INTEGRATION OF BIOGENIC EMISSIONS IN ENVIRONMENTAL FATE, TRANSPORT, AND EXPOSURE SYSTEMS

BY CHRISTOS I. EFSTATHIOU

A dissertation submitted to the

Graduate School—New Brunswick

Rutgers, The State University of New Jersey

and

The Graduate School of Biomedical Sciences

University of Medicine and Dentistry of New Jersey

in partial fulfillment of the requirements for the

Joint Degree of Doctor of Philosophy

Graduate Program in Environmental Sciences - Exposure Assessment

Written under the direction of

Dr. Panos G. Georgopoulos

and approved by

_____

_____

_____

_____

_____

New Brunswick, New Jersey

May, 2009

ABSTRACT OF THE DISSERTATION

Integration of Biogenic Emissions in Environmental Fate, Transport, and Exposure Systems

by Christos I. Efstathiou

Dissertation Director: Dr. Panos G. Georgopoulos

Biogenic emissions make a significant contribution to the levels of aeroallergens and secondary air pollutants such as ozone. Understanding major factors contributing to allergic airway diseases requires accurate characterization of emissions and transport/transformation of biogenic emissions. However, biogenic emission estimates are laden with large uncertainties. Furthermore, the current biogenic emission estimation models use low-resolution data for estimating land use, vegetation biomass and VOC emissions. Furthermore, there are currently no established methods for estimating bioaerosol emissions over continental or regional scale, which can impact the ambient levels of pollent that have synergestic effects with other gaseous pollutants.

In the first part of the thesis, an detailed review of different approaches and available databases for estimating biogenic emissions was conducted, and multiple geodatabases and satellite imagery were used in a consistent manner to improve the estimates of biogenic emissions over the continental United States. These emissions represent more realistic, higher resolution estimates of biogenic emissions (including those of highly reactive species such as isoprene). The impact of these emissions on tropospheric ozone levels was studied at a regional scale through the application of the USEPA's Community Multiscale Air Quality (CMAQ) model. Minor, but significant differences in the levels of ambient ozone were observed,

In the second part of the thesis, an algorithm for estimating emissions of pollen particles

from major allergenic tree and plant families in the United States was developed, extending the approach for modeling biogenic gas emissions in the Biogenic Emission Inventory System (BEIS). A spatio-temporal vegetation map was constructed from different remote sensing sources and local surveys, and was coupled with a meteorological model to develop pollen emissions rates. This model overcomes limitations posed by the lack of temporally resolved dynamic vegetation mapping in traditional pollen emission estimation methods. The pollen emissions model was applied to study the pollen emissions for North East US at 12 km resolution for comparison with ground level tree pollen data. A pollen transport model that simulates complex dispersion and deposition was developed through modifications to the USEPA's Community Multiscale Air Quality (CMAQ) model. The peak pollen emission predictions were within a day of peak pollen counts measured, thus corroborating independent model verification. Furthermore, the peak predicted pollen concentration estimates were within two days of the peak measured pollen counts, thus providing independent corroboration. The models for emissions and dispersion allow data-independent estimation of pollen levels, and provide an important component in assessing exposures of populations to pollen, especially under different climate change scenarios.

Acknowledgements

Table of Contents

List of Tables

List of Figures

List of Abbreviations

ABL   Atmospheric Boundary Layer

ADE   Atmospheric Diffusion Equation

AERMAP Terrain Data preprocessor

AERMET Meteorological Data preprocessor

AERMOD American Meteorological Society EPA Regulatory MODel

AIS   Aerial Information System

AML   Arc Macro Language

ARL   Atmospheric Resources Laboratory (EPA)

ATP   Adenosine-5'-triphosphate

AQMS   Air Quality Modeling System

AQS   Air Quality System (EPA)

AVOC   Anthropogenic Volatile Organic Compound

BEIGIS   Biogenic Emissions Inventory Geographic Information System

BEIS   Biogenic Emissions Inventory System

BIOME   Biogenic Model for Emissions

BVOC   Bogenic Volatile Organic Compound

CAAA   Clean Air Act Amendments

CARB   California Air Resources Board

CBM   Carbon Bond Mechanism

CEMPD Center for Environmental Modeling for Policy Development

CIR   Color Infrared

CFCC   Census Feature Class Code

CLM   Community Land Model

CMAQ-CTM Community Multi-scale Air Quality - Chemical Transport Model

CMSA   Consolidated Metropolitan Statistical Area

CO   Carbon monoxide

CTM   Chemical Transport Model

DEM   Digital Elevation Model

DMAPP   Dimethylallyl Pyroposphate

DWM   Diagnostic Wind Model

EDAS   ETA Data Analysis System

EMS   Emission Modeling System

EOS   Earth Observing System (NASA)

EPA   Environmental Protection Agency

EROS   Earth Resources Observations and Science System

ESRI   Environmental Systems Research Institute

ETM+   Enhanced Thematic Mapper (Landsat)

EWDB   Eastwide Forest Inventory and Analysis Database

FDDA   Four Dimensional Data Assimilation

FTP   Federal Test Procedure

FIPS   Federal Information Processing Standards

GEMAP   Geocoded Emissions Modeling and Projection System

GIS   Geographic Information System

GIRAS   Geographic Information Retrieval and Analysis System

GloBEIS Global Biosphere Emissions and Interactions System

GM   Genetically Modified

HYSPLIT Hybrid Single-Particle Lagrangian Integrated Trajectory Model

IGBP   International Geosphere-Biosphere Programme

IIP   Isopentenyl Pyrophosphate

ITUM   Integrated Terrain Unit Maps

I/M   Inspection and Maintenance

LAI   Leaf Area Index

LDD   Long Distance Dispersal

LRT   Long Range Transport

LSM	Land Surface Model
LS	Lagrangian Stochastic
LULC	Land Use Land Cover
MCIP	Meteorology Chemistry Interface Processor
MEP	Methylerthritol 4-phosphate
MM5	5th Generation Mesoscale Model
MRF	Medium Range Forecast
MRLC	Multi-Resolution Land Characterization
MSA	Metropolitan Statistical Area
MVA	Mevalonic acid
NAAQS	National Ambient Air Quality Standards
NASA	National Aeronautics and Space Administration
NCAR	National Center for Atmospheric Research
NHANES	National Health and Nutrition Examination Survey
NJDOT	New Jersey Department of Transportation
NJDEP	New Jersey Department of Environmental Protection
NLCD	National Land Cover Database
NMVOC	Non Methane Volatile Organic Compound
NOAA	National Oceanic and Atmospheric Administration
NWP	Numerical Weather Prediction
NWS	National Weather Service
NOx	Nitrogen Oxide
NPP	Net Primary Productivity
OTC	Ozone Transport Committee
PAQSM	Photochemical Air Quality Simulation Model
PAR	Photosynthetically Active Radiation
PAVE	Package for Analysis and Visualization of Environmental Data
PBL	Planetary Boundary Layer
PFT	Plant Functional Types

PSU   Penn State University

ROG   Reactive Organic Gas

RADM   Regional Acid Deposition Model

RAMS   Regional Atmospheric Modeling System

REMSRAD Regional Modeling System for Aerosols and Deposition

RFG   Reformulated Gasoline

ROM   Regional Oxidant Model

RRTM   Rapid Radiative Transfer Model

SAPRC   Statewide Air Pollution Research Center

SIP   State Implementation Plan

SOA   Secondary Organic Aerosol

TIGER   Topologically Integrated Geographic Encoding and Referencing

TNRCC Texas Natural Resources Conservation Commission

UAM   Urban Airshed Model

USGS   United States Geological Survey

UTM   Universal Transverse Mercator

VMT   Vehicle Miles Traveled

VOC   Volatile Organic Compounds

VRS   Vapor Recovery System

WRF   Weather Research Forecast

Chapter 1

Introduction

Aside from accidental releases, extreme air pollution episodes during which the concentration of air pollutants, in particular around urban-industrial areas, can reach excessively high levels for periods of several hours to several days, can cause extreme discomfort, diseases, and even deaths among the most vulnerable part of the population (children, elderly, and sensitive groups like asthmatics). Industrialized and developing countries experience such conditions in various environmental settings, and from both anthropogenic and biogenic emission sources. The various sources of air pollution can be divided into three broad categories: (1) urban and industrial sources; (2) agricultural and other rural sources; (3) natural emissions. Each of these categories can further be subdivided into several subcategories (Figure 1.1). With respect to their potential as either direct or indirect health stressors, they can be organized in the following two main groups of interest:

1. **Volatile organic compounds** whose predominant source of biogenic origin is the growth and death of vegetation;

2. **Bioaerosols**, that contain a number of aeroallergens such as pollen spores and fungi.

1.1 Background and significance

1.1.1 Health impacts of allergenic air pollutants

The American Academy of Allergy, Asthma and Immunology (AAAAI) estimates that 36 million Americans suffer from seasonal allergy and 20 to 30% of the population suffers from seasonal *allergic rhinitis* (also known as "hay fever") [Knowlton et al., 2007]. Allergies are among a host of factors that can trigger an asthma attack. Asthma is a chronic and potentially life-threatening lung disease characterized by difficulty breathing [A.L.A., 2007]. Worldwide asthma

rates doubled between 1998 and 2003 and self-reported cases in the U.S. rose by 75% between 1980 and 1994. In addition to an increase in prevalence, there has also been an increase in the severity of asthma. Between 1986 and 1993, the number of hospitalized children in California who experienced a negative outcome, such as intubation or cardiopulmonary arrest, doubled.

At the same time, a number of epidemiological and chamber exposure studies including asthmatics have demonstrated associations between several individual air contaminants and increased frequency or severity of diseases of the upper respiratory tract. Air contaminants including: ozone, sulfur dioxide, nitrogen oxides, acid particulates (hydrogen ion), sulfates, fine and coarse particulate matter, total particulates and wood smoke, in addition to a varying spectrum of bioaerosols such as pollen and fungal spores have all been strongly associated with respiratory diseases. These studies have also suggested that particulate air contaminants can cause an increase in both acute respiratory effects, and long-term cardiovascular effects as measured by emergency room visits [for review see Dockery, 2001; Dockery and Pope, 1994; Peterson and Saxon, 1996]. However, the temporal correlation among air contaminants (and even temperature in warm weather) makes it tough to pinpoint associations between individual contaminants and broad exposure endpoints such as asthma or other common diseases of the respiratory tract. Many of the studies investigating relationships between ambient air quality and acute asthmatic attacks are based on evaluation of only a few contaminants or markers (e.g. PM_{10}). Furthermore, particulate matter is composed of many compounds and only a limited number of studies have explored which components might be the most important for certain effects like asthma exacerbations [Bernstein et al., 2004; Thurston et al., 1992, 1994; Tolbert et al., 2000]. A growing number of studies provide evidence that climate-induced changes in temperature, concentration of atmospheric CO_2 and pollen seasons will increase the production and allergenicity of airborne allergens, effectively compounding the threat of deteriorating air quality [D'Amato and Cecchi, 2008]. While more studies need to confirm this link, substantial evidence correlates the global rise in asthma with climate-induced changes in air pollution and aeroallergens, such as ragweed [Knowlton et al., 2007].

1.1.2 Biogenic emissions of ozone precursors

The presence and effects of vegetative growth in the interaction layer of the lower troposphere can contribute significantly to the reactive organic gas (ROG) inventory in both rural and urban areas. The significance of this contribution from biogenic sources is enhanced by the greater atmospheric reactivity of many biogenic hydrocarbons in comparison to anthropogenic byproducts. As a result, volatile organic compounds (VOCs) emitted by growing vegetation are important chemical species that affect the oxidative capacity of the troposphere [National Research Council, 1991; Seinfeld and Pandis, 2006], as well as the levels of other species (e.g. carbon monoxide, methane, aerosols) that are known to play an important role in climate forcing [Collins et al., 2002; Shallcross and Monks, 2000]. Biogenic VOCs (BVOCs) are also precursors to surface-level ozone (O_3), which has a well-documented impact on human health [Reeser et al., 2005], and agricultural productivity [Felzer et al., 2004; Fuhrer and Booker, 2003]. On the global level, the BVOC emissions are estimated to be close to an order of magnitude greater than the global total anthropogenic source [Guenther et al., 1995; Wang and Shallcross, 2000; Wang et al., 1998a,b,c]. Their impact is complicated by the fact that the interactions between ozone precursors are highly nonlinear [Jacob, 2000; Kang et al., 2003; Roselle, 1994; Sillman et al., 2002], and are affected by transport processes, meteorology, and the differential reactivity of individual VOC species [National Research Council, 1991; Seinfeld and Pandis, 2006]. O_3 levels are also dependent on the regional background component that is known to be affected by long-range transport (LRT) of O_3 and its precursors [Fiore et al., 2002].

Grid-based photochemical air-quality simulation models (PAQSMs) offer computerized representations of the atmospheric processes responsible for air pollution, including ozone and secondary aerosol formation. These models simulate the atmosphere in varying degrees of detail by mathematically representing emissions; initial and boundary concentrations of chemical species; the chemical reactions of the emitted species and their products; and the effect of local meteorology (sunlight, wind, and temperature). In this way, an understanding of atmospheric chemistry and meteorology is combined with estimates of source emissions to predict possible control strategy effects.

The development and success of specific emissions control strategies is expected to be greatly dependent on the estimated fluxes of biogenic hydrocarbon species. Considerable attention has

be given to determining BVOC emission rates in past research. However, biomass and leaf mass quantification and plant species composition and dominance are believed to be the weaker links in the development of BVOC emission estimates, both for plants in urban settings and for regional-level inventories [Karlik et al., 2002]. Therefore, most biogenic emissions models belong to the broad class of methods that involve the use of phenomenological, i.e. "observation-based" approaches in which empirical relationships are deduced from smog chamber experiments or open-field atmospheric measurements. In order to ensure that land-surface processes are accounted for in these models, surface characteristics such as soil and vegetation properties have to be specified as accurately as possible. Experimental and modeling studies on an area-wide basis have demonstrated that biogenic hydrocarbons can constitute a significant contribution to the overall VOC inventories of both urban and rural regions [Chameides et al., 1988; Lamb et al., 1993; Pierce et al., 1990; Winer et al., 1983; Zimmerman, 1979a]. In the eastern US, the total annual amount of BVOC emissions has been estimated to exceed the corresponding anthropogenic releases [Fuentes et al., 2000; Guenther et al., 2000; Kinnee et al., 1997; Pierce et al., 1998]. Consequently, incorporating BVOC emissions into existing air quality models results in substantial increases in predicted ozone concentrations, although areas with low nitrogen oxide levels can exhibit the opposite effect [Horowitz et al., 1998; Liang et al., 1998; Pierce et al., 1998; Roselle, 1994]. On average, BVOCs are estimated to be 2-3 times more reactive than emissions from mobile sources, a major anthropogenic VOC (AVOC) contributor [Atkinson, 1987, 1990, 2000; Atkinson and Arey, 1998; Atkinson and Carter, 1984; Atkinson et al., 1995; Carter, 1994; Carter et al., 1995; Corchnoy and Atkinson, 1990].

1.1.3 Emissions and transport of biogenic emissions

As mentioned before, the representation of the land-surface processes is an important component of atmospheric and environmental models since it has a direct impact on precipitation and on the evolution of the atmospheric boundary layer (ABL). A key question addressed here is whether the same general modeling framework that has been developed for simulating regional photochemical episodes, can cover a variety of sources of biogenic origin that can be important in human population-based exposure modeling. There is a clear need for modeling tools that can associate background emissions from biogenic sources which follow the natural growth and

seasonality of the local ecosystems. BVOC and bioaerosol emissions with occasional episodes (forest fires, volcanic eruptions) that release pollutants, frequently involved in long-range transport (LRT) due to their slow removal from the atmosphere (e.g. $PM_{2.5}$). Recent studies have shed light on the complexity of interactions between gas-phase pollutants (Figure 1.2), and have highlighted the importance of studying the co-occurrence of such contaminants. It is also well established that atmospheric pollen allergens are not carried only by intact pollen grains, but also by smaller particles measuring just a few microns *(paucimicronic particles)* [Emberlin, 1995; Spieksma and Nikkels, 1999]. Furthermore, it has been suggested that the pollen component of urban aerosols may undergo chemical transformations, described by the mechanism of protein nitration, upon contact with pollutants such as nitrogen dioxide and ozone, and in this way acquire enhanced allergy-inducing properties [Franze et al., 2005]. This interaction of photochemical smog constituents and bioaerosols has been also verified in highly polluted areas of India and Iran [Bist et al., 2004; Chehregani et al., 2004].

The main problem associated with regional modeling studies of BVOC emissions is that they are assumed to be static on the timescales relevant to the air pollution policies. The predicted changes in emissions for recent decades have been small, because the equilibrium vegetation models used in such studies inherit the assumption that current vegetation has reached a steady-state with respect to the current climate. However, climate change can affect emissions both directly, since plant-level emission rates depend on the surrounding environmental conditions, and indirectly, due to the evolution of vegetation at the ecosystem level.

This framework can be extended for population exposure assessment applications and a number of additional processes can be incorporated. For example, application of pesticides to croplands by spraying from aircrafts may result in transport and exposure to residential areas. The soil may also naturally emit contaminants (e.g. Radon), or be contaminated by radionuclides or heavy metals which in turn can be taken up by plants and become airborne again during fire events. These situations can be modeled by using the same land use/cover, geological, elevation, and vegetation-related *geodatabases*. More in-depth modeling tools can be used by applying allocation methodologies [see the related USGS report Thelin and Gianessi, 2000] and in some cases direct coupling with transport models (atmospheric, groundwater, *etc.*) that follow the pollutant(s) of concern and relate to a potential pathway of exposure. Increasing

interest has been shown in assessing the impact of *genetically modified* (GM) plants in such scenarios. Evidence presented in a recent project funded by the European Environment Agency, suggest that there is a clear risk that GM plants of various species would cross-pollinate non-GM plants, up to and beyond their recommended isolation distance under favorable meteorological conditions [Eastham and Sweet, 2002].

Hence, there is a clear need not only for broader and more versatile ambient monitoring networks, but also for the development of a framework for multi-pollutant exposure modeling applications by taking advantage of the existing state-of-the-art computer-based methods and environmental information databases.

1.2 Background on air quality modeling components

1.2.1 Chemical transport models

The principal objective of a chemical transport model is to mathematically reproduce a variety of air pollution phenomena. In this way, CTMs have been used to simulate air quality (concentration levels of each pollutant) in time and space. It is clear though, that in order to benefit from CTMs and to perform comprehensive air quality assessments, a combination of air quality measurements and CTMs should be employed [De Leeuw et al., 2001]. To use such models, some information intrinsic to the chemical transport model is needed, such as grid structure, resolution, and initial and boundary conditions. Inputs to CTMs can be broadly grouped as those dealing with meteorology and emissions:

1. *Meteorological inputs:* Usually CTMs require hourly, vertically and horizontally resolved wind fields, as well as hourly temperature, humidity, mixing depth, and solar insolation fields. Some also use the vertical diffusivities, cloud characteristics and rainfall as simulated by meteorological models. Meteorological inputs are typically developed de-coupled from the chemical transport model. The data sparsity is the main reason of preference towards the usage of *dynamic* or *prognostic* meteorological models.

2. *Emissions:* As previously discussed, accurate emission inputs are key to good model performance. Emission inputs are developed to be compatible with the chemical mechanism and the model's spatiotemporal resolution. Detailed, speciated VOC emissions are usually

lumped into the appropriate chemical mechanism categories. Typically, this would include gridded, hourly estimates of the emissions of CO, NO_x, SO_2, and various primary VOCs. For particulate matter modeling, primary emissions of SO_3, NH_3, $PM_{2.5}$, and PM_{10} should be included.

CTMs, in relationship to the coordinate system can be classified into *Lagrangian* or *Eulerian* models. *Lagrangian* models consider a mobile coordinate system, which in the case of atmospheric phenomena, follows a defined air parcel. Conversely, the *Eulerian* approach is based on a fixed coordinate system. *Box models* are the simplest air pollution models, and a particular category of *Eulerian* photochemical dispersion model. They are based on the mass conservation of a pollutant inside a single cell, or box, inside which emissions are considered homogeneous [Jacobson, 1999]. The ground as defined by land cover/type characteristics bounds this cell on the bottom, the inversion base (or some other upper limit to mixing) on the top, while there are east-west and north-south boundaries on the sides. Box models can be applied for both inert and reactive pollutants. Fundamental to the model concept is the assumption that the pollutant concentrations in a volume of air are spatially homogeneous and instantaneously mixed. Under this condition, pollutant concentrations can be described by the simple balance among the rates at which they are transported in and out of the air volume, their rates of emission from sources within the volume, the rate at which the volume expands or contracts, and the rates at which pollutants react chemically or decay.

Trajectory models use a moving-coordinate approach to describe the atmospheric diffusion and pollutant transport. A hypothetical column of air is defined, which given a specified starting point, moves under the influence of the prevailing winds, passing over emission sources which inject primary pollutant species in the column [Seinfeld, 1988]. Chemical reactions may also be simulated in the column which can be partitioned horizontally or vertically in many layers or cells. The formulation employed by trajectory models to describe atmospheric process is based on the mass conservation, approximated by the atmospheric diffusion equation (ADE) in a moving coordinate system. The air parcel of interest is assumed to travel solely with the horizontal wind.

Grid models employ a fixed Cartesian reference system within which the atmospheric dynamics are described. The region to be modeled is bounded on the bottom by the ground, on the top by the inversion base (or some other maximum height), and on the sides by the desired east-west and north-south boundaries. This space is then subdivided into a two- or three-dimensional array of grid cells. Most global scale models assume vertically well-mixed cells extending from the ground surface to the base of the inversion layer: others subdivide the modeled region into a number of layers in the vertical direction. The basis for grid models is the solution of the atmospheric reaction diffusion equation using an *Eulerian* coordinate system [Dabdub and Manohar, 1997]. Most common applications of grid models to date have been related to photochemical ozone and aerosol dynamics, because grid models provide the only means to predict three-dimensional concentration distributions over a specified region. Their limitations emerge in principal from the considerable information database needed as input [Seinfeld, 1988].

One of the most important components of chemical transport models is the photochemical mechanism. A mechanism for tropospheric chemistry is a mathematical description of the photochemical processes of low atmosphere through a series of chemical reactions involving primary and secondary pollutants. Divergence points between different chemical schemes are [Kuhn et al., 1998]: (1) formulation of the reaction mechanism, (2) rate constants for the reactions and their temperature and pressure dependencies, and (3) temporal integration of the reaction rates by a chemical solver. Chemicals considered in a photochemical mechanism distinguish between inorganic compounds (NO_x, O_x, and SO_x) and organic compounds, mainly VOCs. The variety of VOCs emitted to the atmosphere is wide, and its speciation and determination through emission inventories is very complicated. A more detailed comparison of the existing tools and databases will be presented in Chapter 3.

1.2.2 Meteorological models

Meteorological models provide the necessary information regarding the atmospheric state to the chemical transport model. The dispersion of atmospheric pollutants is based on the advection transport, mixing by eddy diffusion and dry or wet deposition. These phenomena depend on the meteorological state of the atmosphere, leading to the minimal need for wind

patterns and information regarding the atmospheric turbulence. Meteorological models can be classified as either *prognostic* or *diagnostic*:

- Prognostic models are based on the solution of the time-dependent hydrodynamic and thermodynamic equations, appropriately modified for atmospheric application. These models are also known as *dynamic* or *primitive equation models* [Pielke, 1984];

- Diagnostic models provide information about the wind fields and other meteorological parameters, via satisfying established physical constraints. By imposing the continuity equation to the meteorological variables measured in fixed locations, they describe the state of the field of interest providing a diagnostic of the variable. These models are also called *mass consistent* or *kinematic* models.

The predominant tendency in air quality modeling evolves towards the use of prognostic models as pre-processor meteorological packages to extract and reformat the variables needed by the CTM. Prognostic models used in photochemical modeling employ the same algorithms that are used in the Numerical Weather Prediction (NWP) models. The main differences lay in the meteorological scale of the study and the related strength of the processes that drive the model. Usually, chemical transport models are applied over regions with dimensions less than 1,000 km (mesoscale) with a spatial resolution of a few kilometers. Models used for weather prediction work on more extensive regions (macroscale). However, both types are based on the same primitive equations to resolve the physics of the atmosphere [Seaman, 2000].

1.2.3 Emission models

An atmospheric emission inventory is a compilation of the estimates of pollutant emissions into the atmosphere, distributed over a determined geographical area, during an established period of time. In practice, atmospheric emissions are estimated on the basis of selected or representative *in situ* measurements. Models can also be used to relate the activity of that source with the amount of any kind of substances that are emitted to the atmosphere. The basic model for an emission estimate is the product of at least two variables: (1) an activity statistic; and (2) a typical average emission factor for the activity. Emission estimates are gathered together to compile inventories or databases which also contain a variety of supporting information including:

location of the source of emissions, emission measurements, emission factors, temporal profiles, production or activity rates in the various source sectors, external conditions, etc.

An *atmospheric emission model* can be defined as a set of mathematical submodels of differing degrees of complexity that are integrated. They are useful for estimating atmospheric emissions within an "airshed" of concern, from different sources in the spatial extend it covers, during an established period of time. The varying complexity can result in a spectrum of estimates; from simple resume tables specifying the type of pollutant and nature of the source, to more complicated allocation schemes that assign information about the flux of pollutants in the different cells that divide the domain of interest. Two distinct approaches to emission modeling have been developed in recent years:

1. *Top-down approach:* Emissions are estimated for the entire geographical area under study and then are distributed to the individual cells proportionately to certain parameters associated with the source type and properties (e.g. traffic, demographics, industrial density, biomass density).

2. *Bottom-up approach:* Emissions are estimated at an individual cell-level, by means of establishing every parameter for that cell in particular. The total emission value is obtained by aggregation of estimates carried out for all the cells within the area of interest.

1.2.4 Modeling exposures to co-occurring pollutants

Human exposures to atmospheric pollutants can be extremely complex due to the spatial and temporal nature of emissions, meteorology, and human activities. Variations in both the ambient pollution concentrations and behavioral factors influence individuals contact with pollutants found indoors and outdoors. Traditionally different types of models have been used to provide the critical linkages between pollutant emissions from natural and anthropogenic sources, concentrations in various media, human exposures to indoor and outdoor pollutants and the delivered dose to the body resulting from contact with these pollutants. The U.S. Environmental Protection Agency (US EPA) uses a wide range of models in linking air pollution emissions to ambient concentrations to human exposures and to delivered pollutant dose to human respiratory system. However, each modeling component within the source-to-dose continuum (Figure 1.3)

contributes imprecision to predictions depending on the complexity of the underlying environmental, personal exposure or biological condition represented by each model. Furthermore, new maps resulting from analysis by the Natural Resources Defense Council (NRDC) suggest that regions most affected by ragweed and smog substantially overlap with one another (Figure 1.4), leaving these regions particularly vulnerable to the effects of global warming. As global warming boosts levels of both ragweed and smog, the risk of asthma and allergic reactions for people living in these overlapping regions will likely increase.

1.3 Objectives

Photochemical episodes are associated with meteorological conditions that favor both the transformation and transport of chemicals and require a broad and rigorous analysis of the fluxes of pollutants involved in the region. The effective characterization of biogenic emission fluxes and sources can have a significant influence on control strategies developed by policy-makers. In addition, there is a strong linkage on the source-to-dose population exposure continuum (Figure 1.3) that remains unexplored when biogenic sources and the associated uncertainties are lumped in broader pollutant groups. The utilization of multi-scale, multi-dimensional databases and geodatabases, despite its complexity, can be a beneficial tool for assessing air quality via environmental transport/fate models. Incorporating the vegetative characteristics of a particular region into the model can enhance the estimation of the potential contribution to population exposure. In addition to this main hypothesis, a variety of related biogenic emissions (aeroallergens, forest fires) can be studied in a unified manner in the same modeling framework. Keeping in mind the role of vegetation as the underlying information base, the objectives of this thesis can be defined as:

Objective A

- Improve biogenic VOC emission inventories by incorporating additional land use/land cover and vegetation databases;

- Study the impact of refined estimates on regional surface ozone levels.

Objective B

- Improve the characterization of pollen emissions;

- Develop modules for studying the transport of pollen particles;

- Implement modules in a framework that allows for studying co-exposures.

1.4 Outline of the thesis

- Chapter 1 presents a brief introduction to the major atmospheric processes relevant to biogenic emissions, their transport, and transformation. It also discusses the steps involved in air quality modeling applications that have been currently used in exposure systems, and the associated limitations. Additionally, Chapter 1 summarizes the objectives and presents a brief overview of this thesis.

- Chapter 2 presents the relevant background information on the biogenic processes and released agents that accompany them. The focus of the chapter will be on emissions, transport, and transformation of such pollutants and aeroallergens. In addition, Chapter 2 provides a link to the major model formulation and emission parameter development for each of the involved species.

- Chapter 3 reviews and aggregates geodatabases and modeling tools to support biogenic emissions modeling.

- Chapter 4 presents the application of integrated emissions-chemistry-transport modeling of biogenic VOC species relevant to the Northeast region. In Chapter 4, the effect of the aggregate geodatabase that includes recent satellite data for the area of interest will be also discussed.

- Chapter 5 presents the development and application of a module that incorporates emission and transport processes of aeroallergens at the regional scale. The main focus of Chapter 5 will be pollen particles and more specifically Birch and Ragweed, a set of very significant allergenic particles that affect most of the population of the Northeast.

- Finally, Chapter 6 presents the conclusions of this thesis, and recommendations for future work. This is followed by bibliography.

Figures
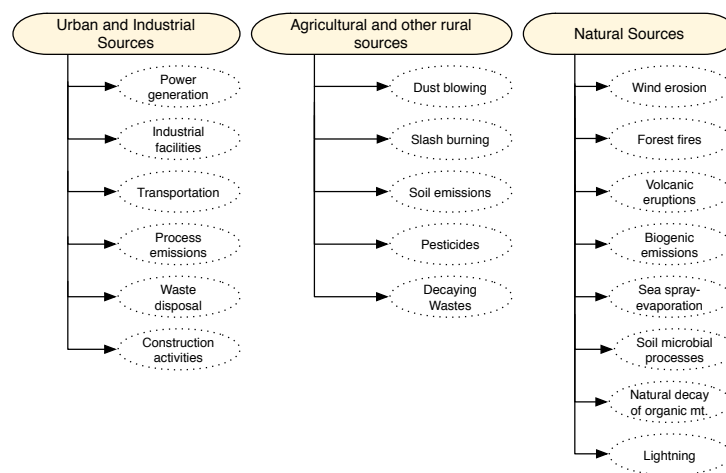
Figure 1.1: Grouping of the various sources of air pollution [Source: Finlayson-Pitts and Pitts, 2000].
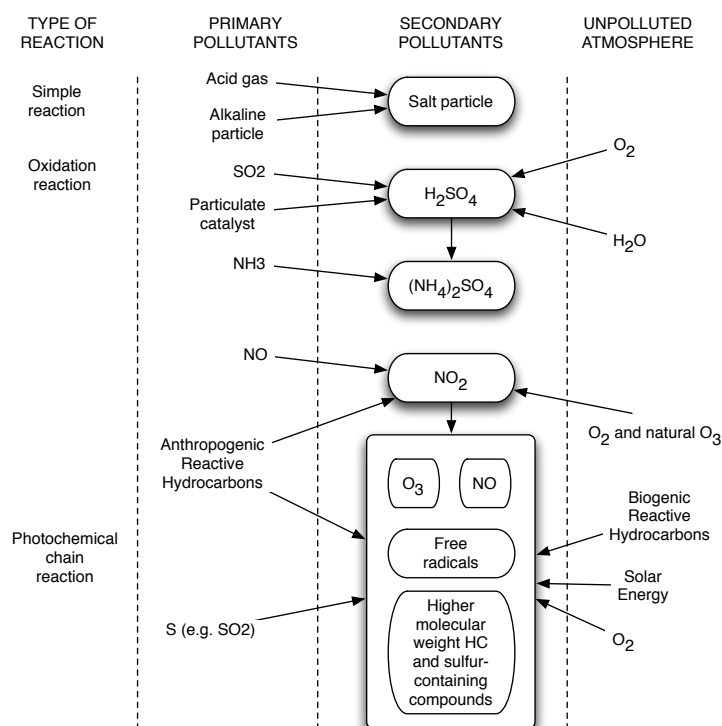
Figure 1.2: A schematic of interactions between chemical species and particulate matter leading to the formation of secondary pollutants [Source: Franze et al., 2005].
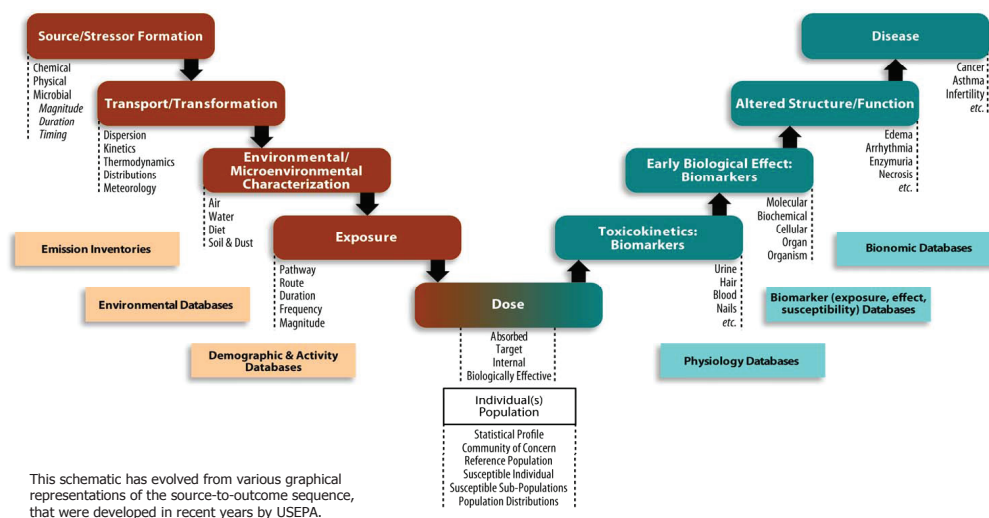
Figure 1.3: The *source-to-dose-to-effect* exposure assessment framework extended to modeling co-exposures to various contaminants, including those of biogenic origin [Source: Georgopoulos, 2008].
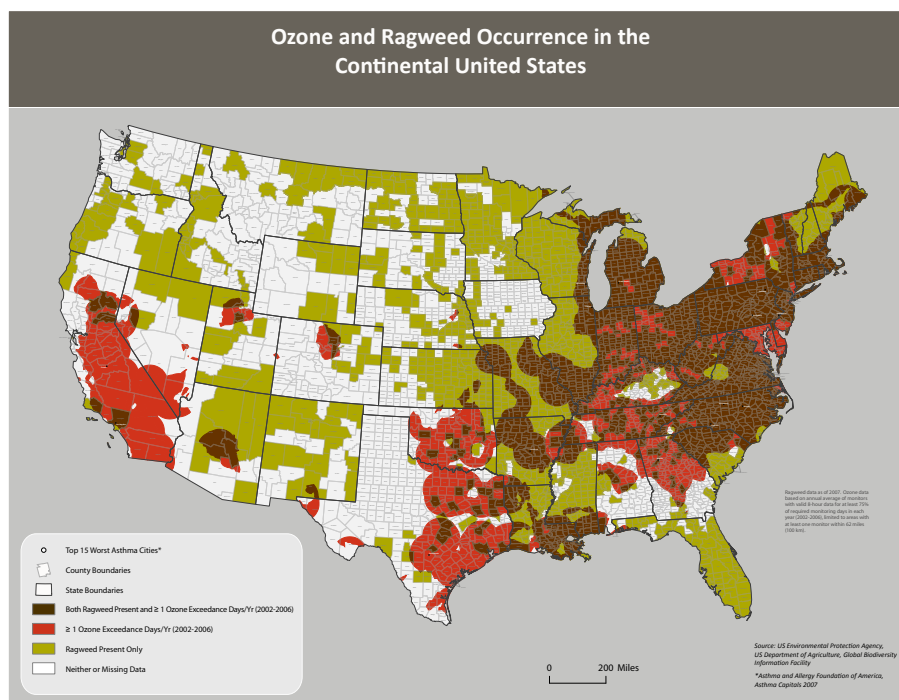
Figure 1.4: Ozone and ragweed co-occurrence in the continental United States. Together they can exacerbate asthma, allergic symptoms, etc. [Source: Knowlton et al., 2007].

Chapter 2

Background on the emission, transport and transformation of major biogenic releases

Chemical compounds and bioaerosols in the surface interaction layer between the biosphere and atmosphere are released from vegetation via a number of natural processes. The purpose of this chapter is to review the current approaches for modeling these processes on the regional scale. The releases that are covered in this study fall into the two main categories mentioned before: (1) biogenic non-methane volatile organic compounds (NMVOCs), and (2) bioaerosols. Volatile organic compounds (VOCs), nitrogen oxides (NO_x), and greenhouse gases such as methane (CH_4), nitrous oxide (N_2O), ozone (O_3) and carbon dioxide (CO_2) may originate from a variety of biogenic sources. Bioaerosols can be found in the atmosphere in the form of pollens, fungal spores, bacteria, viruses, and a number of fragments coming from plants and animals. The focus of this study for the group of bioaerosols concentrates on pollen particles. These two main groups of biogenic emissions may significantly impact air quality on the local scale during periods of adverse meteorological conditions. The following sections present information on the production, release, and transport processes for the major representatives of the first two groups of interest: BVOCs and pollen particles.

2.1 Biogenic Volatile Organic Compounds

It was first recognized over 40 years ago that isoprene [2-methyl-1,3-butadiene] is emitted into the atmosphere from plants [Rasmussen and Went, 1965; Sanadze and Dolidze, 1961]. Since then, numerous studies have revealed that a wide variety of NMVOCs are produced and emitted from certain parts of vegetation (see Figure 2.1) [Arey et al., 1991a,b, 1995; Ciccioli et al., 1993; Evans et al., 1982; Fuentes et al., 2000; Geron et al., 2000b; Hewitt, 1999; Isidorov et al., 1985; Konig et al., 1995; MacDonald and Fall, 1993; Rasmussen, 1970]. Table 2.1 provides a subset of the total

number of NMVOCs observed in literature as plant emissions along with their reaction products, chosen to be representative of the organic compound classes involved. The group of compounds referred to as isoprenoids or terpenoids, is of great importance and consists of isoprene (C_5H_8), monoterpenes (two isoprene units), and sesquiterpenes (three isoprene units). They are usually characterized as volatile, poorly water soluble, and very reactive compounds with a strong scent. The structures of some terpenoids and common oxygen-containing compounds, also considered to belong to the terpenoids group, are illustrated in Figure 2.2.

Published emission inventories of biogenic and anthropogenic NMVOCs imply that in regional and global scales the emissions of biogenic NMVOCs are comparable to, or exceed, those of anthropogenic origin [Guenther et al., 1995; Lamb et al., 1987, 1993]. On a global scale, it is estimated that $1150\,$Tg of carbon are released annually in the form of NMVOCs ($1\,$Tg $= 10^6$ metric tons) [Guenther et al., 1995]. Although there are large uncertainties in the emission rates of total biogenic NMVOCs and of individual compounds, 44% and 11% of biogenic VOC emissions have been attributed to isoprene and monoterpenes, respectively [Guenther et al., 1995]. Recent annual estimates for the North America suggest that of the $86\,$Tg of biogenic NMVOCs, 30% is isoprene, 30% is methanol, 20% are monoterpenes and sesquiterpenes, 8% are hexene derivatives, and 5% is 2-methyl-3-buten-2-ol, with the remainder being relatively nonreactive species [Guenther et al., 2000].

2.1.1 Biosynthetic pathways for the isoprenoid group

The biochemical pathways involved in the synthesis of biogenic hydrocarbons have been the subject of extensive recent research [Ajikumar et al., 2008; Calfapietra et al., 2008; Illarionova et al., 2006; Lopes et al., 2007; Rohdich et al., 2002; Sharkey et al., 2005, 2008; Weathers et al., 2006]. Estimating biogenic hydrocarbon emissions relies on empirical models of emissions based on observations. Whenever possible, mechanisms involved in the synthesis and emission of biogenic hydrocarbons are used to compare and improve models. Mechanistic models are further improved when the season and location of emissions is well understood. However useful such models can be, a fundamental understanding of the pathways and chemistry of BVOC synthesis is necessary. The biosynthetic pathways of the isoprenoid group (see Figure 2.3) share a common precursor compound, dimethylallyl pyrophosphate (DMAPP). This precursor and its

isomer, isopentenyl pyrophosphate (IPP), are also precursors for important biological molecules such as the carotenoids and cholesterol. Although the pathways of this group are not completely known, initial thoughts pointed to the well known mevalonic acid (MVA) pathway [McGarvey and Croteau, 1995]. However, later research revealed that higher plants have two distinct routes for the biosynthesis of DMAPP; the MVA pathway and the 2-deoxyxylulose 5-phosphate/2-methylerythitol 4-phosphate (MEP) pathway [Lichtenthaler et al., 1997]. In the MEP route, DMAPP is formed from glyceraldehyde 3-phosphate and pyruvate, as opposed to the mevalonate precursor [Sharkey and Yeh, 2001]. The mevalonate-independent isoprenoids (such as isoprene, carotenoids, and phytol) are those formed in the chloroplasts. Sesquiterpenes and triterpenes are synthesized from mevalonic acid in nonplastid compartments and isoprene, monoterpenes, phytol (C_{20}) and carotenoids (C_{40}) are synthesized from IPP generated from the MEP pathway [Lichtenthaler et al., 1997; Zeidler et al., 1997]. The IPP is isomerized into DMAPP, which is the precursor for synthesis of isoprene, in a pathway that is not well understood. The final step of isoprene synthesis is the elimination of pyrophosphate from DMAPP by the enzyme isoprene synthase, which appears to be a membrane-bound, light-activated enzyme [Wildermuth and Fall, 1996]. Additionally, changes with this enzyme's activity are well correlated with changes in isoprene emission. Isoprene synthase is one of the reasons that light is a primary factor in controlling isoprene emissions.

It is also clear that the "energy currency" (Adenosine triphosphate - ATP) of the cellular level is produced during photosynthesis and is required for the synthesis of isoprene [Monson and Fall, 1989]. This is in agreement with the experimental evidence that isoprene production and emission are closely linked to photosynthesis [Loreto and Sharkey, 1990; Monson and Fall, 1989; Tingey et al., 1981]. With a better understanding of the biosynthetic pathway, the energy cost associated with isoprene emission can also be determined. The MEP pathway is reported to be more efficient than the MVA pathway, but it is still substantial, and benefits associated with isoprene emission must be compared to the cost of carbon and energy given up by the plant [Sharkey and Yeh, 2001]. This way, the primary requirements for isoprene synthesis are light, warm temperatures, and availability of MEP pathway precursors from photosynthetic processes.

2.1.2 Environmental factors affecting biogenic VOC emissions

The factors affecting biogenic VOC emissions at the single-leaf level have been reviewed by a number of authors [Fuentes et al., 2000; Guenther et al., 1993; Hewitt, 1999]. As described above, the biosynthetic pathway for the group of isoprenoids has revealed the full effect of the environmental driving forces. It is known that, for compounds such as monoterpenes that are released from resin ducts or glands, temperature is the dominant control factor [Tingey et al., 1980]. The increasing vapor pressure of these compounds with temperature explains the temperature response of the emission (Figure 2.4-a). On the contrary, some plants have been found to emit monoterpenes that are not stored in the plant, directly after a light-dependent synthesis (*e.g. Pinus densiflora, Picea Abies, Quercus ilex, Pinus Pinea, Sunflower and Beech* [Bertin et al., 1997; Loreto et al., 1996; Schuh et al., 1997; Schurmann et al., 1993; Staudt et al., 1997, 2000; Yokouchi and Ambe, 1984]). Plants are believed to emitt monoterpenes for a variety of reasons, including defense against insects and other herbivores, and attraction of pollinators and enemies of herbivores [Hewitt, 1999]. Singsaas [2000] suggested that the emission of isoprene benefits plants by increasing their thermotolerance.

Isoprene emission does not follow the relationship of monoterpenes to volatility; it is instead related to metabolism [Monson et al., 1994]. In other words, isoprene and a part of the plant monoterpene emissions do not come from preexisting pools. The temperature effects are instead enzymatic, with two distinct phases of increase in the emission. For small temperature rate changes, the isoprene emissions change as quickly as the leaf temperature (average time constant 8.2 s). For larger rate changes, the plant will make metabolic adjustments and activate enzymes to increase isoprene emissions (average time constant of 116 s) [Singsaas and Sharkey, 1998, 2000]. The activation energy for isoprene emission is relatively constant across a wide range of conditions, and most investigators have reported similar values ranging from 60 to $90 \, \text{kJ mol}^{-1}$ [Guenther et al., 1993]. Although the activation energy is relatively constant, the leaf's capacity to emit isoprene has been found to vary. The base emission capacity (or basal emission rate) is defined as the rate of emission at $30\,^\circ\text{C}$ and $1000 \, \mu\text{mol m}^{-2}\,\text{s}^{-1}$ of photosynthetically active radiation (PAR). Figure 2.4-b shows the variation of the emission rate of isoprene as a function of leaf temperature, a curve that was found to vary within a growing season [Fuentes et al., 2000]. The dependence on temperature is very different for isoprene emissions versus

photosynthesis. A maximum photosynthesis rate for most plants occurs around $30\,^{\circ}\text{C}$, whereas isoprene emissions continue at temperatures above $30\,^{\circ}\text{C}$. Most plants studied, cease to emit isoprene at temperatures above $40\,^{\circ}\text{C}$ where it is assumed that biosynthetic enzymes are denatured [Guenther et al., 1993; Hewitt, 1999]. Another effect of this temperature dependence is that the ratio of fixed carbon emitted as isoprene increases rapidly with temperature, in particular when they exceed $30\,^{\circ}\text{C}$.

Isoprene and some monoterpene emissions are also dependent upon light. The light dependence is often similar to that of photosynthesis, but many reports have shown that isoprene emission can continue to respond to increasing light after photosynthesis is saturated (Figure 2.4-c) [Harley et al., 1996]. Plants do have the capability to draw on carbon reserves for isoprene production. This is usually experienced as long term drought stress, during which photosynthesis shuts down and stomata are closed, but isoprene continues to be emitted. When drought stress is relieved, isoprene emission exceeds prestress rates [Sharkey and Loreto, 1993]. Not only have short-term effects of temperature and light intensity on isoprene emission rates been observed, but also leaves that develop in full sun emit isoprene at a higher rate than leaves that develop in the shade (Figure 2.4 -d) [Harley et al., 1996]. For example, isoprene emissions measured in deciduous oak canopy at two heights, were found to be significantly higher for sun leaves compared to shade leaves when expressed on a leaf area basis (51 and $31\,\text{nmol}\,\text{m}^{-2}\,\text{s}^{-1}$; $P < 0.01$) [Harley et al., 1997]. Recent studies have shown that the light and/or temperature environment over several days can influence the isoprene emission rate. One approach to characterize these variations in isoprene emissions is to determine emissions as a function of thermal degree units [Fuentes and Wang, 1999; Geron et al., 2000a; Hakola et al., 2000; Monson et al., 1994].

2.1.3   Tropospheric photochemistry and biogenic VOCs

The gas-phase chemistry of the troposphere involves the oxidation of organic species in the presence of oxides of nitrogen under the action of sunlight. Atmospheric oxidation proceeds via chains of radical reactions, which for the case of organic compounds can be long and complex. A key process in atmospheric formation is photolysis of species such as NO_2, HCHO, and HONO. On the other side, *heterogeneous* or *aqueous-phase chemistry* involving reactions in aerosol particles and cloud droplets may affect ozone concentrations in a number of ways

including production and loss of OH radicals and nitrogen oxides, direct loss of ozone, and production of halogen radicals [Jacob, 2000]. Both direct and indirect measurements of photolysis rates in the atmosphere can be a difficult task. To calculate the photolysis rate of a chemical compound, one has to consider: the fraction of solar radiation it absorbs, the distribution of wavelengths and intensity of solar radiation. The photolysis rate of a biogenic chemical, A, in the troposphere, given in molecules $cm^{-2} s^{-1}$, can be expressed in the following way [Roselle et al., 1999]:

$$K_c = \int\limits_{\lambda=290\,nm}^{\lambda_i} \sigma(\lambda) J(\lambda) \phi(\lambda) [A] \, d\lambda \tag{2.1}$$

where,

$\lambda \quad \rightarrow \quad$ wavelength (nm)

$J(\lambda) \quad \rightarrow \quad$ actinic flux (photons $cm^{-2} nm^{-1} s^{-1}$)

$\sigma(\lambda) \quad \rightarrow \quad$ absorption cross-section in base e (cm^{-2} molecules^{-1})

$\phi(\lambda) \quad \rightarrow \quad$ primary quantum yield of A (molecules/photons)

$[A] \quad \rightarrow \quad$ concentration of A

This rate can be considered as a first-order rate constant $K_c = K_a[A]$, and the integral can be substituted by a summation in an interval of wavelengths, where a mean value takes the place of the variable's value within that interval. Absorption cross-sections and quantum yields are functions of wavelength, and may also be a function of temperature and pressure, something that is unique to species and reactions [Jacobson, 1999]. The actinic flux is usually estimated with radiative transfer models, depending on the solar zenith angle [Roselle et al., 1999]. Another approach is to measure the light intensity and convert this to an actinic flux. Photolysis of a molecule may produce one or more sets of products, and the probability of each set of products is embodied in the *quantum yield* term. The production of excess ozone in the atmosphere requires NO_x, VOCs, and sunlight. Under normal atmospheric conditions, the photolysis of NO_2 (at wavelengths < 424 nm), leads to the formation of ozone through reactions 2.2 and 2.3, and the cycle is balanced, because NO and O_3 react to regenerate NO_2 (Eq. 2.4).

$$NO_2 \xrightarrow{h\nu} NO + O\cdot \tag{2.2}$$

$$O \cdot + O_2 \xrightarrow{M} O_3 \tag{2.3}$$

$$NO + O_3 \rightarrow NO_2 + O_2 \tag{2.4}$$
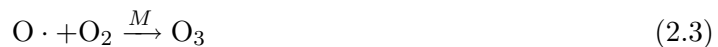
The above three reactions occur rapidly, establishing a steady-state ozone concentration:

$$[O_3] = \frac{J[NO_2]}{k[NO]} \tag{2.5}$$

where k is the rate constant for reaction 2.4, and $J[NO_2]$ is the photolysis rate of NO_2. However, if NO can be converted to NO_2 without scavenging O_3, excess O_3 will be generated. The conversion of NO to NO_2 can occur with biogenic VOCs as the fuel as illustrated in Figure 2.5. The primary removal for the major BVOCs is oxidation by the OH radical, but similar reactions can occur by O_3 and NO_3 oxidation. Various reviews describe in great detail the reaction pathways for the degradation of VOCs, both biogenic and anthropogenic [Atkinson, 1997, 2000; Finlayson-Pitts and Pitts, 2000]. The right portion of Figure 2.5 shows the generalized reaction pathway for VOCs in the atmosphere, where the important intermediate products are alkyl radicals (R·), which quickly combine with O_2 to form alkyl peroxy radicals (RO$_2$·), and alkoxy radicals (RO·). Regions with low NO_x levels (typically less than 5-10 pptv) are termed "clean" atmospheres, and those with significant NO_x (in the ppb range) are termed "dirty" [Finlayson-Pitts and Pitts, 2000]. The rates of reactions are related to the concentration of NO_x in a very complex manner. When NO_x is low, nitric acid (HNO$_3$) and hydrogen peroxide are formed, both playing an important role in the formation of acid rain [Gaffney and Marley, 1991]. However, when NO_x levels are high, the reaction steps outlined above occur creating excess O_3. The formation of O_3 is a non-linear process that is a function of the (HC/NO$_x$) ratio, temperature, and sunlight [Fehsenfeld et al., 1992; Logan, 1985].

Lifetimes and reaction mechanisms of biogenic VOCs

Rate constants for the gas-phase reactions of many of the NMVOCs emitted from vegetation with OH radicals, NO_3 radicals and O_3 have been measured and reported in recent literature. These rate constants can be combined with assumed ambient tropospheric concentrations of OH radicals, NO_3 radicals and O_3 to calculate the biogenic VOC lifetimes with respect to each of these loss processes (Table 2.1). Considering both day and night, the half-life of isoprene ranges from 1.5 to 3 hours. Since it has such a short lifetime, the amount of isoprene that escapes from the boundary layer can be considered negligible. Kesselmeier et al. [2000] measured vertical profiles of isoprene and some monoterpenes over a pristine forest in Amazonia. The lowest mixing ratios were found at the highest altitudes (500 m), and the highest at the surface (Figure 2.6). A diurnal variation is also noticed at a considerable degree as we get closer to the surface. Monoterpenes generally contain at least one unsaturated carbon-carbon bond and often have one or more rings in their structure. For α-pinene, an important monoterpene, the lifetime may range from as little as 5 minutes to 3 hours, while other monoterpenes have even shorter lifetimes [Kesselmeier and Staudt, 1999]. Plants also emit a wide range of other highly reactive VOCs, including many oxygenated species [Winer et al., 1992]. Although many of these fluxes are small when compared to those of isoprene and monoterpenes, they are often of similar magnitude to the anthropogenic sources.

During the past two decades, a lot of research has tried to shed light into the chemical mechanisms and the identification and quantification of the oxidation products involved. Several product studies under atmospheric conditions have faced difficulties due to analytical problems in detecting multifunctional groups, as well as the lack of commercial standards for the anticipated products. The reactions and products have been reviewed by a number of researchers [Atkinson, 1990, 1997, 2000; Atkinson and Arey, 1998, 2003a,b; Calogirou et al., 1995; Fuentes et al., 2000]. Two general mechanisms can be identified: (1) addition to C=C bonds by OH radicals, NO_3 radicals and O_3, and (2) H-atom abstraction from C-H bonds (and to a much lesser extent, from O-H bonds) by OH radicals, and NO_3 radicals. Ozone reacts only by addition to the C=C bonds, and for such BVOCs, addition of OH and NO_3 will generally dominate over H-atom abstraction by these radicals and will lead to hydroxy- or nitrooxy- substituted alkyl radicals, respectively. H-atom abstraction by OH radicals and NO_3 radicals occurs from the

various C-H bonds in alkanes, ethers, alcohols, carbonyls and esters. This reaction pathway is of minor importance for isoprenoids, alcohols, ethers, esters, and ketones containing C=C bonds, but is important for aldehydes with C=C bonds (*e.g.* methacrolein). The reactions of the alkyl or substituted alkyl radicals (R·) formed after H-atom abstraction from C-H bonds or after OH or NO_3 radical addition to the C=C bonds are illustrated in Scheme 1 of Figure 2.7, with the reactions proceeding through the intermediary of organic peroxy and alcoxy radicals. In the atmosphere, alkoxy radicals can decompose by C-C bond scission, isomerize by a 1,5-H shift through a six-membered transition state and react with oxygen. Scheme 2 in Figure 2.7 shows details for the OH radical initiated reactions of isoprene as a representative mechanism. In this scheme, the reactions are followed for only one of the six possible hydroxyalkyl radicals [Atkinson, 1997]. The same source of research provides us with a summary table of the products observed when isoprene reacts as an alkane with OH radicals, NO_3 radicals and ozone (see Table 2.2). Recent studies provide new constraints on the chemistry of the poorly understood isoprene resonance channels, which account for more than one third of the total isoprene carbon flux and a larger fraction of the nitrate yields [Paulot et al., 2008]. The same study indicates that the *cis* branch dominates the chemistry of the isoprene resonance channel with less than 5% of the carbon following the *trans* branch. The yield of isoprene nitrates, which when oxidized release nearly 50% of the NO_x, was found to be approximately 11%. The large molar yields of formic acid during chamber experiments suggest a novel mechanism describing its formation from the organic nitrates [Paulot et al., 2008].

Initial studies attempting to quantify an isoprene-initiated secondary organic aerosol (SOA) suggested that isoprene was not a significant precursor of SOA [Pandis et al., 1991]. Claeys et al. [2004a,b] analyzed aerosol samples from the Amazonian forest and proposed that isoprene oxidation could provide an additional source of SOA via multiphase acid-catalyzed reactions with hydrogen peroxide. Recent laboratory chamber studies found a yield of 1-2% at high NO_x levels [Kroll et al., 2005], and 3% at low NO_x levels [Kroll et al., 2006]. The presence of SO_2 has been found to attribute around 2.8% to the yield of SOA due to ozone [Edney et al., 2005]. An in-cloud process for SOA formation from isoprene has also been identified [Lim et al., 2005]. Field experiments provide evidence that the isoprene oxidation products hydroxyacetone, methylglyoxal, and glycoaldehyde contribute between 10 and 120 Tg of organic aerosol to the troposphere

[Matsunaga et al., 2005]. Terpenes are oxidized in the atmosphere during the day by both OH radicals and ozone, at night by NO_3 radicals and O_3, while the reaction with O_3 leads to the formation of additional OH radicals [Aschmann et al., 2001]. While reaction rate coefficients for many of these reactions have been determined [Atkinson and Carter, 1984], there is a lack of data regarding their products [Hakola et al., 2000, 2003]. A number of researchers observed particle formation in the chemistry of terpenes, revealing that the mass-based aerosol yields were strongly associated with the structure of the hydrocarbon, the initial hydrocarbon-to-NO_x ratio and the amount of seed aerosol initially present [Koch et al., 2000]. Kanakidou et al. [2005] review the current understanding of organic aerosol sources and sinks.

Measurement of BVOCs and development of standardized emission factors

The research agenda on biogenic hydrocarbons is driven, to a large extent, by the need to derive accurate emission inventories so that assessments can be made on the contribution of hydrocarbons upon regional and global atmospheric chemistry. Ambient concentration levels of biogenic NMVOCs, even in heavily forested rural areas, rarely exceed 5% of the total NMVOCs [Arnts and Meeks, 1981]. This caused a great deal of confusion, leading many researchers to erroneously conclude that biogenic NMVOCs do not contribute significantly to the formation of O_3 or aerosols in the troposphere [Altshuller, 1983; Arnts and Meeks, 1981]. The development and application of measurement techniques, capable of identifying the variety of biogenic species and determining emission fluxes at very low ambient levels, and the resulting discovery of different associated reaction pathways, have been the main reasons to think otherwise.

Depending on the scale, such measurement techniques range from enclosures and environmentally controlled gas exchange systems to measuring hydrocarbon fluxes from individual foliage elements, branches, or entire plants, to micrometeorological methods to derive emissions at the plant ecosystem level. Enclosure systems were based on the first conceptual design for BVOC sampling, being particularly useful for defining the forcing variables controlling their emission. Such systems range from whole-plant enclosings to controlled-environment cuvette systems. Canopy-level flux estimation methods were also developed to overcome the limitations of leaf-based fluxes and allow us to measure BVOC for many seasons without interfering with

environmental conditions. Additionally, canopy-level measurements provide direct spatial averages of BVOC fluxes entering the atmospheric environment. The methods applied to determine hydrocarbon fluxes at the canopy level by simultaneously analyzing micrometeorological parameters are: (a) gradient diffusion approach, (b) modified Bowen-ratio technique[1], (c) relaxed eddy accumulation technique, and (d) eddy covariance approach. Several authors discuss the experimental techniques used for quantifying: (a) leaf, (b) canopy, or (c) landscape level fluxes [Fuentes et al., 2000; Guenther et al., 1996]. Kaharabata et al. [1999] found that under similar temperature and light levels canopy fluxes derived from the gradient diffusion approach varied by 27% when compared against their leaf-level equivalent. Their analysis demonstrated that the variability observed in measured hydrocarbon fluxes could be accounted for by varying numbers of heterogeneously distributed clumps of emitter species within a varying footprint. Also, they confirmed previous analysis [Lamb et al., 1996] in that the heterogeneous source distribution of hydrocarbons has to be explicitly considered when estimating and comparing emissions based on above-canopy measurements.

The variation of isoprene emissions primarily occurs at the *genera* level, with no real taxonomic pattern [Martin et al., 1991]. The developmental stage of the leafy biomass is also expected to affect the isoprene emission rate. Most plants do not reach their basal emission rates until full leaf development and expansion [Fuentes and Wang, 1999; Monson et al., 1994]. Ambient concentrations of isoprene above a central Pennsylvania deciduous forest have been found to range from 0 to more than 30 ppbv during daytime, while typical midday levels were between 5-10 ppbv [Martin et al., 1991]. In other ecosystems such as the tropical forests of Brazil, inside-canopy isoprene levels of 8 ppbv have been reported [Martin et al., 1991]. As a result, the compilation of a database with standardized emission factors factors is an extremely difficult task, and a very important link between modeling algorithms and land cover/vegetation databases. The Environmental Protection Agency (US EPA) has undertaken the task of developing and maintaining a database for the entire U.S., which is a part of the standard modeling tools and supporting databases for regulatory applications [Kinnee et al., 1997; Lamb et al.,

---

[1]The modified Bowen-ratio (MBR) technique is a micrometeorological method that can be used to estimate air-surface exchange rates, providing differences in concentrations between two heights can be resolved. Application of the MBR method requires that fluxes and gradients for at least one scalar entity be measured in order to directly compute the exchange coefficient k, which is assumed to be applicable for all scalars.

1993].

2.2 Bioaerosols

Bioaerosols are defined as airborne particles that are living, contain living organisms or were released from living organisms, including plants. Until recently, the atmospheric fate and transport of bioaerosols has not been thoroughly studied in relation to peacetime society. Yet, modern societies have been experiencing a continuous increase in allergic diseases, as a result of elevated levels of aeroallergens and pollutants in metropolitan settings that are considered to be "dirty". Bioaerosol emissions in the atmosphere are also highlighted by another "modern Pandora's box", the problem of cross-pollination and the control of the pollen dispersal from genetically modified (GM) crops [Aylor et al., 2003]. Recent worldwide events, such as epidemics, call for new tools to assess, predict and manage the aerial spread and associated risk of such aerosols. The first step in assessing the risks of bioaerosols is determining their source, composition, and geographically specific behavior as atmospheric aerosols. It is suggested that the volumetric total of the airborne particulates made up by biological material in remote continental, populated continental, and remote maritime environments is 28, 22, and 10% , respectively [Matthias-Maser et al., 2000]. In some regions of the earth, biological material may comprise a substantial proportion of the total aerosol mass concentration (e.g. in tropics, the range can be from 55 to 95%). The size of a bioaerosol particle may vary from $100\,\mu\text{m}$ to $0.01\,\mu\text{m}$. Assuming spherical equivalent particles, pollens from anemophilous plants have typical diameters of 17-58 μm [Stanley and Linskens, 1974], fungal spores are typically 1-30 μm in diameter [Gregory, 1973], bacteria are typically 0.25-8 μm in diameter [Thomson, 1981], while viruses have diameters which are usually less than $0.3\,\mu\text{m}$ [Taylor, 2007]. Table 2.3 contains information regarding pollen size, volume, and weight for several different species. The fragments from plants and animals may also be of various sizes. In addition to size, an important characteristic of biological material is that it does not necessarily occur in the air as independent particles. Past research identified the majority of bacteria at inland sites as being associated with particles of an aerodynamic diameter greater than $3\,\mu\text{m}$. Unexpectedly, new scientific findings document that in the natural environment, bacterial dispersal is faster and occurs over longer distances than previously assumed [Lighthart and Shaffer, 1997]. The magnitude of this new potential risk is extremely difficult

to assess, because there are insufficient data on quantity, identity, viability, and dispersal of airborne microorganisms [Jones and Harrison, 2004].

2.2.1 Aeroallergen production and release

In this section, several environmental (external) and ecological (internal) factors related to aeroallergen production are discussed. Phenology is a state within a sequence of growth stages in the development process of vegetation or any organism. The general phenological stages that most plants transition through include emergence, early vegetation, late vegetation, flowering, fructification, and senescence (Figure 2.8). Plant communities within a spatial unit at any moment in time are at different developmental stages. Pollen is the male gametophyte, the structure responsible for the production and storage of the gametes of seed-producing plants. There are two main types of seed-producing plants, the angiosperms and the gymnosperms. Most of the plants producing allergic pollen belong to the angiosperms. Gymnosperms, the group just below the angiosperms on the evolutionary scale are of minor allergological importance [Falagiani, 1990]. The pollen particles and fragments develop in the pollen sacs (gymnosperm) or anthers (angiosperms) which open when ripe, exposing it to the air. The majority of the plants have not evolved like the anemophilous angiosperms but have maintained a vector-mediated pollinator system. Yet some animal-polinated (zoophilus) species produce abundant pollen and are partially adapted to wind-dispersal as a secondary mode of pollination [Faegri et al., 1989; Lewis et al., 1983]. Because of such cases of either facultative anemophily or incidental release of pollen, it is fallacious to ignore all zoophilus species as potential offenders in localized cases of inhalant allergy. Pollen is released once the mechanism of dehiscence, opening of anthers or microstrobili and release of pollen is initiated. The process and product properties vary in the different plant families, and has been well described for the anemophilous species [Keijzer, 1987a,b; Keijzer et al., 1987]. The onset and duration of dehiscence depends in part on meteorological conditions which change from day to day. Under identical conditions, every species has its specific time of anther dehiscence [Ogden et al., 1974]. Animals that depend on vegetation during their lifetime have evolved in such way that their phenological stages are synchronized with those of the plants they exploit.

Pollen production depends on different factors, such as the climate of the preceding year,

the weather of summer and autumn, or simply on biological rhythms [Stanley and Linskens, 1974]. Distribution patterns of aeroallergens primarily reflect size, density, quantity of pollen available and environmental conditions during dehiscence. The quantity of pollen produced per plant unit is usually measured volumetrically and is found to vary significantly within different species. Anemophilus species almost always outproduce entomophilus species while the hydrophilus species produce only a few grains per plant. Reddi [1986] noticed a great individual variation in anemophilus species, with the grains released per anther to be between 32 (*Bothriochloa*) and 89,000 (*Phoenix dactylifera*). Quantities of 10^7 grains per plant are typical in *Zea mays*, while *Vallisneria* produces 72 to 144 grains per plant. Table 2.4 contains information regarding pollen volume production for several different species on an annual and 50-year basis. In a more detailed approach, Molina et al. [1996] determined the number of pollen grains produced at the branch, tree or crown level for different anemophilus species. However, when modeling vegetation as a source of pollen, the chief interest concerns the number of grains produced per area unit. Understanding the temporal component of the pollen flux is equally important. In previous attempts to calculate the amount of pollen released from a specified area, the numbers tended to be overestimated at the beginning and end of the season since the variations in flowering time within the area of interest were not taken into account [Kawashima and Takahashi, 1999]. Bringing these components together results in the concept of the spatiotemporal flowering map, which is consisted of the land use/land cover database along with a pollen release module that describes the availability of pollen particles. More information on the development and restrictions of this map, along with the related datasets will be provided in the following chapters.

2.2.2   Fate and transport of allergenic pollen grains

The effects of meteorological factors on atmospheric bioaerosol levels have been discussed in several publications [Aylor, 1999; Aylor and Irwin, 1999; Jones and Harrison, 2004; Li and Kendrick, 1994]. Major points from these reviews include the following facts regarding pollen:

- they are of irregular shape and diameter [Gregory, 1973; Stanley and Linskens, 1974];

- they can hydrate and dehydrate [Aylor, 2002, 2003];

- they may build up aggregates (entomophilous species have a pollen kit on their surface [Keijzer, 1987b]);

- they have different densities and settling velocities [Jarosz et al., 2003];

- they have species-specific, limited, and mostly unknown viability [Aylor, 2004];

- the concentration thresholds that cause allergic symptoms at the exposure endpoint depend on the species [Reponen et al., 2001].

Pollen occurs in a number of shapes, mostly variations of spheres with a geometry determined to some extent by the number and position of the germinal apertures. The pollen of certain conifer trees contains an air sac resulting in a low density particle, which will behave like a smaller higher density one [Jones and Harrison, 2004]. The size of pollen is related to the following list of factors [Stanley and Linskens, 1974] : (1) chromosome numbers, (2) heteranthery[2], (3) temperature, (4) individual flower character, (5) mineral nutrition, (6) water conditions and (7) number of germination pores. The rate at which particles are deposited from the atmosphere by turbulent deposition can be presented in terms of a deposition velocity, which is a function of the aerodynamic diameter [Nicholson, 1988b].

The upper limit of the convective ascent of air during the daytime is given by the thermal inversion over which *cumulus* clouds indicate the position of actual updrafts. The horizontal air speed within this layer for a medium wind is 5-10 m s^{-1}, almost two orders of magnitude greater than the free fall velocity of the grains. According to Stoke's law, a pollen grain of size 25 µmwould have a free fall velocity of 7.5 cm s^{-1}. Assuming a horizontal wind speed of 5 m s^{-1}, the pollen is capable of traveling 67 m when released from a height of 1 m. However, if released from a height of 20 m, it would travel 1333 m. A parameterization methodology of the pollen settling velocity, which is necessary to determine the sedimentation flux, has been discussed in the literature [Aylor, 2002; Helbig et al., 2004]. Deposition of the grains is assumed to be negligible compared to their sedimentation. Coagulation is neglected as well, since the typical atmospheric number densities of the pollen grains are quite low. Particle size will also affect

---

[2]Heteranthery, the production of two or more stamen types by individual flowers reduces this conflict by allowing different stamens to specialize in "pollinating" and "feeding" functions.

the likelihood of entering the atmosphere, depending on the deposition surface characteristics [Reynolds, 2000]. Nicholson [1988a,b] provides an extensive review of the pollen re-suspension processes.

The vertical profile of the wind along with the average height of the vegetation have an important role in the large-scale transport of pollen. The nighttime temperature inversion is accompanied by still air, and after sunrise, the solar heat flux affects the convection currents in the anther microenvironment. Under the influence of such currents, pollen can reach a relatively high altitude. Independent of the pollen species and size, the highest density during field experiments has be found to occur at heights between 250-650 m [Stanley and Linskens, 1974]. In the same experiment, particle sedimentation is noticed when the night-time convection currents are reduced significantly. This return of the pollen grains to the lower air strata at nighttime is demonstrated in ragweed pollen trapping studies [Ogden et al., 1974].

Long distance dispersal of pollen

Long-distance dispersal (LDD) of pollen is important due to several reasons: (1) species expansion following climate change, (2) recolonization of disturbed areas and (3) control of pests. Current knowledge suggests that the frequency and the spatial extent of LDD events are extremely difficult to predict. Researchers agree that mechanistic models coupling seed release and aerodynamics with turbulent transport processes provide accurate probabilistic descriptions of LDD of seeds by the wind [Kuparinen, 2006; Nathan et al., 2002]. Nathan et al. [2002] showed that uplifting above the forest canopy is necessary and sufficient for LDD, setting an upper bound on the probability of long-distance colonization. Most seeds were not uplifted and are predicted to travel only up to several hundred meters, with a modal distance of roughly the canopy height. On the contrary, the few seeds that were uplifted are predicted to travel at least several hundred meters, and perhaps tens of kilometers. This suggests that the pollen escape fraction, or the uplifting probability, or equivalently the frequency of LDD, is predictable from the statistical distributions of seed release height, seed terminal velocity, and turbulent flow at the time of release [Nathan et al., 2002]. Further experiments indicate that foliage shedding from deciduous forests can also significantly increase the uplifting probability of pollen grains [Nathan and Katul, 2005]. Keeping in mind these findings, release height was considered a key

parameter for the dispersion output at coarse spatial resolution (12 km). Results from further investigation will be presented in the relevant aeroallergen modeling implementation section of Chapter 5.

Chapter 2: Figures
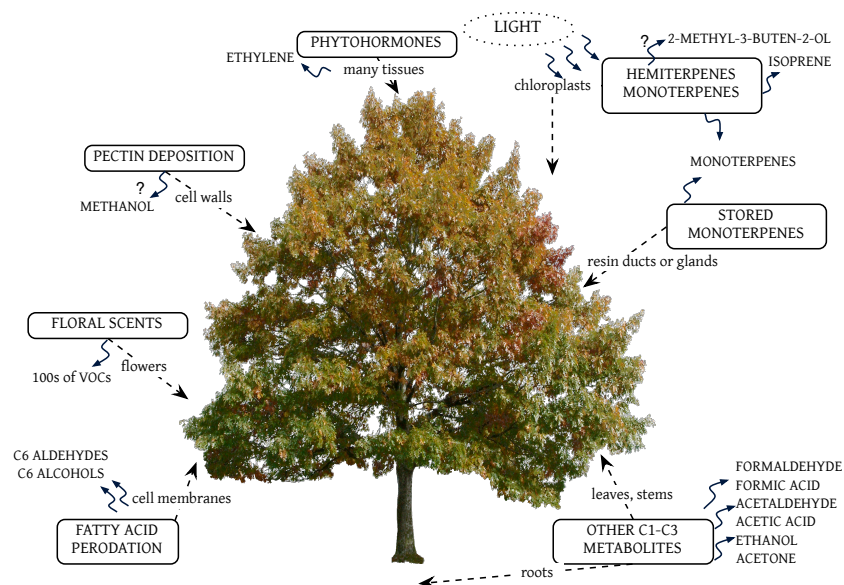
Figure 2.1: Mechanisms and location of production for the major biogenically emitted VOCs. In this scheme a hypothetical tree emits all known major plant VOCs plus floral scents. The probable plant tissues and compartments are indicated. Major uncertainties, indicated by question marks, and the various VOC pathways are discussed in the text [Source: Hewitt, 1999].
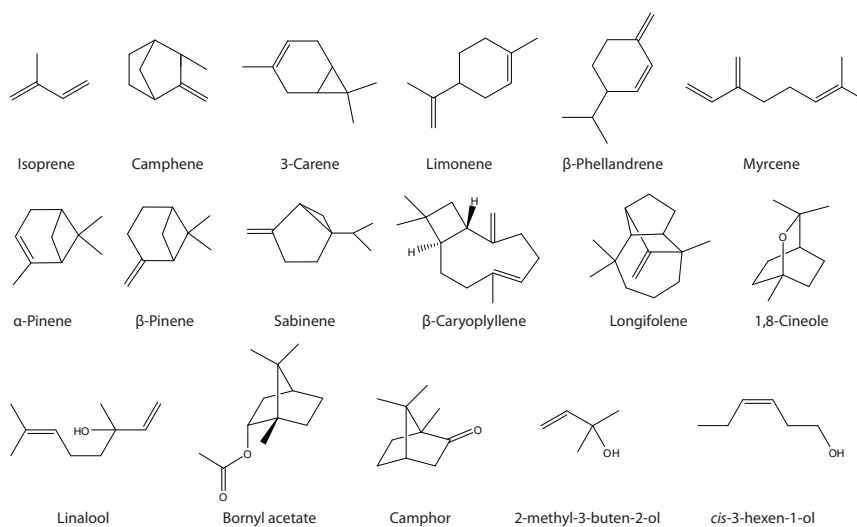
Figure 2.2: Chemical structures of major terpenoids and common oxygen-containing compounds, also considered to belong to this broad biogenic VOC group.
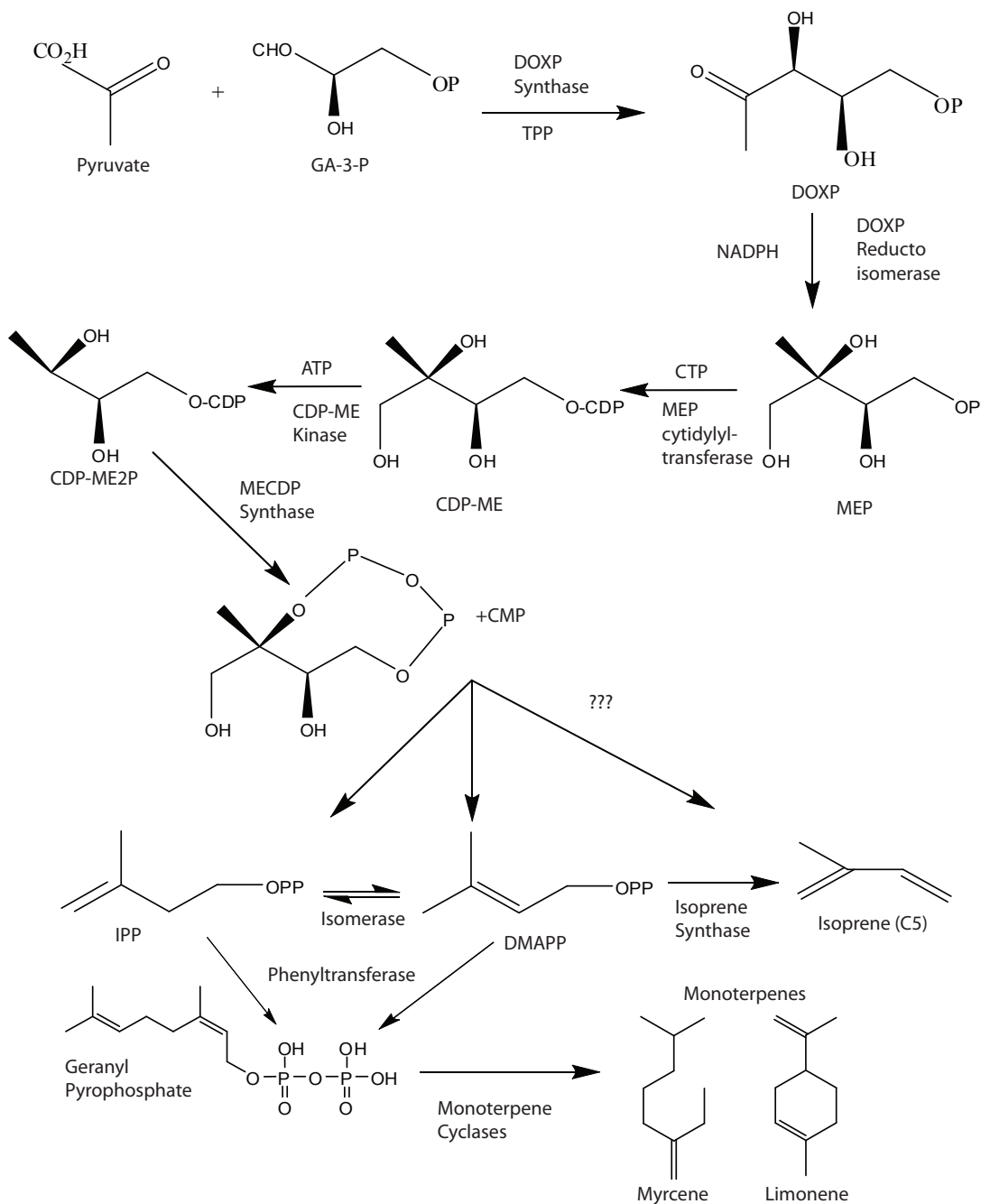
Figure 2.3: The general biosynthetic pathway for isoprene and monoterpene production in plants. Uncertainties in the pathway process are indicated by question marks. [Source: Fuentes et al., 2000].
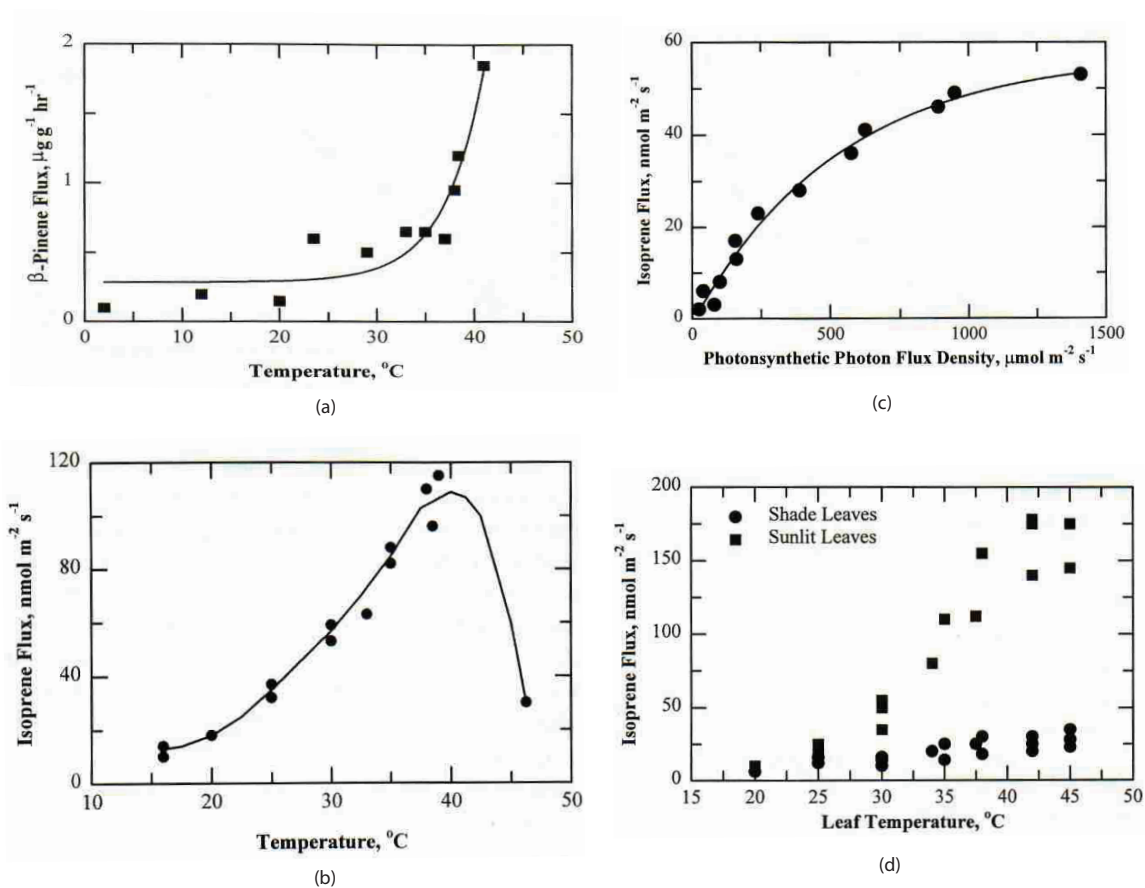
Figure 2.4: Environmental controls on isoprene and monoterpene emission flux [Source: Fuentes et al., 2000; Harley et al., 1996, 1997].
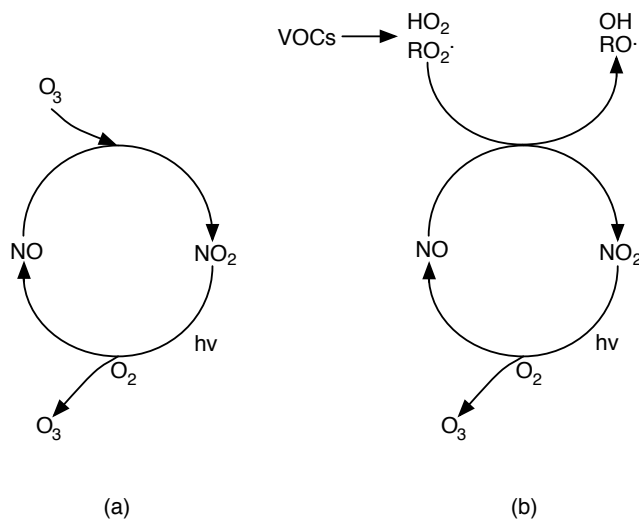
Figure 2.5: Generalized reaction pathway for VOCs in the atmosphere (right) and the NO to NO$_2$conversion in the presence of O$_3$ (left).
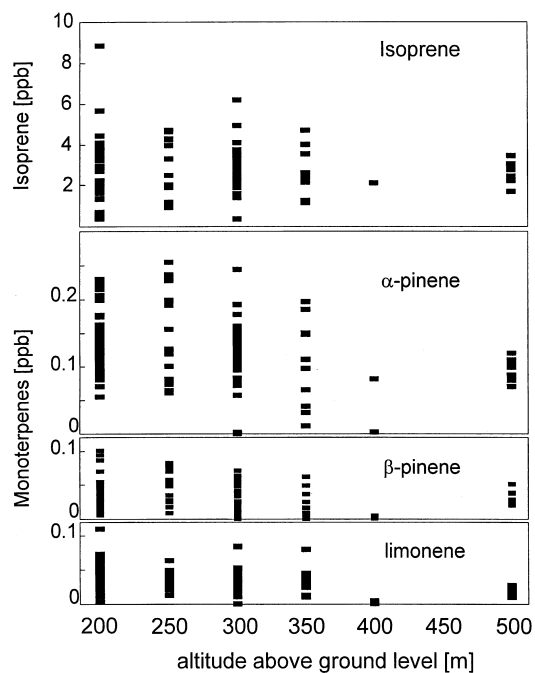
Figure 2.6: Vertical profiles of isoprene and some monoterpenes over a pristine forest in Amazonia [Source: Kesselmeier et al., 2000].
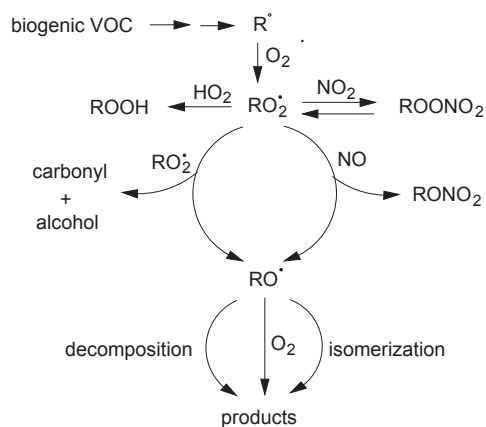
Scheme 1
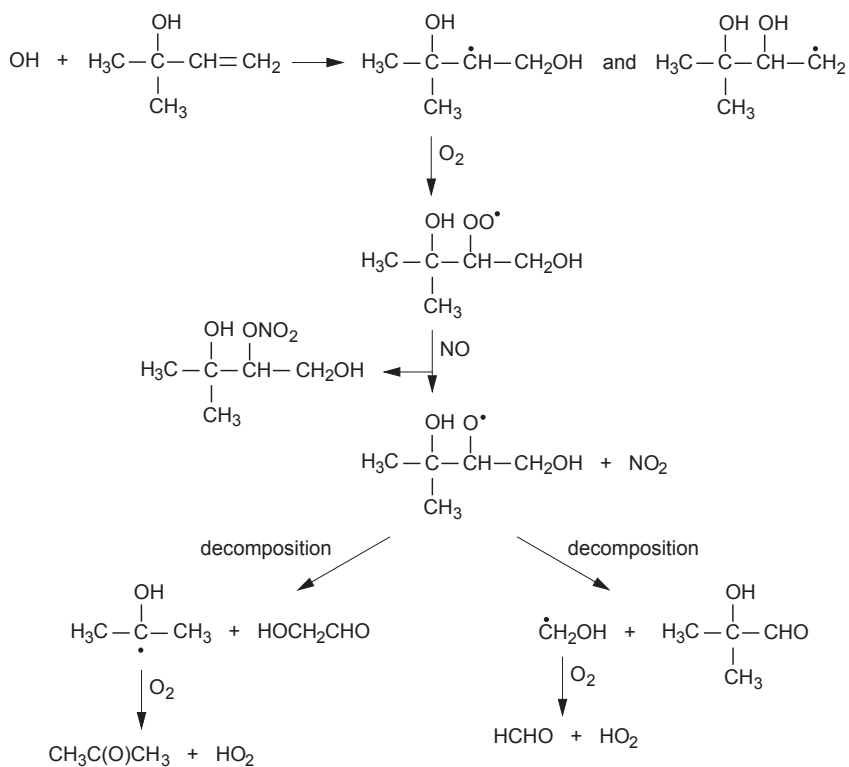
Scheme 2

Figure 2.7: General reaction scheme of alkyl or substituted alkyl radicals (Scheme 1) and details for the OH radical initiated reactions of isoprene followed for one of the six possible hydroxyalkyl radicals (Scheme 2) [Source: Atkinson, 2000; Atkinson and Arey, 2003a,b].
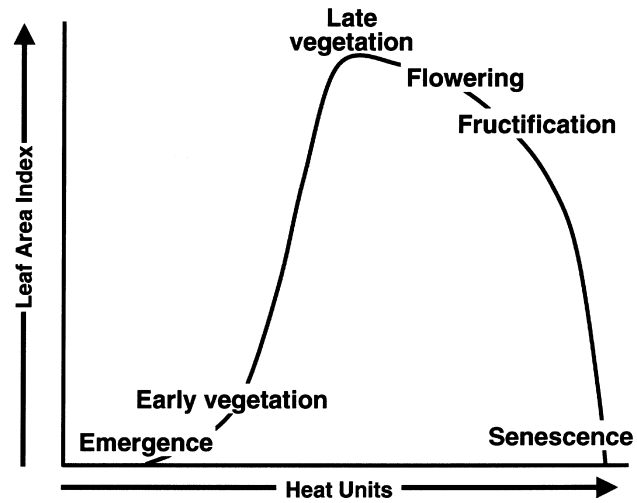
Figure 2.8: Typical representation of the phenological stages in foliage growth of higher plants, as measured by the leaf area index shown as function of accumulated heat units [Source: Gage et al., 1999].

Tables

Table 2.1: Selected biogenic NMVOCs emitted from vegetation and calculated tropospheric lifetimes with respect to Gas-Phase reaction with OH radicals, NO_3 radicals, and O_3.

VOC class	Compound	Chemical Formula	lifetimes for reaction with		
			OH	**NO$_3$**	**O$_3$**
Alkanes	n-butane	C_4H_{10}	5.7 d	2.8 yrs	-
	n-hexane	$CH_3(CH_2)_4CH_3$	4.95 h	10 d	-
	C_{10}-C_{17}alkanes	C_nH_{2n+2} (n=10-17)	-	-	-
Alkenes	Propene	C_3H_6	6.6 h	4.9 d	1.6 d
	Benzene	C_6H_6	12 d	-	-
	Toluene	C_7H_8	2.4 d	1.9 yrs	-
	Isoprene	C_5H_8	1.4 h	1.6 h	1.3 d
	Camphene	$C_{10}H_{16}$ monoterpenes	2.6 h	1.7 h	18 d
	3-carene		1.6 h	7 min	11 h
	Limonene		50 min	5 min	2 h
	Myrcene		40 min	6 min	50 min
	Terpinolene		49 min	7 min	17 min
	b-phellandrene		50 min	8 min	8 h
	α-pinene		2.6 h	11 min	4.6 h
	β-pinene		1.8 h	25 min	1.1 d
	β-ocimene		2.2 h	7.6 min	0.7 h
	Sabinene		1.2 h	7 min	4.6 h
	β-caryophyllene	$C_{15}H_{24}$ sesquiterpenes	40 min	4 min	2 min
	Longifolene		3.0 h	1.6 h	>33 d
Alcohols	methanol	CH_3OH	12 days	1 year	>4.5 yrs
	2-methyl-3-buten-2-ol	see Figure 2.2	2.1 h	8 d	1.7 d
	cis-3-hexen-1-ol		1.3 h	4.1 h	6 h
Continued on next page					

Table 2.1 – continued from previous page

VOC class	Compound	Chemical Formula	OH	NO$_3$	O$_3$
	Linalool		50 min	6 min	55 min
Aldehydes	Formaldehyde	CH$_2$O	1.5 d	80 d	-
	Acetaldehyde	C$_2$H$_4$O	11 h	17 d	-
	n-hexanal	CH$_3$(CH$_2$)$_4$CH$_2$CHO	-	-	-
	trans-2-hexenal	C$_6$H$_{10}$O	-	-	-
Ketones	Acetone	CH$_3$C(O)CH$_3$	66 d	-	-
	6-methyl-5-hepten-2-one	C$_8$H$_{14}$O	55 min	9 min	1.0 h
	Camphor	see Figure 2.2	-	-	-
Ethers	1,8-cineole	see Figure 2.2	1 day	1.5 yr	>4.5 yrs
Esters	3-hexenyl acetate	see Figure 2.2	1.8 h	4.5 h	7 h
	Bornyl acetate	see Figure 2.2	-	-	-
Biogenic	Methyl Vinyl Ketone	-	6.8 h	> 1 yr	3.6 d
Reaction	Methacrolein	-	4.1 h	14 d	15 d
Products	3-methylfuran	-	1.5 h	3 min	19 h
	Pinonaldehyde	-	2.9 h	2.3 d	> 2.3 yrs
	Sabinaketone	-	2.3 days	130 d	> 0.9 yr

Table 2.2: Reaction products of isoprene and yields with respect to Gas-Phase reaction with OH radicals, NO_3 radicals, and O_3.

Product	Yield (percentage)
OH radical reactions	
methyl vinyl ketone + HCHO	32
methacrolein + HCHO	23
3-methylfuran	4-5
$HOCH_2C(CH_3)=CHCHO$ and/or $HOCH_2CH=C(CH_3)CHO$	observed
$CH_2=C(CH_2OH)CHO$	observed
organic nitrates	8-14
NO_3 radical reactions	
methyl vinyl ketone	3.5
methacrolein	3.5
HCHO	11
$O_2NOCH_2C(CH_3)=CHCHO$ and isomers	observed
$O_2NOCH_2C(CH_3)=CHCH_2OH$ and isomers	observed
$O_2NOCH_2C(CH_3)=CHCH_2OOH$ and isomers	observed
Ozone reactions	
methyl vinyl ketone	16
methacrolein	39
HCHO	90
epoxides	5
OH	27
$O(^3P)$	< 10

Table 2.3: Variation in pollen size, volume, and weight [Source: Stanley and Linskens, 1974]

Species	Dimensions in μm)			Volume $(10^{-9}\,\mathrm{cm}^3)$	Weight $(10^{-9}\,\mathrm{g})$
	Length	Width	Height		
Abies alba	97.8	102.9	62.7	499.4	251.6
Abies cephalonica	97.1	98.6	86.2	422.6	212.2
Picea abies	85.8	80.5	66.3	278.2	110.8
Pinus silvestris	41.5	45.9	36.0	35.5	37.0
Larix decidua	76.0	72.0	50.0	180.2	176.3
Pseudotsuga taxifolia	84.8	81.1	54.8	219.2	188.8
Acer saccharum	32.5	23.6	24.6	16.5	6.6
Aesculus hippocastanum	31.0	16.4	18.2	4.8	0.9
Alnus glutinosa	26.4	22.8	13.7	4.4	1.4
Betula verrucosa	10.1	10.1	16.8	2.9	0.8
Fagus silvatica	55.1	40.5	41.1	50.3	26.0
Quercus robur	40.8	26.1	21.5	13.3	5.7
Tilia platyphyllos	40.5	40.1	20.6	15.0	6.5
Ulmus laevis	33.4	32.7	17.7	12.8	6.8
Zea mays	116.3	107.3	107.3	702.4	247.0
Cucurbita pepo	213.8	213.8	213.8	5,117.0	1,068.0

Table 2.4: Seasonal and average lifetime pollen yields per *genus* and *species* [Source: Schopmeyer, 1974]

Genus	Approximate Volume (cm^3)	Species	kg of pollen/tree produced in 50 yrs
Larix	0.3	*Picea abies*	20
Pinus	150	*Fagus sylvatica*	7.6
Pseudotsyga	2	*Pinus sylvestris*	6
Alnus	4	*Corylus avellana*	2.8
Betula	12	*Alnus sp.*	2.5
Fagus	1.3	*Betula verrucosa*	1.7
Liquidambar	25		
Populus	75		
Ulmus	0.3		

Chapter 3

Aggregation of databases and modeling tools to support biogenic emission modeling

The accuracy of meteorological fields is of primary importance in the development and application of air quality modeling systems. In addition to transport, meteorological variables play a major role in determining chemical reaction and mass emission rates, as well as the spatial and temporal distribution of emissions from anthropogenic and biogenic sources. Land Use/Land Cover (LULC) inputs are a critical part of both the meteorological modeling system and the air quality/emissions models. In the absence of synoptic-scale forcing, the role of the land surface is particularly important in driving boundary layer evolution and ultimately precipitation patterns. Inaccurate LULC information often leads to very large errors in surface energy fluxes and thus errors in boundary layer states. Within such models, many land surface variables are commonly defined as a function of LULC via a "lookup table". Variables frequently specified in this way include leaf area index (LAI), fractional vegetation cover, canopy height, emissivity, albedo, surface roughness, rooting depth and parameters related to stomatal resistance. These vegetation-related variables exert significant control on the surface temperature energy balance and subsequently on boundary layer processes and states, most importantly moisture and temperature profiles. The lookup table approach assumes a one-to-one relationship between the surface variable and the LULC category, with no variability represented within a LULC category. In many model applications, seasonal or monthly parameter values are defined, providing an annual cycle of vegetation phenology. In some applications, satellite observations can be used to define a subset of these variables, primarily albedo, LAI and fractional vegetation cover.

3.1 Topography, land cover, and vegetation databases

When considering elevation, LULC, and vegetation data for regional air quality modeling applications, an understanding of the optimal resolutions and formats is necessary. The National Aeronautics and Space Administration (NASA), other U.S. government agencies, and private industry offer a variety of remotely sensed data and LULC products that are relevant to air quality modeling and biogenic emissions. A brief description of the terrain, LULC, and vegetation databases of interest is provided in the following subsections.

3.1.1 Terrain height and digital elevation model data

With respect to meteorological modeling applications, there are six types of terrain height data with geographical resolutions of 1 degree, 30, 10, 5, and 2 minutes, and 30 seconds. The majority of these datasets cover the entire globe (see Table 3.1). The 1-degree and 30-minute data are from PSU/NCAR combined terrain/land-use tapes [Dudhia and Bresch, 2002] and contain land elevation data where the ocean depth is set to be zero. The 5-minute data are from the National Data Center. Both the ocean depth and the land elevation are provided at a vertical resolution of 1 meter. Because of the cavities of 10-minute data in the PSU/NCAR tapes, the 10-minute data are created by a 9-point weighted average method from the 5-minute data. The highest resolution, 30-second terrain height data, is from the Defense Mapping Agency and has a vertical resolution of 1/20 feet. This dataset includes North America as the contiguous United States and a small portion of Canada. GTOPO30[1] is a global digital elevation model (DEM) with a horizontal grid spacing of 30 arc seconds (approximately 1 km) [Systems and USGS, 2002]. GTOPO30 was derived from several raster and vector sources of topographic information [Systems and USGS, 2002]. For easier distribution, GTOPO30 has been divided into tiles which can be selected from an online mapping interface. GTOPO30, completed in late 1996, was developed over a three year period through a collaborative effort led by the U.S. Geological Survey's Center for Earth Resources Observation and Science (EROS) and a variety of collaborating US and foreign agencies and institutes[2].

---

[1]GTOPO30 website: (http://edc.usgs.gov/products/elevation/gtopo30/gtopo30.html)

[2]The following organizations participated by contributing funding or source data: the National Aeronautics and Space Administration (NASA), the United Nations Environment Programme/Global Resource Information Database (UNEP/GRID), the U.S. Agency for International Development (USAID), the Instituto Nacional de

3.1.2 Land Use and Land Cover data

USGS Land Use and Land Cover (LULC) data consists of historical land use and land cover classification data that was based primarily on the manual interpretation of 1970's and 1980's aerial photography [U.S.G.S., 1994]. Secondary sources included land use maps and surveys. Twenty one possible categories of cover type are included in the classification scheme. The LULC files are included along with their associated maps which provide additional information on political units, hydrologic units, census county subdivisions, and Federal and State land ownership. USGS LULC data is available for the conterminous U.S. and Hawaii, but coverage is not complete for all areas. The data is based on 1:100,000- and 1:250,000-scale USGS topographic quadrangles. Files in GIRAS format will have a minimum polygon area of 10 acres (4 hectares) with a minimum width of 660 feet (200 m) for man made features. Non-urban or natural features have a minimum polygon area of 40 acres (16 hectares) with a minimum width of 1320 feet (400 m). Files in CTG format will have a resolution of 30 m. Coarser LULC data can be obtained from PSU/NCAR at resolutions of 1 degree, 30 and 10-minute global datasets. The sources and characteristics of these products are summarized in Table 3.2.

3.1.3 Vegetation characterization databases

A number of vegetation characterization databases have been developed in the recent years for use with general circulation or regional/mesoscale models. In the past decades, the simple biosphere model (SIB) [Sellers et al., 1986] and its revision [Sellers et al., 1996] have been the standard approach applied for global scale modeling. This section describes vegetation products capable of being used with meteorological and air quality models focusing on regional scale applications.

Biogenic Emissions and Landuse Database

The Biogenic Emissions Landuse Database in its latest version (BELD3) offers a classification scheme that incorporates 230 vegetation types, resolved to 1 km [Kinnee et al., 1997]. It is a combinatorial database of the USGS EROS (Earth Resources Observation System) Data Center's 1-km datasets with surveys conducted by various agencies. The EDC data are used for the

---

Estadistica Geografica e Informatica (INEGI) of Mexico, the Geographical Survey Institute (GSI) of Japan, Manaaki Whenua Landcare Research of New Zealand, and the Scientific Committee on Antarctic Research (SCAR)

western US, while other sources such as the US Department of Agriculture's Census of Agriculture and the US Forest Service Eastwide Forest Inventory and Analysis Database (EWDB), are used for the Eastern US [Kinnee et al., 1997; Pierce et al., 1998]. Constructed by the means of a remote sensing model, this database inherits the warning of the parent datasets when used to describe heterogeneous areas. Among its strengths are the number of vegetation species included, and the fact that it uses a combination of county agricultural and forestry data along with remote sensing information [Pierce et al., 2002]. The database was created for estimating emissions of BVOC from vegetation and NO from soil using the standard EPA biogenic and air quality tools included in the Models-3 framework [Pierce et al., 1990]. Its structure includes a lookup table with the emission factors, Leaf Area Index (LAI), biomass density, a summer/winter emission switch, and a leaf correction factor for each vegetation class.

National Land Cover Dataset

The National Land Cover Characterization Project resulted in the development of a nationally consistent land cover data set from Multi-Resolution Land Characterization (MRLC) data called National Land Cover Data (NLCD) [Vogelmann et al., 1998]. In addition to mid-1990s Landsat Thematic Mapper satellite data, a variety of supporting information including topography, census, agricultural statistics, soil characteristics, other land cover maps and wetlands data were used to determine and label the land cover type at a 30 m resolution [Vogelmann et al., 2001]. Twenty-one classes of land cover along with four classes of urban/suburban cover type were mapped, using consistent procedures for the entire U.S. Further information on the remote sensing algorithms and the subsequent accuracy assessment that was performed by USGS can be found in the scientific literature[Vogelmann et al., 2001]. Compared to the BELD3 inventory, the NLCD dataset offers a much finer resolution in exchange for a much broader classification scheme. This dataset is currently being revised based on Landsat Enhanced Thematic Mapper (ETM+) data collected from the early 2000's [Wardlow and Egbert, 2003]. ETM+ is a multi-spectral scanning radiometer that is carried on board of the Landsat 7 satellite. The sensor has provided nearly continuous acquisitions since July 1999, with a 16-day repeat cycle. Among its characteristics, its spatial resolution is 30 m for five visible and one near-infrared bands. The instrument resolution for the panchromatic band is 15 m, and for the thermal infrared band

60 m.

NASA Earth Observing System vegetation products

The NASA Earth Observing System (EOS) provides a variety of platforms and instruments that produce both LULC and vegetation products [Dwyer, 2006]. The MODerate-resolution Imaging Spectroradiometer (MODIS) Land Cover Classification products contain multiple classification schemes describing land cover properties [Cover and Change, 1999; Sulla-Menashe and Friedl, 2007]. The primary land cover scheme (Land Cover Type 1) identifies 17 classes of land cover defined by the International Geosphere-Biosphere Programme (IGBP) which include 11 natural vegetation classes, 3 developed land classes (one of which is a mosaic with natural vegetation), permanent snow or ice, barren or sparsely vegetated, and water. The MOD12 classification schemes are multitemporal classes describing land cover properties as observed during the year (12 months of input data) [Hodges, 2001]. Successive production at quarterly intervals of this "annual" product creates new land cover maps with increasing accuracies as both classification techniques and the training site database mature [Friedl et al., 2002; Myneni et al., 2002]. Additional Science Data Set layers for other classification schemes include the University of Maryland modification of the IGBP scheme (Land Cover Type 2), the MODIS LAI/fPAR (Land Cover Type 3) scheme, the MODIS Net Primary Production (Land Cover Type 4) scheme, and the Plant Functional Types (PFT) (Land Cover Type 5). These were provided to support the Community Land Model (CLM) used in climate modeling. Land Cover Type 5 includes 12 classes, however, only one is an urban class. Four forest and two crop classes are also provided. These data are provided on an annual basis at a 1-km resolution, which are attractive features for use in air quality modeling systems.

The MODIS Global Vegetation Phenology product (MOD12Q2) provides estimates of the timing of vegetation phenology at global scales [Soudani et al., 2008; Zhang et al., 2006]. As such, MOD12Q2 identifies the vegetation growth, maturity, and senescence marking seasonal cycles. The product is produced twice per year using 24 months of data as input (i.e., the 12 months of interest, bracketed by six months on either side) at a 1-km resolution. The first production period highlights July through June, and the second run focuses on January through December. This production schedule accounts for hemispheric differences in the timing

of growing seasons, and enables the product to catch 2 growth cycles if necessary. The 1-km resolution, timely updates, and seasonality features are characteristics that may be beneficial to air quality modeling systems.

3.2 Components of air quality modeling systems for biogenic releases

The current paradigm in the application of air quality modeling systems (AQMS's) in the United States involves their coupling with a mesoscale meteorological model such as the MM5 [Grell et al., 1994] or RAMS [Pielke, 1984]. Including MM5 which is reviewed in the following subsections, this study utilizes a variety of models commonly available for research and regulatory assessment applications: (1) American Meteorological Society/EPA Regulatory Model (AERMOD); (2) HYbrid Single-Particle Lagrangian Integrated Trajectory Model (HYSPLIT), and (3) Models-3 or the Community Multi-scale Air Quality Chemical Transport Model (CMAQ-CTM). A brief description of these models, the meteorological processors and the LULC datasets that they employ is provided in the following sections.

3.2.1 PSU/NCAR Mesoscale meteorological model

The fifth-Generation PSU/NCAR [Dudhia and Bresch, 2002; Grell et al., 1994] MM5[3] system is the most recent in a series of models first developed at Penn State University in the early 1970's [Anthes and Warner, 1978]. Supported by NCAR since its inception, MM5 went through a significant amount of change aimed at broadening its usage. Its use in air quality model applications became common after incorporation of four-dimensional data-assimilation (FDDA) capability. While no further development of MM5 is planned at NCAR, it continues to be the most commonly used meteorological model for air quality applications. As can be seen from the model flowchart (Figure 3.1), MM5 requires a significant amount of geophysical data. These data are interpolated on a user-specified modeling grid through a special processor capable of handling different types of vegetation/LULC and soil datasets (TERRAIN). The output file generated by the processor contains grid-cell average surface elevation, fractional and dominant

---

[3]MM5 website: (http://www.mmm.ucar.edu/mm5/)

LULC, fractional vegetation, and soil type. Physical parameters (e.g., albedo[4], surface roughness length[5], moisture availability, emissivity, thermal inertia) for each vegetation/LULC category are defined within the Land Surface Model (LSM). In an MM5 model run without LSM, the physical parameters are assigned with the help of a look-up table (Table 3.3).

3.2.2 AMS/EPA Regulatory Model

AERMOD[6] is a steady-state dispersion modeling system developed by U.S. EPA for estimating near-field (50-km or less) impacts from surface and elevated sources [Cimorelli et al., 2005; Perry et al., 2005]. The model flowchart (Figure 3.2) shows an integrated system that includes three modules [Prater and Midgley, 2006]:

- A steady-state dispersion model designed for short-range (up to 50 kilometers) dispersion of air pollutant emissions from stationary industrial sources ;

- A meteorological data preprocessor (AERMET) that accepts surface meteorological data, upper air soundings, and optionally data from on-site instrument towers. It then calculates atmospheric parameters needed by the dispersion model;

- A terrain preprocessor (AERMAP) whose main purpose is to provide a physical relationship between terrain features and the behavior of air pollution plumes.

AERMET, the meteorological preprocessor, calculates and provides parameters such as the modified Bowen ratio[7], surface roughness length, surface friction velocity, convective scaling velocity, surface heat flux, and convective and mechanical mixed layer heights to describe the

---

[4]Albedo is a term derived from the Latin word *Albus* meaning "white", is a measure of reflectivity of a surface. Typical values ranges from about 0.1 for water to 0.6 or higher for full snow cover, while most land areas are in an albedo range of 0.1 to 0.4

[5]Roughness length is a parameter which is a measure of terrain roughness as "seen by" surface wind. It is formally the height (in meters) at which the wind speed becomes zero when the logarithmic wind profile above the roughness sub-layer is extrapolated to zero wind speed. In fact, the roughness length lies within the roughness sub-layer, where the wind speed deviates from the logarithmic wind profile. This parameter represents the bulk effect of roughness elements in the surface layer and very approximately has a value of around 0.1 times the height of the roughness elements.

[6]AERMOD website: (http://www.epa.gov/scram001/dispersion_prefrec.htm#aermod)

[7]The modified Bowen-ratio (MBR) technique is a micrometeorological method that can be used to estimate air-surface exchange rates, providing differences in concentrations between two heights can be resolved. Application of the MBR method requires that fluxes and gradients for at least one scalar entity be measured in order to directly compute the exchange coefficient k, which is assumed to be applicable for all scalars.

AERMOD Planetary Boundary Layer (PBL) . AERMOD uses the computed PBL parameters to generate vertical profiles of needed meteorological variables. AERMET requires meteorological observations and LULC-related surface properties, preferably at the source location (Figure 3.2). Observations include morning upper air sounding, either a single surface measurement of wind speed, wind direction, temperature, and cloud cover, or two measurements of temperature (at 1.5 and 10 m), together with a single measurement of solar radiation. Surface properties required by AERMET are surface roughness length, Bowen ratio[8], and albedo. Appropriate values of these variables are a function of eight LULC categories (Water, Deciduous Forest, Coniferous Forest, Swamp, Cultivated Land, Grassland, Urban, and Desert Shrub Land), four seasons (Spring, Summer, Autumn, and Winter) and surface moisture (dry, wet and average moisture) are provided in the AERMET user manual (Tables 3.4 - 3.6). The precise characteristics of the eight LULC categories, seasons and surface moisture conditions have not been defined in the manual. Generally, users specify these values based on LULC properties surrounding the closest National Weather Service (NWS) station. Finally, AERMAP generates location and height data for each receptor location. It also provides information that allows the dispersion model to simulate the effects of air flowing over hills or splitting to flow around hills.

3.2.3 Hybrid Single-Particle Lagrangian Integrated Trajectory Model

The National Oceanic and Atmospheric Administration (NOAA) and Air Resources Laboratory (ARL) developed HYSPLIT4 [Draxler and Hess, 1998], which is used in this project. The HYSPLIT4 model[9] is a system for modeling trajectories, dispersion, and deposition of pollutants that has been under development since 1982. Demonstrated in the flowchart (Figure 3.3), this model uses gridded model output or a series of gridded analyses, such as Eta Data Analysis Systems (EDAS), or output of a forecast model such as MM5/PSU, Eta, and others. The model uses a hybrid between the Eulerian and Lagrangian coordinates to calculate trajectories and dispersion of air parcels. Particle advection and diffusion calculations are performed in a Lagrangian framework, while concentrations are calculated on a fixed grid. Air concentration

---

[8]A Bowen ratio is the ratio of energy fluxes from one medium to another by sensible and latent heating respectively. It is used to determine how much solar heating goes to evaporation of surface moisture and typical values range from about 0.1 (very wet) to 10 (very dry.

[9]HYSPLIT website: (http://www.arl.noaa.gov/ready/hysplit4.html)

calculations associate the mass of airborne particulates with the release of puffs, particles, or a combination of both which can be specified by the user. The dispersion rate is calculated from the vertical diffusivity profile, wind shear, and horizontal deformation of the wind field. Air concentrations are calculated at a specific grid point for puffs and as cell-average concentrations for particles [Draxler and Hess, 1998]. One of three assumptions can be used for the case of computing air concentrations along the parcels trajectory: a puff model, a particle model, and a combination of puff and particle model (called PARTPUF). Other options in HYSPLIT4 allow for gravitational settling, wet and dry deposition, and re-suspension of the pollutants [Draxler and Hess, 1998]. The introduction of a half-life term can be a very useful tool for connecting the pollen viability parameter with a decay rate due to the oxidative properties of the atmosphere. These options give further flexibility to this model to replicate realistic conditions. The accuracy of trajectories has been tested in large-scale experiments, where overall results indicated that no significant differences were seen when compared with the meteorological data sets, with the average error rate in the 20% to 30% range [Draxler et al., 1991].

3.2.4 Community Multi-scale Air Quality Chemical Transport Model

CMAQ-CTM is a component of Models-3 air quality modeling system [Byun and Schere, 2006; Byun and Ching, 1999; Dennis et al., 1996], with state-of-the-science parameterizations of atmospheric processes affecting transport, transformation, and deposition of such pollutants as ozone, particulate matter, airborne toxics, mercury, and acidic and nutrient pollutant species. It is being extensively used for air quality forecasting and emission control strategy development. The model was developed by the Atmospheric Modeling Division of U.S. EPA based in Research Triangle Park, NC, in collaboration with various groups. It was first released to the public in 1998. Support from the U.S. EPA and active participation of the scientific community has facilitated its continued development. The CMAQ-CTM modeling system is currently being maintained by the Center for Environmental Modeling for Policy Development (CEMPD)[10] at the University of North Carolina at Chapel Hill.

CMAQ is an Eulerian air quality model, and solves the discretized form of the Advection-Diffusion Equation (Figure 3.4). Meteorological fields for CMAQ are generally obtained from

---

[10]CEMPD website: (http://cf.unc.edu/cep/empd/index.cfm)

dynamical data assimilating meteorological models (also referred to as mesoscale models). A processor called MCIP (Meteorology Chemistry Interface Processor) [Otte, 2004] is used to create input files for CMAQ. Its main function is to read in meteorological fields simulated by a mesoscale model, compute dry deposition velocities and other variables that CMAQ needs but are not available from the meteorological model, and output data in Models-3 Input/Output Applications Programming Interface (IOAPI) format. Currently, MCIP is capable of processing meteorological fields simulated by PSU/NCAR MM5 [Dudhia and Bresch, 2002; Grell et al., 1994].

3.3   Biogenic VOC emissions algorithms and models

The development of biogenic emission estimates for air quality modeling in the United States received special attention in the late 70's with the release of the first VOC emission factors from Zimmerman's Tampa Bay study in 1979 [Zimmerman, 1979b]. The most detailed modeling scheme has been developed by Guenther et al. [1993] and subsequent improvements have been implemented in later versions of the BEIS and other models. This set of emission models for isoprene, monoterpenes, and other VOCs have been commonly used in the scientific community and are supported by several studies [Lehning et al., 2001; Petron et al., 2001; Pier and McDuffie, 1997; Street et al., 1996; Wang and Shallcross, 2000]. An example of a finer resolution application of Guenther's algorithm is reported in the study of Wiedinmyer et al. [2001] for the State of Texas, USA. The detailed formulation of Guenther's algorithm has been covered extensively in literature and is provided in Appendix A for both the BEIS[11] [Pierce, 2001] and the revised Guenther's version [Guenther et al., 2000]. In the following section, one can find brief description of the individual BVOC models that incorporate Guenther's algorithm along with some key characteristics that have been improved over time. A complete listing and comparison of BEIS with the rest of the models is summarized in Table 3.7.

---

[11]Biogenic Emissions Inventory System website: http://www.epa.gov/asmdnerl/biogen.html

3.3.1 BEIS3 (Authors: Vukovich/Pierce)

The BEIS (Biogenic Emissions Inventory System) [Pierce and Waldruff, 1991; Pierce, 2001; Pierce et al., 1990; Schwede et al., 2005] is a computer algorithm used widely to generate emissions for air quality simulation models such as EPA's CMAQ/Models-3 and the Regional Acid Deposition Model (RADM). The model's framework is presented in Figure 3.5. The FORTRAN code is publicly available through the EPA's website. BEIS was introduced in 1988 to estimate VOC emissions from vegetation and NO emissions from soils. Since 2001, BEIS3.09 is the default version in SMOKE (Sparse Matrix Operator Kernel Emissions) that is capable of generating emission inventories for four species (Isoprene, monoterpenes, Other VOCs or OVOC and NO). BEIS3.13 is the latest research version capable of estimating spatially and temporally resolved emissions of the following:

- Isoprene, monoterpenes, oxygenated and other volatile organic compounds for a total of 34 species, including 14 monoterpenes and methanol;

- Carbon monoxide (CO) induced by photochemical transformation on or in vegetative species; and

- Biogenic nitric oxide (BNO) due to microbial, predominantly from the genera *pseudomonas* and *bacillus*, denitrification processes in soils.

In BEIS Pierce [2001] uses a slightly modified form of the Guenther et al. [1993] formulations to estimate isoprene emissions based on leaf temperature and photosynthetically active radiation (PAR) fluxes. The light correction factor $\gamma_p = C_L$ follows the same formula (Equation A-29), with improvements on the empirical coefficients α and C_{L1} suggested by Harley et al. [1996, 1997], who showed that they will vary with past PAR levels experienced by the leaf. Incorporation of these additional extensions results in a light correction factor of about one for the top of the canopy, to less than 0.30 for a leaf in the bottom of it while keeping PAR equal [Guenther et al., 1999b]. Because these extensions are missing from the previous versions of BEIS, it is likely that the newest implementation slightly overestimates the isoprene emissions, though no study has been conducted to examine this issue. BEIS uses a big-leaf canopy model rather than

a multilayer model that includes a simple sunlit/shaded solar radiation model (Equations A-3 - A-28). A recent review of the updated BEIS3.13 model comparing a multilayer against one that utilizes uniform vertical LAI profiles, found comparable results in the calculations of the affected PAR adjustment factor [Schwede et al., 2005]. Since version 3.11 the model comes with a revised BNO algorithm (Equations A-35 - A-37) to better distinguish between agricultural and non-agricultural land, and to limit adjustments from temperature, precipitation, fertilizer application and crop canopy to the growing season and to areas of agriculture [Williams et al., 1992]. Finally, BEIS3 output can be directly linked with the CMAQ model, while previous versions were being used with RADM (Regional Acid Deposition Model), UAM (Urban Airshed Model) and ROM (Regional Oxidant Model). The Package for Analysis and Visualization of Environmental data (PAVE) is the main tool that has been used for the visualization of the model's results.

3.3.2 GloBEIS2 (Authors: Yarwood/Estes)

The Global Biosphere Emissions and Interactions System (GloBEIS) was developed by NCAR and ENVIRON International Corporation under funding from the Texas Natural Resources Conservation Commission (TNRCC) [Yarwood et al., 1999, 2002]. It is written in Microsoft Access and is fully menu-driven. The code allows users to estimate biogenic emissions of volatile organic compounds, carbon monoxide, and soil NO_x. It includes several isoprene algorithms: BEIS2, BEIS2 with leaf angle correction for estimating PAR, and BEIS99. This option gives the ability to compare different emission factor algorithms (BEIS2, GloBEIS3) in the same model. The model's emission algorithm reflects the method proposed by Guenther et al. [1995, 1993]. Seasonal adjustment of VOC is available as an option in GloBEIS. The model's input is comprised of the domain definition and the land cover/vegetation data, while PAR is calculated externally. Sesquiterpene emissions and secondary aerosol formation have been incorporated for a case study of Southeast Texas [Vizuete et al., 2004]. The canopy can be resolved in a number of layers ranging from 2 to 99. The set of visualization/output capabilities is limited within the Microsoft Access environment. Finally, there is no option for direct output to certain photochemical models such as the SMOKE/CMAQ.

3.3.3 BIOME3 (Authors: Janssen/Wilkinson)

The third generation Biogenic Model for Emissions (BIOME3) is developed by LADCO and Alpine Geophysics. Sensitivity analyses have been conducted to determine the impacts to biogenic emissions predictions over the Midwest United States [Wilkinson and Janssen, 2001]. BIOME3 includes a revised canopy model as well as a revised algorithm to estimate isoprene emissions; however, the monoterpene, oxygenated VOCs, and biogenic nitric oxide formulations remain unchanged. BIOME3 is an equilibrium terrestrial biosphere model that has been implemented globally using a minimal set of just five woody and two grass plant types. The code is written in the SAS environment. In BIOME3, leaf area is expressed as leaf area index (LAI). A small number of ecophysiological constraints are used to select the plant types that may be present in a particular climate. The model then calculates a maximum sustainable LAI and net primary productivity (NPP) for each plant type.

BIOME3 contains the revised isoprene emissions algorithm based on the work of Guenther et al. [1995, 2000, 1993]. Three sets of factors are available within BIOME3: the previous BEIS2 bare factors, additional MEOH (methanol) and MBO (2-methyl-3-butenol) factors, and a new alternative scheme for 34 explicit species. The second improvement is the inclusion of the BEIS3 canopy model as derived from GloBEIS [Yarwood et al., 1999, 2002]. Unlike the BEIS2 formulation which had only a five-type, fixed-canopy model based on forest type (e.g. pine, coniferous, deciduous), the new canopy model is more general and more rigorous in its treatment of energy transfer through a leaf canopy. Leaf-level estimates of temperature and photosynthetically active radiation (PAR) are required in the biogenic isoprene emissions algorithms. In BIOME3, the revised version of the BEIS leaf energy balance is used to adjust PAR levels for sun and shaded leaves as a function of height in the canopy [Guenther et al., 2000]. The third key characteristic of BIOME3 is the inclusion of a user-specified "isoprene ratio" which is a global adjustment factor. In GloBEIS, this value is set to 1.43 which is close to the ratio of isoprene rates determined from cuvette measurements versus leaf enclosure measurements. Guenther suggests using a value of the range between 1.0 and 1.4, although the exact reasoning is not well documented. Model output consists of a quantitative vegetation state description in terms of the dominant plant type, secondary plant types present and the total LAI and NPP for the ecosystem. As in BIOME2, this basic model output is classified

into biomes for comparison with vegetation maps. Output comes as a day specific emissions estimate. These emission estimates can then be speciated and converted to the appropriate format for use with the UAMV/CAMX models, using the available post-processor that comes with BEIS. Additionally, the post-processor can be used to convert those files into IOAPI files for use in CMAQ and Models3.

3.3.4 BEIGIS (Authors: Scott/Benjamin)

The Biogenic Emission Inventory Geographic Information System (BEIGIS) is a spatially and temporally resolved biogenic hydrocarbon emissions inventory model developed by the California Air Resources Board (CARB) [Scott and Benjamin, 2003]. BEIGIS is a model developed specifically for the State of California and is structured in such way that allows for incorporation of best available California-specific data. It is the only model that is structured with a geodatabase procedure (like the Environmental Systems Research Institute's ArcGIS) in mind. A very detailed model description and the accompanying results from the California study are available in scientific literature [Scott and Benjamin, 2003]. Land use and land cover data were derived from special field studies, the GAP database, and county agricultural offices. The leaf mass database (or Leaf Area Index-LAI) is derived from satellite data. BEIGIS simulates hourly emissions for three species: isoprene, monoterpenes, and MBO (2-methyl-3-butenol) at a 1x1 km resolution. Emission factors are based on UCLA estimates [Benjamin and Winer, 1998; Karlik and Winer, 2001; Winer et al., 1983, 1992]. Since those factors used are branch emissions factors (as opposed to leaf factors used by the previous models), the canopy light extinction is not taken into account in this model. PAR is generated from observed solar radiation data. Similarly to BEIS, the BEIGIS model assumes that 42% of the total solar radiation belongs to the PAR range. Leaf temperatures can be obtained from the first layer of a mesoscale meteorological model such as the MM5 (surface layer height 30m).

3.3.5 Environmental variables of interest in modeling BVOC emissions

The environmental adjustment factors are clearly the backbone of biogenic VOC modeling. As mentioned before for the case of BEIS, improvements have been implemented for the empirical coefficients α and C_{L1} that determine the light adjustment factor (Equation A-29) for

isoprene according to Harley et al. [1996, 1997]. The region has nearly constant C_L at PAR values exceeding what would be found during daytime mostly cloudy conditions (*i.e.*, PAR >1000 μmol m^{-2} s^{-1} or total radiation flux [I] of about 435 W m^{-2}). When compared to the previous versions, it is likely that the newest implementation slightly overestimates the isoprene emissions. The canopy model in BEIS is based on a leaf energy balance and knowledge of the LAI. Campbell and Norman [1998] developed an empirical relationship for sunlit and shaded leaves that requires the calculation of the amount of PAR reaching them, depending on the position of the sun (Equation A-3). Pierce [2001] computes the solar zenith angle from equation A-7 that requires the calculation of the parameter δ_s based on equation A-10, which describes the earth's declination to the solar plane [Duffie and Beckman, 1980]. Although this formulation takes into account the time of the day, it ignores the the day of the year, treating radiation reaching the earth as if every day were the summer solstice in the northern hemisphere. By excluding the effect of the day of the year, BEIS will overestimate the amount of radiation reaching the canopy, resulting in a overestimate of the isoprene emissions. Though the overestimate will be small for most of the summer, it will be noticeably large during warm winter days [Russell et al., 2001]. In the past, the most popular way to estimate PAR for use in the emissions model was the application of the meteorological input preprocessor for BEIS. Currently, there are several approaches for estimating the photosynthetically active radiation (PAR):

- EPA's Biogenic Emissions Inventory System (BEIS) preprocessor calculates PAR based on cloud cover and pressure;

- surface observations from the SURFRAD[12] network;

- using the Community Multiscale Air Quality (CMAQ/MCIP) code;

- using shortwave downward radiation calculated by the PSU/NCAR mesoscale atmospheric circulation model MM5.

The BEIS preprocessor calculates PAR based on the angle of the sun, time of the day, atmospheric pressure, and horizontal cloud fraction. A limitation of BEIS is that it does not take

---

[12]SURFRAD monitoring network is a part of NOAA's Earth System Research Laboratory (Global Monitoring Division) and U.S. Department of Commerce (http://www.srrb.noaa.gov/surfrad/)

into consideration the vertical cloud position. More recent methods include the application of a conversion factor applied to the short-wave downward radiation calculated by a meteorological model and use of satellite PAR data. The advantage of this approach is that the attenuating effects of the clouds have already been accounted for in the the meteorological model (MM5). Baker et al. [2001] published a preliminary comparison of the different approaches for the Ozark Isoprene Experiment (OZIE) regional photochemical episode on July 18th of 1998. The results of this study indicate that the MM5 methodology produces values which best match both satellite and ground-based observations. The CMAQ/MCIP code appears to generate unrealistically high values of PAR (daily maxima greater than $500\,\mathrm{W\,m^{-2}}$). The ability to use layer 1 (surface layer, ranging 2-30 m depending on the project) MM5 calculated temperatures, supports the idea of coupling MM5 with the emissions model described above. In addition, a surface radiation monitoring network, SURFRAD, provides surface measurements of PAR for 8 locations of the U.S. at 3-minute intervals. Satellite data may also be a useful tool for capturing the spatial characteristics of PAR [Van Laake and Sanchez-Azofeifa, 2005]. Due to their limited temporal availability, they are mainly applied to assure the quality of meteorological model estimates of cloud cover.

Though Pierce [2001] accounts for canopy attenuation of PAR in his formulations, there is still some debate in the literature about how to account for canopy effects not only for PAR, but also for temperature. Lamb and Coordinating Research [1999] summarize the issues surrounding the debate, pointing to the well-known discrepancies that exist between the higher measured leaf-level isoprene emissions and the lower measured above-canopy levels. Even with the application of isoprene canopy escape efficiency, coupled with a canopy attenuation model [Goudriaan and van Laar, 1994], in a modified version of GloBEIS [Yarwood et al., 2002], that is more rigorous than that used by Pierce [2001], Guenther et al. [1999a,b] calculated a difference between the two of the order of 5%. Incorporating such a model could be critical when dealing with forested areas with dense and high canopy. In addition, canopy adjusted temperature will also affect the total monoterpene emissions. However, our knowledge of canopy effects is still incomplete and requires further investigation so that these effects can be modeled in an improved way.

Several scientific groups (EPA/OAQPS, IL EPA, MCNC, and LADCO) have conducted various tests to assess the sensitivity of air quality model results to biogenic inputs. The conclusions

of these studies can be used as key-characteristics for establishing the current biogenic modeling framework:

- BIOME3 takes a full advantage of the PAR output from MM5;

- A multi-layer canopy model may have insignificant effects (difference of 5%) in national scale studies, but can be important for regional assessments;

- BEIS2 to BEIS3 comparison showed increased values on the order of 5 ppb or more, and model to monitor comparisons showed better agreement when using BEIS3;

- The model's uncertainties are associated with emission factors that need continued updating, and land cover/vegetation data that are of limited resolution;

- Only few biogenic models provided output for use with certain photochemical models;

- BEIGIS is the only example that used high-resolution data and provided output through a Geographical Information System (ArcGIS).

3.4 Models for the pollen release and dispersal

The dispersal of seeds is directly connected to the ability of a population to spread, invade, and migrate, whereas genetic information is transmitted by pollen flow. This way many plant diseases are also dispersed along with the pollen particles. Kuparinen [2006] reviews several types of models that have been developed for modeling airborne particle dispersion. The author lists these models in four categories in increasing order of complexity:

- The simplest dispersal models are used as sub-models in models describing a larger process, such as in a spatially explicit metapopulation model. They are based on a simplified and computationally easy description of the shape of the particle dispersal pattern with only a few model parameters;

- Empirical models with varying numbers of model parameters have been used for modeling observed dispersal patterns. The parameters of the traditional empirical dispersal models are shape parameters of the mathematical curves, describing for example, the density of the tail of the dispersal pattern;

- Quasi-mechanistic models have been recently developed for pollen applications. These models have descriptive parameters that are estimated by statistical methods from dispersal data;

- Fully mechanistic models incorporate the description of the physical factors affecting particle dispersal and are able to predict the dispersal process based on measurements of the environmental conditions during the dispersal period.

The development of realistic emission inventories is a very important area in all cases of dispersion modeling, including the release of pollen particles. One problem arises from the fact that currently no detailed maps of the spatial distribution of the relevant plants are available. As described in the previous chapter, the emission of pollen particles is determined by several factors. Phenological observations indicate that pollen emissions depend on the start and the intensity of the flowering season. Modeling the state of vegetation over time and space scales of our interest can be an extremely uncertainty-bound task. For example, it is well known that the birch pollen flowering shows inter-annual variations [Clot, 2001; Estrella et al., 2006], and long-term trends [Dose and Menzel, 2004; Rousi and Heinonen, 2007; Schleip et al., 2006]. The emission of pollen depends on meteorological variables, such as temperature, wind gusts and longer-term temperature and drought stresses [Mullins and Emberlin, 1997; Puls, 1987; Rempe, 1938]. Helbig et al. [2004] proposed a parameterization that was modified for the needs of this and takes into account these individual factors. The authors applied their parameterization to an isolated field in the Rhine Valley, Germany showing that pollen grains can travel large distances, especially in inhomogeneous terrain where secondary circulation systems are generating vertical velocities substantially greater than zero. In the relevant pollen modeling section significant attention will be paid to the numerous issues faced in such pollen studies, along with the fact that the lack of observational data does not allow for any comparison with real-time results.

3.4.1 Phenological modeling applications

There are several semi-empirical models for predicting the start and duration of the flowering season at the species-level. Descriptions of the flowering start time are based on three main principles:

- climatological averaging of long-term observations;

- heat sums, such as the growing degree-days, and period units;

- dynamic models (*i.e.* promoter-inhibitor model of Schaber and Badeck [2003]

The estimates based on climatological averages are not suitable for performing dynamical short-term simulations, in which conditions can be substantially different from climatic averages [Adams-Groom et al., 2002; Emberlin et al., 2002]. However, the climate-based values are available or can be easily developed for the entire U.S., while the other methods mentioned above are usually based on local or, at best state-wide observations. Therefore, their application for the case of nation-wide modeling is a difficult task. The description of other parameters of flowering such as its intensity and the total amount of released pollen also require the use of semi-empirical models that predict the next-year flowering features, based on conditions of the previous growing season [Masaka and Maguchi, 2001; Ranta et al., 2005].

Chapter 3: Figures
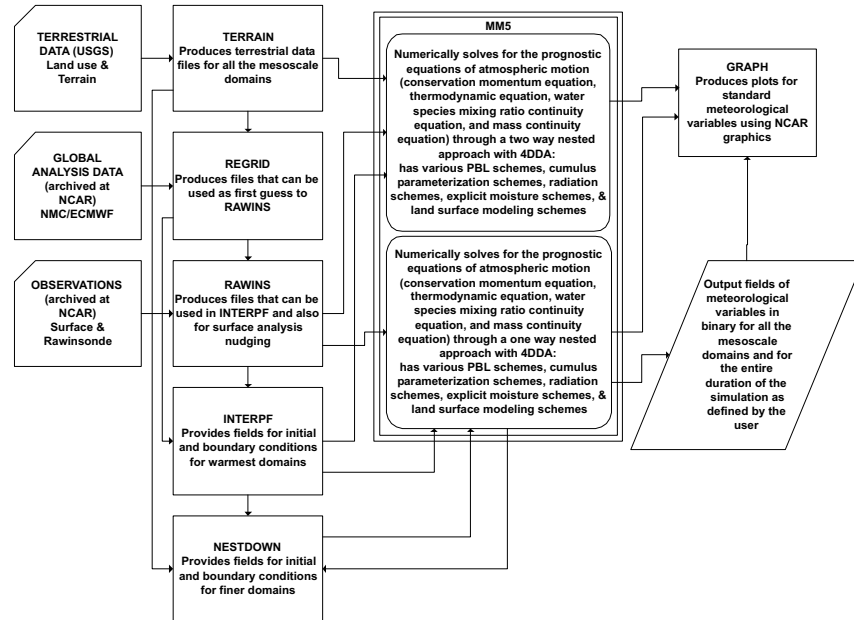
Figure 3.1: Schematic flowchart of the 5th Generation Meteorological Model (MM5) [Source: Dudhia and Bresch, 2002].
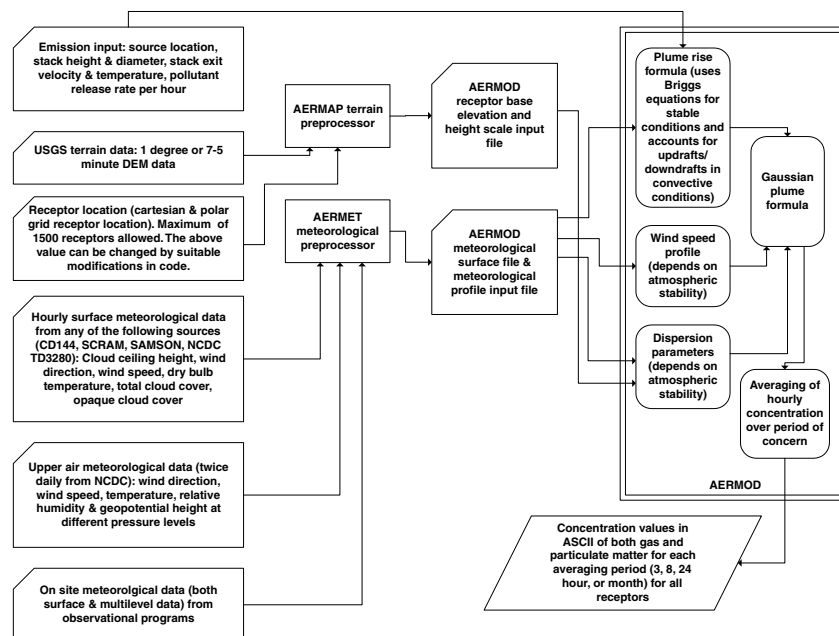
Figure 3.2: Schematic flowchart of the AMS-EPA Regulatory Model (AERMOD)[Source: Prater and Midgley, 2006].
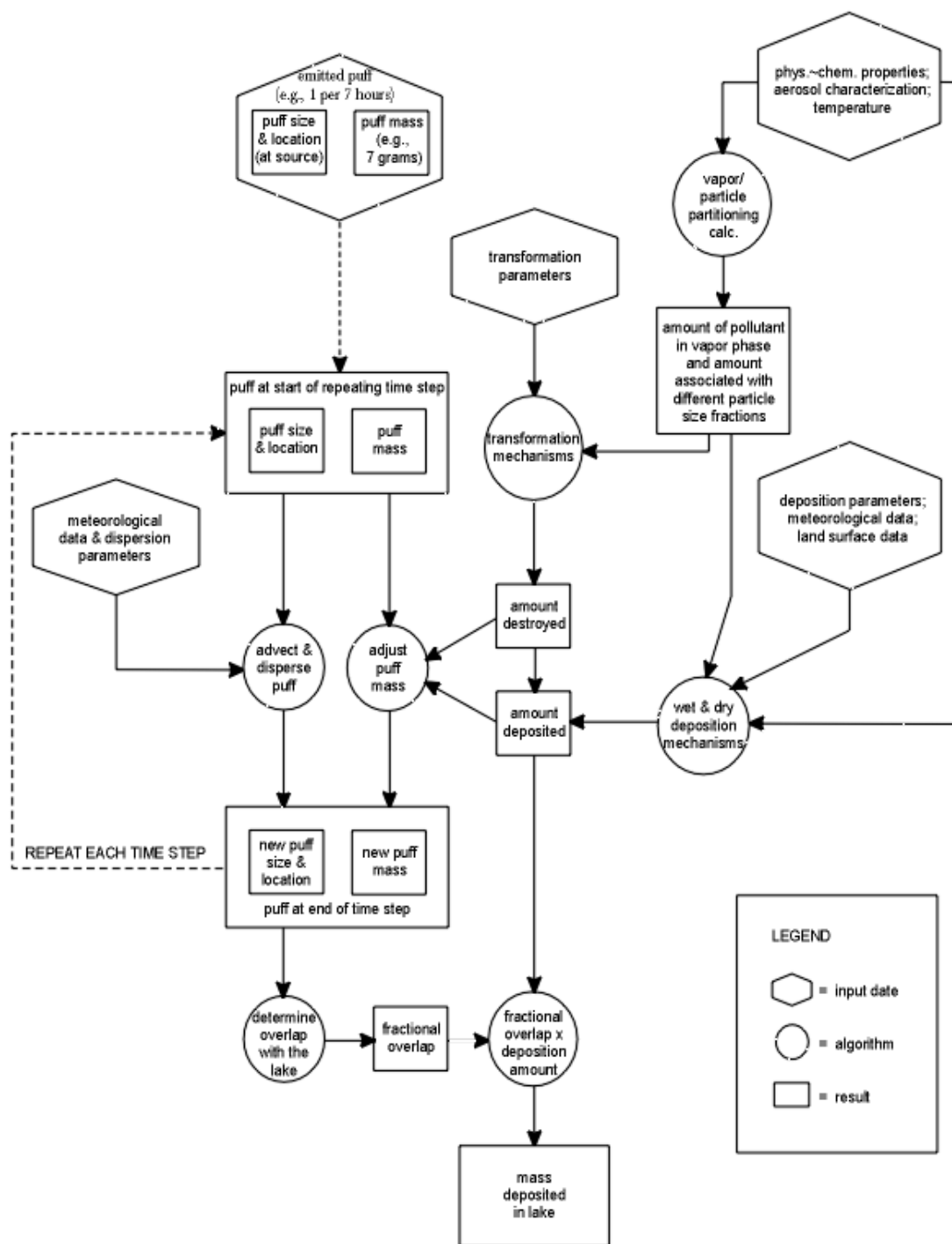
Figure 3.3: Schematic flowchart of the Hybrid Single-Particle Lagrangian Integrated Trajectory model (HYSPLIT - ARL/NOAA.) [Source: Draxler and Hess, 1998].
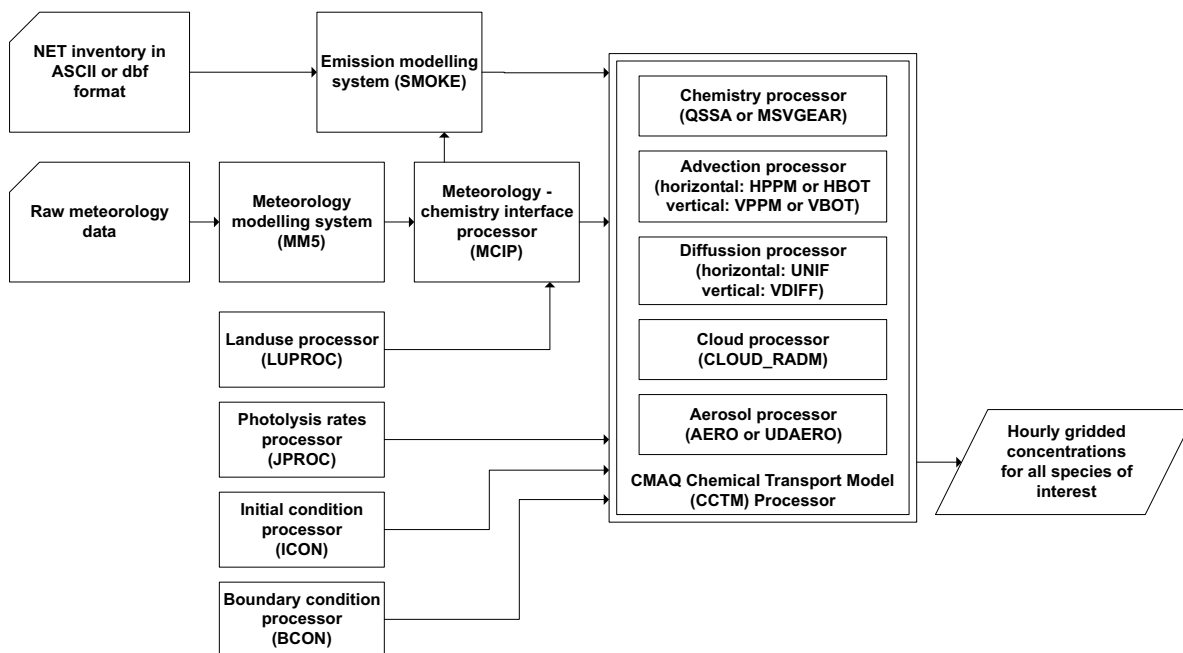
Figure 3.4: Schematic flowchart of the Community Multiscale Air Quality (CMAQ/Models-3) chemical transport model [Source: Byun and Schere, 2006].
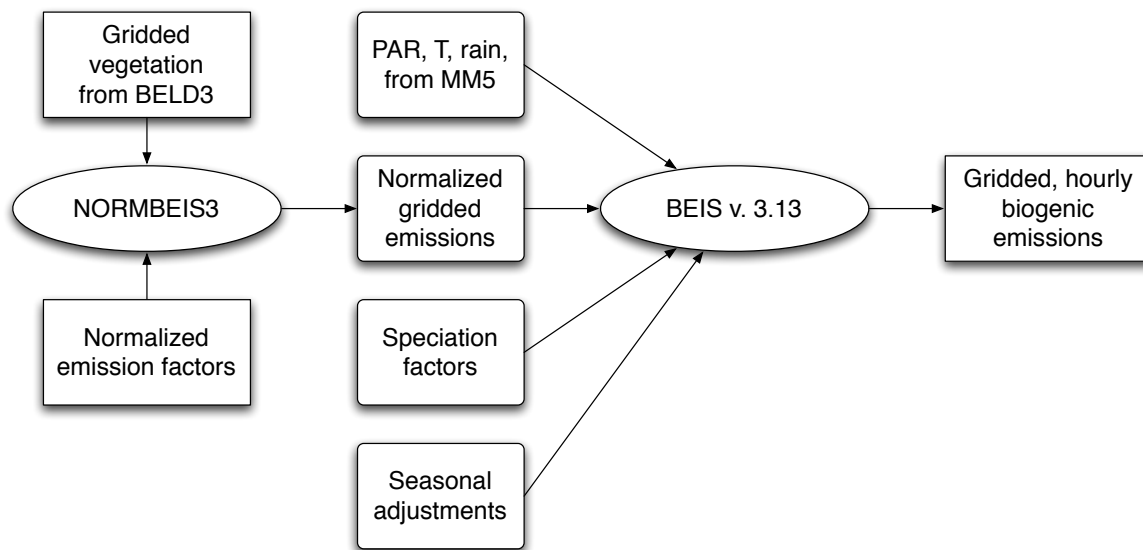
Figure 3.5: Schematic flowchart of the Biogenic Emissions Inventory System (BEIS) model [Source: Pierce, 2001].

Tables

Table **3.1**: Terrain height and elevation model products

Resolution	Data source	Coverage	Size(bytes)
1 deg. (111.0 km)	USGS	Global	129,600
30 min. (55.0 km)	USGS	Global	518,400
10 min. (18.5 km)	USGS	Global	4,665,600
5 min. (9.25 km)	USGS	Global	18,662,400
2 min. (3.70 km)	USGS	Global	116,640,000
30 sec. (0.925 km)	USGS	Global	1,866,240,000
Tiled 30 sec. (0.925 km)	GTOPO30 by USGS EROS Data Center in 1996	Global (33tiles)	57,600,000 or 51,840,000 for each tile

Table **3.2**: Land Use and Land Cover (LULC) mapping products

Resolution	Data source	Coverage	Size(bytes)
1 deg. (111.0 km)	PSU/NCAR	Global	842,400
30 min. (55.0 km)	PSU/NCAR	Global	3,369,600
10 min. (18.5 km)	PSU/NCAR	Global	30,326,400
200 and 30 meters	USGS	Global	varying

Table 3.3: Description of the 13 categories involved in the PSU/NCAR classification scheme for MM5 and the physical parameters for the North Hemisphere seasons [Source: Grell et al., 1994]

Land use	Albedo		Moisture		Emissivity		Roughness length		Thermal inertia	
	Sum	Win	Sum	Win	Sum	Win	Sum	Win	Sum	Win
Urban land	18	18	5	10	88	88	50	50	0.03	0.03
Agriculture	17	23	30	60	92	92	15	5	0.04	0.04
Range-grassland	19	23	15	30	92	92	12	10	0.03	0.04
Deciduous forest	16	17	30	60	93	93	50	50	0.04	0.05
Coniferous forest	12	12	30	60	95	95	50	50	0.04	0.05
Mixed forest	14	14	35	70	95	95	40	40	0.05	0.06
Water	8	8	100	100	98	98	0.01	.01	.06	0.06
Wetland	14	14	50	75	95	95	20	20	0.06	0.06
Desert	25	25	2	5	85	85	10	10	0.02	0.02
Tundra	15	70	50	90	92	92	10	10	0.05	0.05
Permanent ice	80	82	95	95	95	95	.01	.01	0.05	0.05
Sub/Tropical forest	12	12	50	50	95	95	50	50	0.05	0.05
Savannah	20	20	15	15	92	92	15	15	0.03	0.03

Table 3.4: Albedo as a function of season and LULC as specified in the AERMOD modeling system [Source: U.S.E.P.A, 1998]

Land use	Spring	Summer	Autumn	Winter
Water (fresh and sea)	0.12	0.10	0.14	0.20
Deciduous Forest	0.12	0.12	0.12	0.50
Coniferous Forest	0.12	0.12	0.12	0.35
Swamp	0.12	0.14	0.16	0.30
Cultivated Land	0.14	0.20	0.18	0.60
Grassland	0.18	0.18	0.20	0.60
Urban	0.14	0.16	0.18	0.35
Desert Shrubland	0.30	0.28	0.28	0.45

Table 3.5: Surface roughness length as a function of season and LULC as specified in the AERMOD modeling system [Source: U.S.E.P.A, 1998]

Land use	Spring	Summer	Autumn	Winter
Water (fresh and sea)	0.0001	0.0001	0.0001	0.0001
Deciduous Forest	1.00	1.30	0.80	0.50
Coniferous Forest	1.30	1.30	1.30	1.30
Swamp	0.20	0.20	0.20	0.05
Cultivated Land	0.03	0.20	0.05	0.01
Grassland	0.05	0.10	0.01	0.001
Urban	1.00	1.00	1.00	1.00
Desert Shrubland	0.30	0.30	0.30	0.15

Table 3.6: Bowen ratio as a function of season, LULC and moisture levels as specified in the AERMOD modeling system [Source: U.S.E.P.A, 1998]

Land use	Spring			Summer			Autumn			Winter		
Moisture levels	Dry	Avg	Wet	Dry	Avg	Wet	Dry	Avg	Wet	Dry	Avg	Wet
Water (fresh and sea)	0.1	0.1	0.1	0.1	0.1	0.1	0.1	0.1	0.1	2.0	1.5	0.3
Deciduous Forest	1.5	0.7	0.3	0.6	0.3	0.2	2.0	1.0	0.4	2.0	1.5	0.5
Coniferous Forest	1.5	0.7	0.3	0.6	0.3	0.2	1.5	0.8	0.3	2.0	1.5	0.3
Swamp	0.2	0.1	0.1	0.2	0.1	0.1	0.2	0.1	0.1	2.0	1.5	0.5
Cultivated Land	1.0	0.3	0.2	1.5	0.5	0.3	2.0	0.7	0.4	2.0	1.5	0.5
Grassland	1.0	0.4	0.3	2.0	0.8	0.4	2.0	1.0	0.5	2.0	1.5	0.5
Urban	2.0	1.0	0.5	4.0	2.0	1.0	4.0	2.0	1.0	2.0	1.5	0.5
Desert Shrubland	5.0	3.0	1.0	6.0	4.0	1.5	10.0	6.0	2.0	10.0	6.0	2.0

Table 3.7: Biogenic emission models - attribute comparison table

Model	BEIGIS	BEIS3	BIOME3	GloBEIS
Sponsors	CARB	EPA MCNC	LADCO/ Alpine Geophysics	TNRCC Environ
Programming Language	ArcView	FORTRAN	SAS	Microsoft Access
Canopy Model	BEIS2 (No light Attenuation)	BEIS2 (No light Attenuation)	BEIS2 or Guenther	Guenther
Canopy layers	5	5	2 to 99	2 to 99
PAR calculation	Read in	Calculated	Read in	Read in
Isoprene ratio	none	none	variable	1.43 (variable)
Primary Landuse	California State-specific	BELD3	BELD3	TNRCC Specific
Visualization	ArcView	PAVE	SAS commands FSVIEW/GRAPH	Microsoft Access
Photochemical model output	Not Available	CMAQ	CMAQ	UAM-V CMAQ

Chapter 4

Modeling emissions of biogenic VOCs and their effect on tropospheric ozone levels

Despite significant progress in photochemical modeling science in the last decades, large uncertainties still remain associated with the role of biogenic emissions in the formation of surface ozone. While it is extremely difficult to quantify the uncertainty levels of biogenic emission estimates due to insufficient monitoring data, an uncertainty factor of three has been suggested as a reasonable estimate for total VOCs nationwide [National Research Council, 1991]. The objective of this chapter is to evaluate the impacts of using biogenic emission estimates from the BEIS modeling system on ozone predictions for the Northeastern United States. For the area of interest as defined by the Ozone Transport Committee (OTC domain), biogenic emissions account for about 5% of the total NO_x emissions. During the summertime months, biogenic VOCs including isoprene and monoterpenes account for 64%, 88%, and 91% of the domain-wide emissions of paraffinic carbons (PAR), higher aldehydes (ALD2), and olefins (OLE), respectively, when BEIS model output is converted to chemical mechanism species (Table 4.1). In order to estimate the effect of biogenic emissions, the standard biogenic modeling methodology will be compared against a set of standard and modified vegetation databases, performing a basic sensitivity analysis for the domain of interest.

4.1 Description of the BVOC sensitivity studies

Several approaches have been used to estimate the contribution of biogenic emissions to O_3 based on modeling studies. In the first approach, the current situation and modeling methodology are treated as a "base case". Then biogenic emissions are removed to calculate their contribution to O_3. Here, the contribution of biogenic emissions to O_3 concentrations under current conditions can be estimated. It should be noted, however, that this contribution estimate may vary

according to the degree of perturbation (*e.g.* -10% slightly, -100% totally). By selecting a total perturbation, one can address the "global" sensitivity and bypass the possible issue of nonlinearity in the effect of biogenic emissions on O_3 and particulates. A second approach consists of simulating the natural atmosphere with no human influence. The O_3 concentrations calculated in such a simulation would represent the absolute contribution from biogenic emissions. There are, however, two major issues associated with this approach:

- Current urban-to-regional scale air quality models have never been evaluated under such conditions and the validity of those models in such applications is uncertain (*e.g.* in a similar manner that global models systematically underestimate O_3 concentrations by 5 to 10 ppb [Wang et al., 1998c]);

- Biogenic emissions interact with anthropogenic emissions to produce ozone and particulate matter.

Due to the above reasons, simulating an atmosphere with only biogenic emissions may not be of relevance, a point particularly valid for the densely populated Northeast United States. A third general category of approaches includes techniques that can "tag" each molecule to a specific source, or calculate the sensitivity coefficient of O_3 to biogenic emissions. However, the non-linearity of the response of O_3 and particulates to changes in biogenic and anthropogenic emissions will lead to different results depending on the source attribution, or the local sensitivity techniques being used. In this study, we elected to bound the problem by applying the first approach along with extensive testing and modification of the spatial allocation methodology of the BEIS model. The contribution of biogenic emissions and natural boundary conditions (BC) to O_3 and particulates deduced by removing these components from the base case is expected to be different from the concentrations of O_3 and particulates in a simulation with natural BC and only biogenic emissions. This is due to non-linearity in the chemical production of secondary air pollutants. The range of values predicted in these simulations for biogenic influences on O_3 should, therefore, provide reasonable bounds for this study.

The first step in the modeling approach involves testing the model's spatial components and allocation methodology under standardized environmental conditions in order to exclude the effect of meteorology. The latest emission factors for the United States and Canada produce small

differences in emissions that affect mostly the Canadian forests. Coupling these factors with the CBM-IV [Gery et al., 1989] chemical mechanism gives very close results in surface O_3 concentrations within the United States. Most chemical mechanisms include a number of aggregate biogenic stable species, established to attend different criteria (Table 4.2). CACM for example, classifies biogenics attending to the potential to generate secondary organic aerosols [Griffin et al., 2002]. On the other hand, LCC [Lurmann et al., 1987] and RACM [Stockwell et al., 1997] treat individual species explicitly as pinene, limonene, myrcene, and carene. CBM-IV has been widely used for O_3 studies, and therefore is selected for the sensitivity studies that will be presented in this chapter. The second step focuses on comparing the intermediate phenological variables (biomass density, leaf area index) calculated in BEIS, with relevant remote sensing products from the MODIS instrument. The biogenic emission estimates were adjusted to account for the difference between the static and dynamic approach in obtaining these variables, and a new set of simulations were performed with the CMAQ model. Based on these improvements, the following three sensitivity cases will be considered:

- Lower limit sensitivity case with no biogenic emissions, but with base case BC that include the contribution of natural species;

- Best estimate sensitivity case A with (a) standard, and (b) updated biogenic emissions calculated using BEIS, and natural contribution to BC;

- Best estimate sensitivity case B using remote sensing products for leaf area index adjustments on (a) isoprene, and (b) total biogenic emissions.

4.2 Application of the Models-3 system with refinements to the BEIS module

4.2.1 Meteorological data preprocessing - MM5 simulation description

The MM5 mesoscale atmospheric model has been widely used to generate meteorological data for air quality studies in the United States. Meteorological fields generated by the University of Maryland for MANE-VU/OTC modeling, featured two nested domains with a grid spacing of 36 and 12 km respectively (see Figure 4.1). A modified Blackadar PBL scheme uses a first-order

diffusivity formulation suitable for stable and neutral environments and a nonlocal closure for unstable regimes. MM5 was resolved vertically into twenty-nine variably spaced full sigma levels. While the first layer had a height of $28\,\mathrm{m}$, 11 layers were used in the lowest kilometer of the PBL. The chosen model physics options included the rapid radiative transfer model (RRTM, [Mlawer et al., 1997], Kain-Fritsch *cumulus* parameterization [Kain, 2004], medium range forecast (MRF) boundary layer parameterization [Hong and Pan, 1996], and simple ice microphysics scheme [Dudhia, 1989]. The initial and boundary conditions for the outer grid of the MM5 simulation were provided by the National Center for Environmental Prediction (NCEP spatial resolution: $2.5°$). The USGS elevation and LULC databases that were utilized in the MM5 setup are presented in Figures 4.2 and 4.3. The standard USGS database is sufficient for the purpose of our study and consistent with the BEIS methodology. It should be noted that modifications in the LULC component of the meteorological model should be always encompassed in the biogenic model. A bridge between the microphysics modules of the meteorology model and the biogenic model itself, is a missing component that would be extremely useful in air quality modeling studies.

The MM5 simulated period covered the entire year of 2002, and the MCIP preprocessor was used to convert monthly output for the Models-3 system. As described in the previous chapter, temperature and incoming radiation at the top of the canopy are the critical variables being passed from the meteorological output to the biogenic emissions model. MCIP calculates the temperature for the surface layer at both its bottom and top. Since leaf temperature is such a critical variable, the BEIS formulation provides with the option to choose from two different heights (1.5 and $10\,\mathrm{m}$ respectively). This decision should be based on the domain characteristics and the final MM5 performance at each level. In addition, total incoming radiation for the top of the layer is passed from MM5 output, and half of this amount is assumed to be equal to the fraction of photosynthetically active radiation (fPAR). As a quality assurance test of the meteorological output for biogenic modeling, the modeled variables were compared against the U.S. surface radiation (SURFRAD) monitoring network. Time series plots of these variables for the cells that enclose the three SURFRAD monitors found within the 12 km OTC domain, are presented for the month of August in Figures 4.4 - 4.6. A good correlation to the monitor values can be observed in the resulting comparison scatter plots of each individual variable and

SURFRAD station involved in this study (Figure 4.7). Additional MCIP variables used in the BEIS model include surface pressure, convective and non-convective precipitation. The basic set of variables handled by BEIS was considered enough for the purpose of our study, when the employed chemical mechanism is considered (CB-IV). More information on the mechanism will be provided in the following subsection.

4.2.2 Application of improved BEIS modules for the Northeast United States

Biogenic emissions were calculated using versions 3.09, 3.12, and the experimental 3.13 of the BEIS model along with MCIP meteorology fields for the entire 2002. As described in the previous chapter, the general processing approach has not changed significantly in the most recent versions. Version 3.09 involves a simplified method that uses only the USGS part of the BELD database, leaving out the high-detail species-level component. The updated methodology (versions 3.1x) is used to estimate emission fluxes for each one or a group of the 34 biogenic species/compounds based on individual vegetation densities mapped using the BELD database. Those species are then subsequently assigned to the species covered by each chemical mechanism. For the case of the CBM-IV chemical mechanism it results to 12 species (Table 4.1 with the addition of CO, NR), while using the older 3.09 version would produce only 4 CBM-IV species. In total, CBM-IV includes 37 chemical species (12 of which are photolytic) and 78 reactions. Additionally, BEIS treats natural emissions of NO from soils, biomass burning, and lightnings. The Campbell and Norman methodology was incorporated in order to calculate appropriate light correction factors for isoprene and methyl butenol (MBO) [Campbell and Norman, 1998]. An analysis of each step followed in the BEIS modeling approach will be the subject of the following subsections.

Spatial allocation of the BVOC emission potential using the BEIS model

The spatial allocation of the biogenic VOC emission potential under the BEIS modeling framework is determined by the function **Normbeis**. **Normbeis** utilizes the BELD vegetation database in conjunction with the standardized emission factor look-up table that corresponds to the speciation profiles described before. For some plant species, emission factors for specific terpenes, sesquiterpenes, and oxygenated compounds remain to be investigated [Lamb and Coordinating Research, 1999]. Since for the majority of these species the factors are based on taxonomical

assignment of the plant species whose emission factors are relatively well defined, the emission factor lookup table is under continuous review [Benjamin and Winer, 1998]. Table 4.3 lists a lumped version of the BEIS lookup table for the 10 most abundant tree families that are present within the OTC domain based on the BELD vegetation database. In addition to the the emission factors for the major biogenic VOCs, the vegetation emission database contains the associated leaf area index and dry leaf biomass factors that are used in phenological modeling. As it is well known for the Northeast U.S. and Canada, the density of the oak trees ranks among the highest. This, along with the fact that oak is one of the strong isoprene emitters, identifies them as a very significant family for regional air quality modeling. In contrast to the Southern U.S., monoterpene emitters have a weak presence in the MANE-VU/OTC domain. For the rest of the biogenic emission factors (OVOC and NO), uncertainties involved in quantification are obvious from the almost uniform emission potential.

The current version of BEIS (3.13) features an updated emission factor table along with minor modifications in the environmental correction factor formulation. In earlier versions of BEIS-3, standardized isoprene emission factors for black spruce, blue spruce, white spruce, and Englemann spruce were assumed to be $14 \, \mu g \, C/g/h$. Based on detailed measurements of spruce emissions, this emission factor has been lowered to $7 \, \mu g \, C/g/h$ (Isebrands et al. [1999], Pattey et al. [1999], and Westberg et al. [2000] report a range of 6-8 $\mu g \, C/g/h$. Assuming a leaf biomass of $1500 \, g \, m^{-2}$, this translates into an area flux of $10.500 \, g \, C/km^2/h^2$. A map showing the spatial distribution of the total spruce species density for the OTC domain is provided in Figure 4.8. The reduction in the isoprene emission factor for all the spruce species has consequently resulted in reductions in the emission fluxes for USGS-defined coniferous forests (from $11.383 \, g \, C/km^2/h^2$ to $7.918 \, g \, C/km^2/h^2$ and for USGS-defined deciduous forests (from $8.232 \, g \, C/km^2/h^2$ to $6.707 \, g \, C/km^2/h^2$. USGS-defined forest data are used for estimating biogenic emissions from Canada (Figure 4.9), where species-specific densities are not available for the BELD3 database. Additionally, the USGS portion of BELD3 is used in the standard version of BEIS (3.09). Comparison of the **Normbeis** (Figures 4.10 - 4.12) output suggests that the isoprene changes are expected to affect emissions from Canada and slightly the Northeast United States.

The standardized emission factors for monoterpenes were also updated. In earlier versions of

BEIS-3, the emission factor for Douglas fir was $1.41\,\mu g\,C/g/h$. Based on extensive measurements of Pressley et al. [2004], this factor was reduced to $0.39\,\mu g\,C/g/h$ in BEIS-3.13. Assuming a leaf biomass of $1500\,g\,m^{-2}$, it translates into an area flux of $585\,g\,C/km^2/h^2$. In the same manner, the emission for hemlock was changed from $0.18\,\mu g\,C/g/h$ to $0.95\,\mu g\,C/g/h$. With a leaf biomass of $700\,g\,m^{-2}$, the monoterpene area flux for hemlock is assumed to be $665\,g\,C/km^2/h^2$. A map showing the spatial distribution of the total Douglas fir and hemlock species density for the OTC domain is provided in Figure 4.13. Comparison of the **Normbeis** output reveals that the monoterpene changes are expected to have barely noticeable effect in the Northeast United States (Figures 4.14 - 4.16).

Phenology modeling using BEIS-3: Leaf Area Index modifications

Leaf biomass provides the energy that drives the growth of the tree stand and is therefore the subject of several models [Makela, 1986; Valentine, 1985]. It is also possible to describe changes in the leaf biomass using less formal techniques including expert knowledge, which is subject to verification using visual estimation or photogrammetric techniques. The leaf biomass values that are listed in Table 4.3 reflect peak foliar density (*e.g.* these values are the maximum leaf biomass factors that occur during the growing season). Leaf area index (LAI) is defined as the total one-sided green leaf area per unit ground surface area. LAI describes a fundamental property of the plant canopy in its interaction with atmosphere, especially concerning radiation, energy, momentum, and gas exchange [Monteith and Unsworth, 1990]. Leaf area plays an important role in the absorption of radiation, in the deposition of photosynthates during the diurnal and seasonal cycles, and in the pathways and rates of biogeochemical cycling within the canopy-soil system [Bonan, 1995].

BEIS-3 calculates summer and winter LAI for each cell within the modeling domain based on the lookup table for emissions processing (Table 4.3) along with a wintertime adjustment factor. This factor indicates the fraction of the emissions factors to use when estimating biogenic emissions in the winter months (*e.g.* zero indicates that the plant species does not emit in the winter months). It is unclear how this factor was determined, therefore is likely to be highly uncertain. The resulting map for the OTC domain based on the BEIS model is presented in Figure 4.17. The methodology developed for the study of the biogenic VOCs was based on

incorporating a satellite leaf area index product (MODIS), in order to calculate the intermediates to the biogenic emissions variables. The MODIS instrument has been used in monitoring of canopy phenology from the perspective of examining potential effects of climate change [Ahl et al., 2006; Myneni et al., 1997]. Computational limitations along with known satellite issues during the winter months (*e.g.* cloud/snow coverage affects 4 out of 5 days), restricted our application to the month of August. Algorithms to convert the geographical coordinate system and resample to the 12 km grid for the OTC domain were developed. The final result for the area of interest during the first week of August is provided in Figure 4.18. Comparison against the MODIS 8-day LAI product for the first acquisition period of August 2007 reveals significant differences between the calculated and the remotely sensed vegetative stage (Figure 4.19). Since it is well established that most of the monoterpenes are not emitted by the leafy part of the vegetation, two separate scenarios were developed. In the first scenario, only the isoprene emissions were adjusted according to MODIS LAI product. In the final scenario, a "worst case" approach with all biogenic emissions (except soil NO and CO) adjusted according to MODIS LAI was implemented. Results from the comparison of the strength of emission source, and its effect on O_3 levels, will be presented in the following section.

4.3 Biogenic emissions and photochemical modeling simulation results

This section provides modeling results for the OTC/MANEVU domain for the scenarios established before. It is separated into two areas of interest: the improvement of the Biogenic Emission Inventory System (BEIS) implementation in the Sparse Matrix Operator Kernel Emissions (SMOKE) model, and the application of the Community Multiscale Air Quality model (CMAQ) using the relative emission inventories. A Geographical Information System (GIS) was established for the relative inputs and output of each step of the modeling procedure for better visualization purposes. Additionally, relevant portions of the USEPA air quality system (AQS) database were incorporated in the GIS database along with the location of each monitoring station. For verification purposes CMAQ output was compared against the USEPA monitoring stations that were operating in the domain and period of interest.

4.3.1 Emissions comparison with different BEIS formulations

Emissions inputs for the CMAQ model are typically developed using the Sparse Matrix Operator Kernel Emissions (SMOKE) processing system. A schematic overview of the data collection processing that includes both anthropogenic and biogenic emissions from the OTC domain is provided in Figure 4.20. Total biogenic emission estimates for the OTC domain during the month of August 2002 were calculated for each scenario. Figure 4.21 shows the total emission for each biogenic species included in the CBM-IV mechanism, with individual LAI adjustments (excluding NO and CO emissions). Detailed time series plots of the isoprene and monoterpene emissions in the domain were created using hourly BEIS output for the simulated scenarios (Figure 4.22). The domain-wide contribution of the biogenic emissions to their anthropogenic counterparts for the simulations performed in this study is summarized in Table 4.4. From data above, it can be concluded that the BEIS emission factor updates do not have a significant contribution to the total biogenic emissions assigned to the OTC domain. On the other hand, leaf area index adjustments seem to have a quite significant effect on the emissions of isoprene and the rest of the biogenic groups involved in the CBM-IV mechanism.

In order to examine the spatial effect of the emission model modifications, August 12th of 2002 was selected as a day with strong biogenic influence, suitable for further investigation. A set of maps showing the allocation of these emission totals during the morning hours of August 12th is provided for the domain of interest. Figure 4.23 and 4.24 show a comparison of the LAI-adjusted and the updated BEIS allocation of isoprene emissions respectively, as calculated for the morning of August 12th of 2002. Similar comparison maps are presented for the case of monoterpene emissions in figure 4.25 and 4.26. For both cases a significant increase can be noticed in the Southwest portion of the OTC/MANEVU domain and in Northern areas covered by dense Canadian forests. Densely populated areas that are classified under urban land cover are, as expected, associated with decreased biogenic emissions when the MODIS-adjusted scenario is applied.

4.3.2 Surface ozone levels during the August 2002 scenarios

In the sensitivity simulations with biogenic influences adjusted or removed, both the spatial and temporal distribution of O_3 changed following the changes in emissions and BC. The response,

in terms of absolute and relative changes in O_3, also varies as a function of time and location. We first analyze the response as a function of location. Hourly surface ozone concentrations were obtained for each modeling scenario across the entire OTC/MANEVU domain. The four time periods considered are 0800-0900, 1200-1300, 1600-1700, and 2000-2100 EST. Briefly these four periods can be characterized as follows. During the early morning period, there is injection of fresh emissions in the surface layer, and the mixing layer starts to grow rapidly. The 1200-1300 EST period reflects the time during which, photochemical reactions, vertical mixing, and advection processes dominate. During the 1600-1700 EST period, the mixed layer starts to collapse with decreasing solar insolation. The 2000-2100 EST period is characterized by the dominance of nighttime chemical and removal processes. It should be noted that the relative roles of different atmospheric processes are not constrained to these specific time periods since they can overlap; these periods are considered here for examining the overall temporal response of the modeling systems in relation to the spatial effect of the biogenic emissions.

Figures 4.27-4.30, 4.31-4.34, 4.35-4.38, and 4.39-4.42 provide hourly ozone maps for each computational scenario for 8 am, 12 pm, 4 pm, and 8 pm EST during the 12th of August, respectively. From this set of figures, we can observe the strong influence that biogenic emissions impose on the East Coast, and more specifically along the northeastern urban corridor region. The importance of the southeastern states is apparent when O_3 maps that include biogenic emissions are compared against the anthropogenic-only scenario. More specifically, this effect can be demonstrated in Figures 4.31-4.34, where the Southeast areas that experience concentrations above 50 ppb have greatly expanded when compared against the Northeast, where the effect has a smaller spatial extent.

Finally, the temporal distribution of ozone was examined for the duration of the entire modeled period. Figure 4.43 shows the response of O_3 to different emission and BC scenarios using two spatially aggregated metrics: domain maximum O_3 and domain average O_3. The daily time series reveal that the simulation maximum and average was strongly influenced by the biogenic emissions and for some days by the overwhelming anthropogenic component (August 23rd). As a result, the overall modeled domain maximum was not affected by the inclusion of biogenic emissions. Domain-wide average daytime and nighttime ozone concentration time series were created from the CMAQ output and can be found in Figure 4.44. As expected, the

observed daytime effect of biogenic emission results to an increase of 5 ppb or more of O_3, while the reduced nighttime influence is less significant (around 2-3 ppb).

4.3.3 Statistical analysis of model performance

The map presented in Figure 4.45 shows a subset of the AQS monitoring database, more specifically the ozone monitoring station network, established and maintained by the USEPA. The database was processed for all monitors within the OTC/MANEVU domain, and each of them was compared against cell-specific model output. Daily maximum ozone concentration plots are provided for a subset of O_3 monitors within the State of New Jersey (Figure 4.46). In order to have a direct comparison against the NAAQS standards, time series plots for the hourly and 8-hour average O_3 concentration are shown in Figures 4.47 and 4.48. Tesche and McNally [1997]; Tesche et al. [1990] and the E.P.A. [1991] recommended several statistical measures to perform evaluation of the grid-based urban-scale photochemical models. A number of investigators have applied some of these measures in the evaluation of urban and regional-scale photochemical models. In this study, we applied a total of four statistical measures, the first three of which have been recommended by the EPA to assess model performance; these are (i) unpaired accuracy, (ii) normalized bias, (iii) normalized absolute gross error, and (iv) correlation coefficient, as defined in the list presented in Appendix B. The database used in this section of the study, consists of the predicted and measured hourly ozone concentrations at all monitoring stations for each episode day, and as such these data are paired in both space and time. In other words, for the duration of the episode there is one set of measured and predicted maximum ozone, providing 744 pairs for the modeled month (spin-up time was also allowed) for each monitoring location within the data analysis grid. The statistical metrics have been calculated taking in account all the ozone monitors located within the State of New Jersey, and the results are summarized in table 4.5.

4.3.4 Ozone response to increasing biogenic emissions

Several investigators focused on the policy-making aspect of issue - by answering the question of the different emission reduction options applied uniformly throughout the entire domain. In such simulations, a metric - the index of improvement, or relative change factor- is defined as:

$$\text{Relative Change Factor} = \frac{(\text{O}_3)_{base} - (\text{O}_3)_{control}}{(\text{O}_3)_{base}} \cdot 100\% \qquad (4.1)$$

where O_3 is the hourly ozone concentration at each grid cell.

Previous studies showed have showed differences in the temporal and spatial ozone patterns when biogenic emissions were "perturbed" [Sistla et al., 2001]. The index of improvement was calculated at each monitor location and at each grid cell of the analysis domain, averaged over the entire simulation period. For the case of the Northeast United States, a summary table with the calculated relative change factor is provided in Table 4.6. As we can see from this table the increase in BVOC emission, as it was described in the two major scenarios, resulted in a relative change factor that ranged from 1.01 to 1.05. This change is considered to be important for the summertime months when an increase of 5 ppb can move an area to non-attainment standards for ozone.

Figures
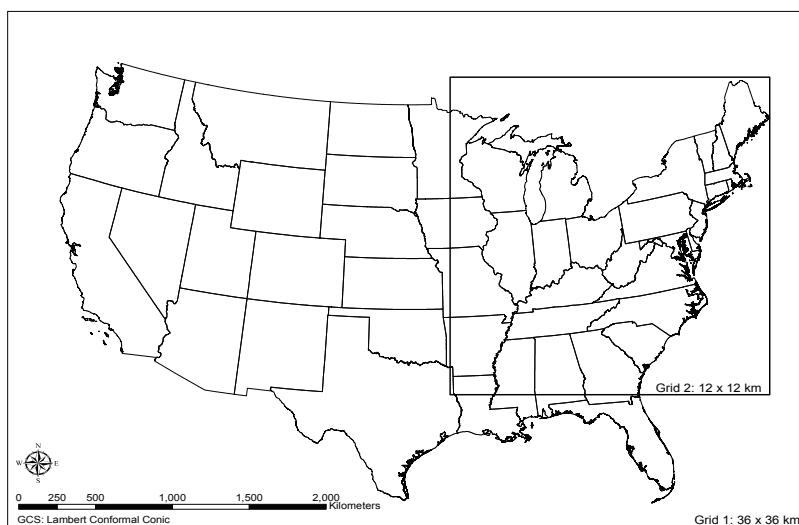
Figure 4.1: The OTC domain with the inner (12 km resolution) and outer (36 km resolution) grids used in meteorological/photochemical modeling.
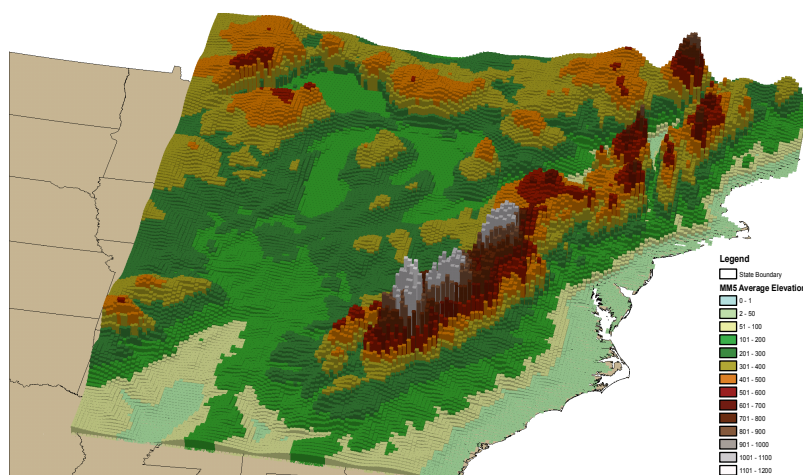
Figure 4.2: A three dimensional view of the OTC domain and topography provided by the USGS elevation data (GCS: NAD83).
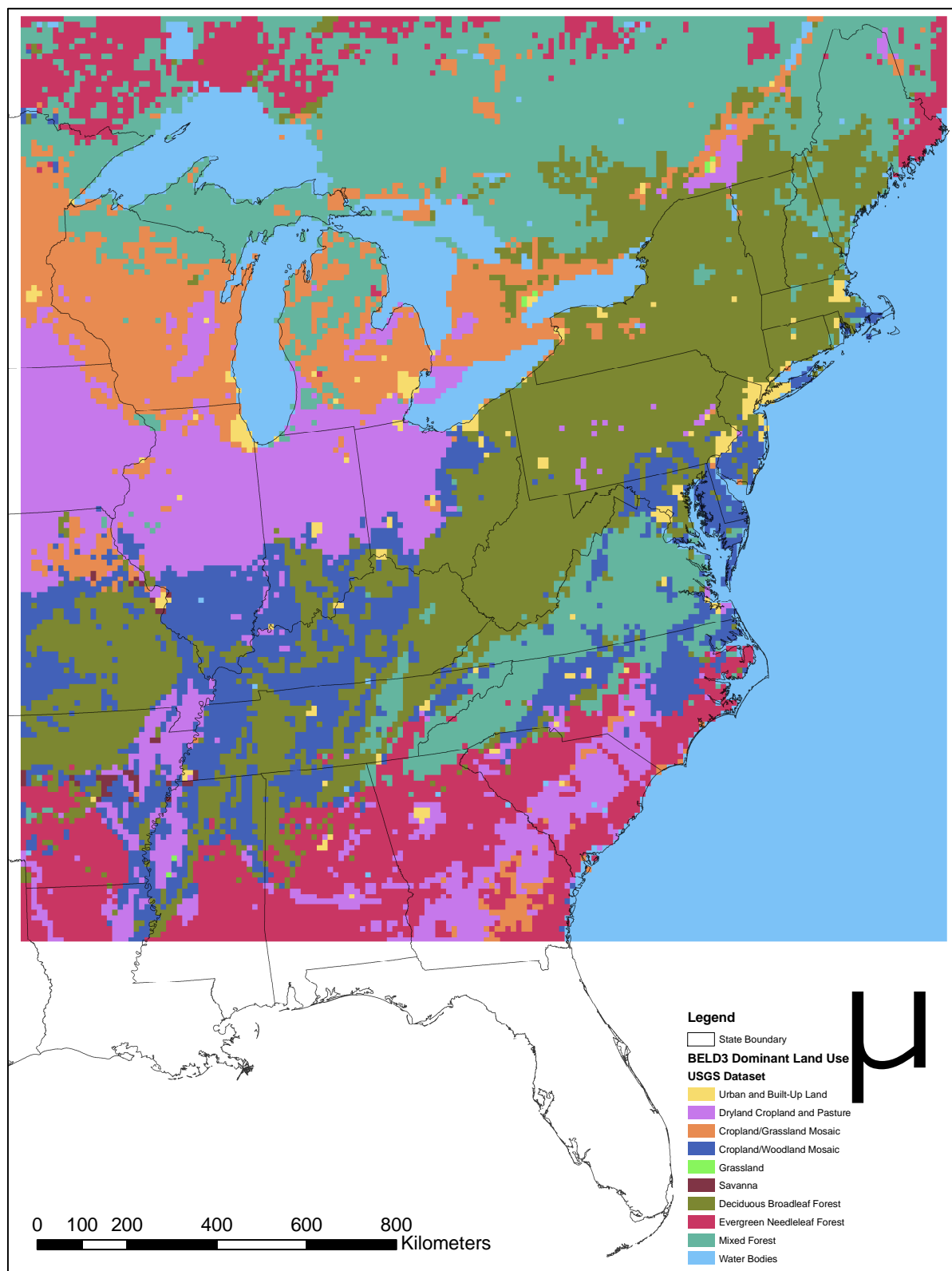
Figure 4.3: Dominant land use classification scheme for the OTC domain according to the USGS database that was used in meteorological modeling with MM5 (GCS: NAD83)
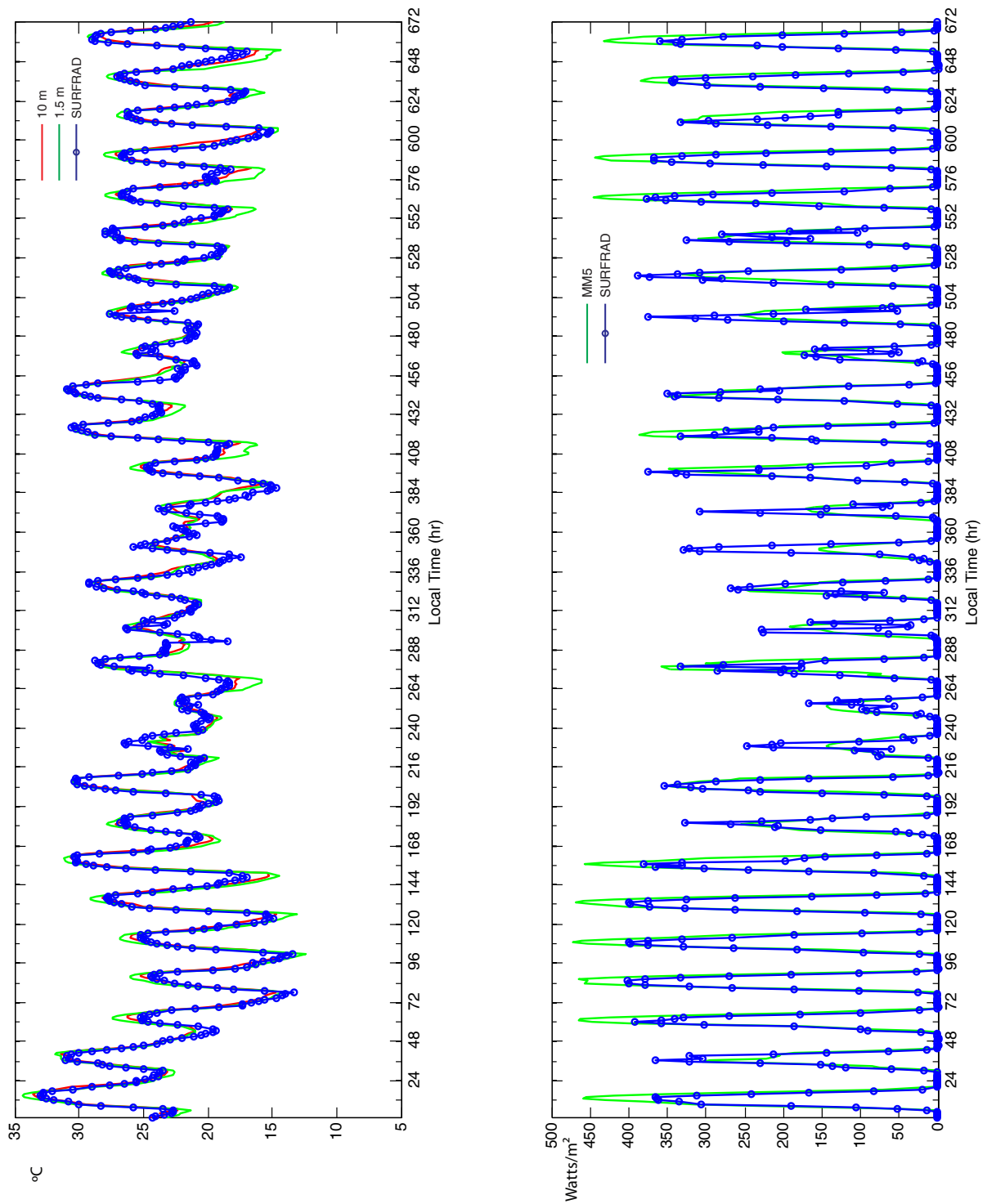
Figure 4.4: Comparison of meteorological variables of interest (Temperature and fPAR) calculated by MM5 (solid lines) and measured at the Penn State University (PA) SURFRAD agro-meteorological station (circles) for the month of August 2002.
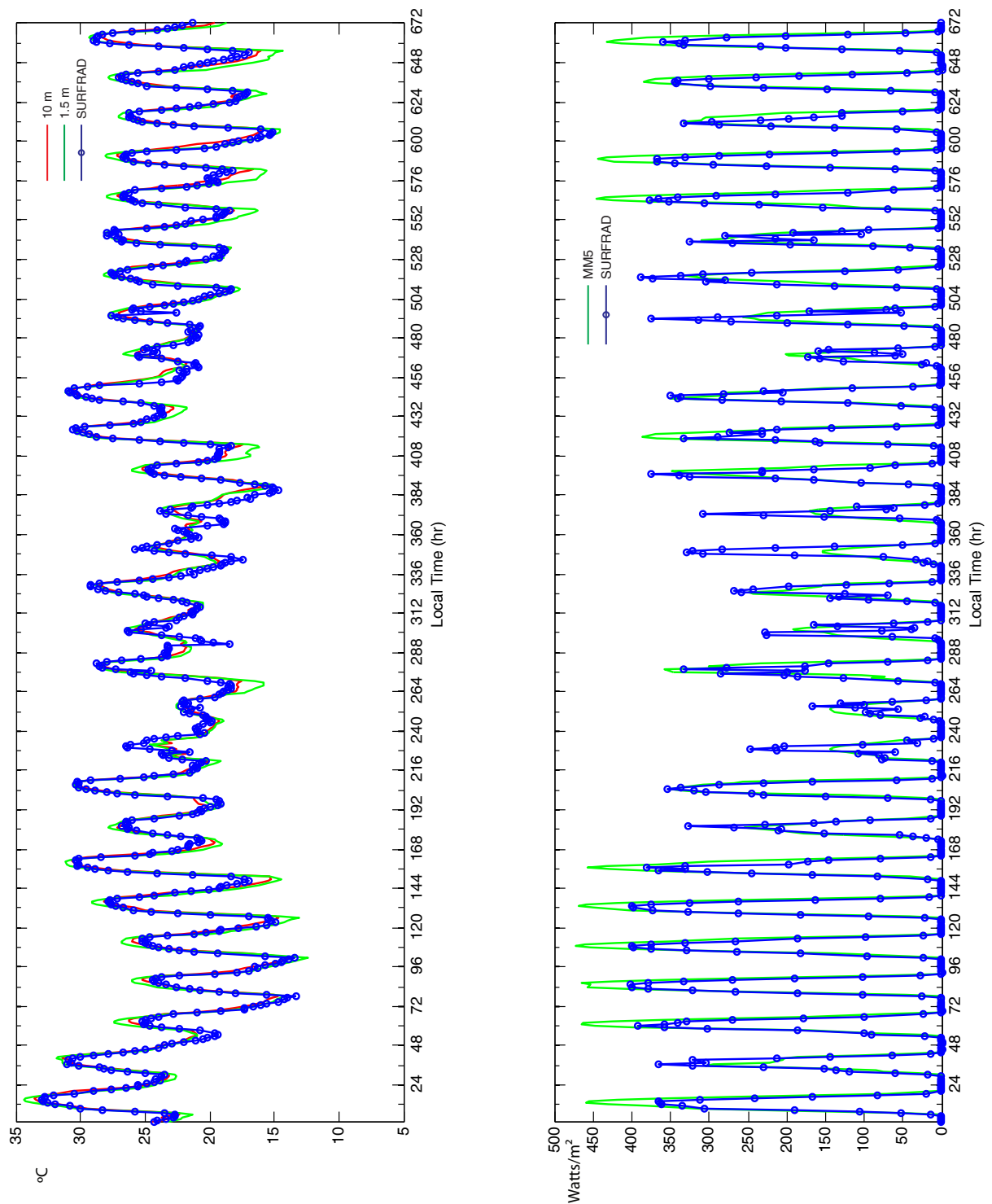
Figure 4.5: Comparison of meteorological variables of interest (Temperature and fPAR) calculated by MM5 (solid lines) and measured at the Bondville (IL) SURFRAD agro-meteorological station (circles) for the month of August 2002.
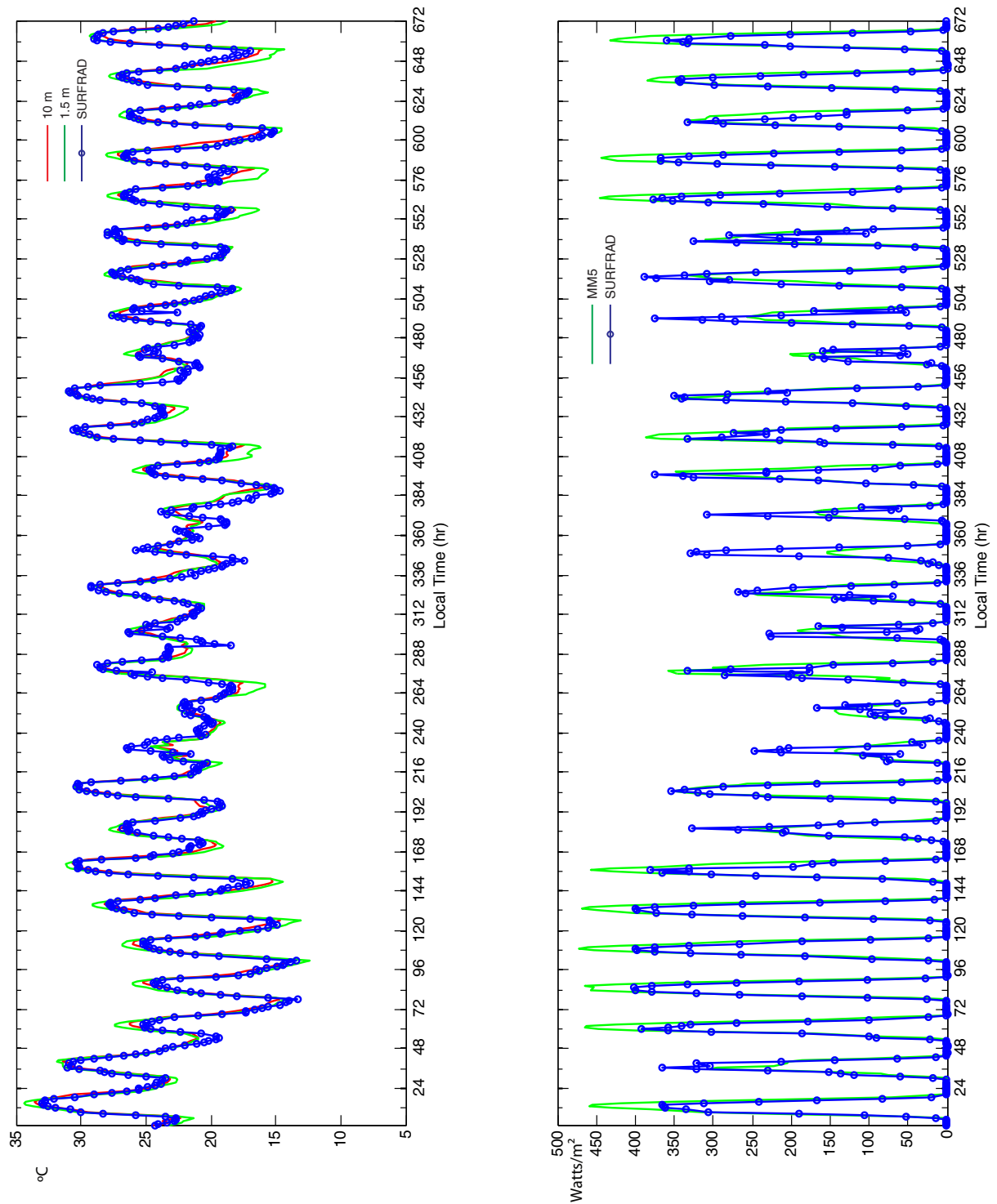
Figure 4.6: Comparison of meteorological variables of interest (Temperature and fPAR) calculated by MM5 (solid lines) and measured at the Goldwin Creek (MS) SURFRAD agrometeorological station (circles) for the month of August 2002.
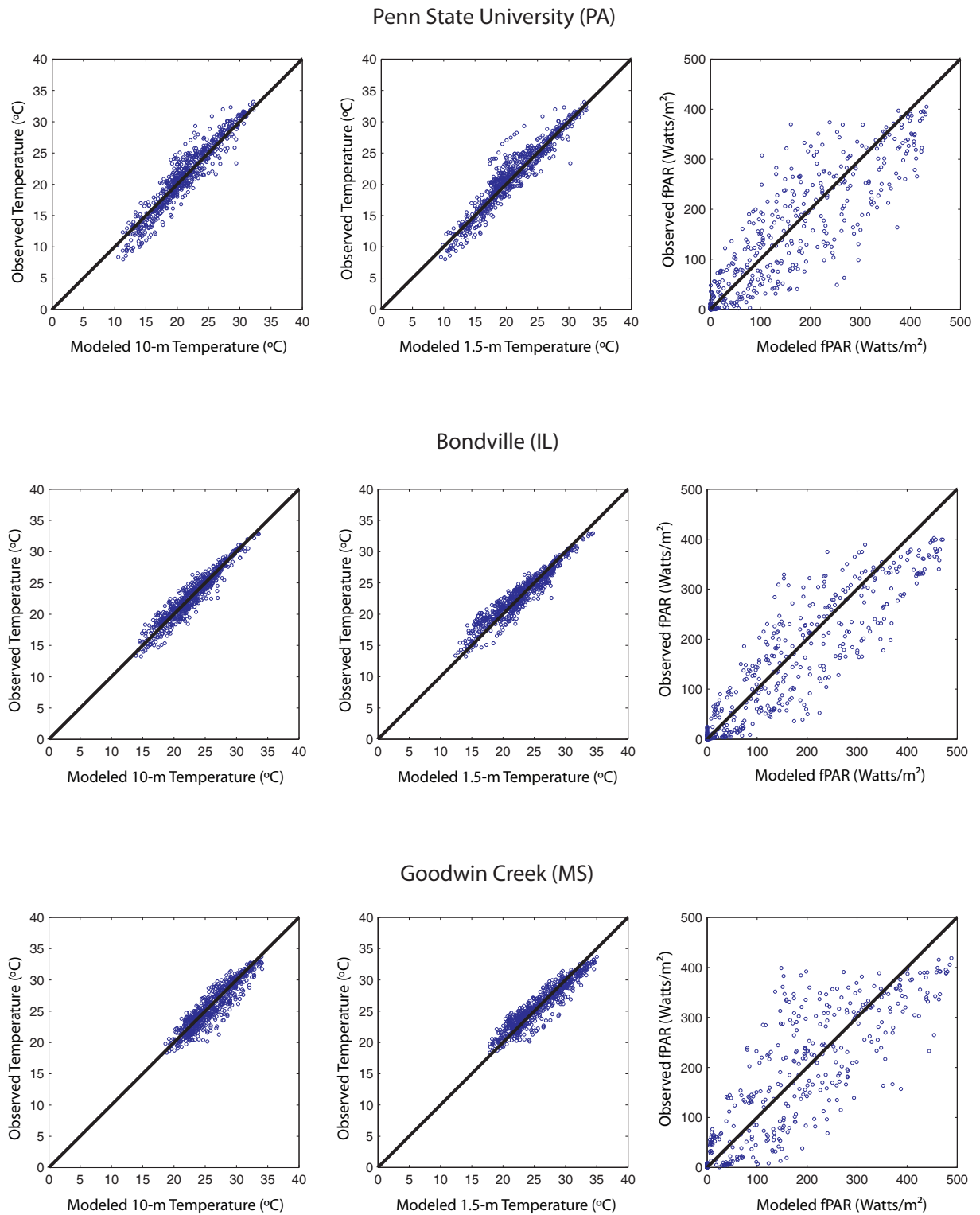
Figure 4.7: Comparison plots showing the correlation of the observed temperature and measured fPAR, versus the MM5 calculations obtained for each cell of the OTC domain enclosing each SURFRAD agro-meteorological station.
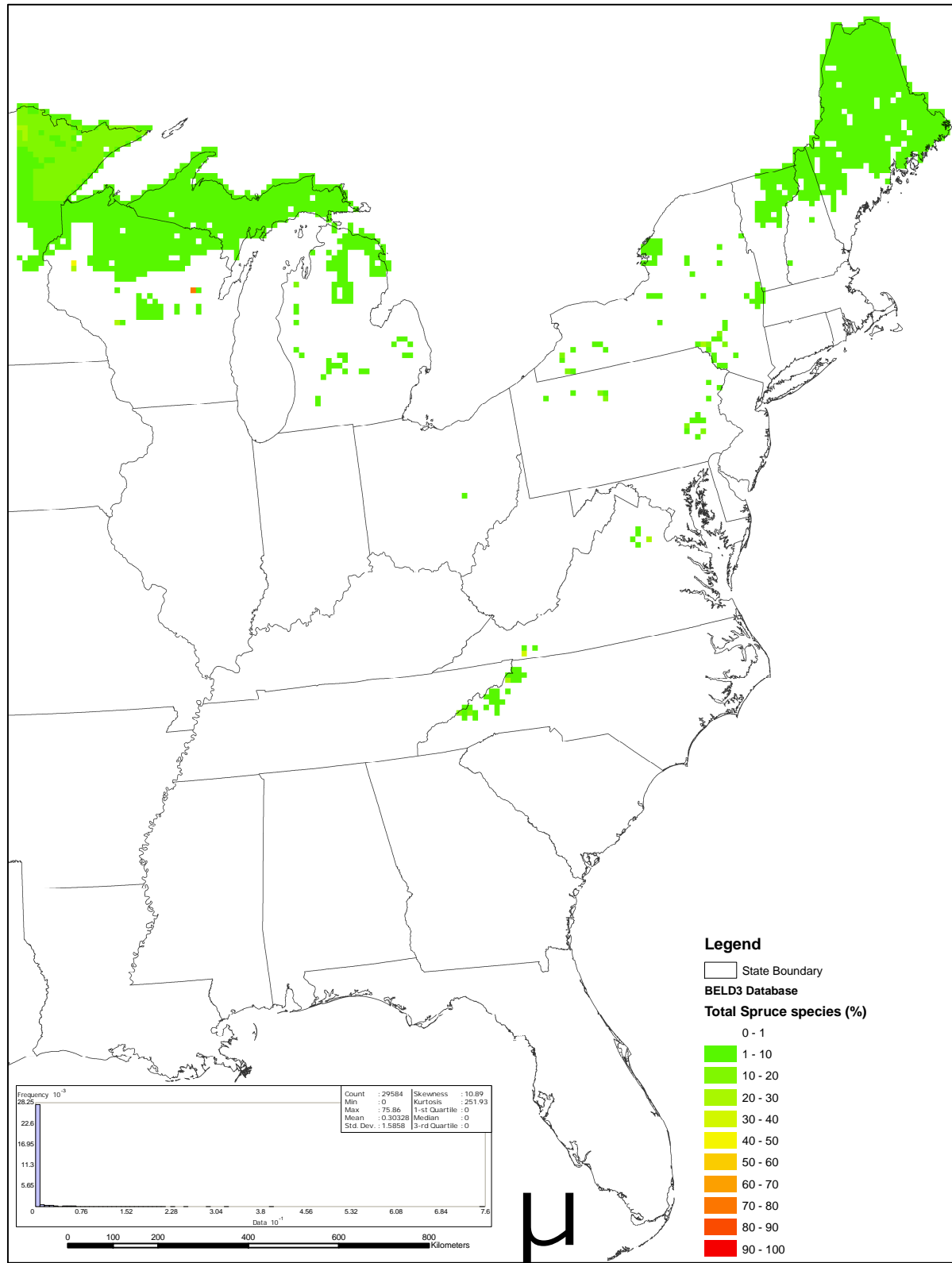
Figure 4.8: Total Spruce species density based on the individual tree species included in the BELD3 geodatabase (GCS: NAD83).
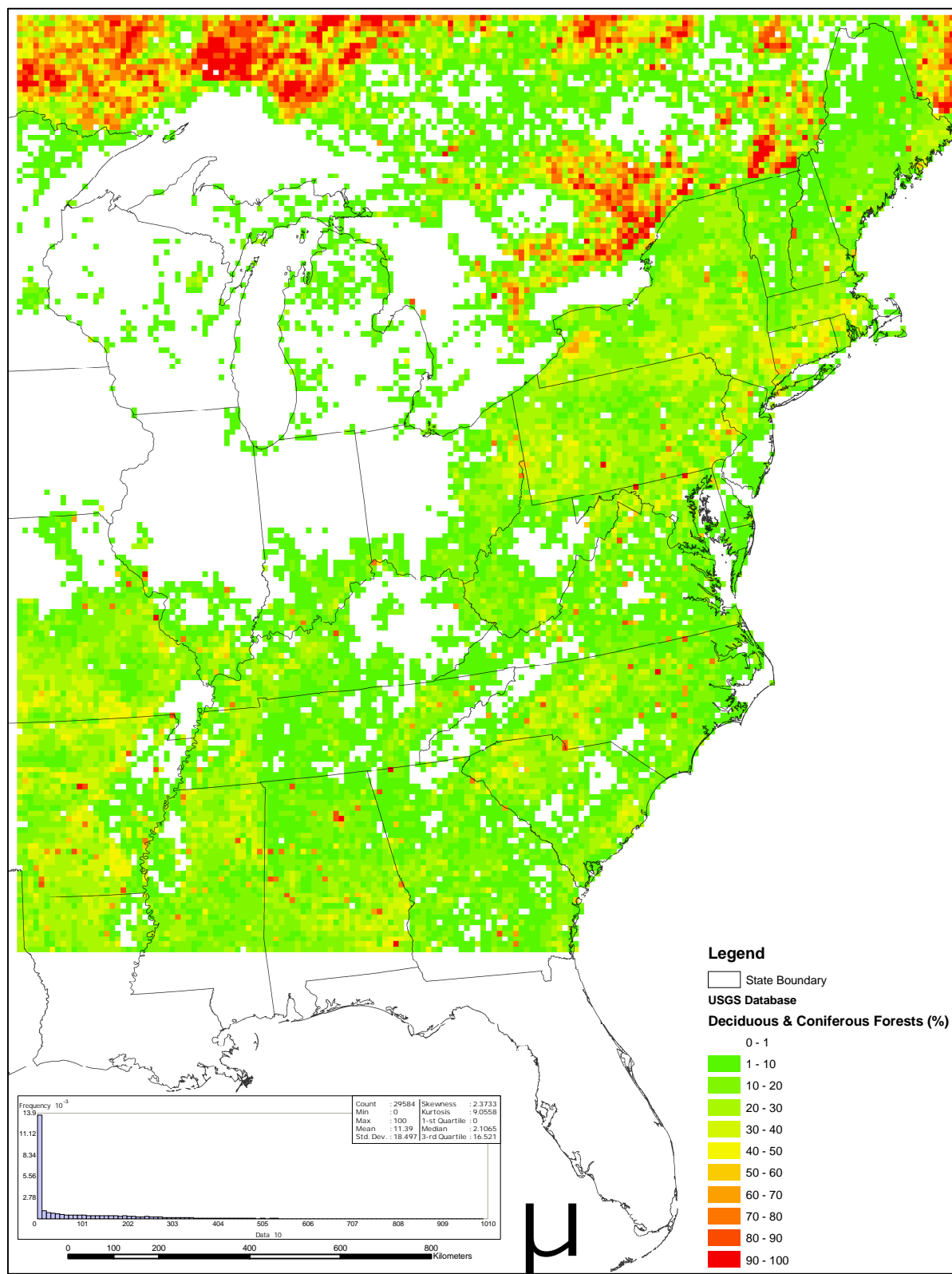
Figure 4.9: Combined deciduous and coniferous forest density based on the USGS forest classification of the BELD3 geodatabase (GCS: NAD83).
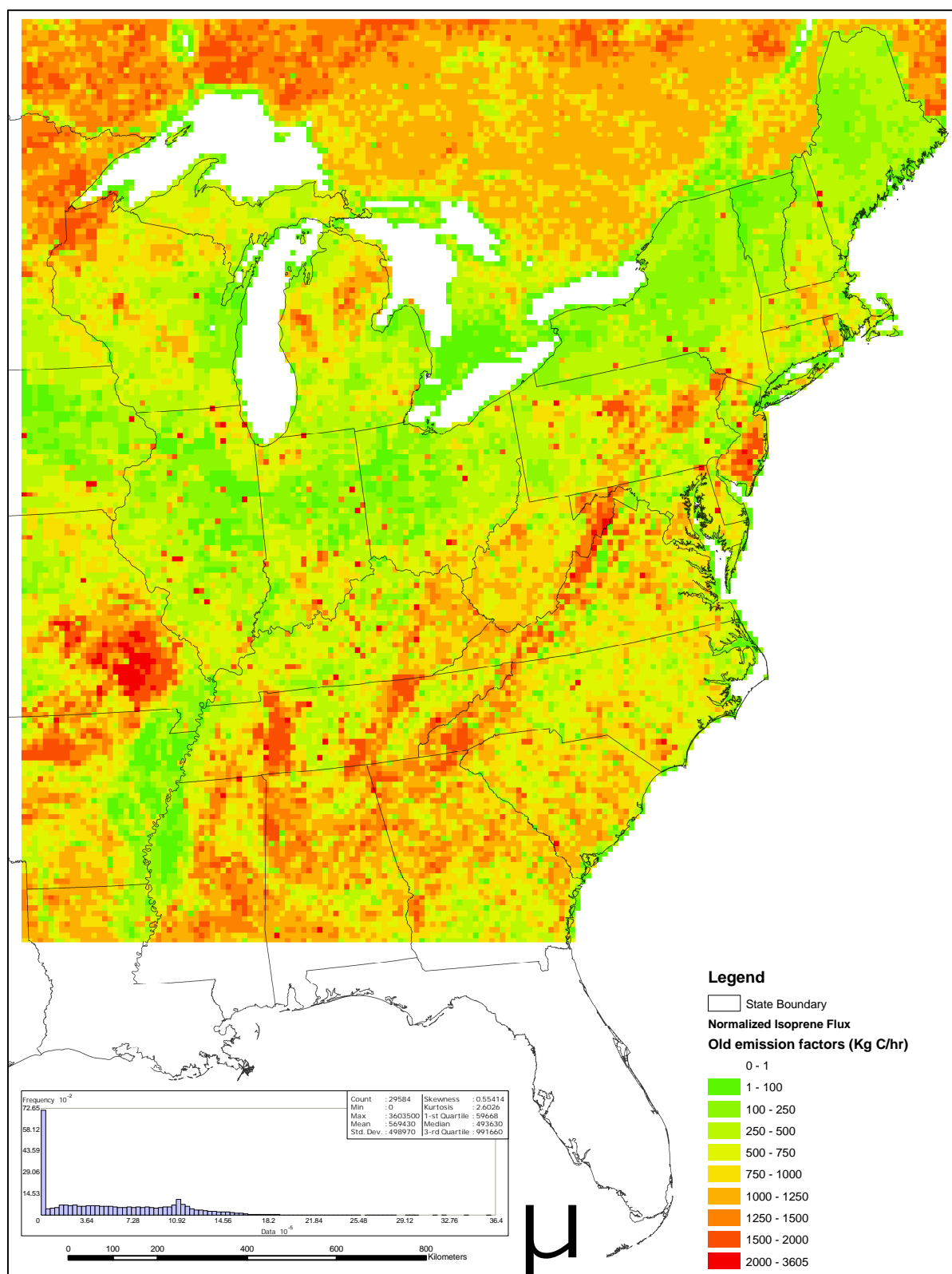
Figure 4.10: Temperature and light normalized isoprene emission using the BEIS allocation methodology and the standard (3.12) emission factors (GCS: NAD83).
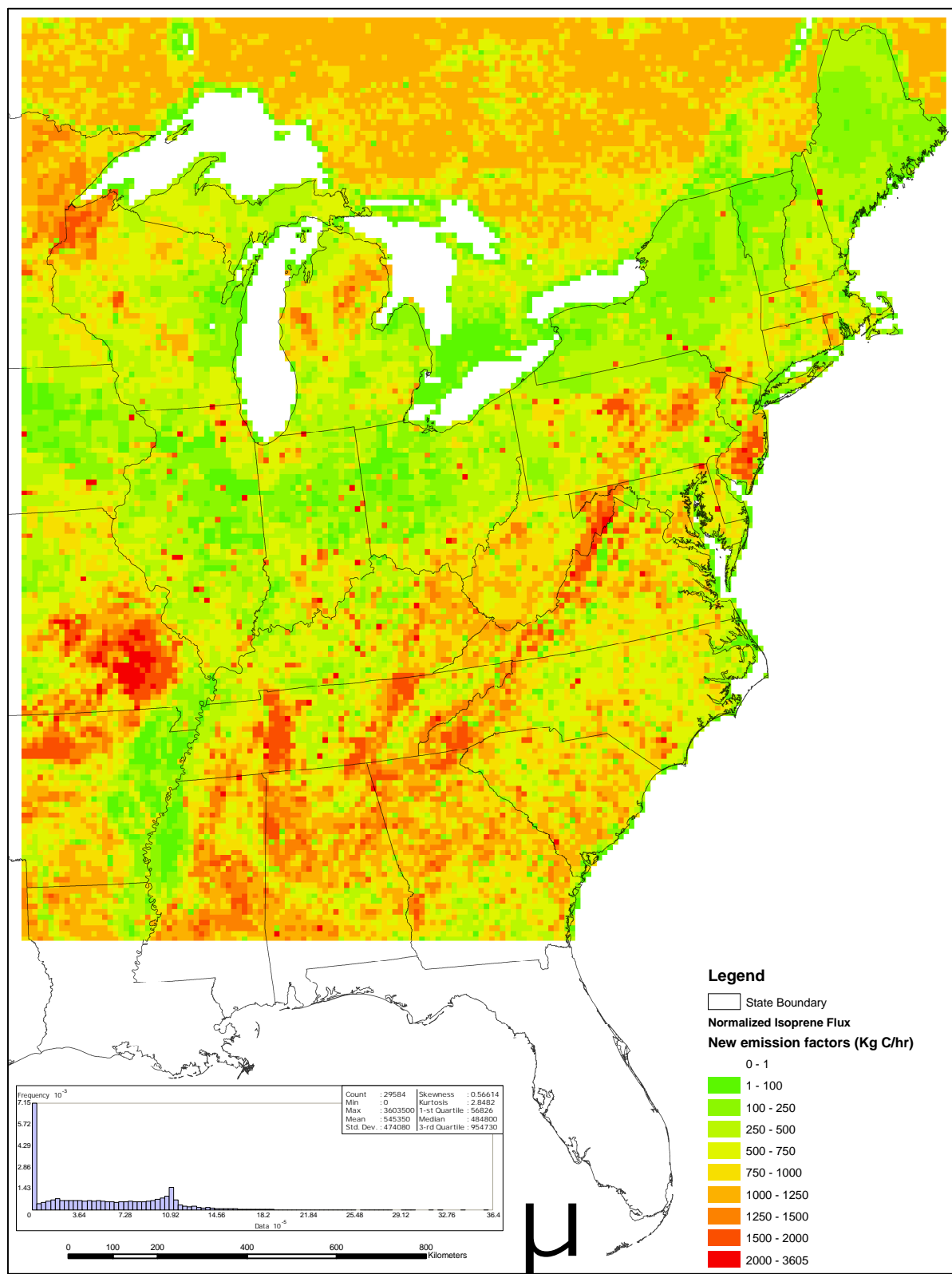
Figure 4.11: Temperature and light normalized isoprene emission using the BEIS allocation methodology and the updated (3.13) emission factors (GCS: NAD83).
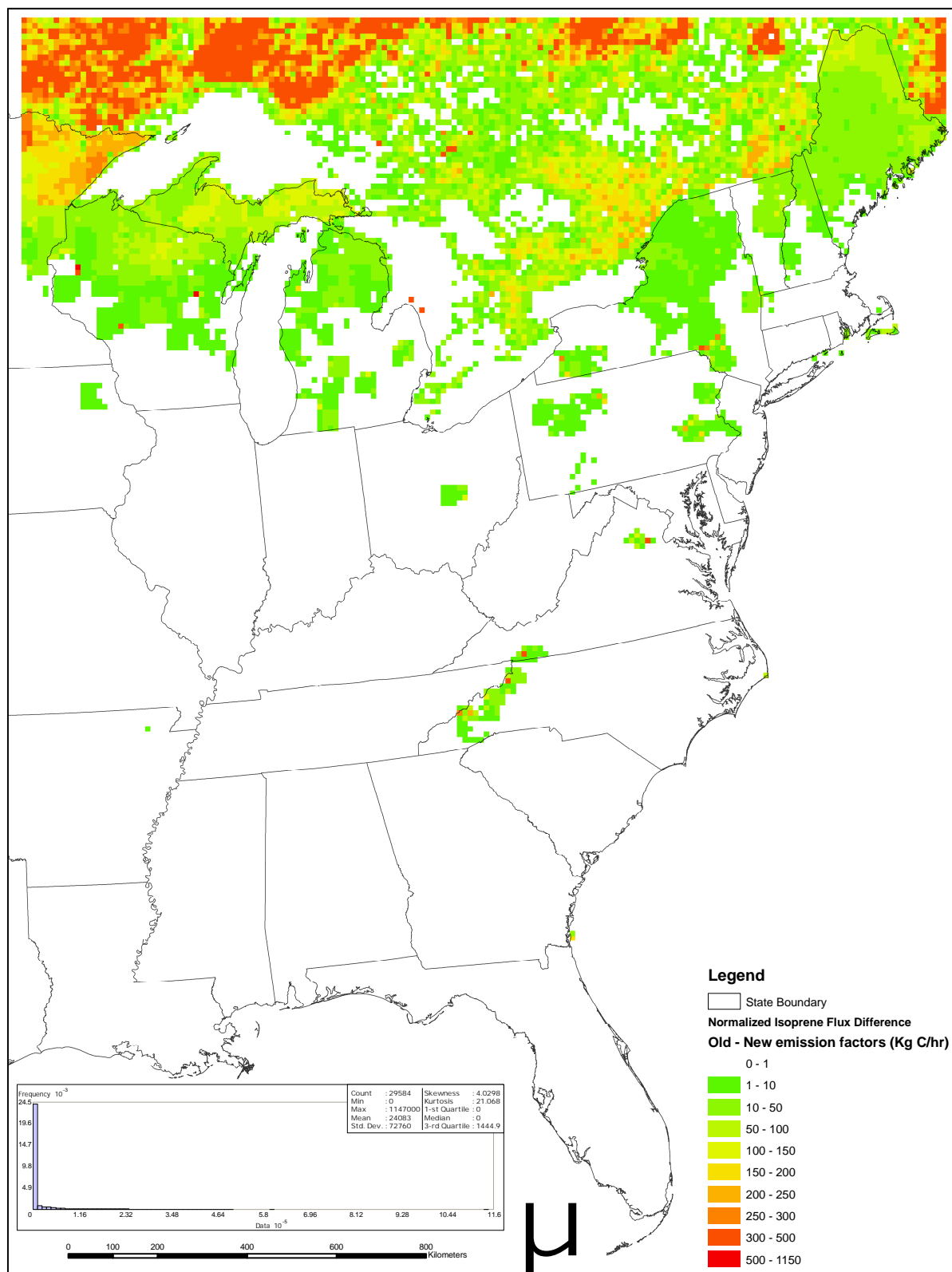
Figure 4.12: Difference between the standard BEIS (3.12) and the updated BEIS (3.13) temperature and light normalized isoprene emission potential (GCS: NAD83).
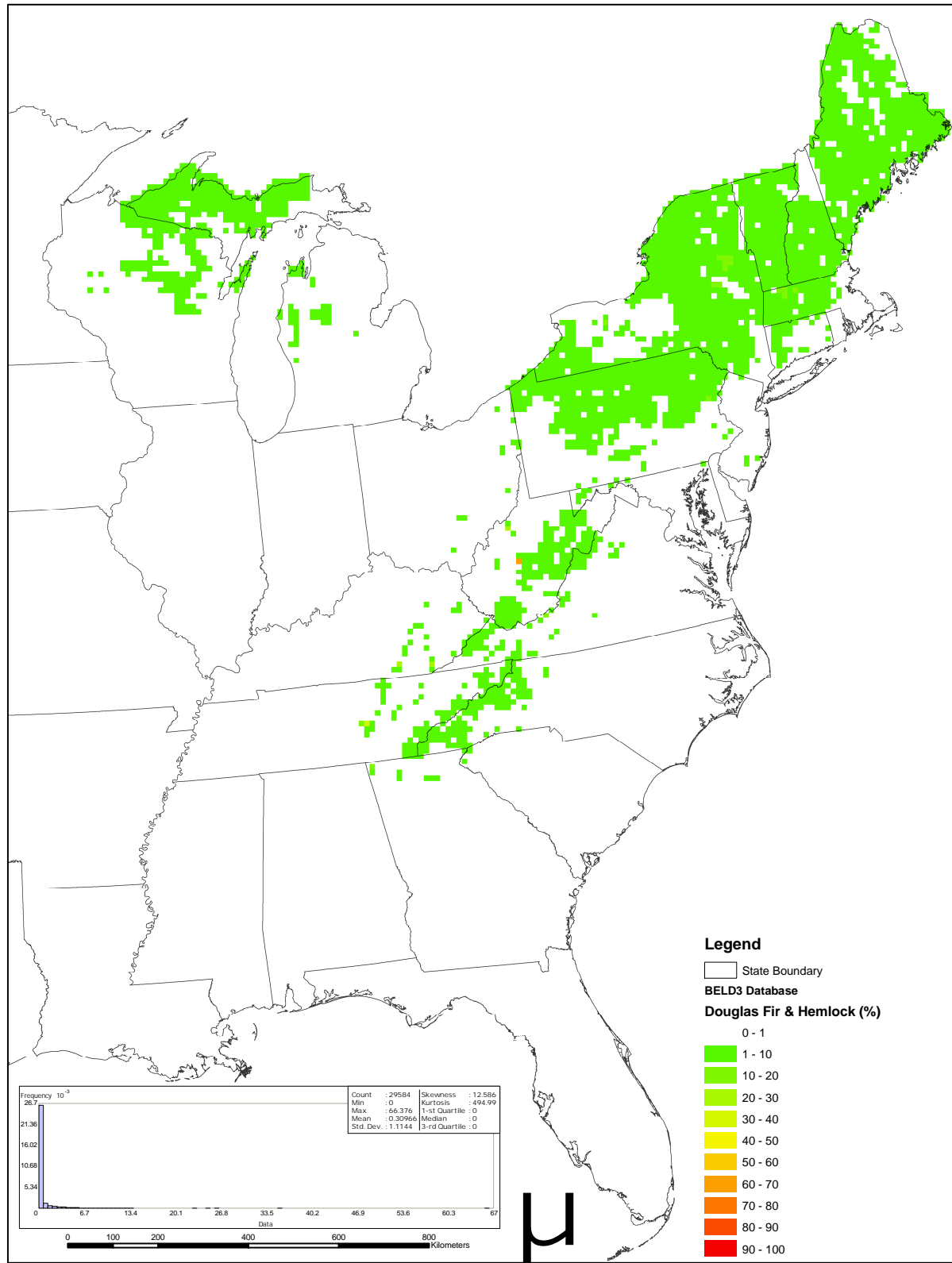
Figure 4.13: Combined Douglas Fir and Hemlock density based on the individual tree species included in BELD3 (GCS: NAD83).
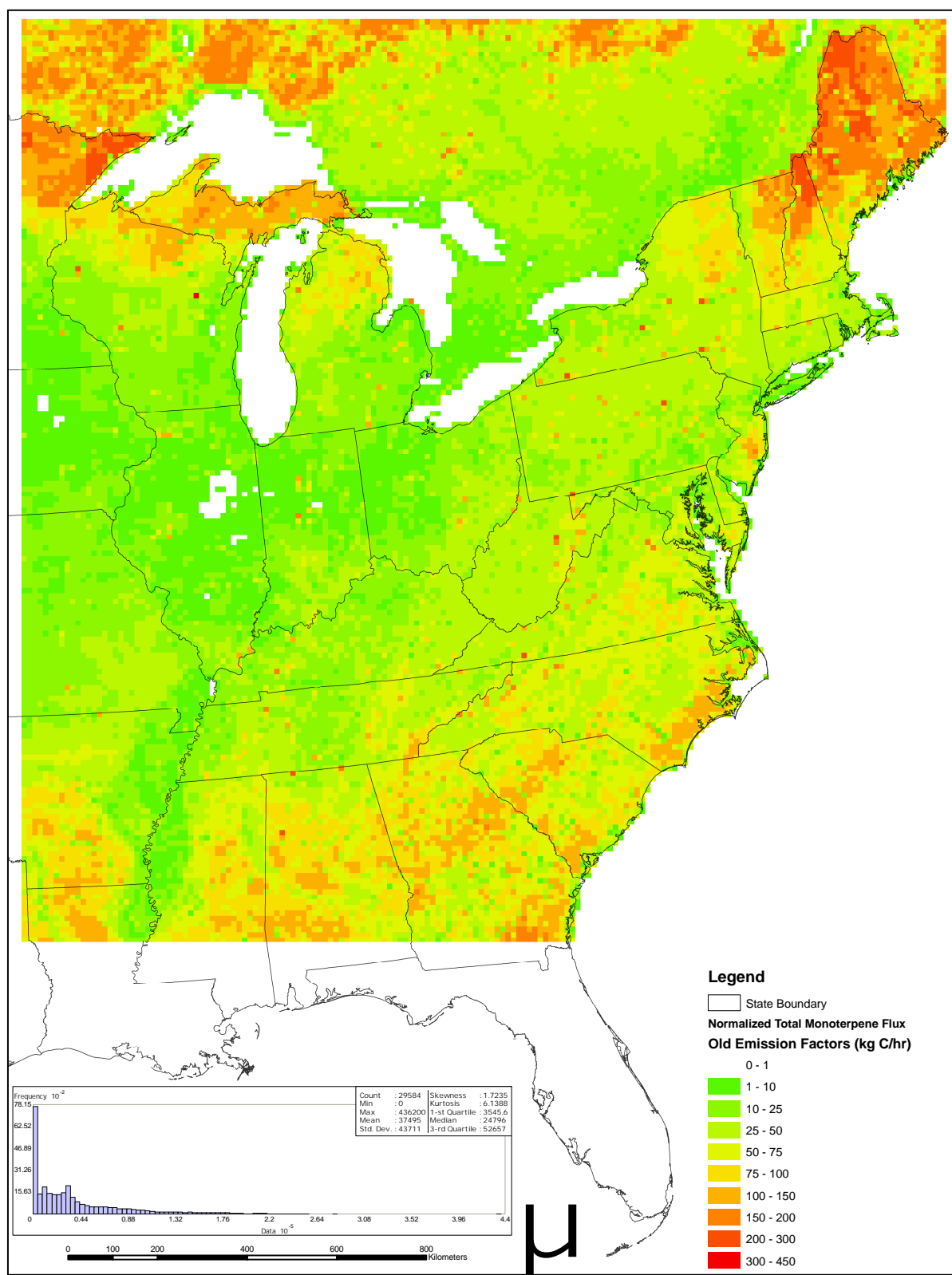
Figure 4.14: Temperature normalized monoterpene emission from the BEIS allocation methodology using the standard (3.12) emission factors (GCS: NAD83).
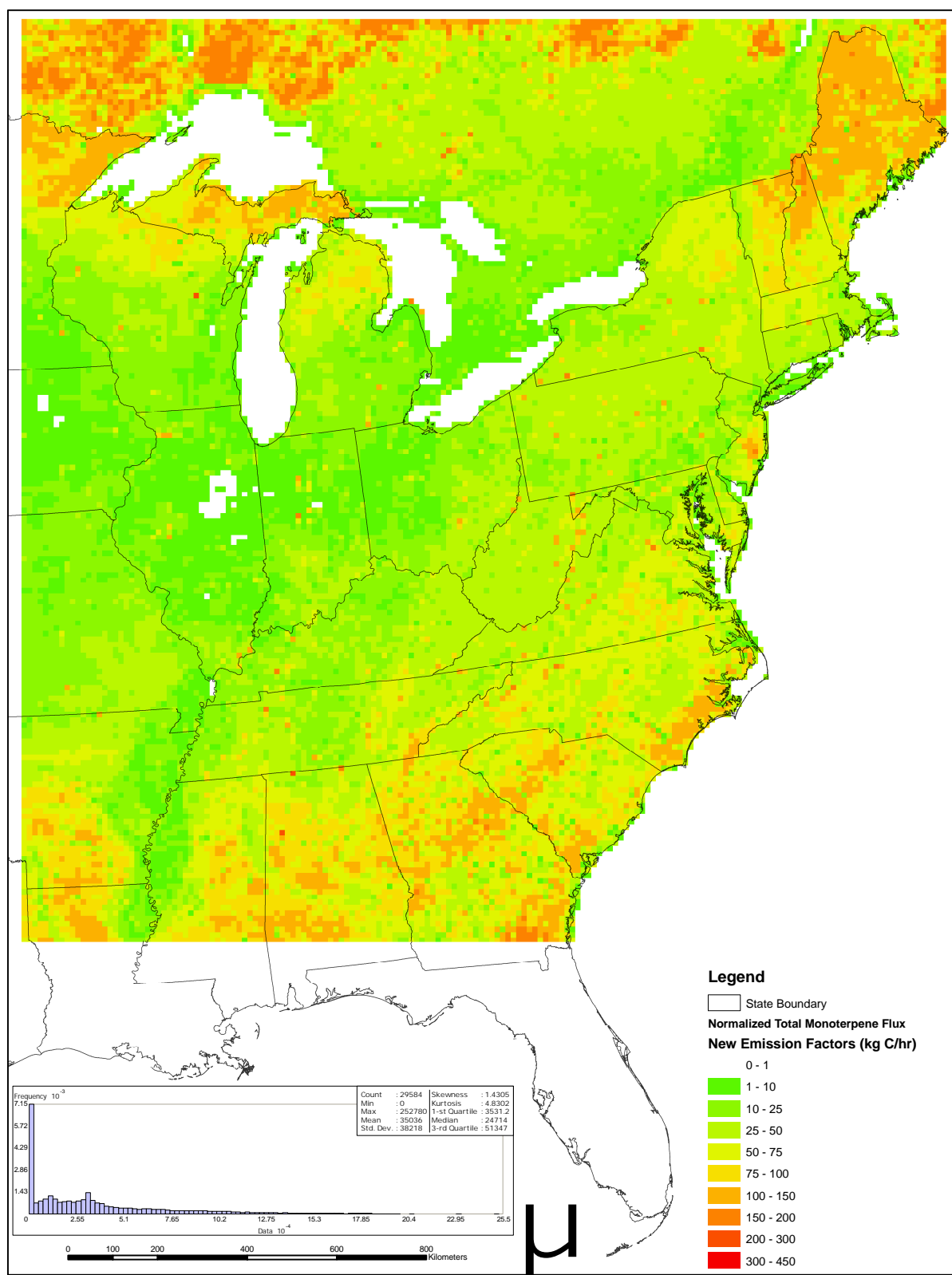
Figure 4.15: Temperature normalized monoterpene emission from the BEIS allocation methodology using the updated (3.13) emission factors (GCS: NAD83).
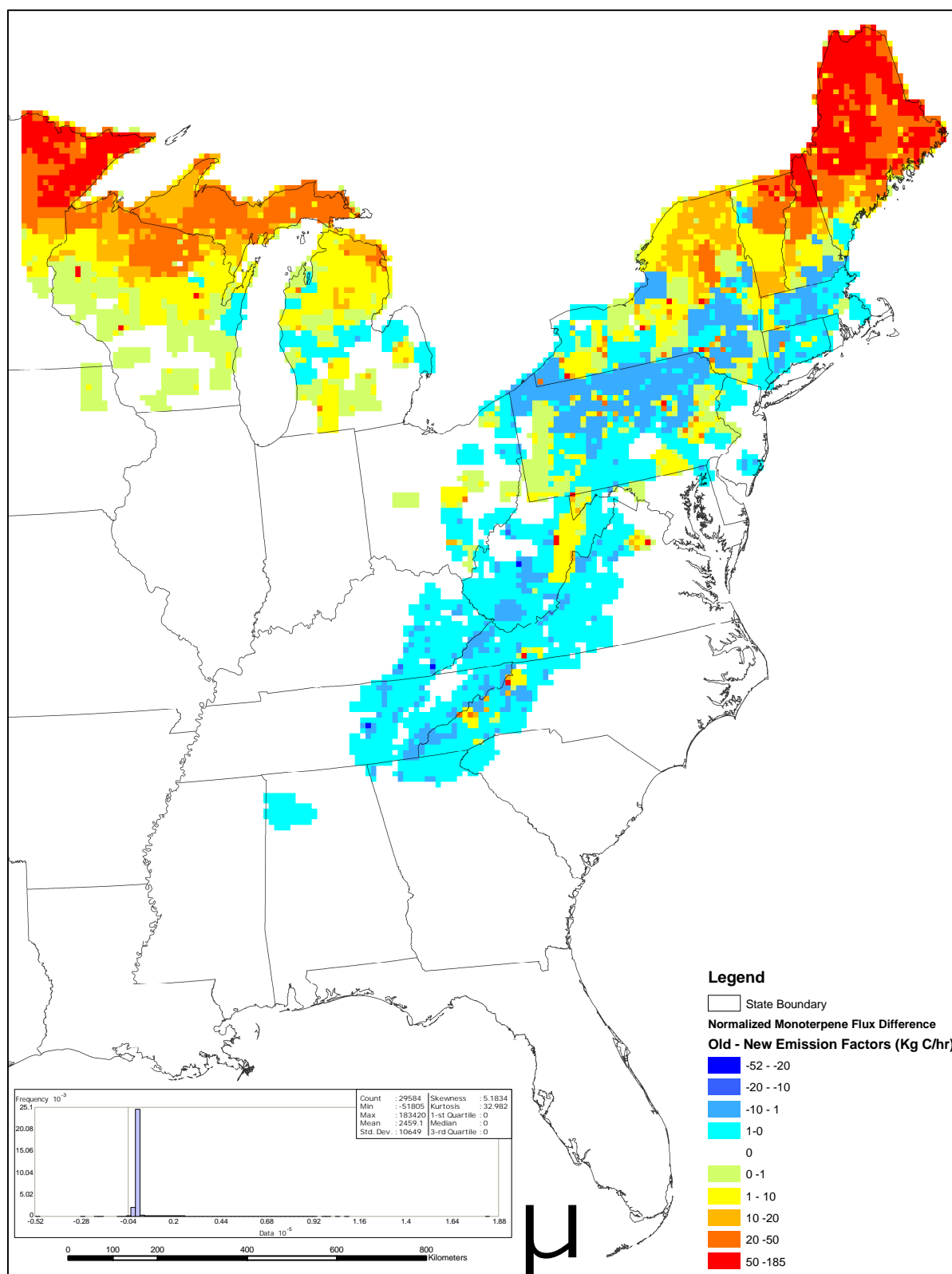
Figure 4.16: Difference between the standard BEIS (3.12) and the updated BEIS (3.13) temperature normalized monoterpene emission potential (GCS: NAD83).
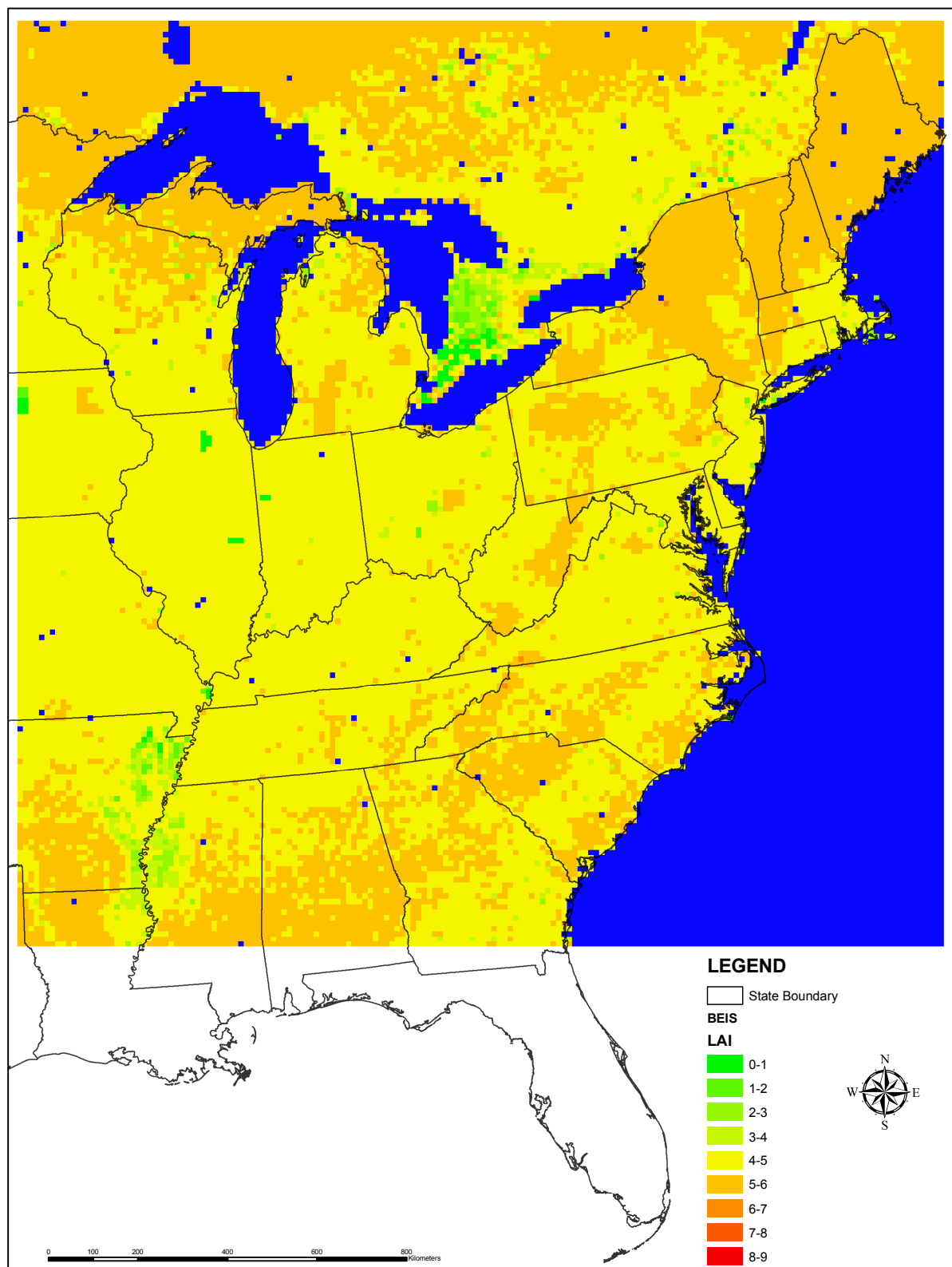
Figure 4.17: Leaf area index calculated based on the BEIS model (GCS: NAD83).
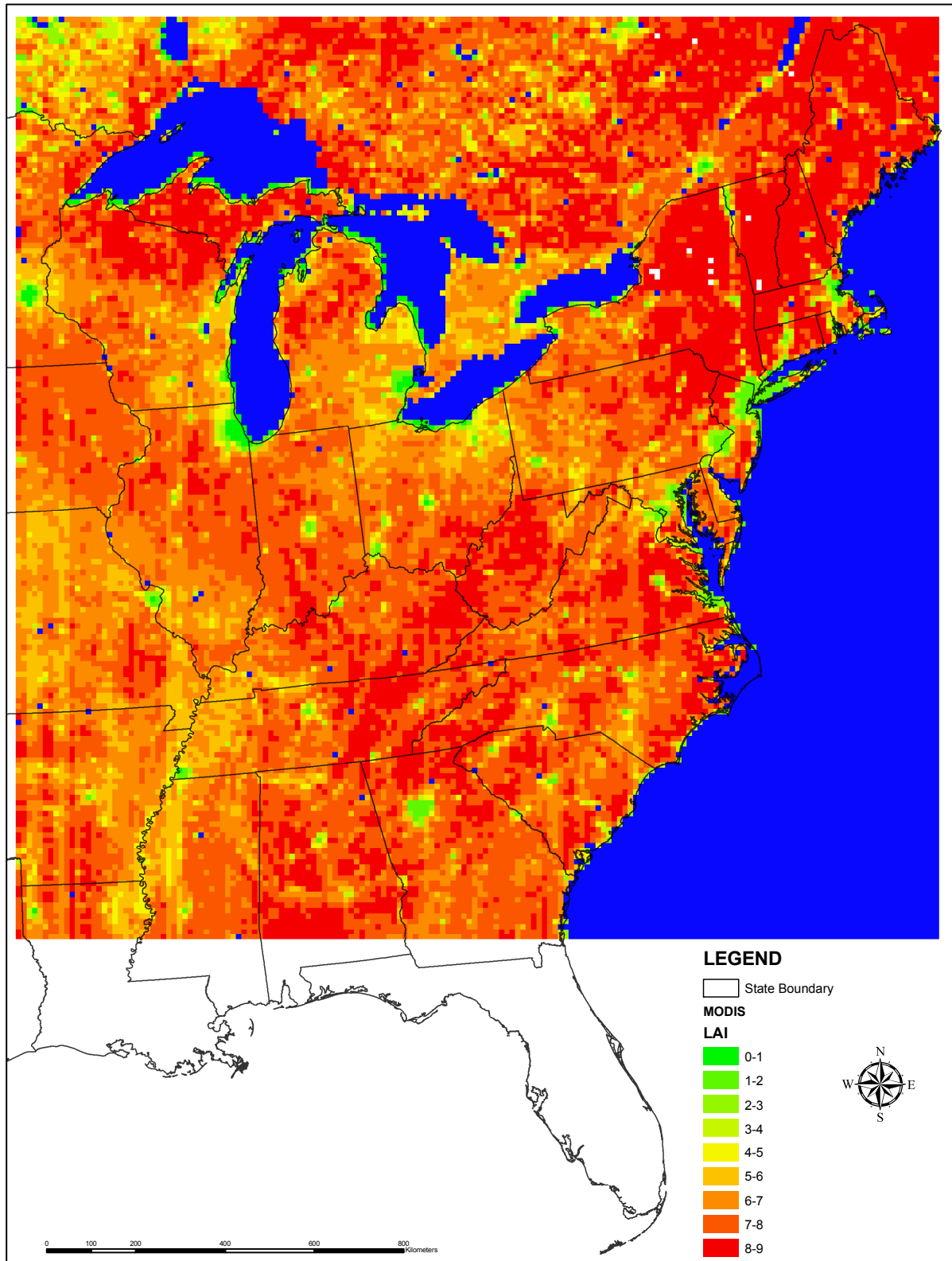
Figure 4.18: Leaf area index obtained from resampling the 8-day composite MODIS satellite product for the first acquisition period of August 2007 (GCS: NAD83).
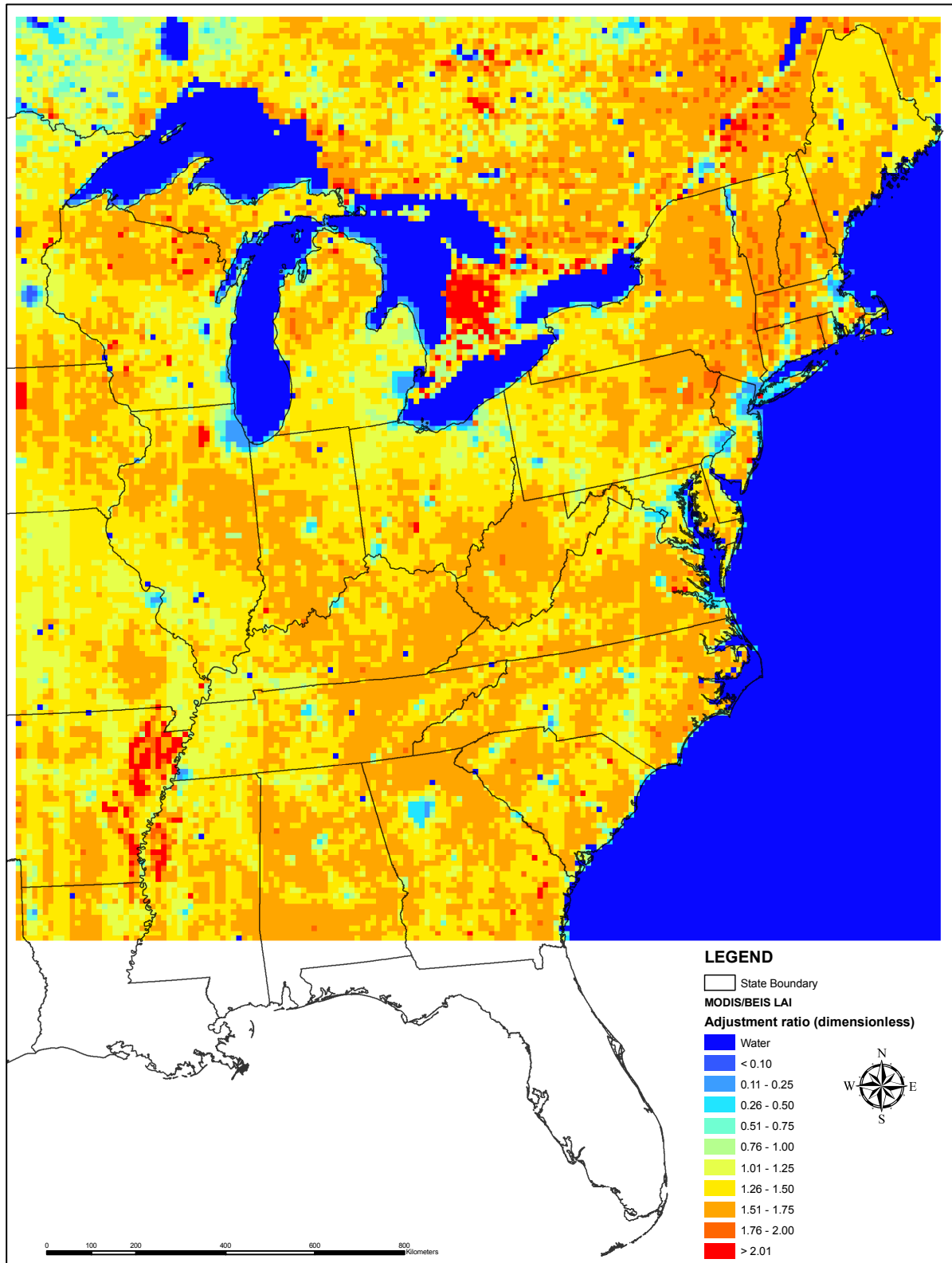
Figure 4.19: Map showing the ratio of the MODIS over the BEIS leaf area index estimate for each cell of the OTC domain (GCS: NAD83).
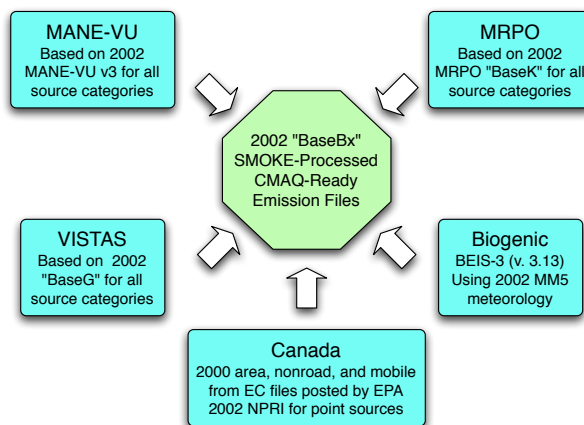
Figure 4.20: Overview of the data collection processing for the OTC/MANEVU domain under the SMOKE/Models-3 framework.
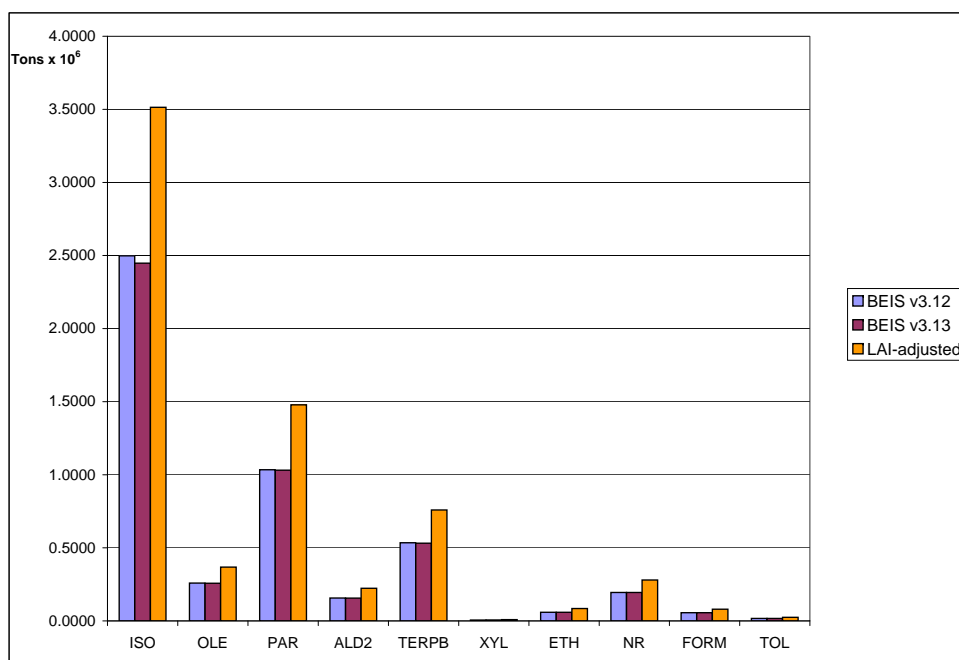
Figure 4.21: Total biogenic emissions during the month of August 2002, mapped according to the CB-IV chemical mechanism species, for the 3 major scenarios developed for the OTC domain.
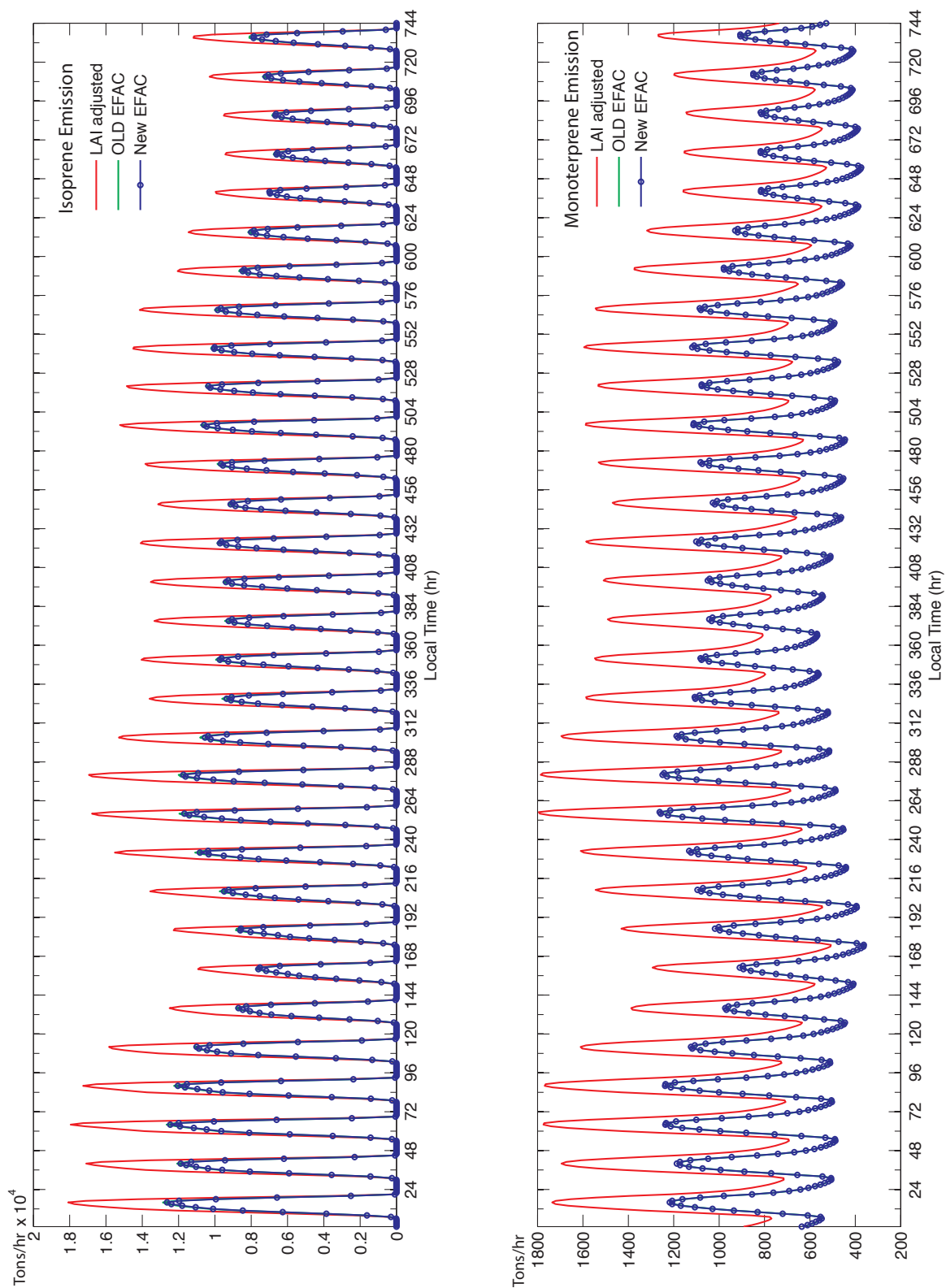
Figure 4.22: Hourly isoprene and monoterpene emission time series for the entire OTC domain, during the three simulated scenarios for the month of August 2002.
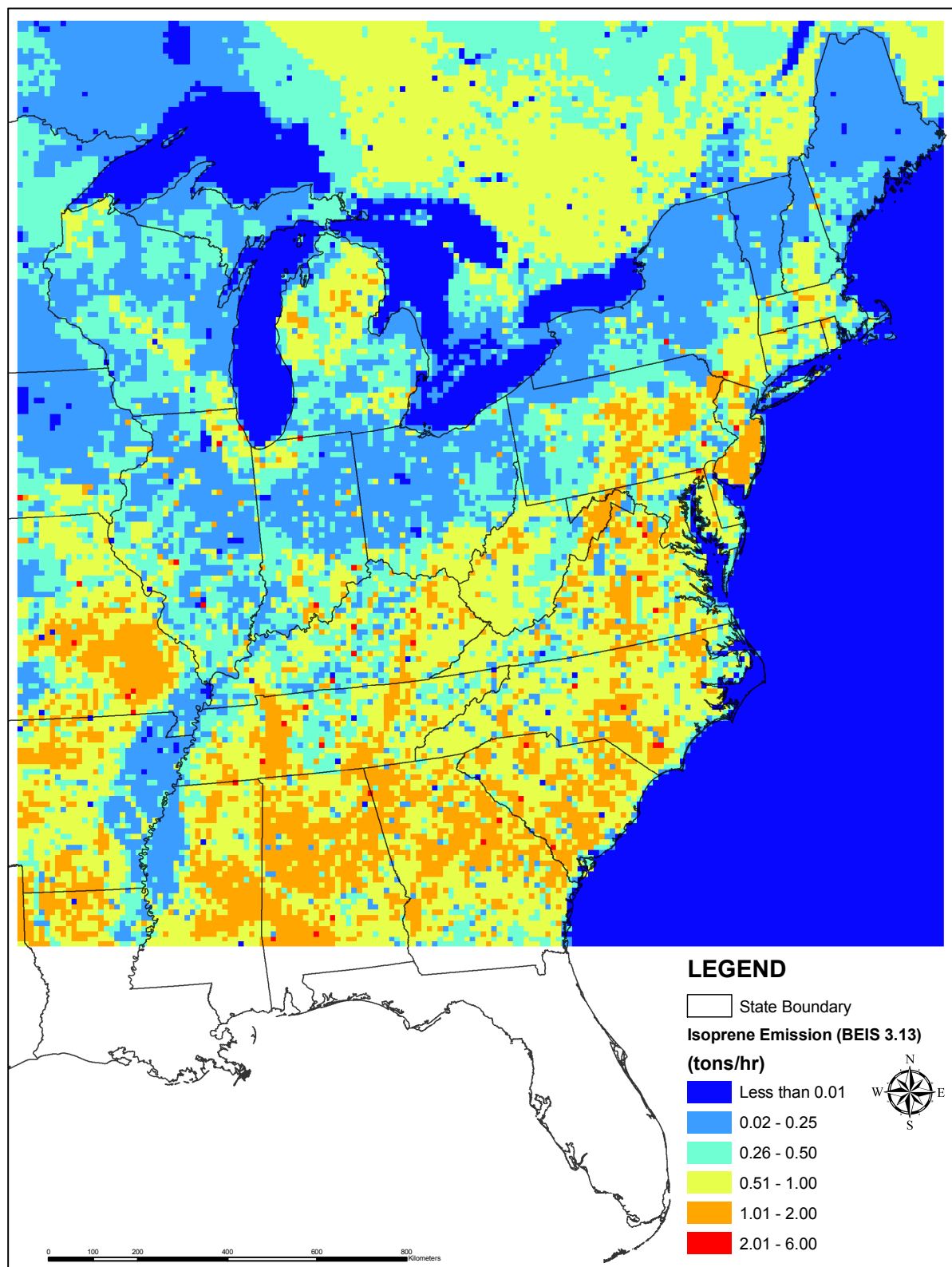
Figure 4.23: Hourly isoprene emission between 10 and 11 am of August 12th calculated with the updated BEIS (3.13) (GCS: NAD83).
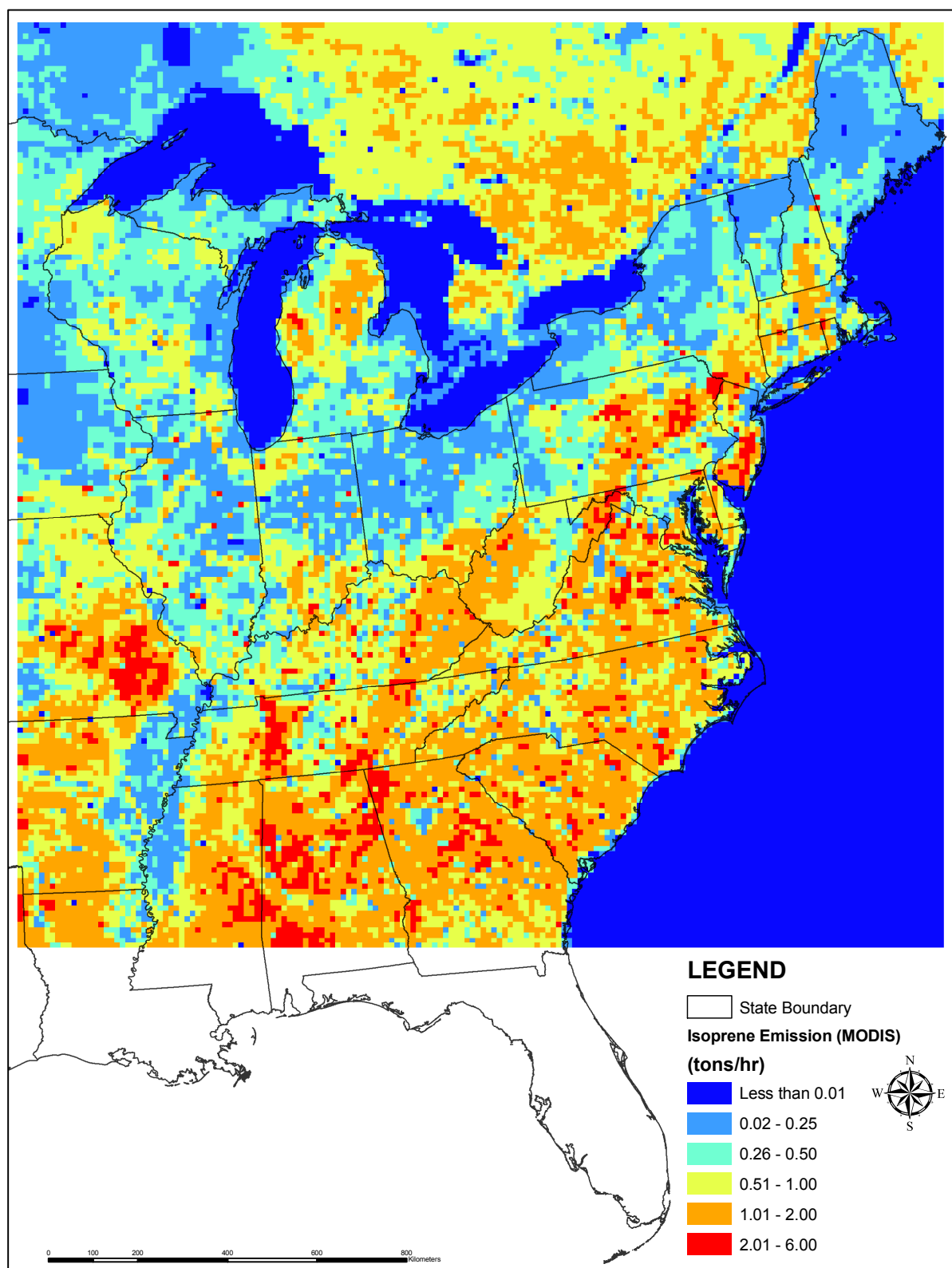
Figure 4.24: Hourly isoprene emission between 10 and 11 am of August 12th calculated with the MODIS adjusted BEIS (GCS: NAD83).
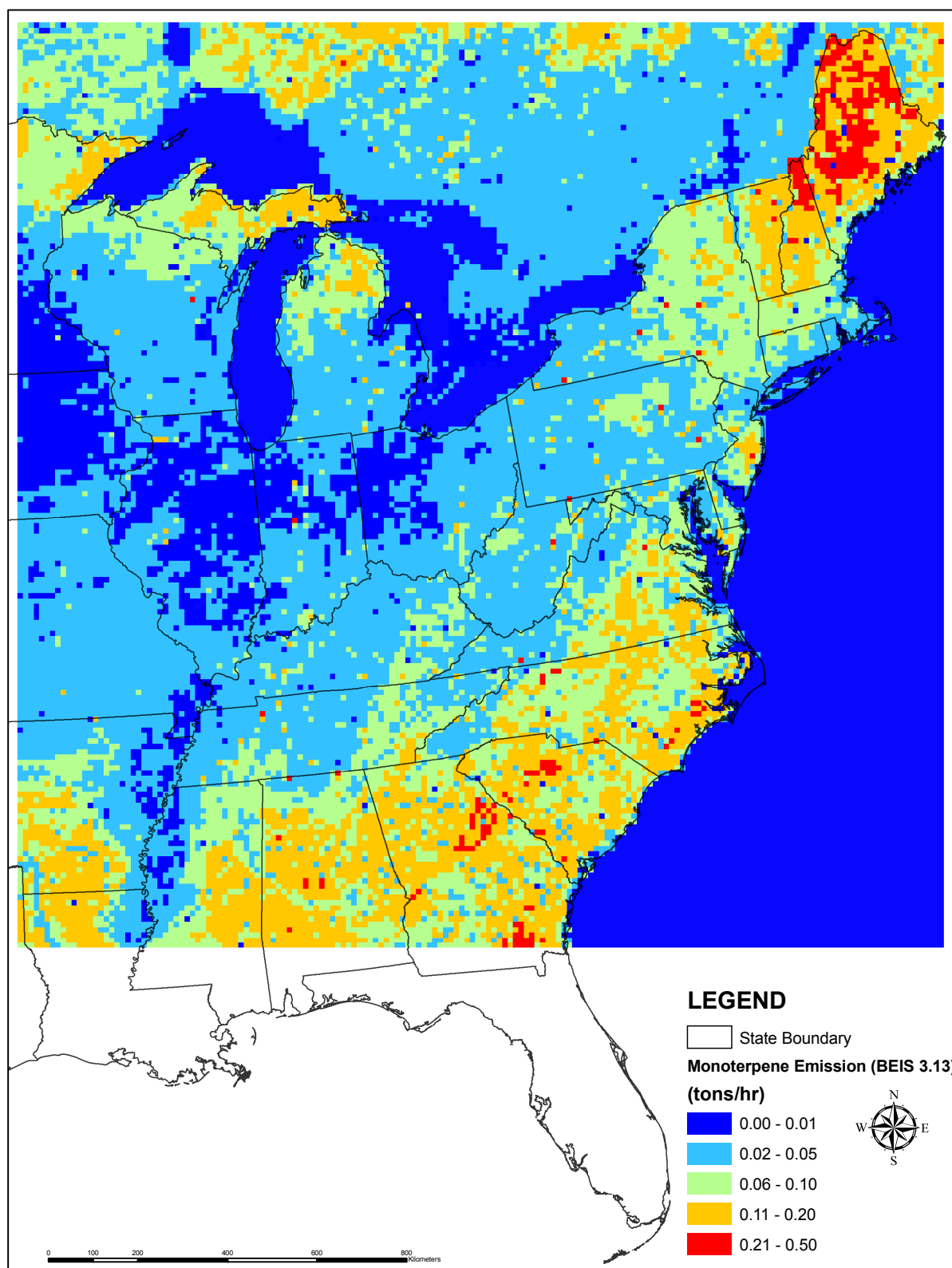
Figure 4.25: Hourly total monoterpene emission between 10 and 11 am of August 12th calculated with the updated BEIS (3.13) (GCS: NAD83).
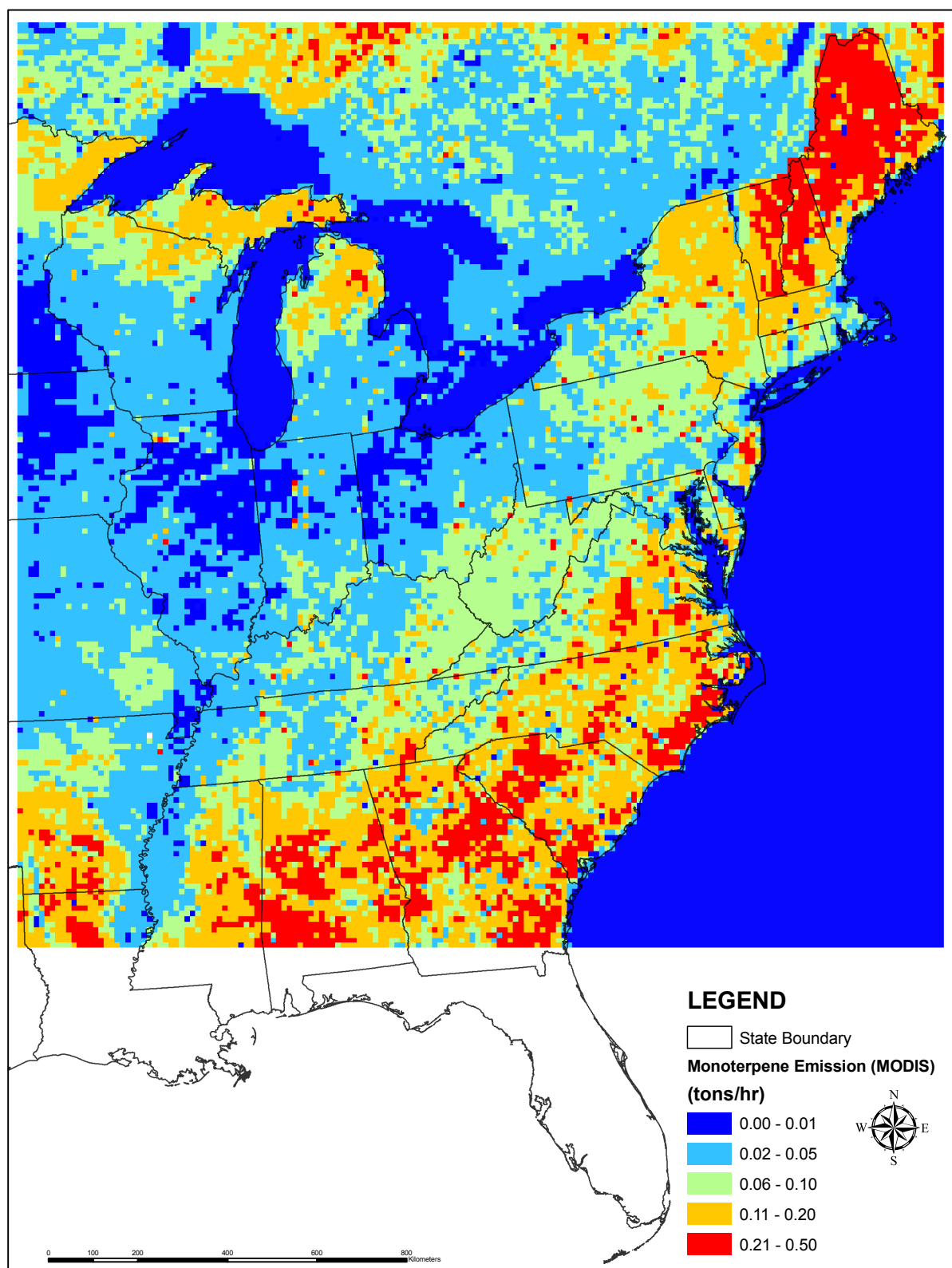
Figure 4.26: Hourly total monoterpene emission between 10 and 11 am of August 12th calculated with the MODIS adjusted BEIS (GCS: NAD83).
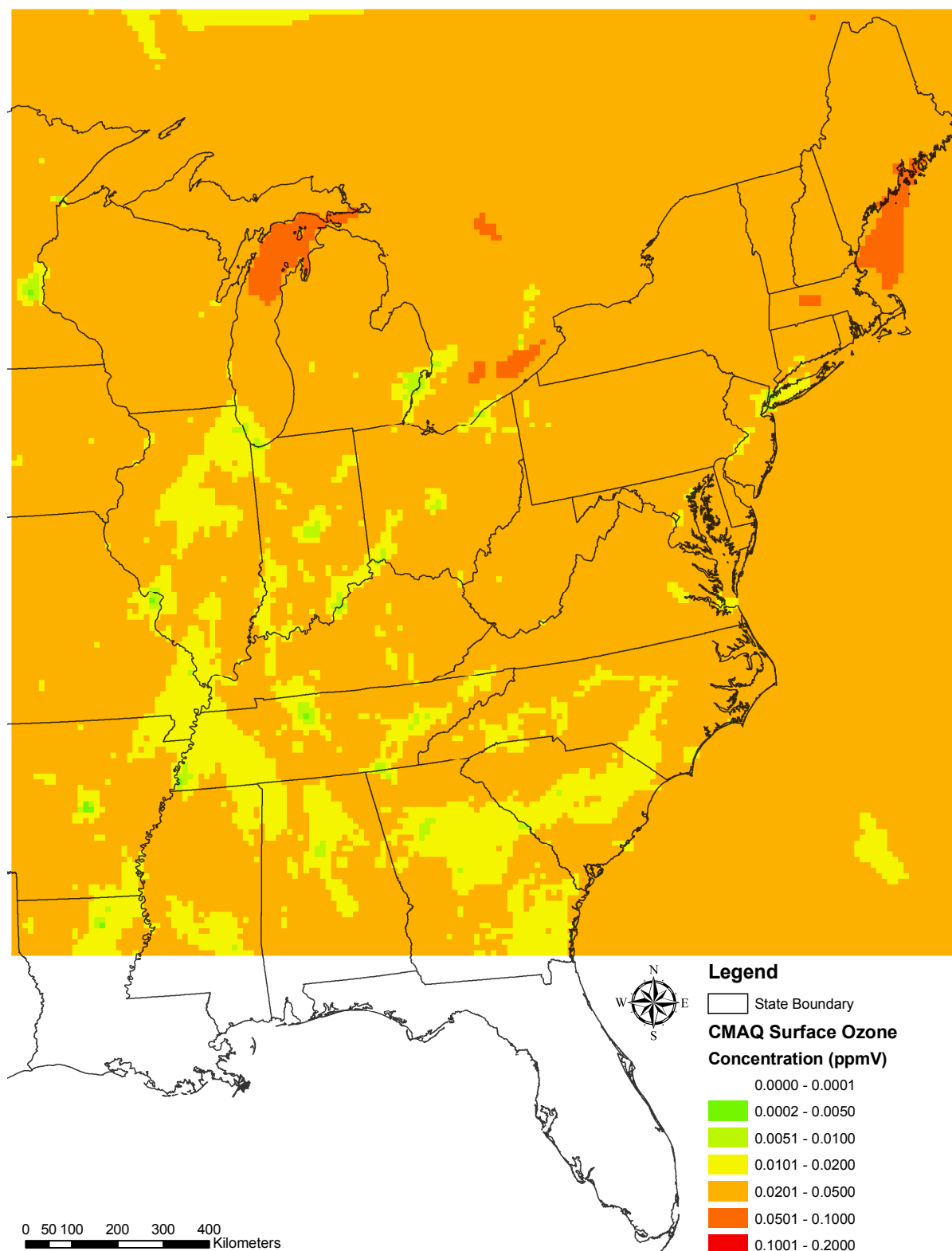
Figure 4.27: Surface ozone concentration calculated with the CMAQ model between 8 and 9 am of August 12th using no biogenic emissions (Scenario 1) (GCS: NAD83).
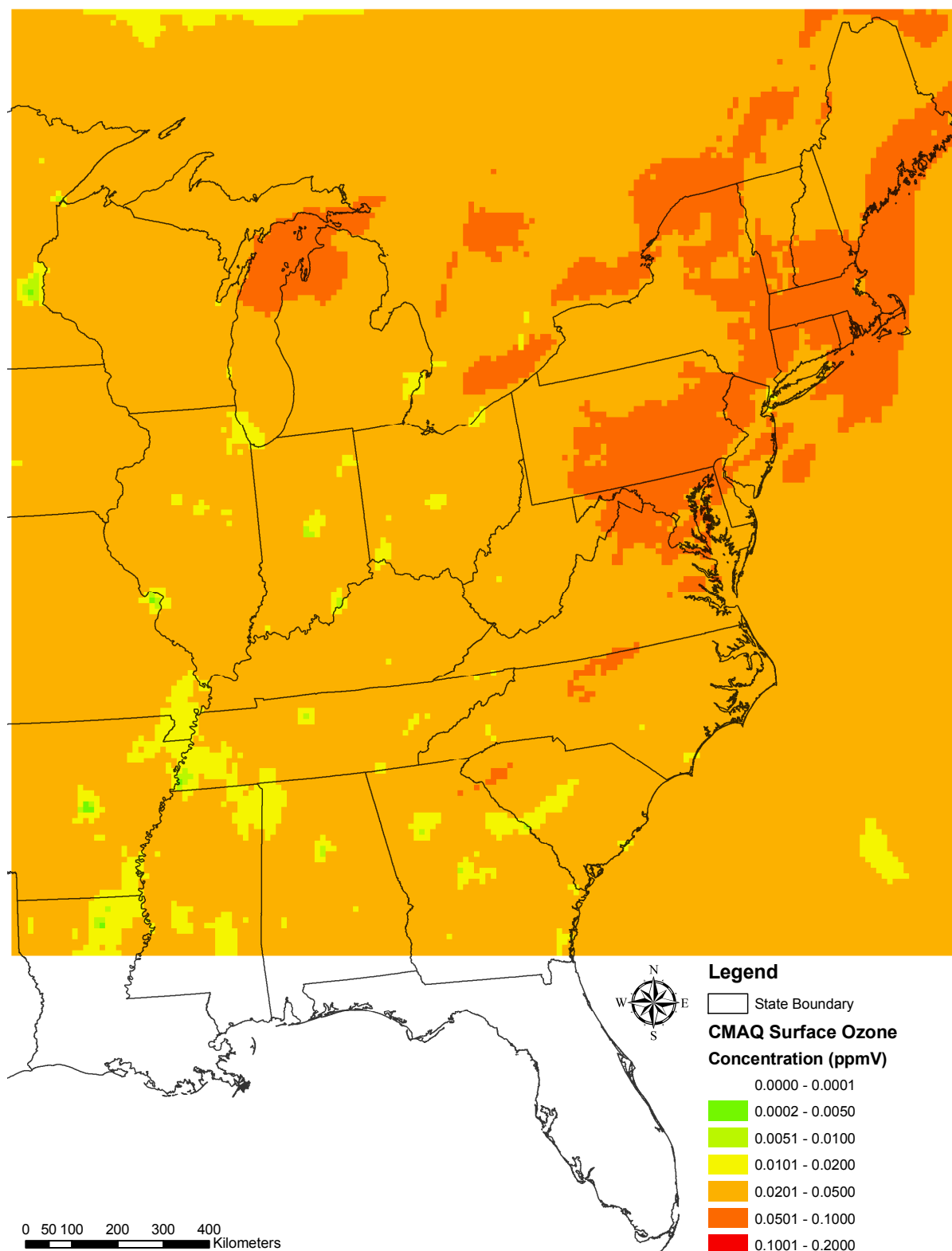
Figure 4.28: Surface ozone concentration calculated with the CMAQ model between 8 and 9 am of August 12th using the updated BEIS 3.13 emission factors (Scenario 2) (GCS: NAD83).
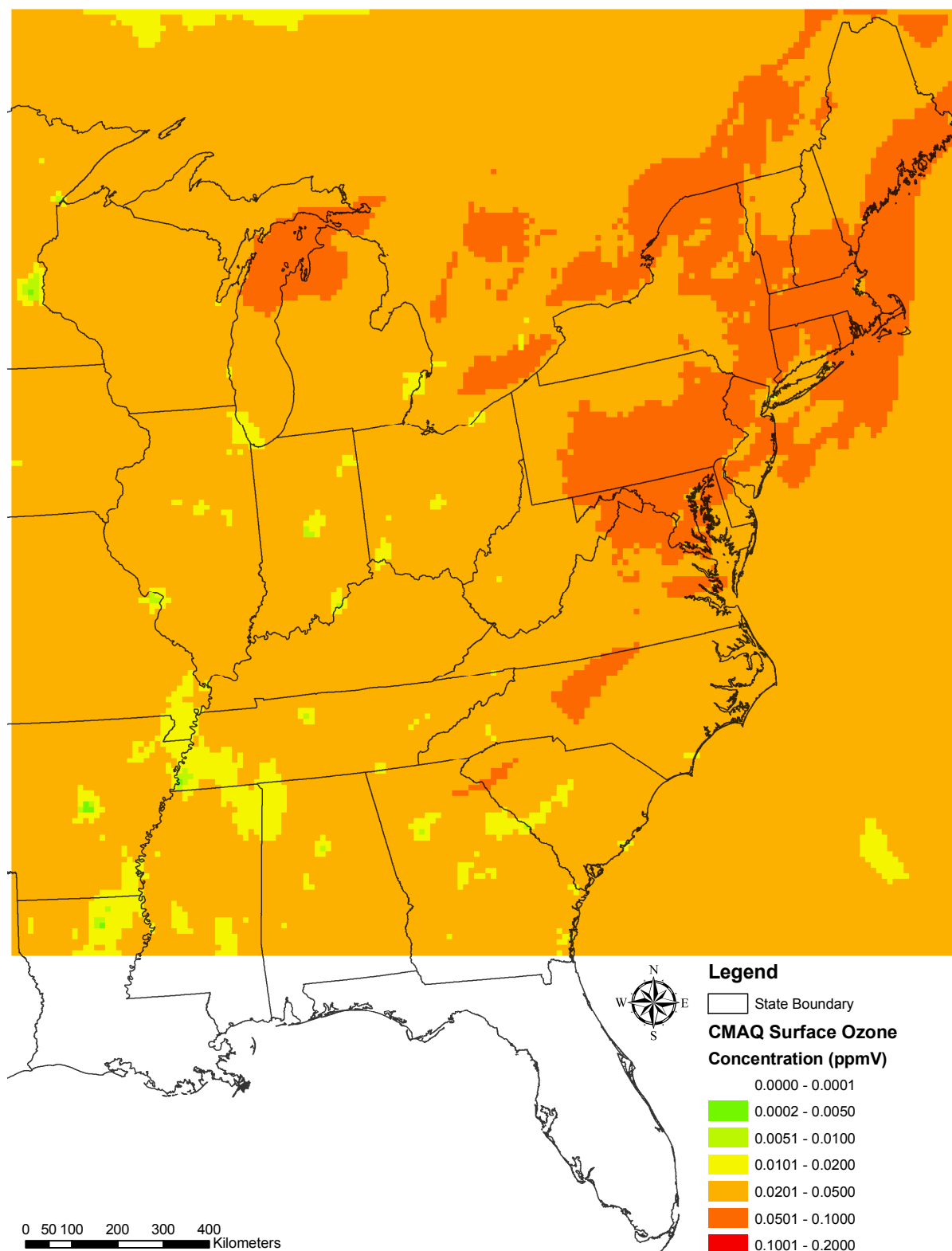
Figure 4.29: Surface ozone concentration calculated with the CMAQ model between 8 and 9 am of August 12th using MODIS adjusted LAI for isoprene emissions (Scenario 3) (GCS: NAD83).
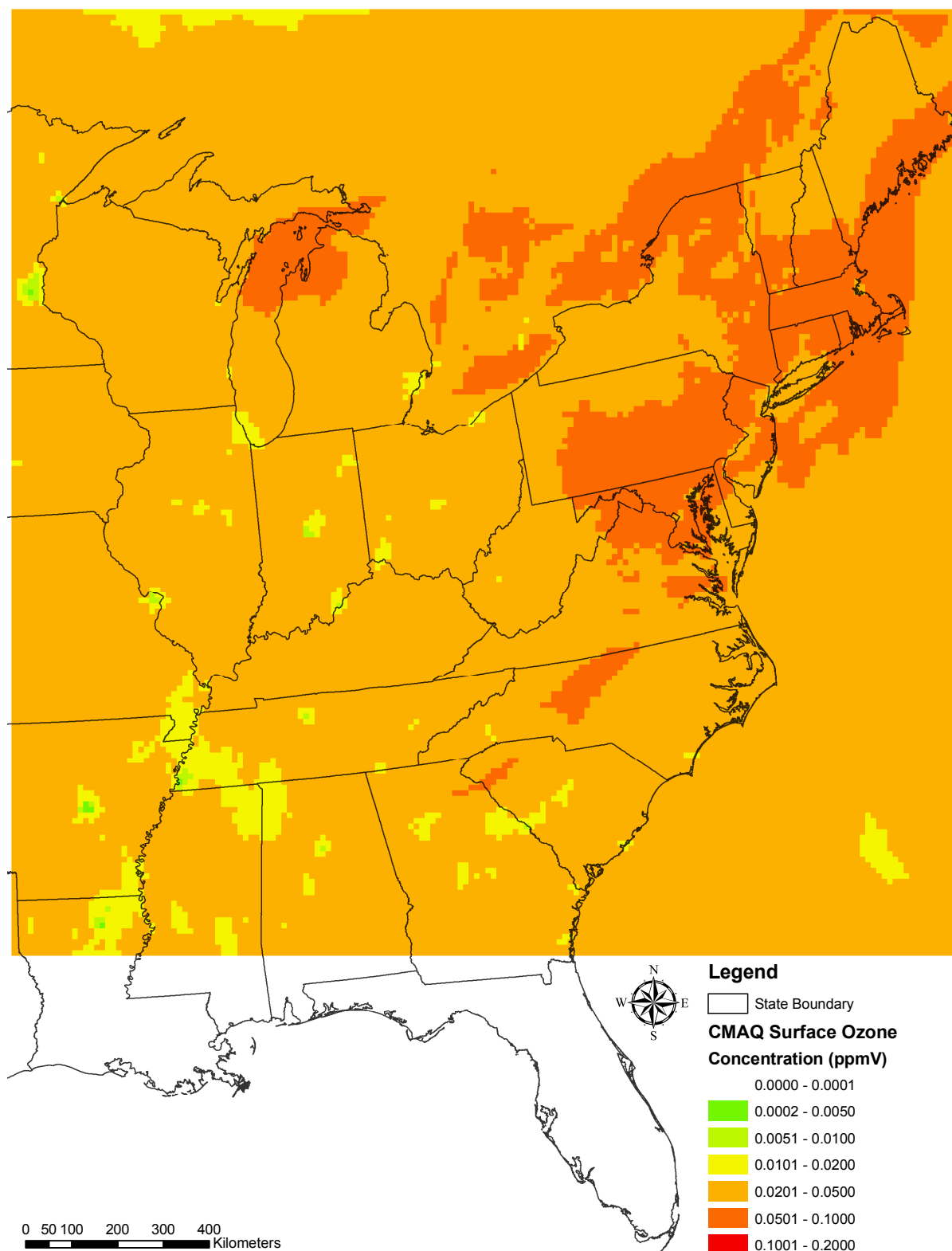
Figure 4.30: Surface ozone concentration calculated with the CMAQ model between 8 and 9 am of August 12th using MODIS adjusted LAI for all biogenic emissions (Scenario 4) (GCS: NAD83).
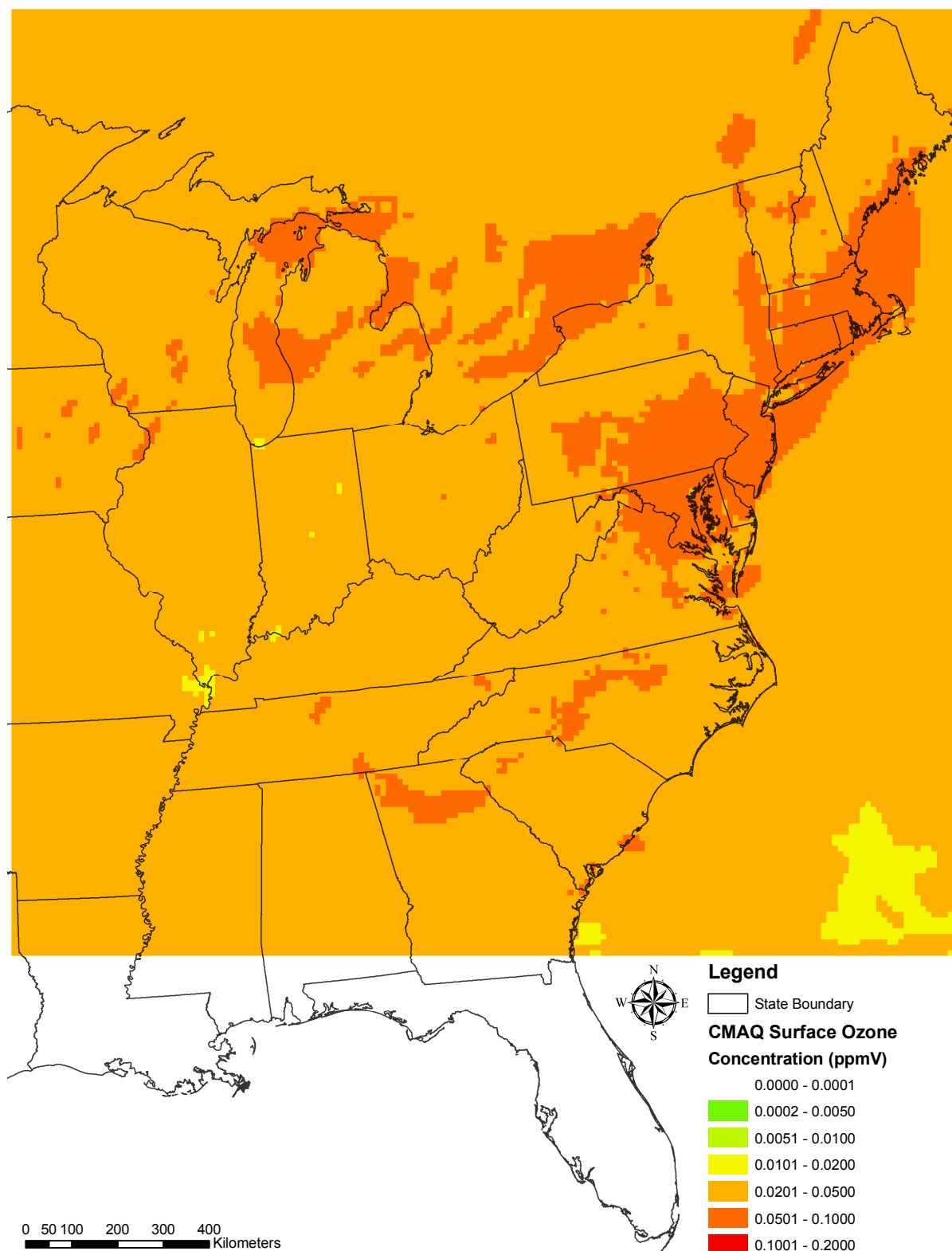
Figure 4.31: Surface ozone concentration calculated with the CMAQ model between 12 and 1 pm of August 12th using no biogenic emissions (Scenario 1) (GCS: NAD83).
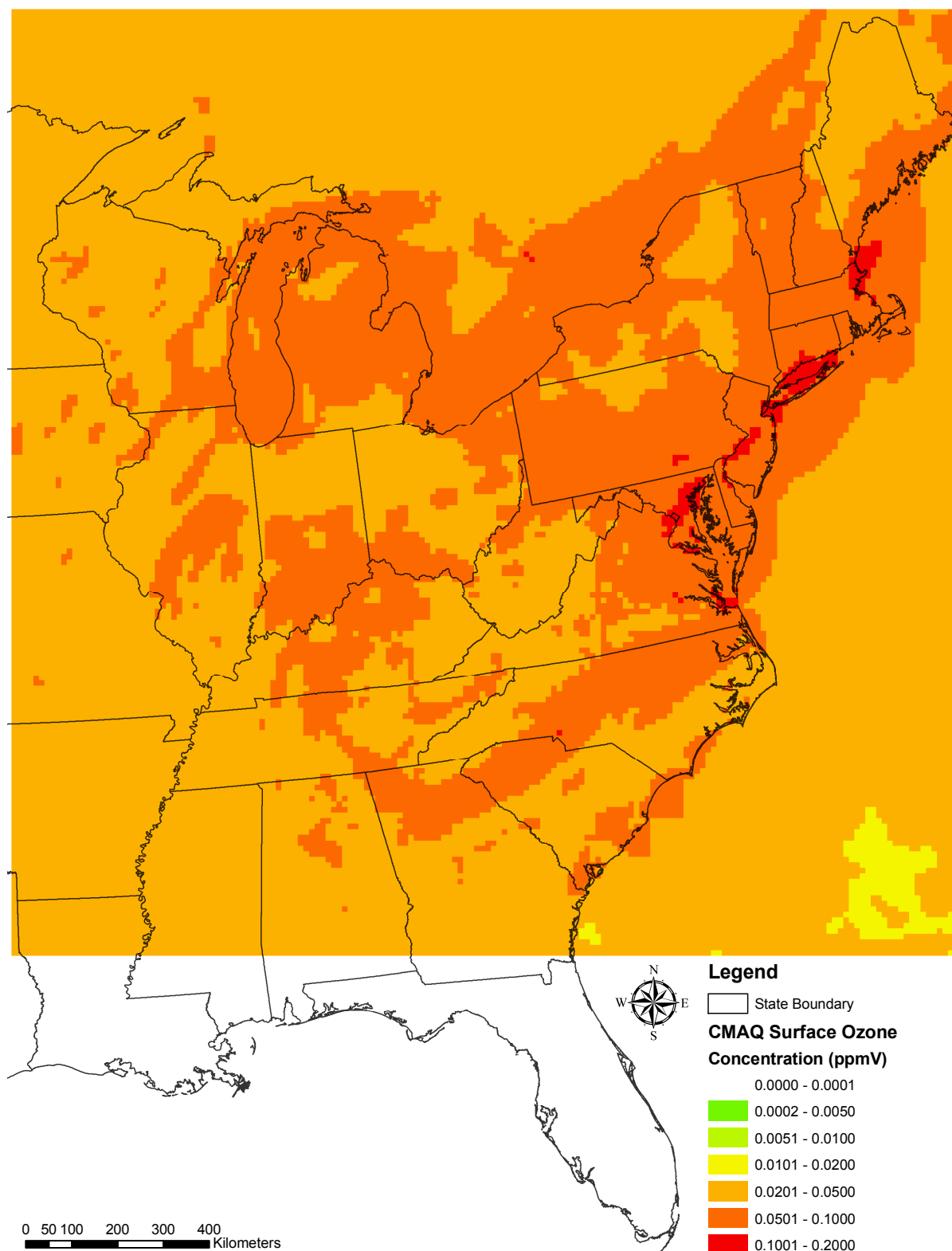
Figure 4.32: Surface ozone concentration calculated with the CMAQ model between 12 and 1 pm of August 12th using the updated BEIS 3.13 emission factors (Scenario 2) (GCS: NAD83).
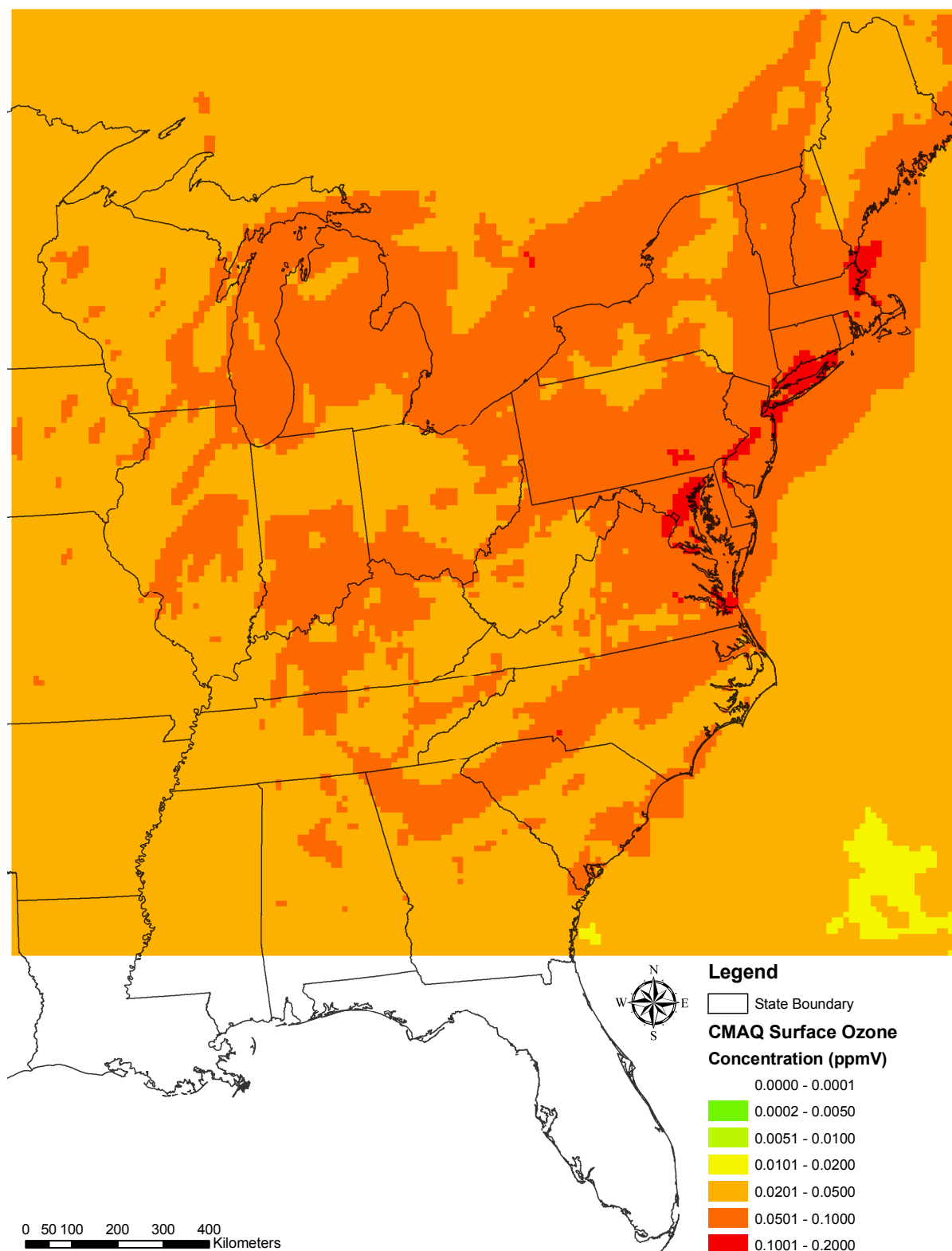
Figure 4.33: Surface ozone concentration calculated with the CMAQ model between 12 and 1 pm of August 12th using MODIS adjusted LAI for isoprene emissions (Scenario 3) (GCS: NAD83).
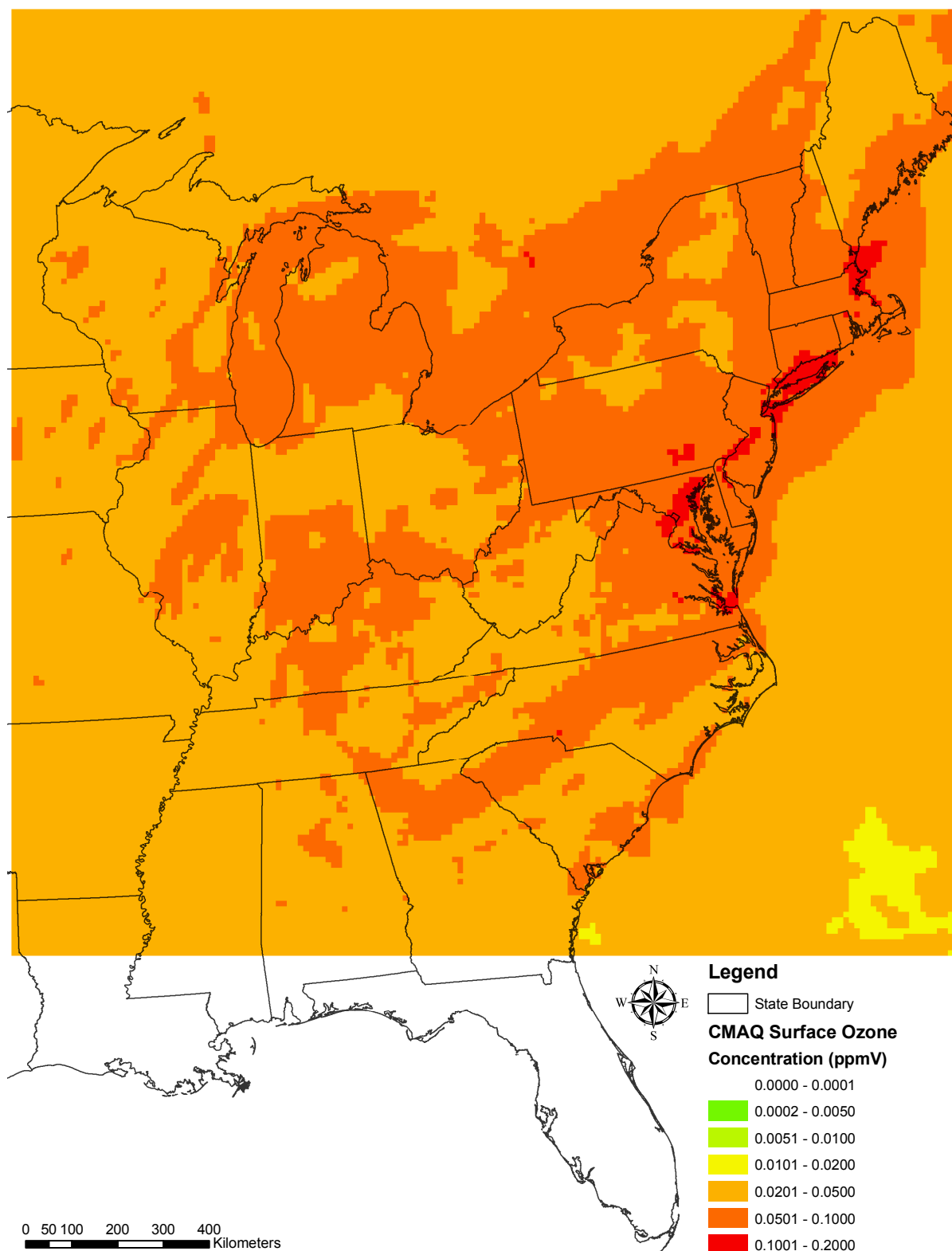
Figure 4.34: Surface ozone concentration calculated with the CMAQ model between 12 and 1 pm of August 12th using MODIS adjusted LAI for all biogenic emissions (Scenario 4) (GCS: NAD83).
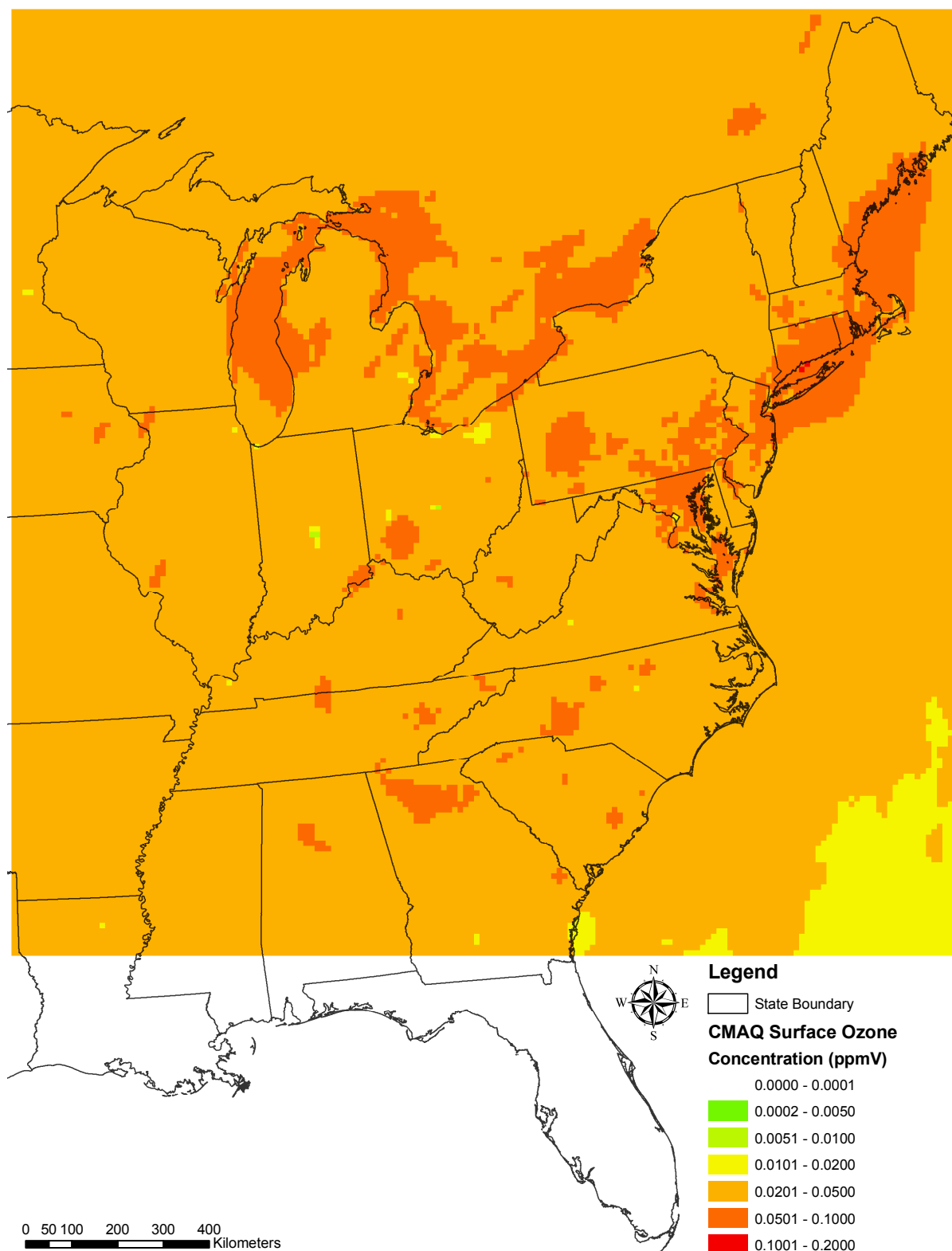
Figure 4.35: Surface ozone concentration calculated with the CMAQ model between 4 and 5 pm of August 12th using no biogenic emissions (Scenario 1) (GCS: NAD83).
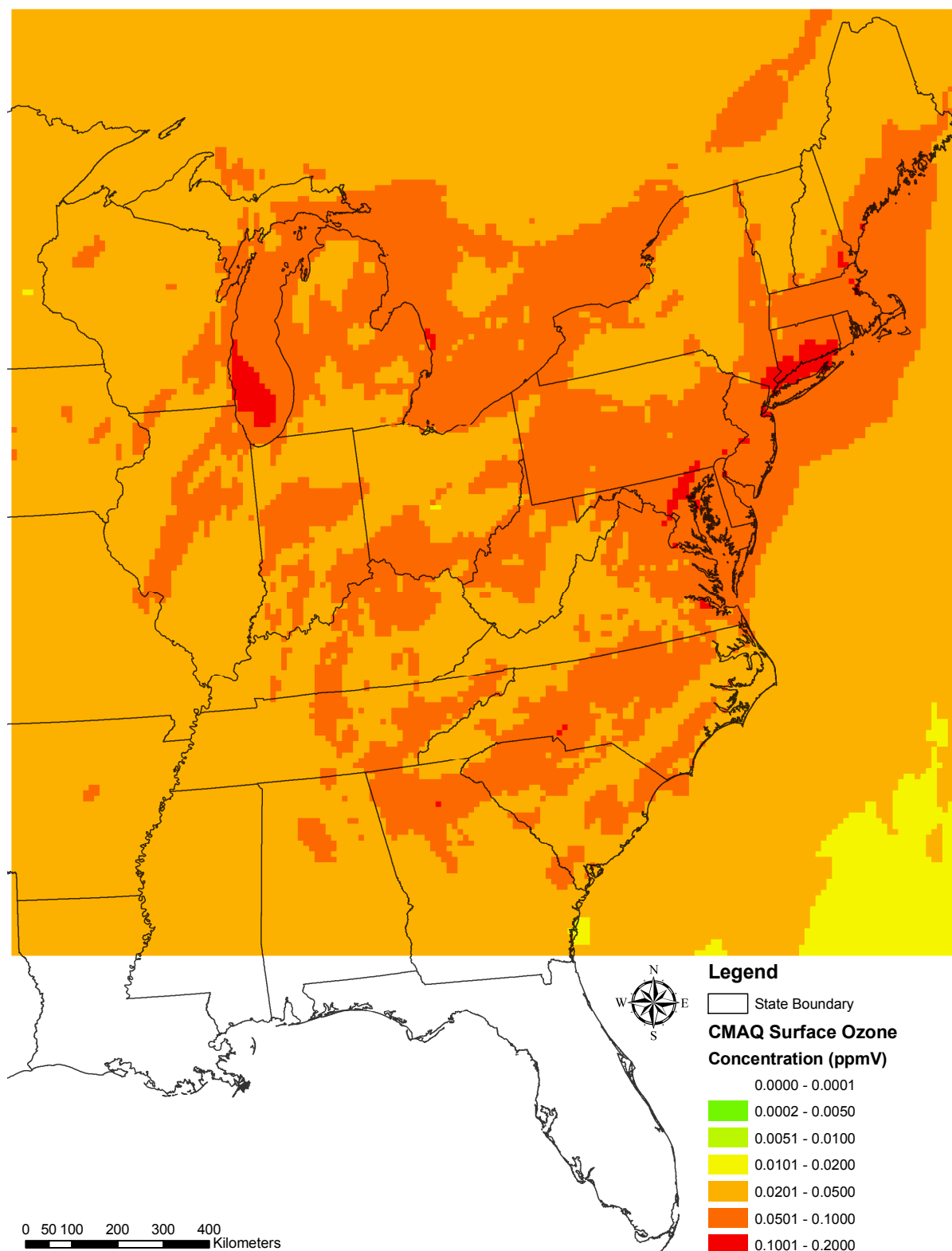
Figure 4.36: Surface ozone concentration calculated with the CMAQ model between 4 and 5 pm of August 12th using the updated BEIS 3.13 emission factors (Scenario 2) (GCS: NAD83).
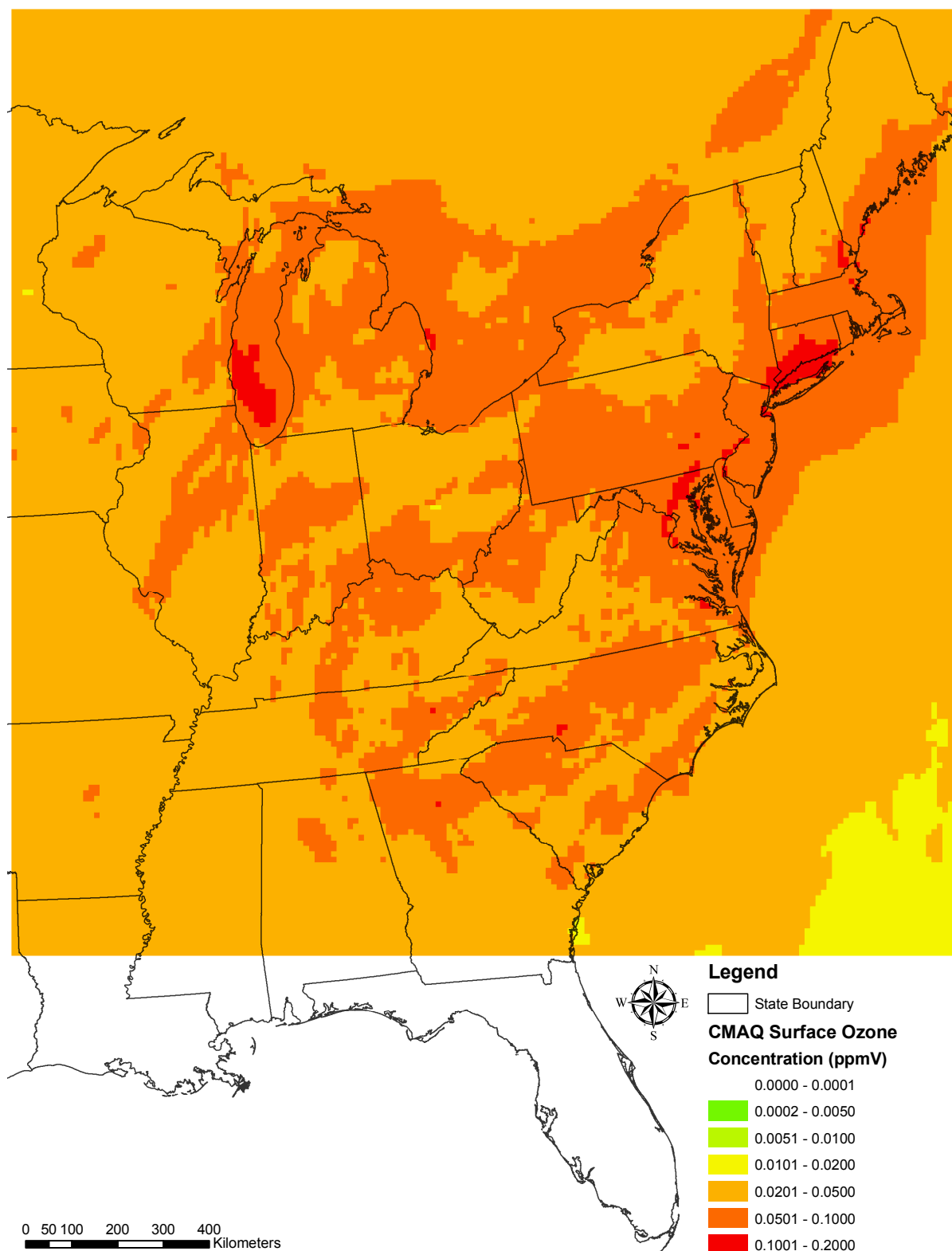
Figure 4.37: Surface ozone concentration calculated with the CMAQ model between 4 and 5 pm of August 12th using MODIS adjusted LAI for isoprene emissions (Scenario 3) (GCS: NAD83).
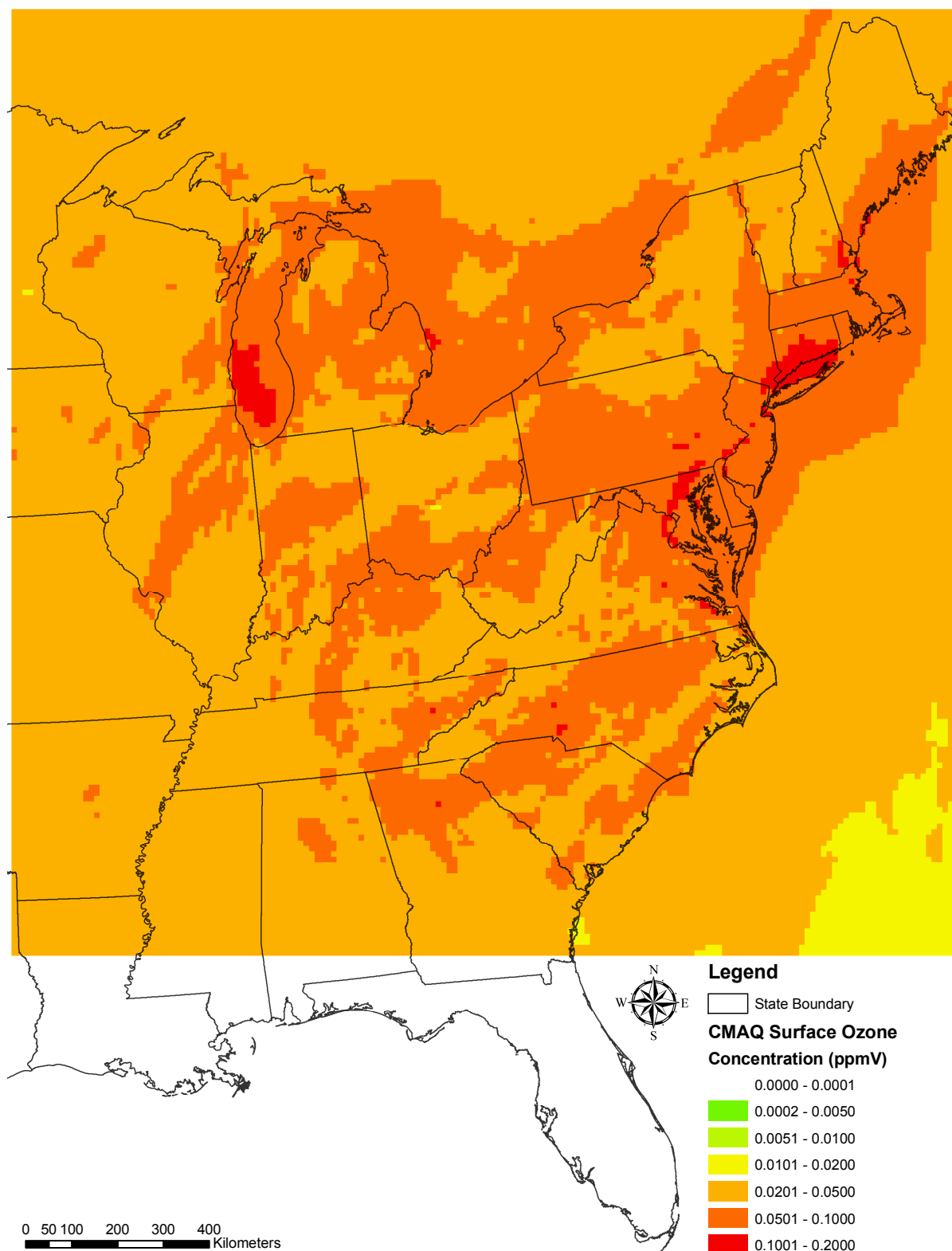
Figure 4.38: Surface ozone concentration calculated with the CMAQ model between 4 and 5 pm of August 12th using MODIS adjusted LAI for all biogenic emissions (Scenario 4) (GCS: NAD83).
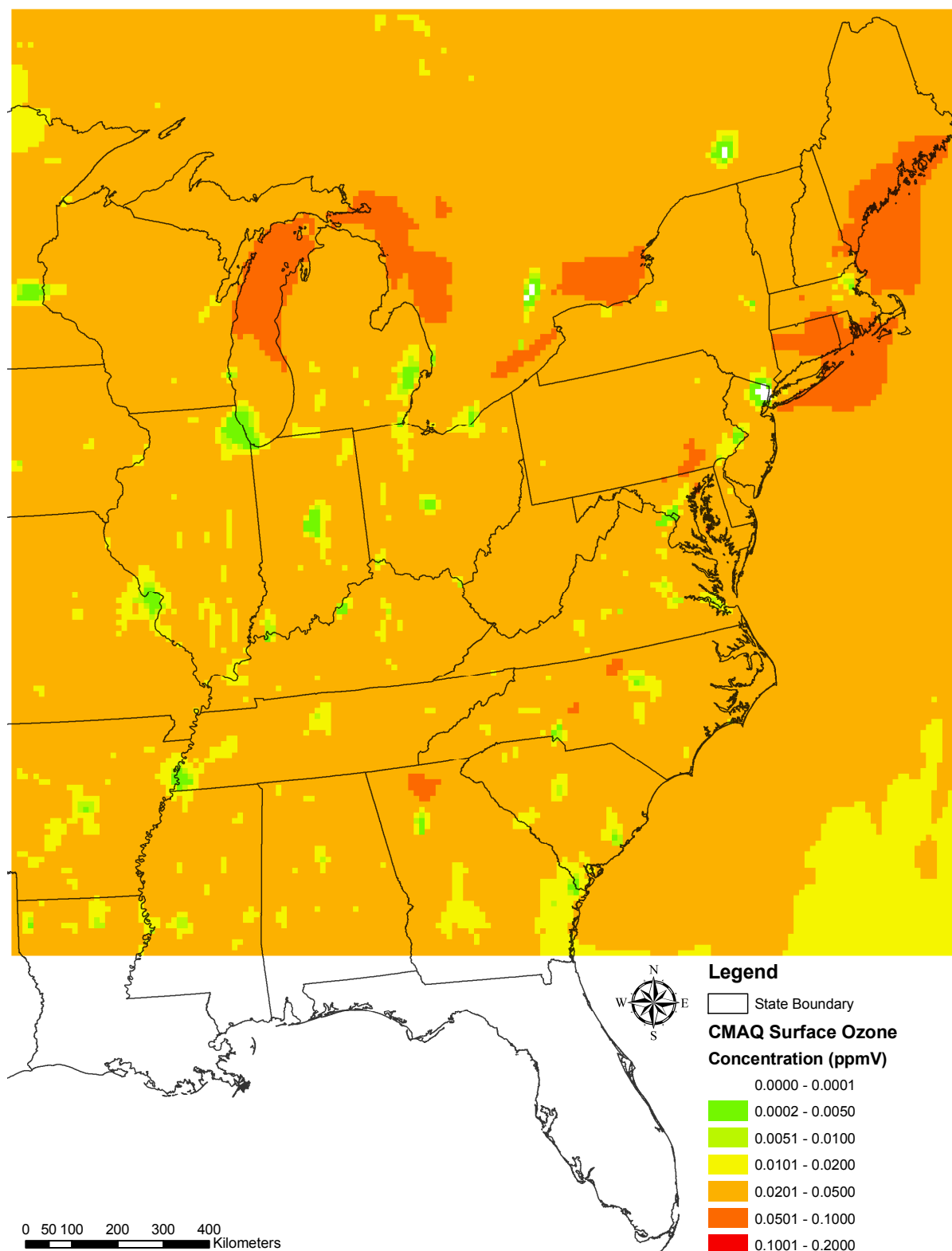
Figure 4.39: Surface ozone concentration calculated with the CMAQ model between 8 and 9 pm of August 12th using no biogenic emissions (Scenario 1) (GCS: NAD83).
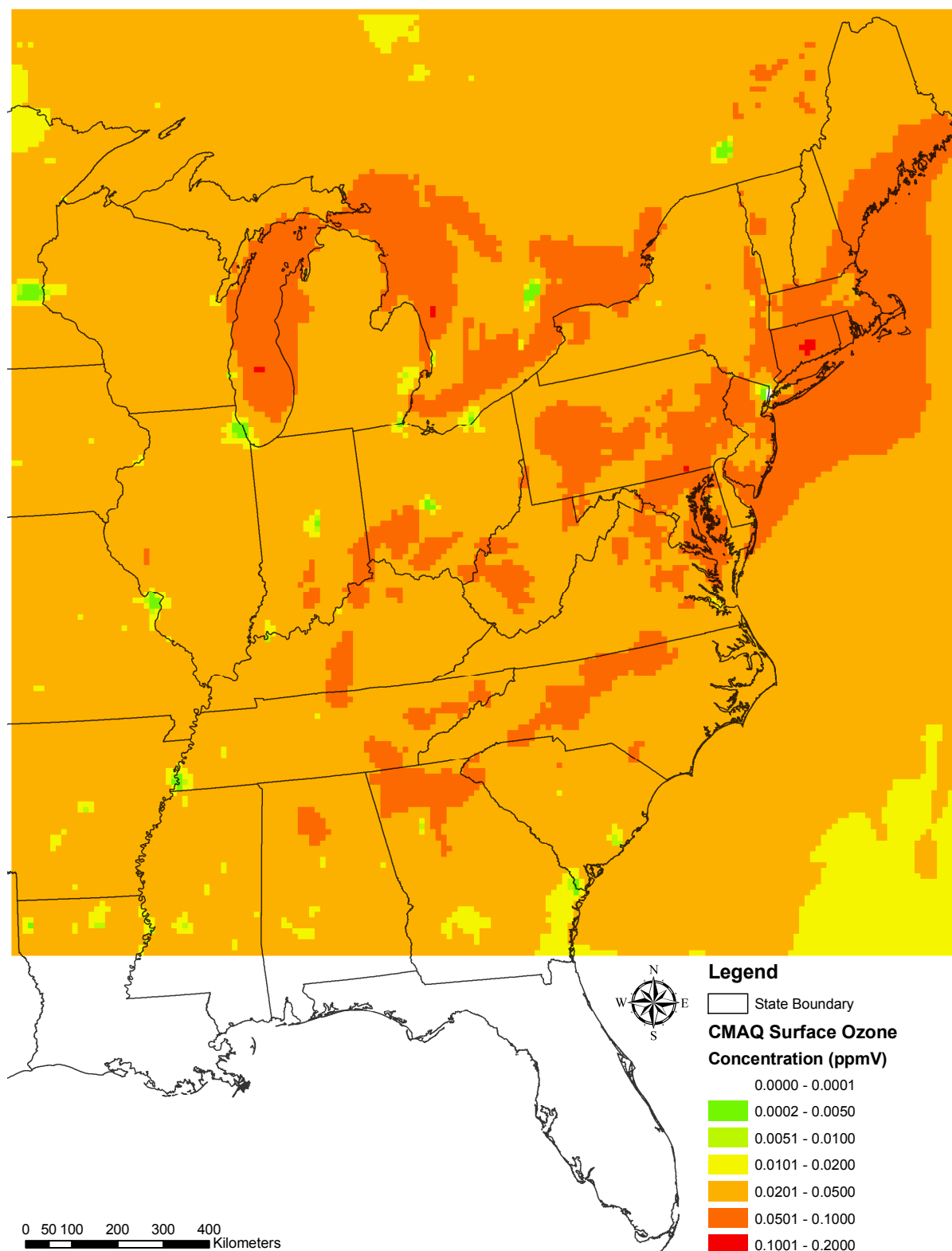
Figure 4.40: Surface ozone concentration calculated with the CMAQ model between 8 and 9 pm of August 12th using the updated BEIS 3.13 emission factors (Scenario 2) (GCS: NAD83).
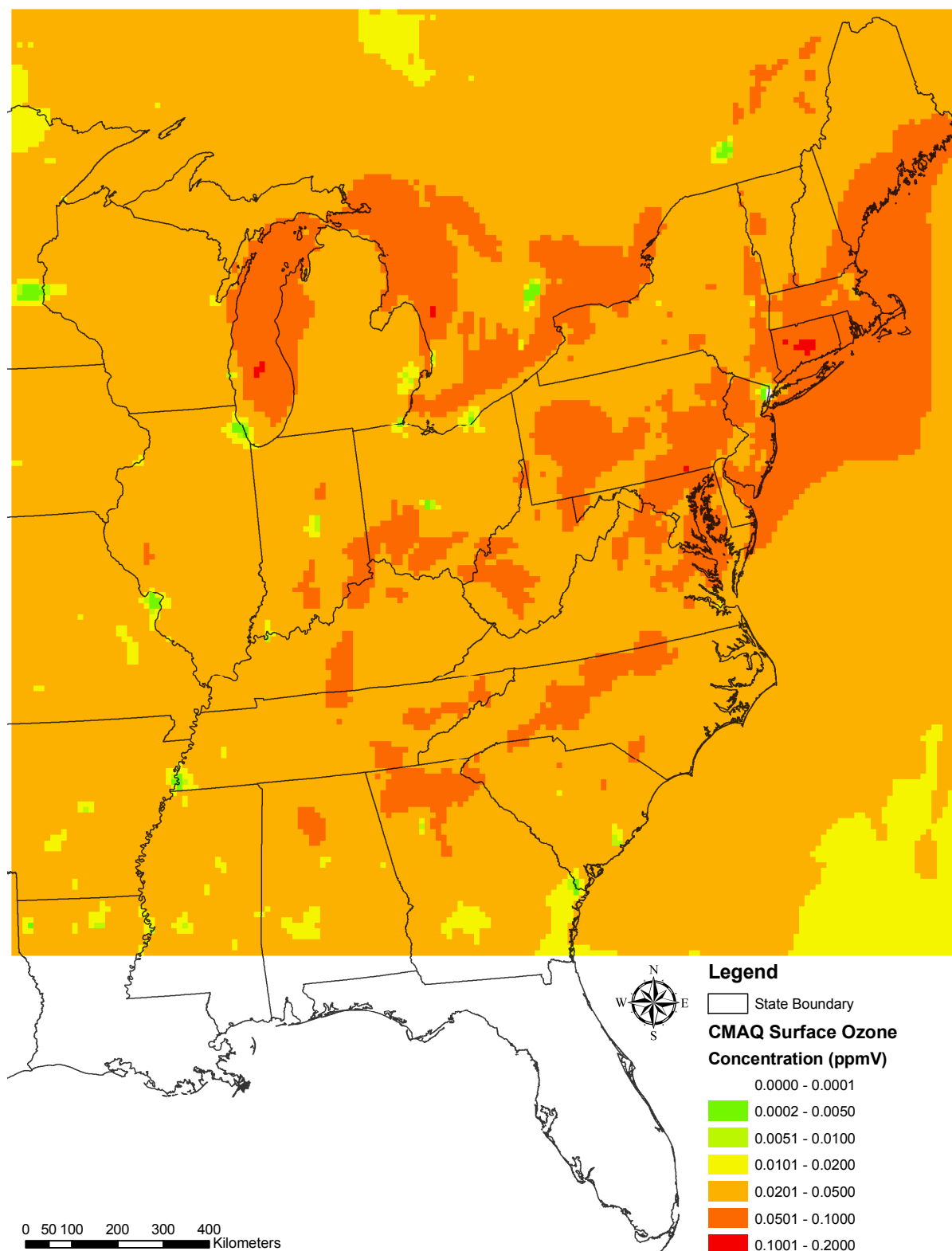
Figure 4.41: Surface ozone concentration calculated with the CMAQ model between 8 and 9 pm of August 12th using MODIS adjusted LAI for isoprene emissions (Scenario 3) (GCS: NAD83).
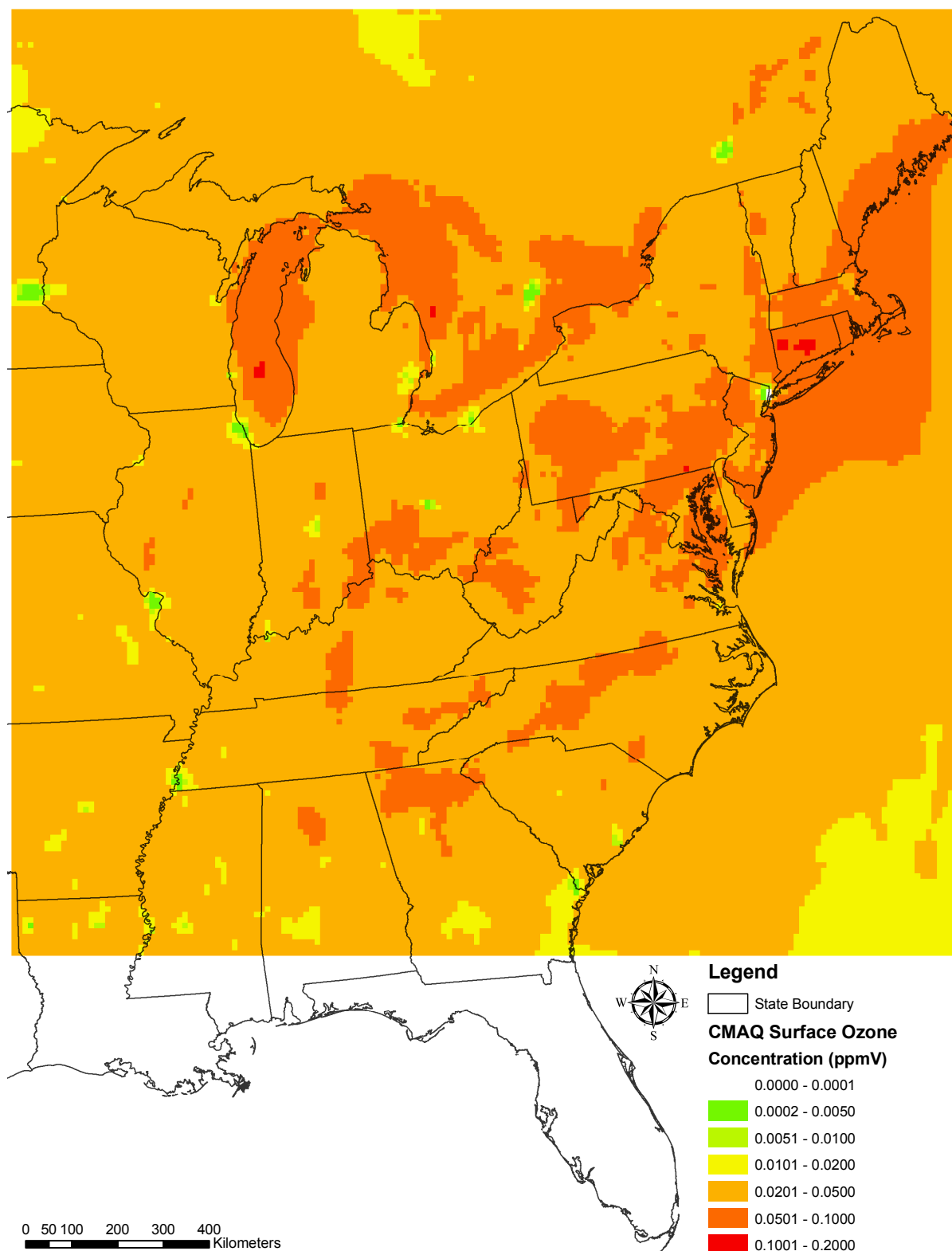
Figure 4.42: Surface ozone concentration calculated with the CMAQ model between 8 and 9 pm of August 12th using MODIS adjusted LAI for all biogenic emissions (Scenario 4) (GCS: NAD83).
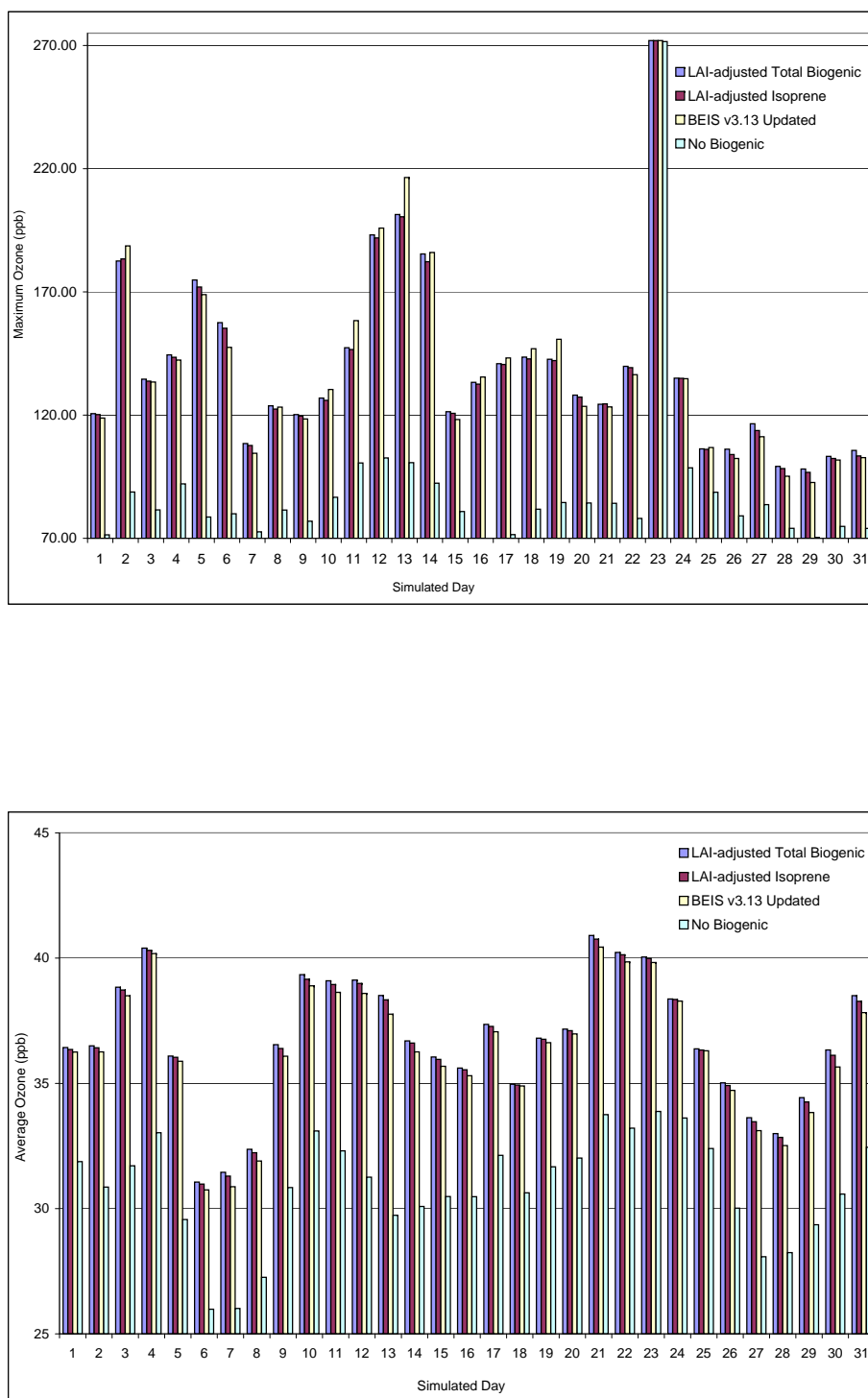
Figure 4.43: Maximum (top) and daily averaged (bottom) domain-wide ozone concentration calculated with the CMAQ model for the biogenic scenarios developed for the OTC/MANEVU domain.
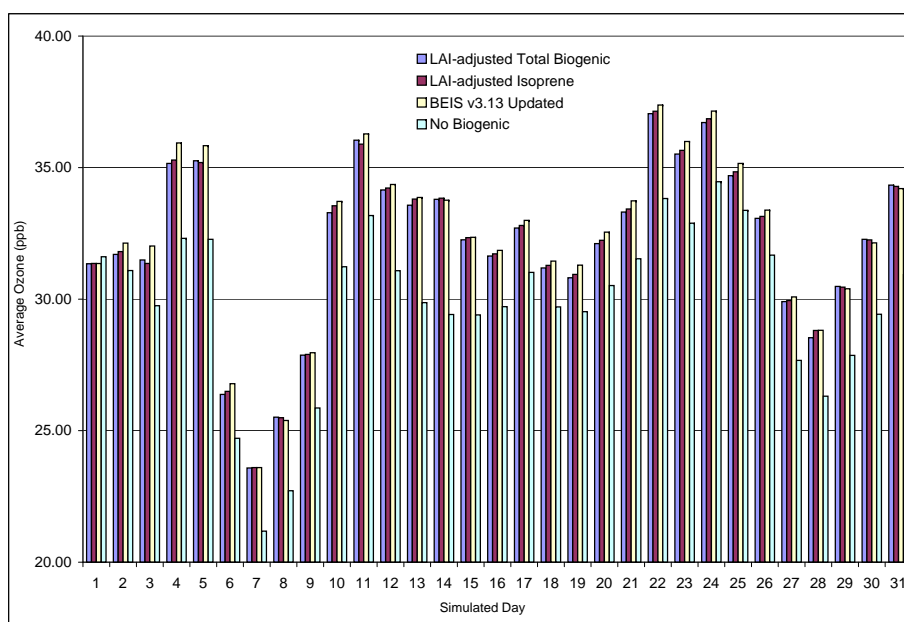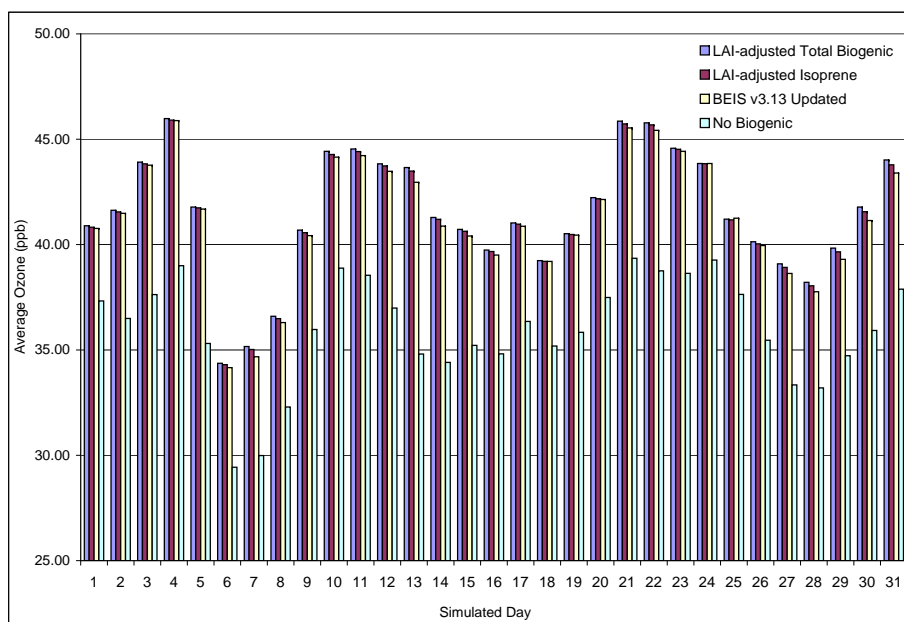
Figure 4.44: Averaged daytime (noon-7 pm, top figure) and nighttime (midnight-7am, bottom figure) domain-wide ozone concentration calculated with the CMAQ model for the biogenic scenarios developed for the OTC/MANEVU domain.
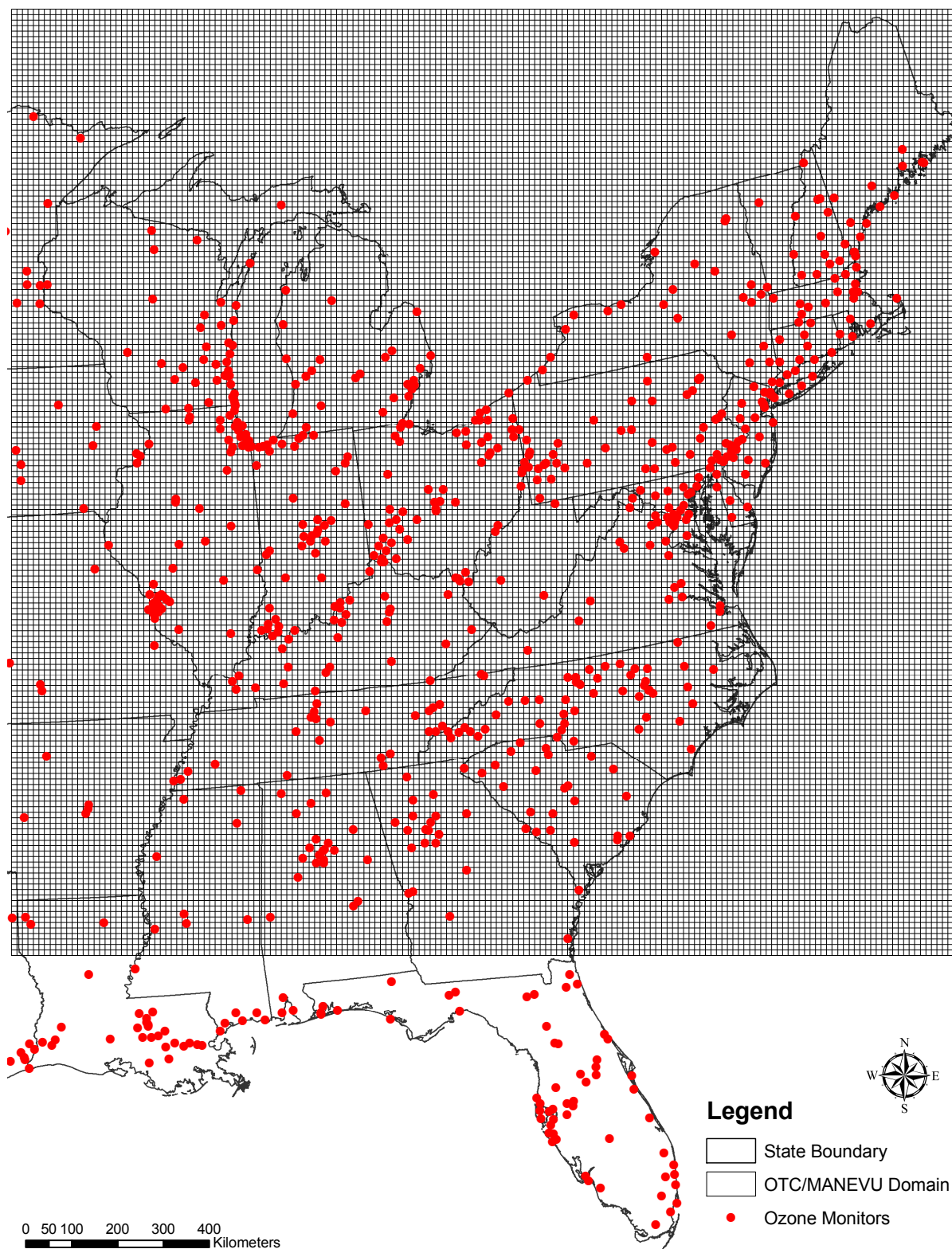
Figure 4.45: Selection of ozone monitors from the PAMS EPA network situated in the modeling region (GCS:NAD83.
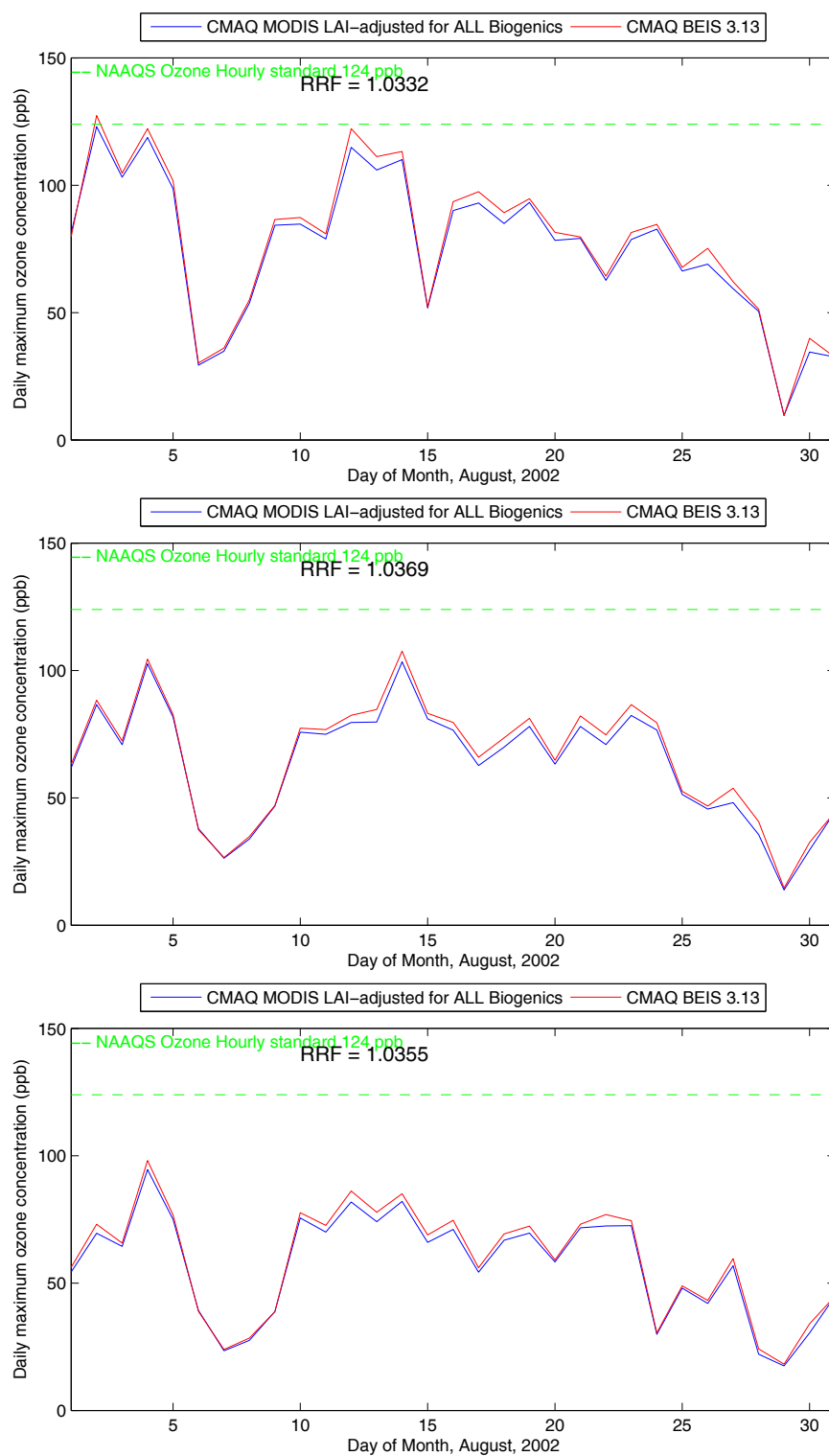
Figure 4.46: Daily maximum ozone concentration comparison between CMAQ simulations using BEIS and MODIS adjusted leaf area index for a selection of PAMS monitors within the OTC domain (340273001 (top), 340190001 (middle), 340150002 (bottom)) during the month August 2002.
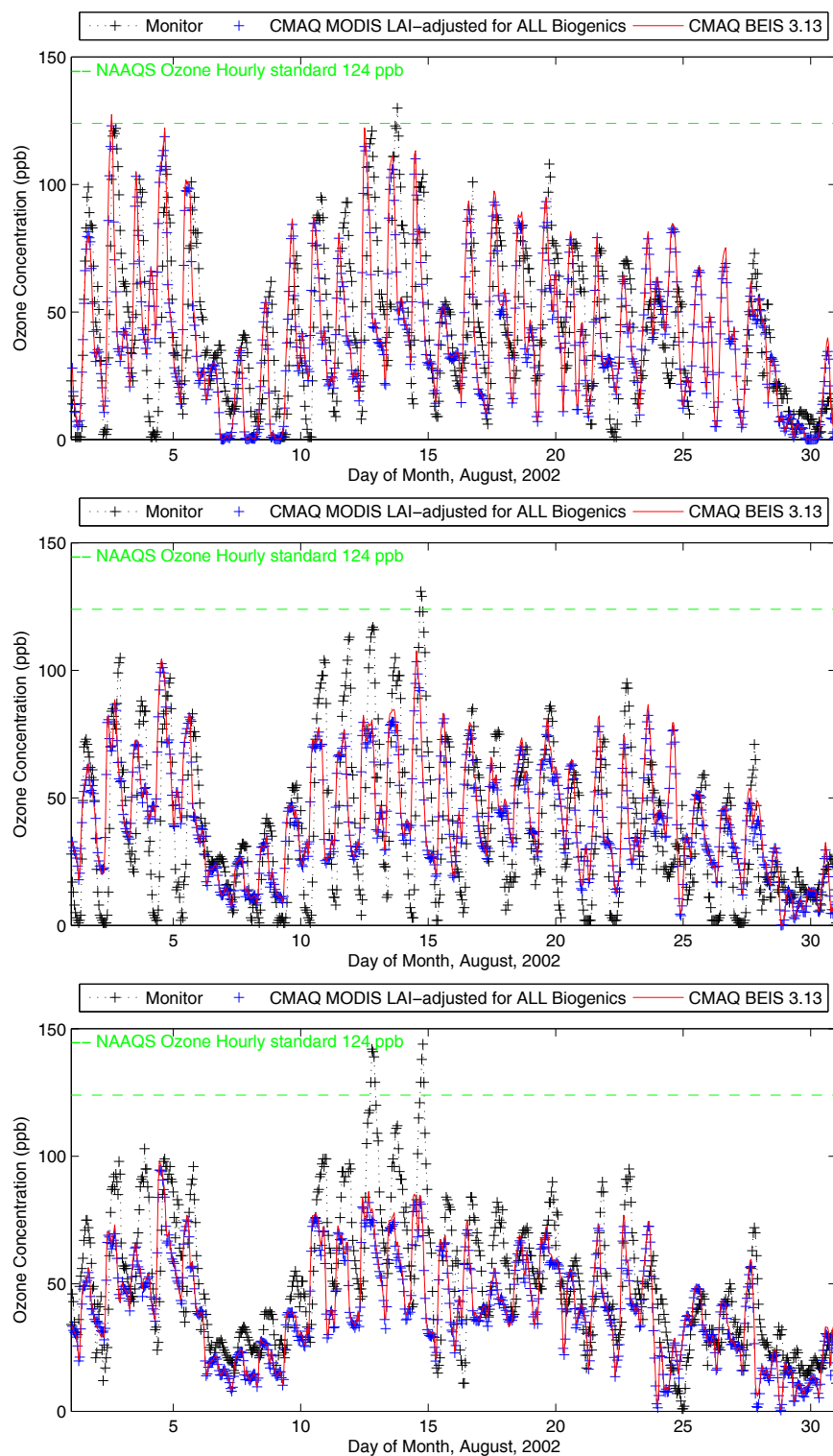
Figure 4.47: Hourly ozone concentration comparison between CMAQ simulations using BEIS and MODIS adjusted leaf area index for a selection of PAMS monitors within the OTC domain (340273001 (top), 340190001 (middle), 340150002 (bottom)) during the month of August 2002.
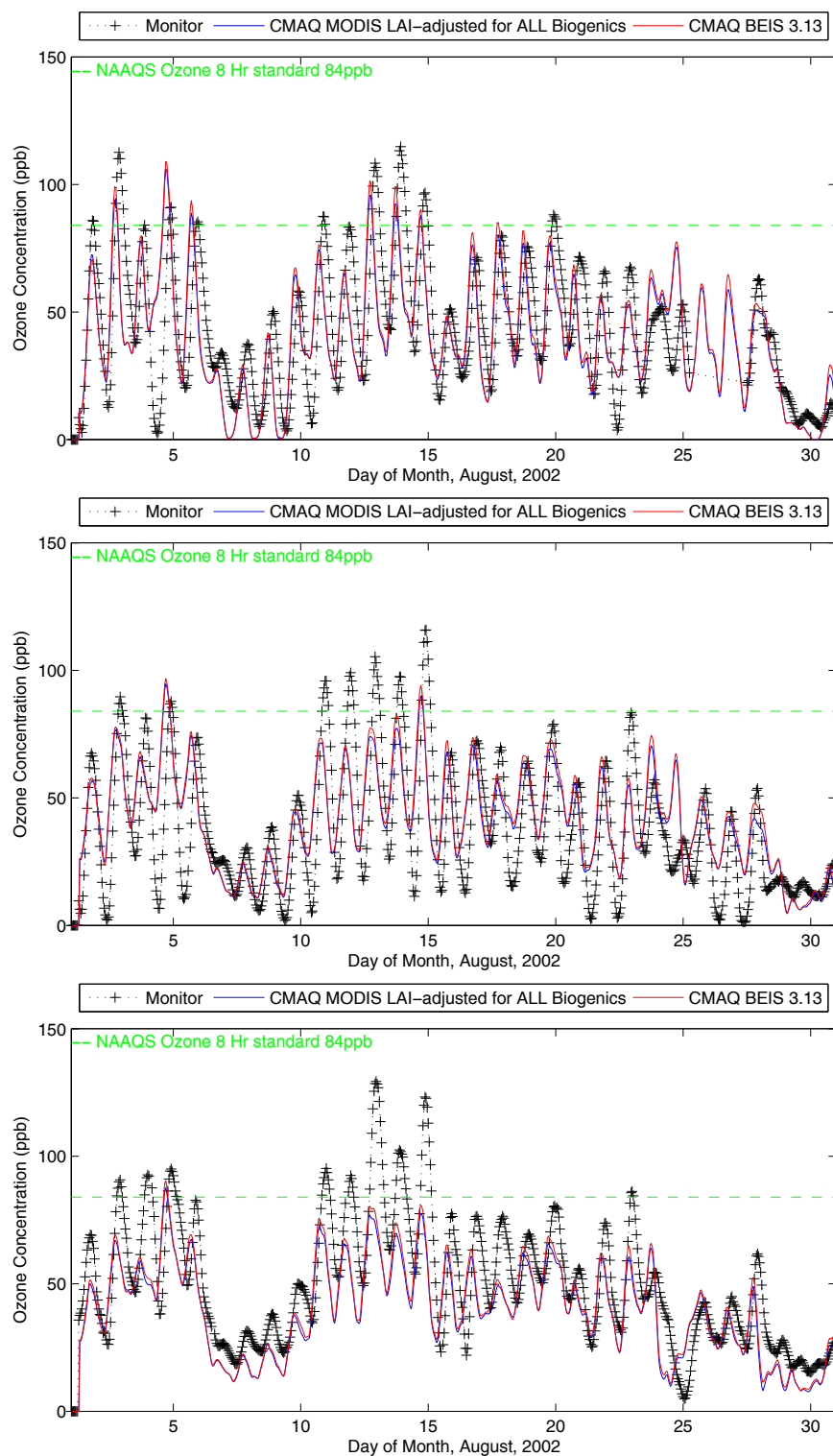
Figure 4.48: 8-hour average ozone concentration comparison between CMAQ simulations using standard and updated biogenic emissions and a selection of PAMS monitors within the OTC domain (340273001 (top), 340190001 (middle), 340150002 (bottom)) for August 2002.

Tables

Table 4.1: Description of major species with biogenic significance under the CBM-IV chemical mechanism.

CBM-IV Species	Description of the lumped structure
ISOP	Isoprene
TERPB	β terpene surrogate species
FORM	Formaldehyde
ETH	Ethene
PAR	The single bonded one-carbon-atom surrogate is used to represent the chemistry of alkanes and most of the alkyl groups found in other organics
OLE	The double bonded two-carbon-atom surrogate is used to represent the chemistry of alkanes whose carbon-carbon double bonds are found in 1-alkenes
ALD2	The two-carbon-atom surrogate is used to represent the chemistry of acetaldehyde and higher aldehydes that contain the -CHO group and adjacent carbon atoms. Used also to represent 2-alkenes that react very rapidly in the atmosphere to produce aldehyde products
TOL	The seven-carbon-atom surrogate is used to categorize monoalkylbenzene structures
XYL	The eight-carbon-atom surrogate is used to categorize dialkylbenzene and trialkylbenzene structures
NO	Nitrogen oxide surrogate

Table 4.2: Reactions of biogenic stable species included in chemical mechanisms for the Models-3 system.

Reaction	LCC	CBM-IV	RADM2	EMEP	RACM	SAPRC99	CACM
Isoprene + OH	x	x	x	x	x	x	x
Isoprene + NO$_3$	x	x	x	x	x	x	x
Isoprene + O$_3$	x	x	x	x	x	x	x
Isoprene + O	x	x			x	x	x
α - Pinene[1] + OH	x				x		
α - Pinene + NO$_3$	x				x		
α - Pinene + O$_3$	x				x		
β - Pinene[2] + OH	x						
β - Pinene + NO$_3$	x						
β - Pinene + O$_3$	x						
Limonene[3] + OH	x				x		
Limonene + NO$_3$	x				x		
Limonene + O$_3$	x				x		
Myrcene + OH	x						
Myrcene + NO$_3$	x						
Myrcene + O$_3$	x						
γ - Carene + OH	x						
γ - Carene + NO$_3$	x						
γ - Carene + O$_3$	x						
BIO-Low[4] + OH							x
BIO-Low + NO$_3$							x
BIO-Low + O$_3$							x
BIO-Low + O							x
BIO-High[5] + OH							
BIO-High + NO$_3$							x
BIO-High + O$_3$							x
BIO-High + O							x

---

[1]α - pinene and other cyclic terpenes with one double bond

[2]β - pinene

[3]d-limonene and other cyclic diene-terpenes

[4]Low SOA monoterpene species (α - terpineol)

[5]High SOA monoterpene species (γ - terpinene)

Table 4.3: Predominant tree families in the OTC domain along with the associated leaf area index (LAI), dry leaf biomass factor, and major biogenic VOC emission factors.

Tree Family	Major Species	BELD Density	LAI	Leaf Biomass	Biogenic Emission Factors			
					Isoprene	Monotrpene	OVOC	NO
Quercus	Oaks	32.35	5	375	26250	66	311	2
Aceraceae	Maples	13.90	5	375	38	529	311	2
Pinaceae	Pines	9.44	3	700	70	1853	581	2
Fagaceae	Beech	4.8	5	375	38	192	311	2
Cupressaceae	Cypress	3.64	3-5	375	38-70	33-609	311	2
Carya	Hickory	3.64	5	375	38	530	311	2
Betulaceae	Birch	3.42	5	375	38	66	311	2
Oleaceae	Ashes	3.15	5	375	38	33	311	2
Moraceae	Mulberries	1	5	375	38	66	311	2

Table 4.4: Biogenic contribution (percentage) to the total CBM-IV species emissions for the month of August 2002 in the OTC domain.

CBM-IV Species	BEIS 3.12	BEIS 3.13	LAI adjusted
NO	5.3	5.3	5.3
CO	7.3	7.3	7.3
TOL	35.8	35.8	44.5
FORM	84	84	88.3
ETH	67.6	67.6	75
XYL	5.8	6.3	8.7
ALD2	87.9	87.9	91.2
PAR	64	63.8	71.5
OLE	91.3	91.1	93.6

Table 4.5: Summary of statistical measures for the analysis grid compared with ozone monitoring stations in New Jersey.

Parameter	BEIS 3.13 modeled	MODIS & BEIS3.13 model
Sample size	9,672	9,672
Unpaired accuracy(%)	10.86	10.45
Ratio of the means	0.9403	0.9676
Normalized bias	1.0704	1.1451
Normalized gross error	1.5596	1.6150

Table 4.6: Relative change factor between the MODIS-adjusted and BEIS 3.13 scenarios calculated using CMAQ output for the cells that contain ozone monitoring stations in the State of New Jersey.

Monitor ID	Relative Change Factor
34—041—0005	1.0516
34—043—0005	1.027
34—045—0002	1.0264
34—053—0006	1.0321
34—055—1004	1.0328
34—063—1006	1.0134
34—065—0004	1.031
34—067—1015	1.0351
34—081—0124	1.0126
34—083—0004	1.0133
34—085—0067	1.0332
34—091—0004	1.0369
34—093—0003	1.0355

Chapter 5

Modeling the emission and transport of aeroallergens at a regional scale

5.1 Background

There is significant evidence that air pollution may contribute to the increase in pollen allergies and asthma in densely populated areas [Aberg, 1989; Asher et al., 1995; Ishizaki et al., 1987; Kogevinas et al., 1999]. However, no direct correlation between pollen release and emission peaks of common pollutants (including fine particulates) has been identified in the literature [Behrendt et al., 1991; Ring et al., 2001]. Modeling the emission and the dispersion of allergenic particles has not been considered in previous air quality modeling studies for criteria pollutants, as most implementations ignore the coexistence of chemicals or other particles. One of the objectives of this chapter is to demonstrate the addition of the most significant aeroallergens in a regional air quality model framework. This allows for studying exposures to co-occuring pollutants and aeroallergens and can be an extremely useful tool for sub-populations of concern (asthmatics, children, etc.).

As described in the first section of Chapter 1, techniques for modeling particle dispersal can be roughly grouped into two modeling approaches: Eulerian and Lagrangian. The Eulerian modeling approach focuses on the density of the particle pattern and, thus, explains the dispersal of an individual particle by modeling the probability of finding it in a given area. The Lagrangian approach models the movement of the particle itself, typically by simulating trajectories for dispersing particles. Before proceeding with analyzing the study design, a brief review of the most significant efforts in modeling pollen particles is presented.

5.1.1 Eulerian modeling approach: analytical models for the dispersal pattern

A characteristic type of a model formulated under the Eulerian framework is based on the theory of atmospheric diffusion. Dupont et al. [2006] reviews the Eulerian framework for pollen dispersal over heterogeneous vegetation canopies. If it is assumed that particle movement can be defined by an uncorrelated, homogeneous random walk (diffusion) around deterministic drift (advection), then the particle dispersal pattern can be described by an advection-diffusion equation (ADE) [Di-Giovanni et al., 1989; Loos et al., 2003; McCartney and Lacey, 1991; Turchin, 1998]. This equation can be considered as describing the random movement of particles around the mean airflow. The ADE can be solved analytically by making several simplifying assumptions [Turchin, 1998]. The simplest solution for the equation is the classical Gaussian plume model [Di-Giovanni and Beckett, 1990; Loos et al., 2003; Turchin, 1998], which is found by omitting the effects of gravity, deposition and spatiotemporal variation on particle movement. The effect of gravity can be incorporated by using an extended version of the Gaussian plume model - a solution called the 'tilted plume' [Andersen, 1991; Di-Giovanni and Beckett, 1990; Di-Giovanni et al., 1989; Okubo and Levin, 1989]. However, some of the parameters needed for these models are not easily measurable [Di-Giovanni and Beckett, 1990; Loos et al., 2003]. At the microscale, it might be justified to use the Gaussian type of models as developed by Walklate et al. [2004] for oilseed rape and by Jarosz et al. [2004] for maize. Such models, however, can only be applied close to the pollen source and are optimized for smaller plants with a shorter release height (*i.e.* a few meters/feet).

The general problem with dispersal models based on the advection-diffusion equation is that all attempts to add realistic features have led to severe modeling difficulties. Modeling deposition at the ground level and within the canopy is complicated [Di-Giovanni and Beckett, 1990; Okubo and Levin, 1989]. A further increase in realism adding vertical variation in horizontal wind and vertical movement leads to difficult boundary-value problems with only non-closed form solutions [Andersen, 1991; Okubo and Levin, 1989]. The effect of the canopy on particle movement - even though it is considered an important factor - has to be omitted because of technical difficulties in solving the equation numerically, and because of several simplifications required for an analytical solution [Andersen, 1991; Di-Giovanni and Beckett, 1990; Loos et al., 2003; Okubo and Levin, 1989]. Because of the difficulties in finding models that include the major biological components

affecting dispersal - but are still simple enough to be analytically tractable - a Lagrangian modeling approach using simulation techniques rather than analytical solutions for determining the particle dispersal pattern is the current preferred method [Andersen, 1991; Di-Giovanni et al., 1989; Nathan et al., 2001].

5.1.2 Lagrangian modeling approach: trajectory models

The simplest way to obtain a straight-line trajectory for an airborne particle is to calculate its landing point based on fixed horizontal and vertical wind speeds [Di-Giovanni et al., 1989; Nathan et al., 2001; Soons et al., 2004]. An important increase in realism is obtained by simulating a particle trajectory so that temporary airflows, particularly vertical airflow, affect the dispersing particle during its flight [Andersen, 1991; Soons et al., 2004; Tackenberg, 2003]. The simplest way to obtain the temporary wind fluctuations is to measure them empirically [Tackenberg, 2003], or to simulate them [Soons et al., 2004]. However, autocorrelation between wind conditions during subsequent moments is an important factor affecting particle dispersal. Therefore, for modeling such airflows, empirical wind measurements collected at a fixed point are not ideal because they might not fully capture the autocorrelation [Soons et al., 2004]. Over the past few years the Lagrangian stochastic (LS) turbulence model has frequently been suggested as a way of producing realistic descriptions of temporary airflows [Aylor and Flesch, 2001; Jarosz et al., 2004; Nathan et al., 2002; Soons et al., 2004]. The LS turbulence model simulates the airflow by estimating the acceleration of an air parcel at given atmospheric conditions [Aylor and Flesch, 2001; Jarosz et al., 2004; Soons et al., 2004]. The LS model has been used in a cross-wind integrated form [Aylor and Flesch, 2001; Jarosz et al., 2004], or in a fully 3D form [Nathan et al., 2002; Soons et al., 2004]. Typically, the canopy has been assumed to be horizontally homogeneous [Aylor and Flesch, 2001; Nathan et al., 2002; Soons et al., 2004], but local changes in ground surface roughness have also been accounted for [Jarosz et al., 2004]. The models have been modified to describe particle dispersal from forest canopies [Nathan et al., 2002], as well as from lower canopies, such as fields or grasslands [Aylor and Flesch, 2001; Jarosz et al., 2004; Soons et al., 2004]. To increase the realism of the dispersal mechanisms, the reduction in particle trajectory autocorrelation time due to a particle falling from one airflow into another because of gravity, has also been added to the LS models [Aylor and Flesch, 2001; Boehm and Aylor,

2005; Jarosz et al., 2004].

5.1.3 Identifying dispersal mechanisms for pollen particles

A comparison between empirical data has shown that analytical models incorporating only the main features of atmospheric transport can predict the average dispersal distances [Bullock and Clarke, 2000; Greene and Johnson, 1995; Loos et al., 2003; Okubo and Levin, 1989; Skarpaas et al., 2003], but they tend to underestimate the tail of the dispersal curve [Bullock and Clarke, 2000; Greene and Johnson, 1989, 1995; Loos et al., 2003; Skarpaas et al., 2003]. As described in the previous chapter, there is convincing evidence that the long-range transport of pollen from remote regions can significantly affect pollinating seasons. That is particularly important for regions on the Northern hemisphere, where the flowering takes place later in spring. This transport causes sudden increases of concentrations of pollen that can occur up to a month before the start of the local pollen season [Siljamo et al., 2004]. Standard mechanisms describing the movement of seeds do not provide information about events such as temporary gusts and updrafts that cause long distance dispersal (LDD) [Higgins et al., 2003]. Because recent attention has been focused in particular on modeling LDD, simple models that only focus on the average environmental conditions have been considered inadequate [Bullock and Clarke, 2000; Higgins et al., 2003; Nathan et al., 2001, 2002; Soons et al., 2004; Tackenberg, 2003]. Simplified attempts to include upward fluctuations in dispersal models have been able to improve the predictions of LDD [Andersen, 1991; Nathan et al., 2001; Skarpaas et al., 2003]. However, irregular, autocorrelated, turbulent fluctuations, such as temporary updrafts, have turned out to be key mechanisms causing LDD [Nathan and Katul, 2005; Nathan et al., 2002; Soons et al., 2004; Tackenberg, 2003], and explaining the shape of the dispersal curve [Nathan and Katul, 2005; Nathan et al., 2002]. Therefore the description of the turbulent fluctuations in the model is at least as important as the description of the mean airflow [Nathan and Katul, 2005].

In our study, we will focus on the dispersion of allergenic pollen grains on the regional scale. Schueler and Schlünzen [2006] used a non-hydrostatic mesoscale model to simulate the dispersion of oak pollen in an area of 200x200 km^2. The proposed parameterization of the emission flux mainly depends on the estimated annual production and the vapor pressure deficit. The pollen grain viability was taken into account according to a function of the particle exposure to sunlight.

Due to a lack of observations, the authors were not able to test and compare their modeling results. Sofiev et al. [2006a] presented a feasibility study of the use of a modeling system originally designed for emergency modeling Siljamo et al. [2004]. Their model was used to study the long range transport of Birch pollen to Finland and subsequently extended to included most of Europe [Sofiev et al., 2006b]. This model includes parameterizations of the settling velocity and of the dry and wet deposition. In order to prescribe the pollen emissions, a detailed Birch forest map in conjunction with climatological values for the pollen emissions were used. Comparison with a limited number of observational data indicated the possibilities and limitations of the modeled pollen distributions. The authors were able to demonstrate that pollen can be transported over quite large distances in the order of several kilometers. Pasken and Pietrowicz [2005] used the HYSPLIT4 model coupled with MM5 meteorology to simulate oak pollen concentrations during a pollen episode that was observed at Clayton, MO. The author used pollen counts to provide with thresholds for a constant source emission model for oak species. Besides the rough assumptions employed in the emission source characterization, oak pollen is a larger particle with lesser allergenic potential when compared to other species found in the Northeast. Comparisons of the above modeling studies have indicated that there are still large discrepancies between observations and simulation results.

5.2   Study design and allergenic species selection for the Northeast

The complex landscape and the wide range of climatic conditions in the Northeast United States are accompanied by a broad spectrum of vegetation species. Pollen calendars differ from one area to the other, however the entire pollination period for the majority of the species starts in late winter and ends in autumn. In typical pollen emission and dispersion simulations, the period of interest is defined by the individual phenology of the major species involved. Grass pollen induced pollinosis has been identified as the most frequent pollen allergy in Europe [Huynen et al., 2003]. The difficulty in modeling pollen emissions from such a source results from the fact that the grass pollen family (*Poaceae*) is comprised of more than 600 genera and over 10,000 species. Ragweed (*Ambrosia*) is the etiologic agent in about half of all cases of pollinosis in the United States. The height of release and particle properties of the average grass pollen family can be approximated by the typical characteristics of the ragweed species. Although the

grass flowering season spans late spring and the entire summer, ragweed is predominant during the late summer to autumn transition period. For trees, one of the most allergenic pollen is produced from birch (*Betula*). However, the phenology of Birch trees is complicated and it remains a challenge to predict the total amount of pollen or the emission rate for a given season. In general, pollen calendars reveal that birch pollen values usually peak one to three weeks after the start of the tree season.

With the above species in mind, a prototype approach for aerobiological applications using existing air quality models (CMAQ/Models-3) along with a variety of supporting databases (BELD3, PLANTS) was developed. The modeled processes under this framework are summarized in Figure 5.1. The resulting methodology can divided in two approaches, the reverse analysis of the pollen release through local pollen counts (pollen calendars) and backward trajectory modeling, and the forward analysis which relies on modeling of the emission and dispersion processes. In order to verify the abundance of the selected vegetation, a number of databases were investigated for their application suitability. The underlying vegetation database that was utilized was the BELD dataset, which provided the species-level spatial density for the domain of interest. Table 5.1 provides a list of the most abundant species in the OTC/MANEVU domain, along with a compilation of species-specific information that includes size, flowering period, and the characteristic allergens they contain. It is easy to identify that the most abundant tree species such as the oaks and pines are not the most important allergen carriers. Furthermore, the particles produced by those species are larger and heavier, and as a result expected to deposit at a smaller distance from their source. Most of the satellite products are expected to face difficulties in identifying ragweed densities, mainly due to the plant size and population dynamics. The BELD 3.1 database does not contain species-level information for ragweed. As a result, the PLANTS database was used as an alternative in order to incorporate county-level ragweed occurrence information. Since ragweed is a rather invasive species, it is expected to be present in most of the area of interest.

5.3 Forward modeling of allergenic pollen aerosol emission and dispersion

Kawashima and Takahashi [1995] presented a method to estimate the distribution of airborne pollen of Japanese cedar by developing a modeling framework using a meteorological model as the basis for predicting the wind fields. One of its drawbacks was related to the flowering time of Japanese cedar, as the calculated pollen numbers tended to be overestimated at the beginning and the end of the season. As the authors reported, the simulation did not take into account the variations in flowering time in the study area, a problem which was later corrected in a revised version of the model [Kawashima and Takahashi, 1999]. A similar method to estimate the detailed mesoscale distribution of airborne pollen, by using a separate simulation to synthesize weather and vegetation data, is incorporated in this study. The methods developed for the Northeast United States will be discussed in the following subsections. A list of the parameters and values used as inputs in the pollen module simulations that will be presented and discussed in later sections is summarized in Table 5.2.

5.3.1 Species phenology and spatiotemporal flowering map development

The pollen emission source has been parameterized by several authors as a function of the total pollen production during a flowering period of n days, with the actual pollen production dependent on the dynamic meteorological conditions [Hilaire, 2007]. Using pollen counts and their statistical interpretations to drive the pollen emission module for forward modeling of the dispersal can be misleading. For the case of total tree pollen the counts are the result of multiple species with overlapping emissions (can be viewed as species-specific distributions), along with the effects of the transport processes involved until the final deposition and particle trapping. The onset of the pollen shedding period can be predicted with simple phenological models utilizing heat degree days along with appropriate species-specific thresholds. Heat degree days are calculated as a cumulative function of the daytime temperatures above a threshold value characterized in the following manner:

$$
D = \begin{cases} \sum_{d=d_s}^{d_e} (\bar{T}_d - T_t) & \text{, when } T_d > T_t \\\\ 0 & \text{, otherwise} \end{cases} \tag{5.1}
$$

where, T_d is the mean temperature of the current day, T_t is a species-specific threshold temperature, and d is the day between the start (d_s) and end (d_e) of the calculations. As a result, the number of degree days applied to any particular day of the week is determined by calculating the mean temperature for the day and then comparing the mean temperature to a base value (typically 65 degrees Fahrenheit). For calculating degree hours the concept remains the same, utilizing hours instead of days. In such a case, the temperature threshold for the same species will be different. Selecting thresholds and starting date for the calculations depend on the definition of the heat sum and the geographical location. A heat degree map for the United States calculated with a 50 degree Fahrenheit base is presented in Figure 5.2. Based on the cumulative heat degree days observed at the Newark meteorological station, a time series plot with the evolution of this variable, indicating the emission threshold developed for the case of Birch phenology is provided in Figure 5.3. The cutoff value that was assigned for this case was selected to be 2000 heat degree days (since Jan 1th of the selected year. Temperature threshold values that have been used in literature for the case of Birch range from 2.3 to 3.5 °C.

5.3.2 Pollen emission model formulation

Due to the numerous uncertainty sources, most authors involved in modeling the pollen emission suggest developing very general source parameterizations. For most of the cases, the maximum occurring pollen grains in a season, the pollen production term is the starting point. In this study a modified version of the emission parameterization according to Helbig et al. [2004] and Sofiev et al. [2006a] was implemented. A similar methodology has been followed by a number of mesoscale modeling groups in Europe [Vogel et al., 2008]. The vertical pollen emission F_{pollen} at the top of the canopy is proportional to the product of a characteristic concentration and a series of meteorological resistances that define the fraction of pollen that can finally be uplifted:

$$F_{pollen} = c_e \cdot K_e \cdot c^*$$ (5.2)

The characteristic concentration c^* is calculated using the following parameterization:

$$c^* = \frac{q_p}{LAI \cdot h_c}$$ (5.3)

where, q_p describes the pollen grains produced in one season in grains per square meter, LAI represents the leaf area index and h_c the canopy height of the corresponding species. In this manner, q_p is reduced by the previously emitted amount of pollen grains. Molina et al. [1996] determined the number of pollen grains for 10 different species. However, pollen grain numbers are traditionally reported per branches, trees, and crown diameter. In this study, a typically suggested area source for birch species and ragweed has been incorporated (Table 5.2). The remaining factor, c_e is considered to be a plant-specific function that describes the likelihood to bloom. This factor takes into account that not all flowers are blooming at the same time, although the meteorological conditions can be ideal for pollen release. To achieve that, the number of flowers increases with time until a maximum is reached. Afterward, the number decreases until we reach the end of the pollen-shedding period:

$$c_e = 4 \cdot 10^{-4} \left(\frac{d}{S} - \frac{d^2}{S^2} \right)$$ (5.4)

where, d is the actual day of the pollen season lasting for the interval S. Outside of the pollen season, c_e is set to zero. The initiation of the pollen period is calculated based on a phenology module that utilizes heat degree days. The simulation result is a spatiotemporal flowering map that will cover the entire period and domain of interest that will be reviewed in the results section.

It is obvious that the available pollen grains cannot be emitted into the atmosphere, if the meteorological conditions are unfavorable. At this point, a daily profile for each of the species of interest (Birch, Ragweed) was compiled from various literature sources at similar latitudes.

This was established in our case with a meteorological trigger system that could optimally assign pollen emission rates. For example, recent literature sources suggest that periods with high tree pollen count are characterized by high maximum temperature, low rainfall and an absolute humidity of around $6\,\mathrm{g\,m^{-3}}$. In general, the strongest positive correlation was with temperature, as described also before for the case of Alder [González Parrado et al., 2009]. In other cases that involve extensive databases that run for decades such that of Basel, Switzerland, it was shown that due to a temperature increase, the start of flowering in the case of Birch occurred about 15 days earlier [Frei and Gassner, 2008]. Finally, the meteorological triggers that will be examined involve the following parameterization for each of the variables of interest:

$$K_e = K_h \cdot K_h \cdot K_w \tag{5.5}$$

where:

- Humidity: For levels below 50, there is full release of pollen. For humidity above 80, there is no pollen release. For intermediate humidity between 50 and 80, the release of pollen is given by:

$$K_h = e_0 \frac{80 - h}{80 - 50} \tag{5.6}$$

- Wind:

$$K_w = e_0 \left(5 - e^{\frac{w_{10m} + u_{conv}}{1.5}} \right) \tag{5.7}$$

- Precipitation:

$$K_r = e_0 \left(1 - \frac{p}{0.5} \right) \tag{5.8}$$

where, e_0 stands for the current value of emission, h represents the relative humidity, w_{10m} is the wind at $10\,\mathrm{m}$ above ground $(\mathrm{m\,s^{-1}})$, u_{conv} is the convective wind $(\mathrm{m\,s^{-1}})$, and p represents precipitation in $(\mathrm{mm\,h^{-1}})$.

5.3.3 Pollen grain as an atmospheric pollutant

The existing methodology for calculating deposition velocities in the CMAQ environment

was reviewed in order to determine its applicability for the case of pollen particles. The deposition velocity calculations under the CMAQ framework (Figure 5.4) are based on the approach described by Seinfeld and Pandis [2006]. As a comparison step, the pollen particle specific formulations of the deposition velocity are presented in the following section, along with experimental results that were obtained from various literature studies and will be included for reference in Appendix C.

The large size of pollen grains, some 5-50 times larger in linear dimensions than conventional atmospheric aerosols, raises a whole set of questions related to the applicability of existing atmospheric dispersion models to the evaluation of atmospheric transport and deposition. There are several ways to check the assumptions underlying virtually all dispersion models. Here we use the Navier-Stokes equation as the basis for such an analysis. In its general form, the Navier-Stokes equation that describes the motion of a small volume of air can be written as follows:

$$\frac{\partial \vec{\nu}}{\partial t} + (\vec{\nu} \cdot \nabla)\vec{\nu} = -\frac{1}{\rho} \ g \ \text{rad} \ p + \frac{\eta}{\rho}\Delta\vec{\nu} \tag{5.9}$$

where $\vec{\nu}$ is a velocity of the volume of air (Lagrangian velocity), ρ is the density of air, p is pressure, and η is the dynamical viscosity (a typical value for air: $\eta_{air} = 1.8 \times 10^{-5} \, \text{kg s}^{-1} \, \text{m}^{-1}$). For slow laminar motion in the (psedo-)stationary case, one may write:

$$\eta\Delta\vec{\nu} - \ g \ \text{rad} \ p = 0 \tag{5.10}$$

Here the stationary condition is:

$$\frac{\partial \vec{\nu_i}}{\partial t} = 0 \tag{5.11}$$

Slow motion means that the Reynolds number is small, i.e., $\text{Re} = |\ \vec{\nu}\ | \ d/\nu \ll \ 1$, where d is a linear dimension (diameter) of the moving object and $\nu = \eta/\rho$ is the kinematical viscosity. The air viscosity can be calculated by the equation C-1 which is derived from the Sutherland's equation (Discussed in relevant Appendix 3, valid between $0 < T < 555$ K). From Equations 5.9 and 5.10, it can be shown that the total force applied to a spherical object moving through the air is:

$$F_{Stokes} = 6\pi r \eta u \left(1 + \frac{3ru}{8\nu}\right) \tag{5.12}$$

where r is a radius of the sphere and u is its velocity relative to the surrounding air. The correction term in brackets is small when Re $\ll$ 1. Using the above equations and the physical characteristics of pollen grains, one can quantify their behavior in an atmospheric flow and evaluate the applicability of existing dispersion modeling approaches to this type of pollutant.

Transport with air masses

A key assumption in all dispersion models is that the pollutant is transported together with the air masses, and follows the airflow, including small turbulent eddies, which means that its inertia is negligible. To check this assumption, it is enough to estimate the relaxation time and distance of the pollen grain in air and compare them with characteristic scales in the troposphere. Below we use the parameters of Birch and Ragweed pollen as one because: (1) most allergic people are sensitive to these species; (2) are the types of pollen that can be classified as one of the furthest-transported class of pollen grain; and (3) both grain shapes are almost spherical, which considerably simplifies the analysis. However, the methodology is applicable for other species, too, as long as the shape-related correction terms are taken into account.

If a particle enters an airflow with its own velocity different from that of the surrounding air, it is forced to follow the main movement with a force represented by Equation 5.9.

$$m\frac{dv}{dt} = -F_{stokes} = -3\pi d\eta\mu \tag{5.13}$$

where m is the mass of the particle. The relaxation time t for Birch pollen will then be:

$$\tau = \frac{d^2 \cdot \rho_{part}}{18\eta} \tag{5.14}$$

Here we have used as a characteristic density of Birch pollen ρ_{part}=800 kg m^{-3} and diameter d=20 μm. Assuming a velocity fluctuation scale of 1 m s^{-1} mm^{-1}, one can see that the grain inertia results in a relaxation distance of the scale of mm, the characteristic path, after which

the grain motion has become adjusted to that of the surrounding air. Therefore, for velocity gradients smaller than $1\,\mathrm{m\,s^{-1}\,mm^{-1}}$, the grain can be considered as noninertial. Since in the real atmosphere the gradients are much smaller, this assumption seems to be well fulfilled. The only comparable spatial scale is the near-surface laminar scale, which can be about several mm thick. However, near the surface, the intensity of turbulence decreases, together with small scale velocity variations, which means that even this layer cannot be penetrated by the pollen grains due to their inertia [Sofiev et al., 2006a]. The above semi-qualitative analysis shows that: (a) for typical atmospheric conditions, the pollen particles (at least Birch and Ragweed particles) do follow the air flows, including turbulent eddies; (b) inertia of grains is also insufficient to penetrate the near-surface laminar layer. Therefore, pollen transport in the atmosphere can be treated via existing advection-diffusion and deposition schemes, which entirely neglect the inertia of the transported species. In addition, the above equations allow straightforward evaluation of dry deposition fluxes, as shown below.

Dry deposition evaluation

The classical scheme for the near-surface dry deposition fluxes includes at least two parallel chains of resistances (see Figure 5.4): one represents gravitational settling; the other consists of aerodynamic, molecular diffusion and surface resistances. Despite the inherently self-contradicting definition of gravitational resistance, this scheme can be used (with clear understanding) to estimate the relative importance of the fluxes through both chains. Considering the stationary motion of a grain due to gravitational force, from equation 5.12 one can derive the particle's terminal settling velocity:

$$u_s = \frac{d^2 \rho_{part} g}{18\eta} \tag{5.15}$$

where g is gravitational acceleration. This is the same expression used by Sofiev et al. [2006a]. The two assumptions behind this formula are: (1) that the correction term in Eq. 5.12 is small, and (2) the Reynolds number is small. For Birch and Ragweed grains, these assumptions are fulfilled:

$$u \sim 1.2\,\mathrm{cm\,s^{-1}};\ \frac{3du}{16\nu} \sim 3.2 \cdot 10^{-3};\ Re \sim 1.7 \cdot 10^{-2} \tag{5.16}$$

The gravitational resistance is the inverse of the settling velocity:

$$R_{grav} = 1/u \sim 85\,\mathrm{s\,m^{-1}} \tag{5.17}$$

The aerodynamic resistance R_A is independent of particle features and has typical values of 1-$100\,\mathrm{s\,cm^{-1}}$, depending on the efficiency of the turbulence. The surface resistance for particles is usually assumed to be zero, which is quite reasonable for the case of pollen grains. The laminar layer resistance R_B representing the process of diffusion through the near-surface thin laminar sublayer is usually computed as:

$$R_B = \frac{2}{\kappa u*}\left(\frac{Sc}{Pr}\right)^{2/3}, Sc = \nu/D \tag{5.18}$$

where $u*$ is a friction velocity, $\kappa = 0.4$ is the von Karman constant, $Pr = 0.72$ is the Prandtl number, and Sc is the Schmidt number. The diffusivity D of the grain due to molecular-scale processes can be computed from Brownian diffusion and the Einstein formula that connects D with kinematical Navier-Stokes considerations:

$$D = \frac{kT}{3\pi d\eta} \tag{5.19}$$

where k is the Stefan-Boltzman constant ($k=1.38 \times 10^{-23}\,\mathrm{J\,K^{-1}}$), and T is the temperature of the air. For Birch and Ragweed pollen, we get approximately:

$$D \sim 10^{-12}\,\mathrm{m^{-2}\,s^{-1}};\ R_B \sim 3.5 \times 10^5\,\mathrm{s\,m^{-1}} \tag{5.20}$$

Comparison of these values and the gravitational settling velocity shows that diffusion plays a negligible role in (Birch and Ragweed) pollen dry deposition from the atmosphere. Since the laminar layer also cannot be penetrated by grains due to their inertia (as described above), the overall dry deposition velocity for this type of pollen will be about $1\,\mathrm{cm\,s^{-1}}$. This estimate is comparable with the values for classical long-range transported species and corresponds to half-lifetime of ~ 1 day in the atmosphere due to dry deposition. This implies that about half of the emitted mass will be transported over a distance greater than $10 \times 10^3\,\mathrm{km}$. In reality part of the grains can stay in the atmosphere considerably longer due to turbulent vertical mixing,

which will oppose the downward motion. A more experimental approach to the estimation of the settling velocity of corn pollen can be found in Aylor [2002] and in applications to other species, in Helbig et al. [2004]. The application of the deposition velocity formula as described in the above literature (excluding the effects of water content on the particle size) is presented in Figure 5.5 on appendix 3. Typical pollen settling velocities calculated with this experimental method are in accordance with the CMAQ methodology (See summary literature values for a spectrum of species on Table 5.3).

5.4 Simulation results for Birch and Ragweed species

5.4.1 Local pollen counts and backward modeling of the pollen dispersion

There are various devices for air sampling for both viable and total spore counts (also referred to as non-viable) analysis [Macher and Macher, 1999]. All these devices operate on only few basic principles: deposition, impaction, and suction. The most common device in the United States, the Rotorod impaction sampler, is present in more than 300 different locations [Frenz, 1999]. A private aerobiological network (Airborne Allergen Network - Multidata Inc.) gathers data collected from each Rotorod monitor after being analyzed according to a common protocol [Frenz et al., 1997]. The mechanism consists of a rotating arm-impactor that collects pollen grains on two plastic rods that the device's motor rotates through the atmosphere (Figure 5.6). The sampling surface is usually analyzed microscopically on a daily basis (excluding the weekends and holidays) to include the following pollen categories with respect to the grain's origin: trees, grasses, total weeds (divided into ragweed and non-ragweed grains).

The Rotorod device used in this study is located in the roof of the UMDNJ building, in Newark, New Jersey. Daily averages were available for the years 1990-2003, excluding the spring of 2000 and some sporadic missing values for tree counts during 1991 and 1998. The annual time series plots for total tree and ragweed counts provided in Figure 5.7 indicate that tree pollen emerges during the late March/early May, while ragweed starts during late August/early September. During 2002 the counts demonstrate a mid-March peak while most of the tree pollen is trapped during late March (Figure 5.8). It is clear that the predominant pollen in the region during the spring is coming from trees, with a study maximum of 9301 grains/m^3 observed during

2002. The spring pollen period of 2002 appears earlier and stronger than usual, comparable only to the 9118 grains/m^3 observed during 1994. Ragweed counts indicated substantially smaller atmospheric levels when compared with the tree component. The year with the maximum counts remained the same with the total tree pollen counts. The study maximum was found to be 690 grains/m^3 during 1994, while the maximum daily counts for 2002 were 187 grains/m^3). Comparison of total pollen counts obtained by two different Rotorod devices located 5.6 km apart has revealed monthly and daily differences [Frenz et al., 1997]. The same study concludes that differences were most pronounced for counts exceeding 100 pollen grains/m^3.

An in-depth analysis of the pollen counts can be provided by including the effect of simulated meteorology along with backward trajectory modeling and pollen source mapping tools that utilize vegetation geodatabases. Independently of the employed methodology, weather conditions should be examined closely as they drive both emission and dispersion of the allergenic particles. For our case, local meteorological data were obtained for the years of interest from the station located in Newark International Airport. The windrose plot presented in Figure 5.9 provides an illustration of the wind component for the entire year of 2002. Representative time series plots of the local meteorological parameters of interest versus the pollen counts for 2002 are presented in Figure 5.10 for total tree pollen and in Figure 5.12 for ragweed pollen particles. Windroses relevant to each pollen season of the same year are presented in Figure 5.11, and Figure 5.13, respectively.

Two modeling scenarios were developed based on the intricacies of 2002, as described above in terms of pollen counts. A period that was carefully examined was the month of April of 2002 which, during the third week, exhibits a strong tree component reaching the monitor location. The second scenario refers to the ragweed simulation for the month of September. The HYSPLIT model offers a computational environment for a variety of transport options, from simple air parcel trajectories, to complex dispersion and deposition simulations. An application of simple 8-hour backward trajectory that reaches 20 m above the surface of UMDNJ location, at 11 am of April 17th is visualized in Figure 5.14. In a more complex setup for the months and species of interest (Figures 5.15 and 5.16), multiple backward trajectories on days with low and high pollen levels can combine to produce a backward plume. April 18th and 19th along with August 5th and 12th were selected as representative days with high pollen counts.

In the same manner, April 15th and 24th along with August 7th and 18th were selected as representative days with high pollen counts. The backward trajectories can be also used to identify and locate clusters of significant pollen sources in the regional scale. In order to achieve that an underlying vegetation information layer was created in a GIS framework based on the tree density map developed by the USGS/USFS/EPA (BELD3). A comparison of the NLCD and USGS databases, as incorporated for the area of interest in the GIS software (ArcGIS), is presented in Figure 5.17. Plumes from 8-hour backward trajectories reaching the device location every two hours are illustrated in Figure 5.18. From these figures we can conclude that high tree pollen counts do not necessarily correspond to trajectories above densely forested areas. This can be potentially due to the fact that the trajectories are outside the "emission window" for specific species-emitters within the area of the air parcel. The only clear finding that can be seen from this analysis is that high counts are correlated positively with winds following the direction of east. A daily vegetation index, characteristic of the pattern of the backward pollen trajectory and the association with the underlying vegetation density, can be a useful metric for such applications. An example of this metric is presented in a raw and distance-weighted manner in Figure 5.19. Further cluster analysis options are available with the use of TrajStat, an external program developed for HYSPLIT [Wang et al., 2009].

5.4.2 Evaluation of pollen emission timing and intensity

One of the most difficult problems in pollen-dispersion forecasting is to evaluate the emission flux of grains and its time evolution. At this point, it has to be pointed that the system developed for "proof of concept" simulations during the Spring of 2002 used an additional "climatological" emission term, which was based on the results of long-term mean observed birch and ragweed flowering dates. The underlying spatial database was BELD3.1 for the case of Birch, and a modified version of the P.L.A.N.T.S. database developed and maintained at the U.S. Department of Agriculture for the case of Ragweed simulations. The result of the emission model for the case of Birch (April 2002) are presented in a set of maps in Figure 5.20. The maps show a good agreement with the monthly temporal profile, as it was recorded in the UMDNJ Rotorod device during the Spring of 2002.

5.4.3 Pollen dispersion results

During the trial reanalysis simulations of 2002, the CMAQ model run once per monthly scenario in order to capture the effects of the entire "emission window" and to allow for certain initial spin-up time for better performance. In the first step of the result analysis, the main focus was on the dispersion comparison of the two modeling options (CMAQ versus HYSPLIT). The patterns observed for a similar area source by each model are provided in Figures 5.21-5.22. As we can see, the entire day was dominated by constant-direction winds that transported particles throughout the Long Island. This flow was consistent throughout the day, as maps with the hourly output (ending at 8 am, 12 pm, 4 pm and 8 pm) indicate. The two models showed significant resemblance in capturing the pattern and intensity of the Birch pollen transport. HYSPLIT calculated plumes covered larger areas than CMAQ output for a variety of dispersion parameterizations (options under the dispersion module).

In the next modeling step, the full month simulations for the case of Birch and Ragweed were explored. Mapped simulation output for Birch and Ragweed pollen is presented in Figures 5.23-5.26 and 5.27-5.30. A different release height was investigated for the case of Birch, with the emission being assigned (to a smaller percentage, usually 20%) in the second layer. The dispersal pattern revealed to be almost identical with some additional area covered by higher atmospheric levels around the 12 by 12 km emission cell. In the same manner, simulations with extended heigh were performed in HYSPLIT and the results of trajectory paths agree to this small increase in longer transport probability. Finally, concentration timeseries plots of the modeled months during 2002 are presented in Figures 5.31-5.32. These plots indicate a good correlation of the modeled pollen source with the observed values of pollen counts at the same cell location as the UMDNJ Rotorod device (Figures 5.15-5.16).

5.5 Discussion

The general attitude towards coarse atmospheric aerosols is that its influence is primarily local or, at most, regional. This study, along with others in the field of aerobiology, shows that from the point of view of atmospheric dispersion modeling, birch pollen grains resemble the behavior of anthropogenic aerosols with a diameter smaller than $10\,\mu m$ (PM_{10}). In particular, pollen

has a similar gravitational settling velocity close to $1\,\mathrm{cm\,s^{-1}}$. A general explanation for this similarity (although pollen is more than twice the size) is that pollen is a low-density particle, which makes it more susceptible to air currents and drastically reduces gravitational settling.

There are also several important differences that bring birch pollen grains into the scale of large-scale transported pollutants. Firstly, the grains are hydrophobic, which significantly reduces the intensity of both in-cloud processes and subcloud scavenging, by far the most intensive sinks of atmospheric aerosol. Secondly, anthropogenic pollutants with concentration levels of $5-10\%$ near the source are often negligible, or at least is not treated as a major problem. In the case of pollen, the opposite situation occurs: concentrations of 100 grains/m^3 of air are considered "high level" while the near-source levels are typically an order of magnitude greater. Therefore, even if dilution and removal of pollen during transport reaches 90% the remaining amount is still considered significant enough to cause health problems. Thirdly, birch forests are abundant over large areas of both Europe and the United States, thus representing an uniquely extensive source area that allows even for transatlantic transport. Finally, pollen emission takes place under conditions that favor large-scale distribution: sunny days in late Spring, no precipitation, moderate wind, and an emission height of more than $10\,\mathrm{m}$. These conditions lead to a quick mixing of the emitted mass over a deep layer due to turbulence. All the above-mentioned factors induce a large-scale dispersion of pollen and confirm at a qualitative level the conclusions derived from formal computations of pollen behavior based on the physical characteristics of the grain. The above factors are reasonably well reproduced by existing meteorological and dispersion models, therefore simplifying their application to pollen dispersion simulations.

Figures
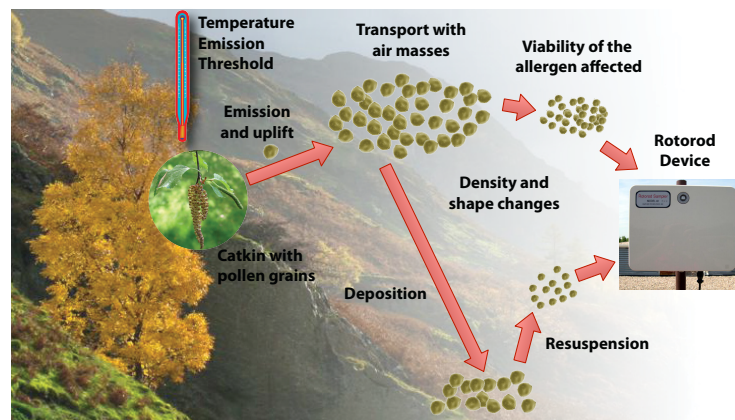
Figure 5.1: Atmospheric processes relevant to the fate and transport of allergenic pollen grains [Source: Helbig et al., 2004].
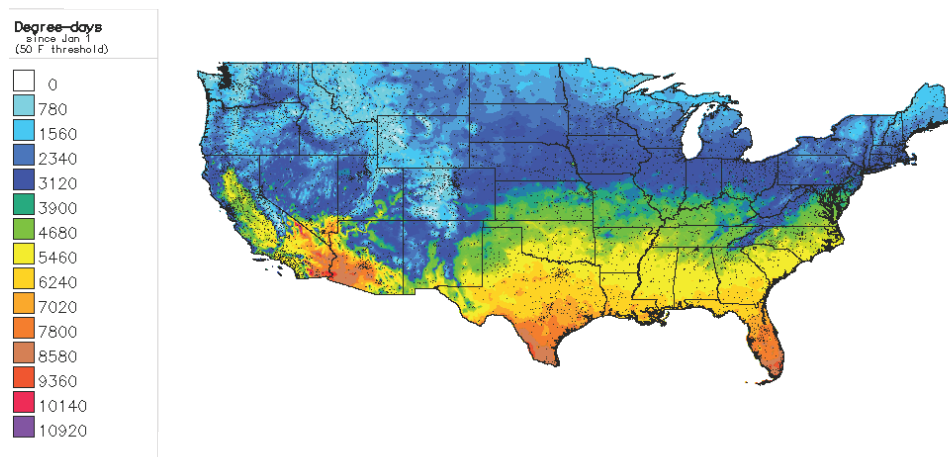
Figure 5.2: Calculated heat degree days for the entire United States during 2002 (50 degrees Fahrenheit threshold).
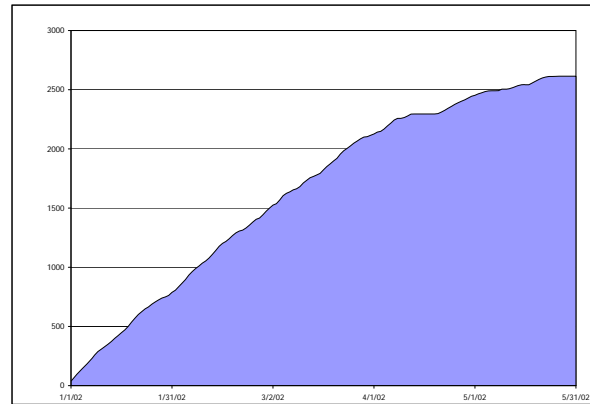
Figure 5.3: Calculated heat degree days for the Newark International Airport meteorological station during 2002 (50 degrees Fahrenheit threshold) using NCDC data.
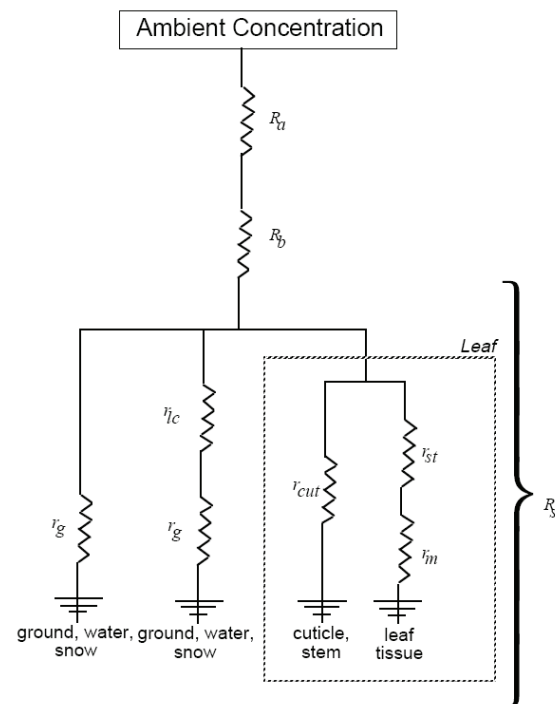
Figure 5.4: Schematic depiction of the processes that influence deposition velocity calculations in the CMAQ model using land-use specific resistances [Source: Seinfeld and Pandis, 2006].
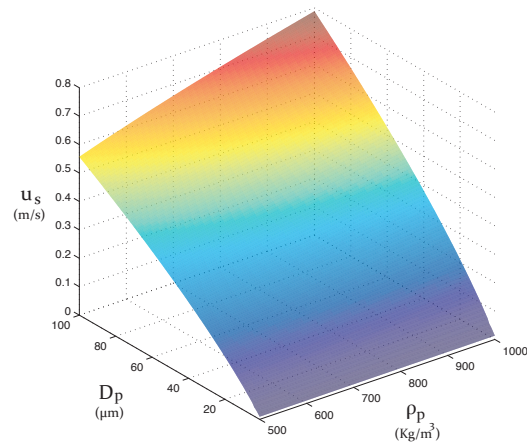
Figure 5.5: Deposition velocity calculations using the method described in Aylor [2002] for a range of pollen sizes and densities, assuming typical temperature and wind speed.
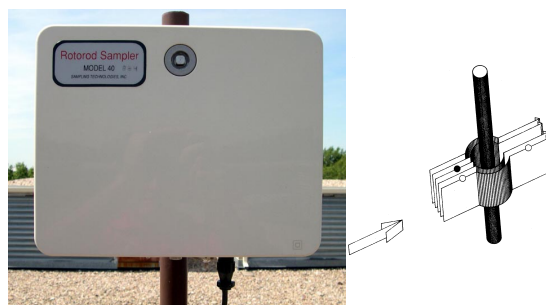
Figure 5.6: The Rotorod device along with a depiction of the sampling principle: air and particle trajectories around an impaction cylinder - only the black particle will impact [Source: Falagiani, 1990].
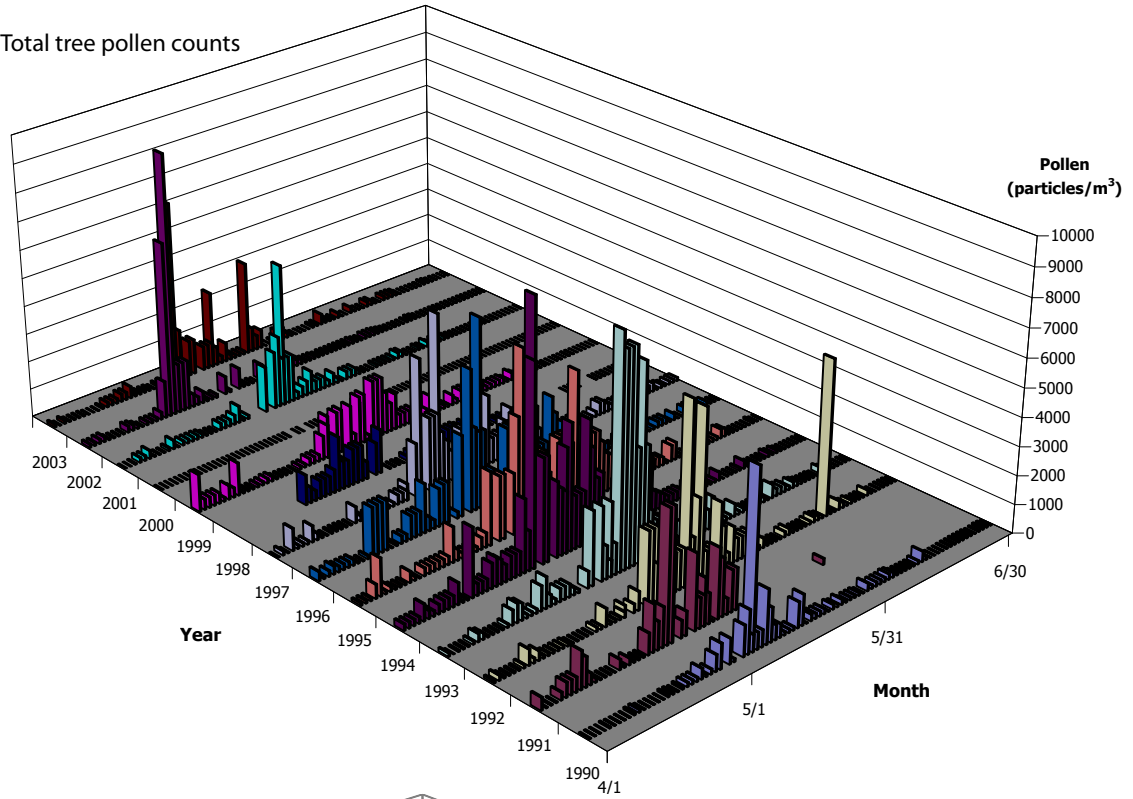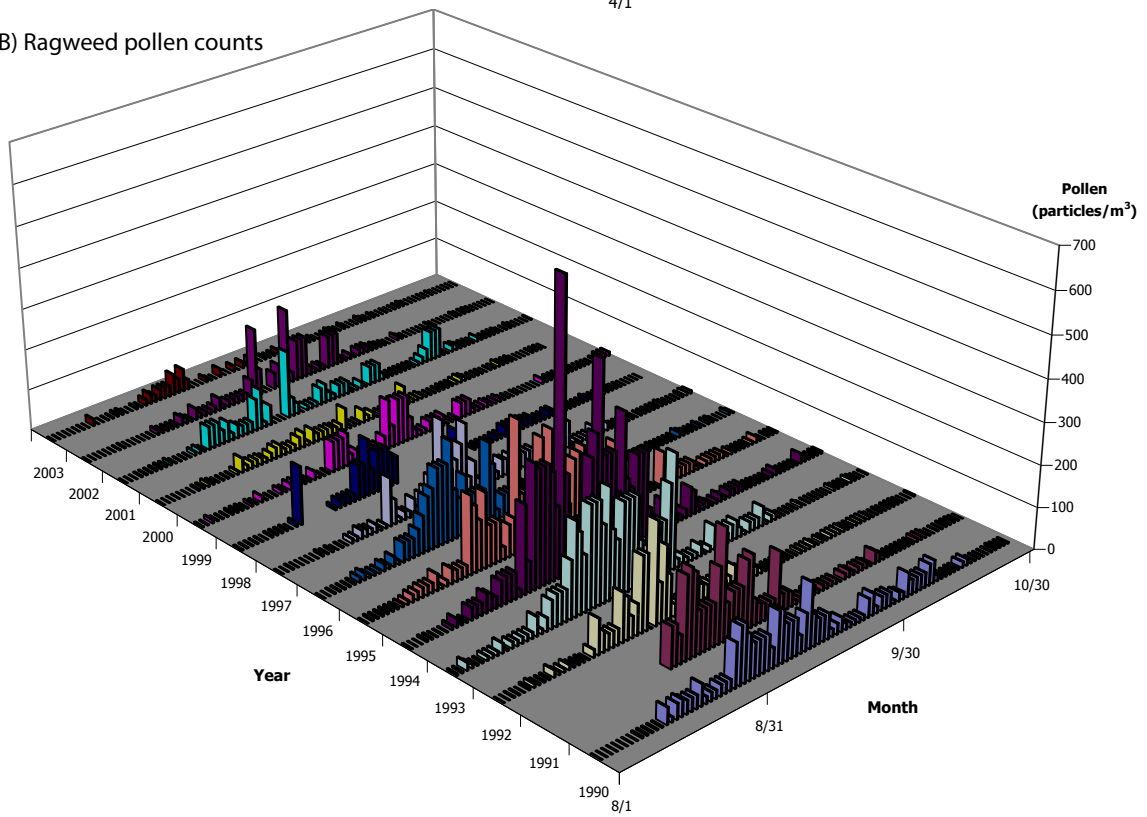
Figure 5.7: Annual tree and ragweed pollen counts in Newark, NJ for the years 1990-2003. Data for UMDNJ Newark were provided by Dr. Bielory.
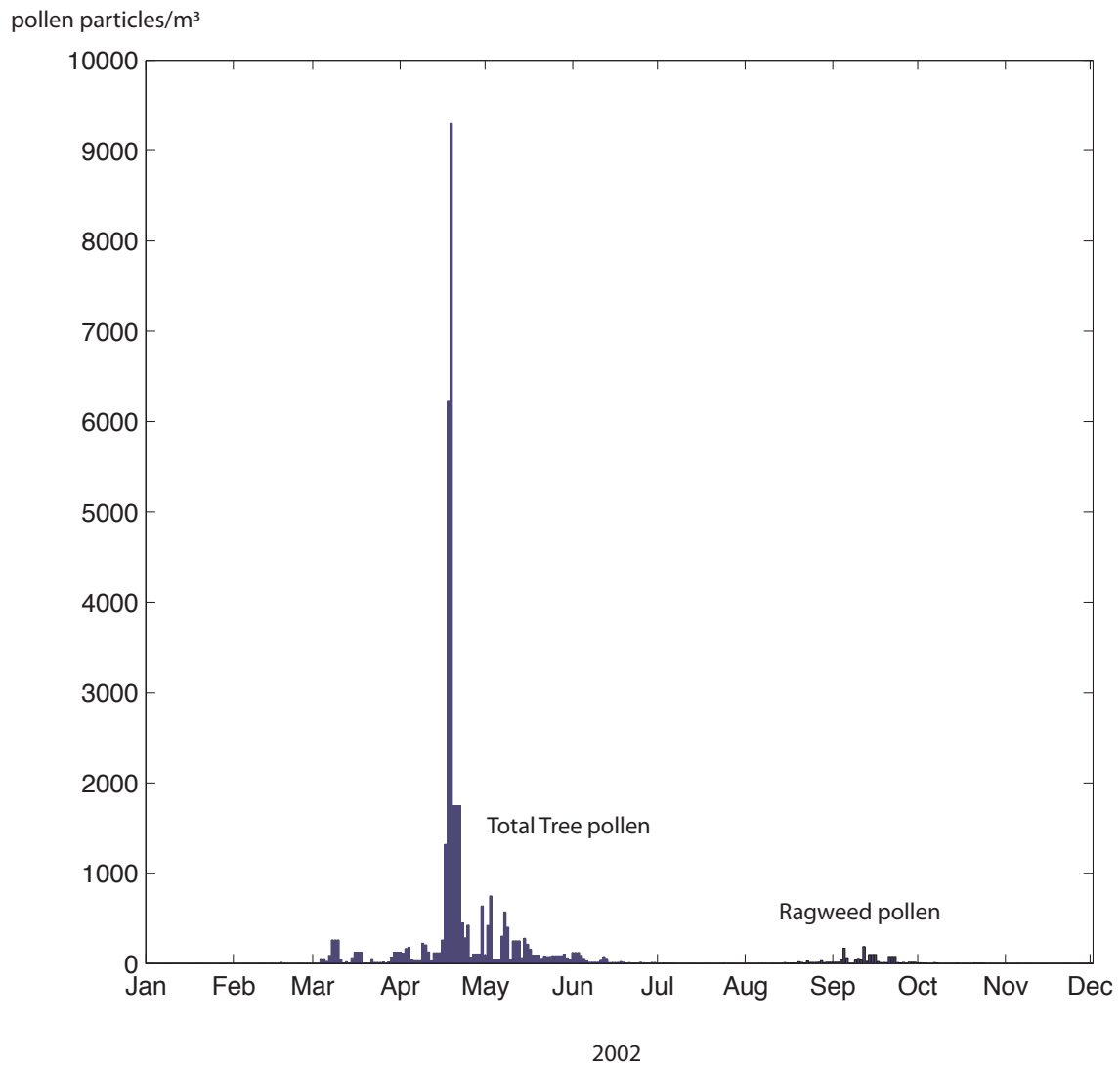
Figure 5.8: Tree and ragweed pollen counts in Newark, NJ for the modeled year of 2002. Data for UMDNJ Newark were provided by Dr. Bielory.

WIND ROSE PLOT:	DISPLAY:
Station #14734 - NEWARK/INT'L ARPT, NJ	**Wind Speed** **Direction (blowing from)**

WIND SPEED (m/s)

- >= 11.1
- 8.8 - 11.1
- 5.7 - 8.8
- 3.6 - 5.7
- 2.1 - 3.6
- 0.5 - 2.1

Calms: 4.39%

COMMENTS:	DATA PERIOD:	COMPANY NAME:	
	2002 **Jan 1 - Dec 31** **00:00 - 23:00**	**CCL**	
		MODELER: **Christos Efstathiou**	
	CALM WINDS: **4.39%**	TOTAL COUNT: **8744 hrs.**	
	AVG. WIND SPEED: **4.55 m/s**	DATE:	PROJECT NO.:
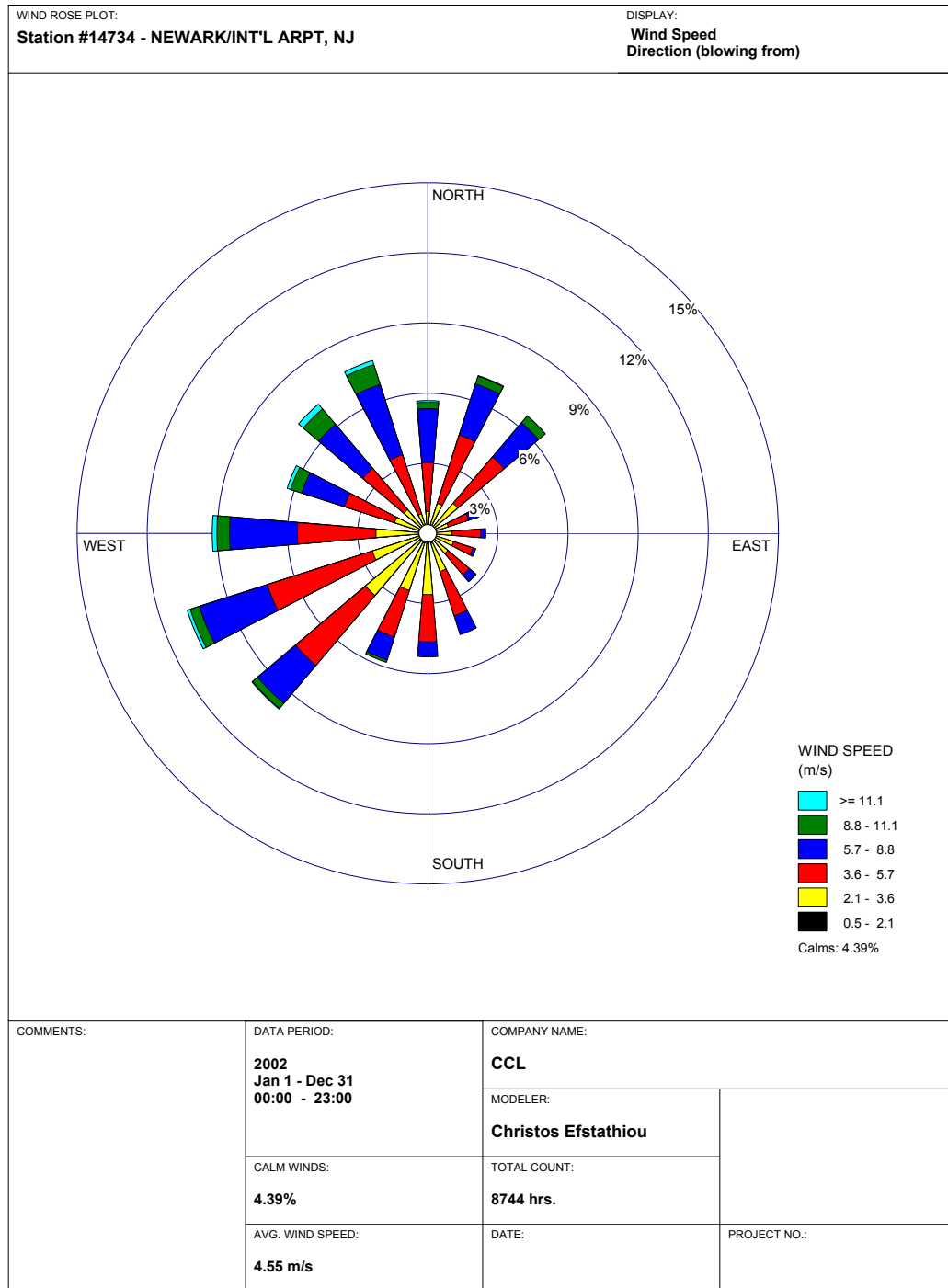
Figure 5.9: Windrose for the Newark International Airport meteorological station during the entire year of 2002.
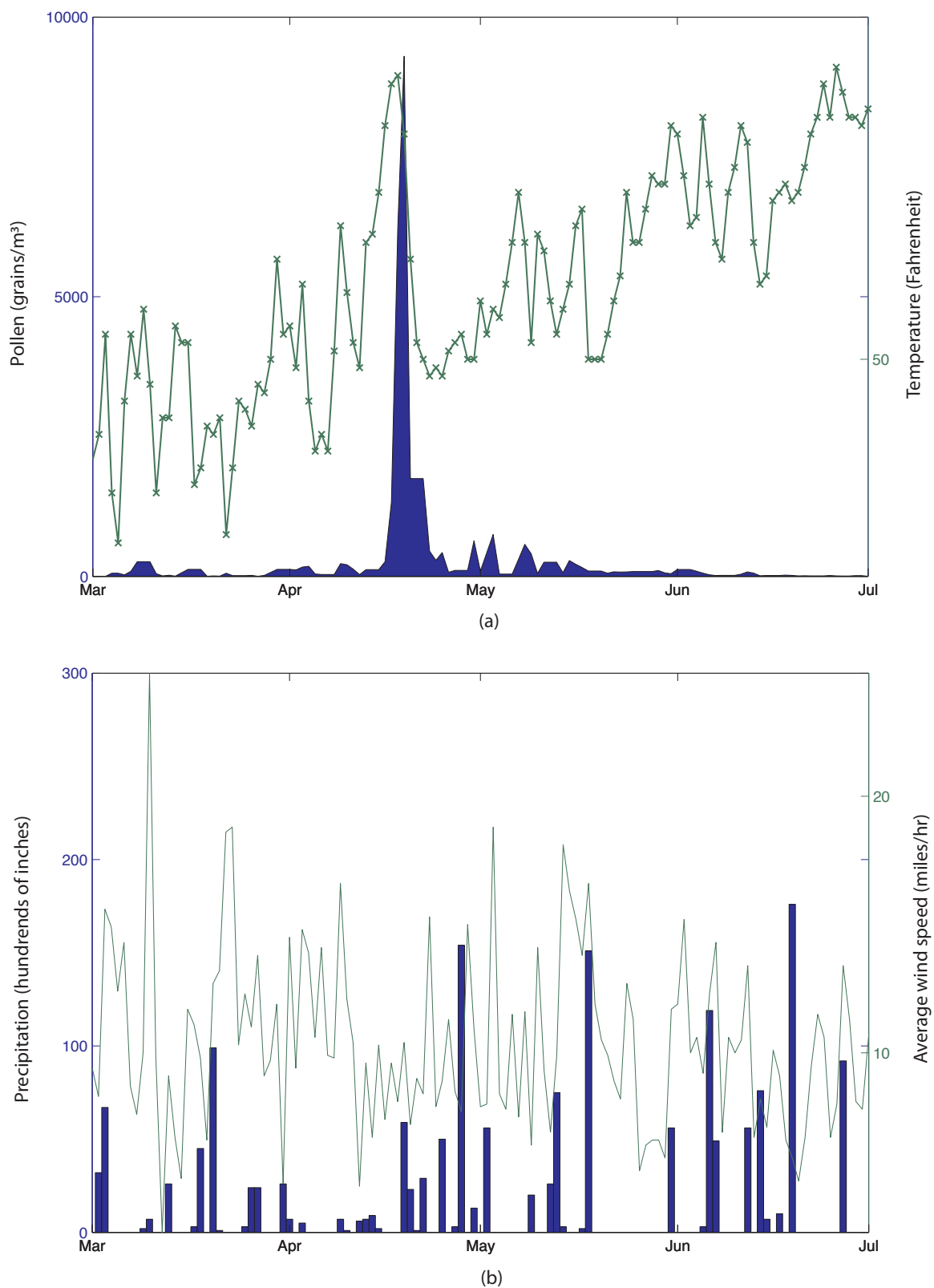
Figure 5.10: Time series plot of the tree pollen counts against the meteorological variables recorded at Newark, NJ during 2002.
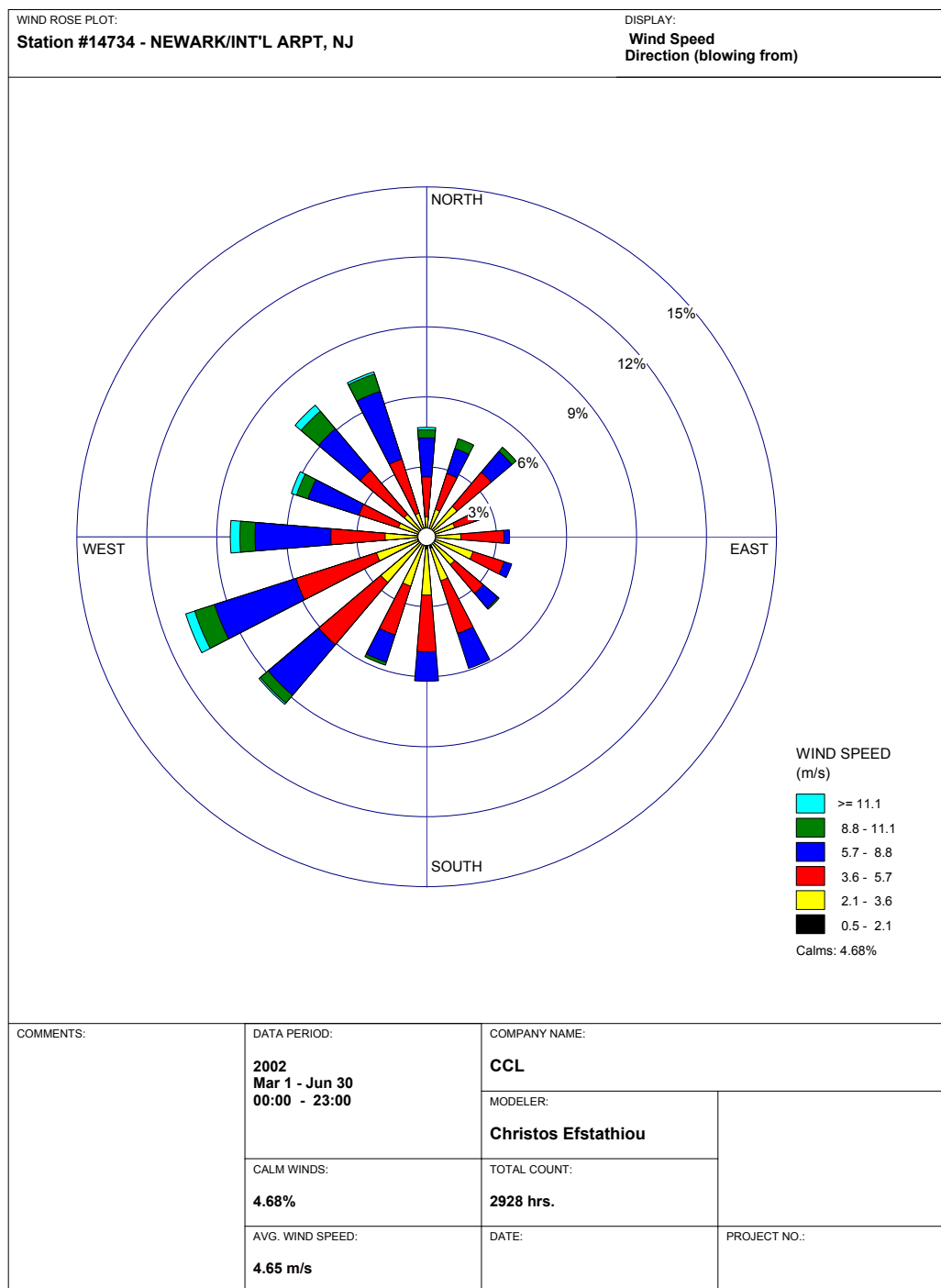
Figure 5.11: Windrose for Newark Meteorological Station - Spring of 2002 (tree pollen).
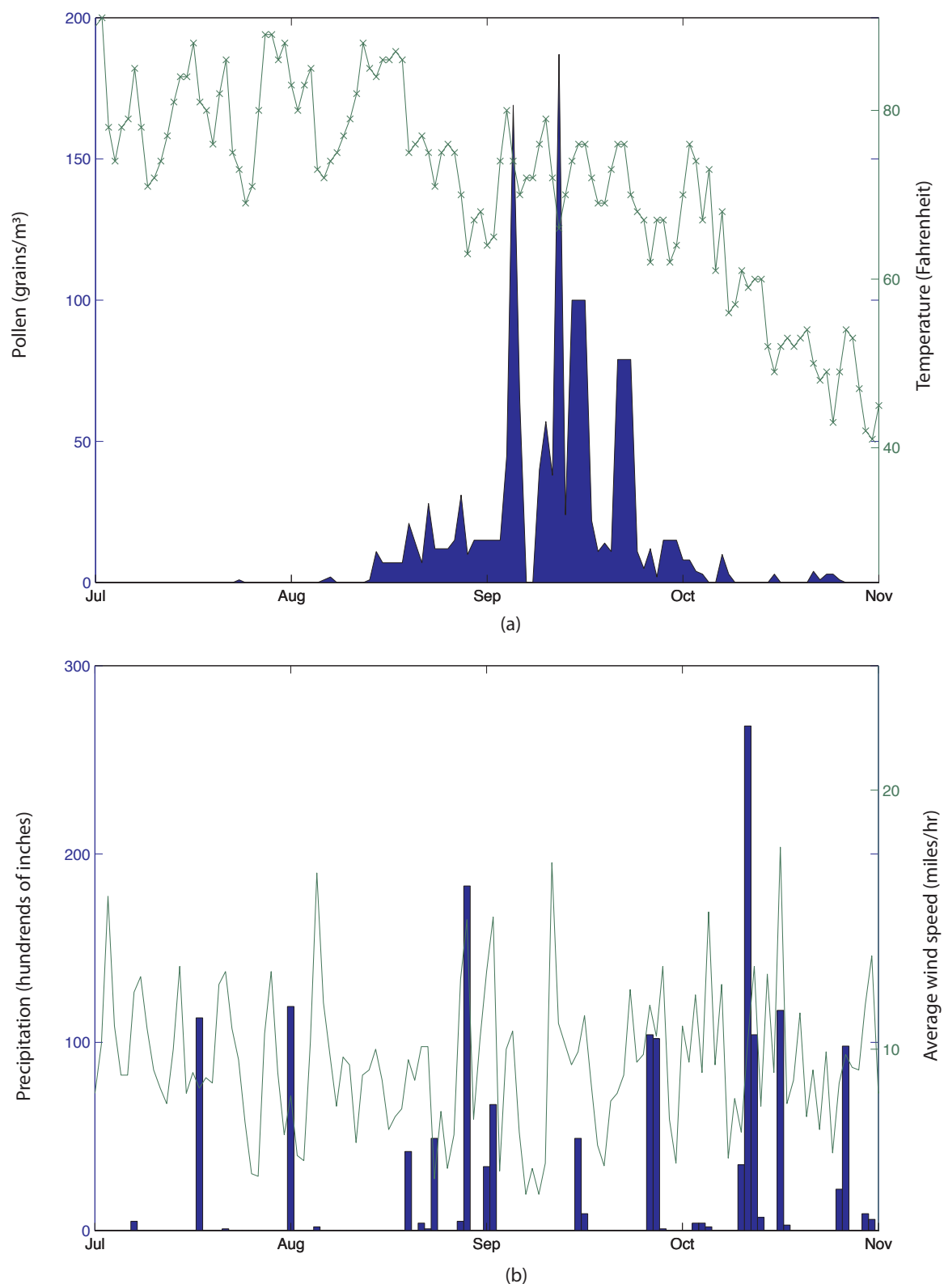
Figure 5.12: Time series plot of the ragweed pollen counts against the meteorological variables recorded at Newark, NJ during 2002.
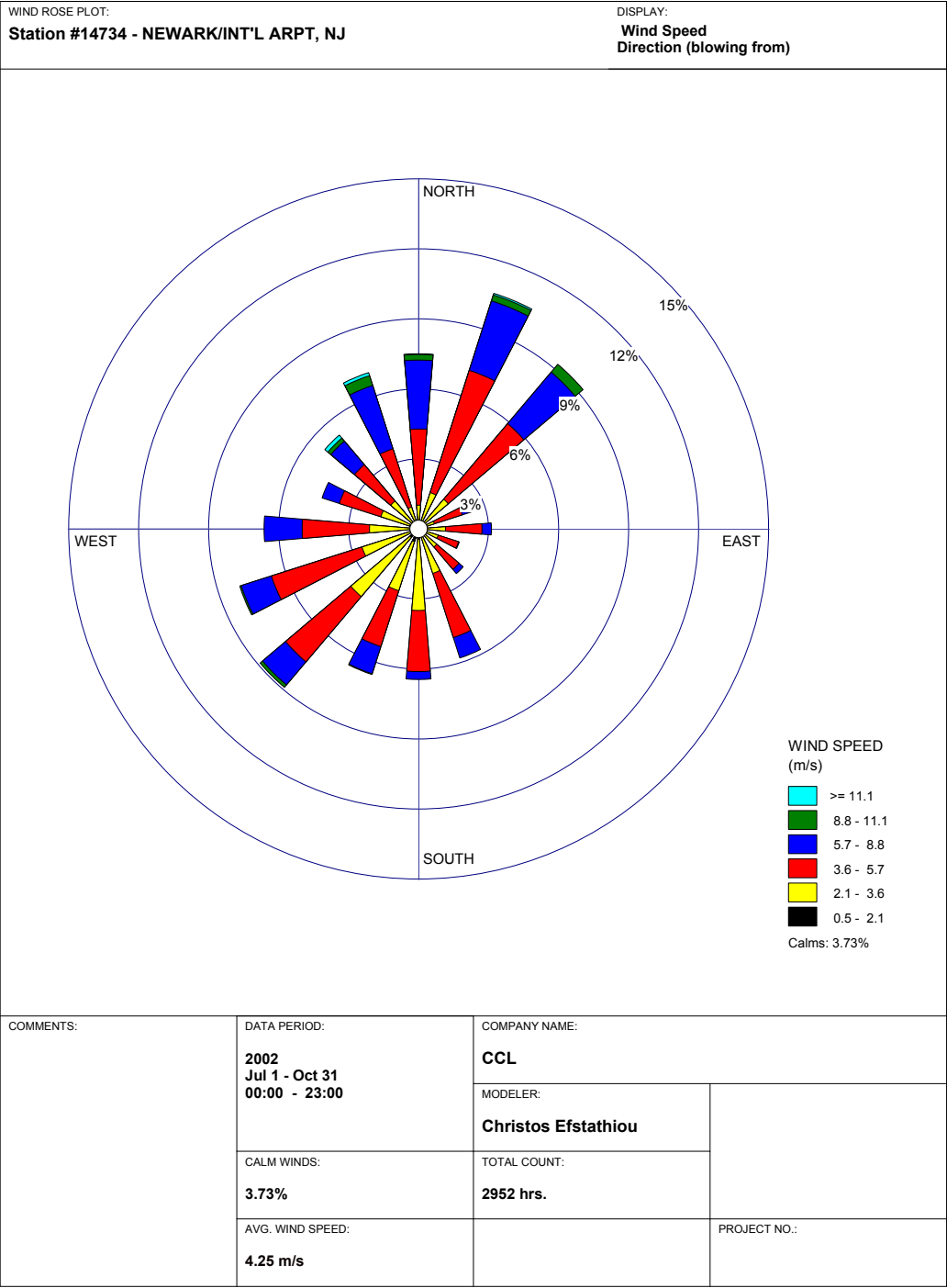
Figure 5.13: Windrose for Newark Meteorological Station - Autumn of 2002 (ragweed pollen).
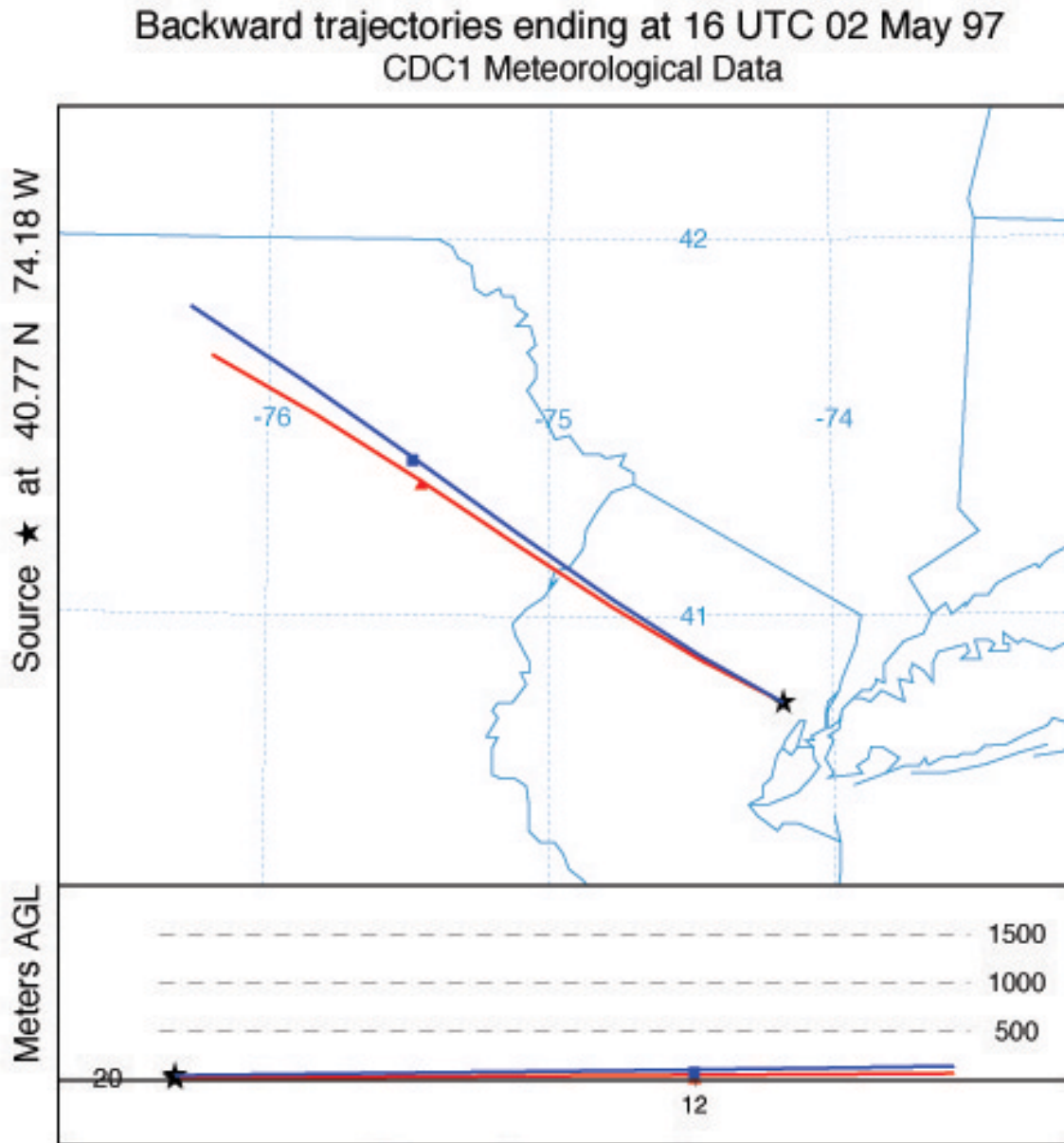
Figure 5.14: 6-hour HYSPLIT backward trajectory that ends at the UMDNJ location at 11AM local time, April 17th of 2002.
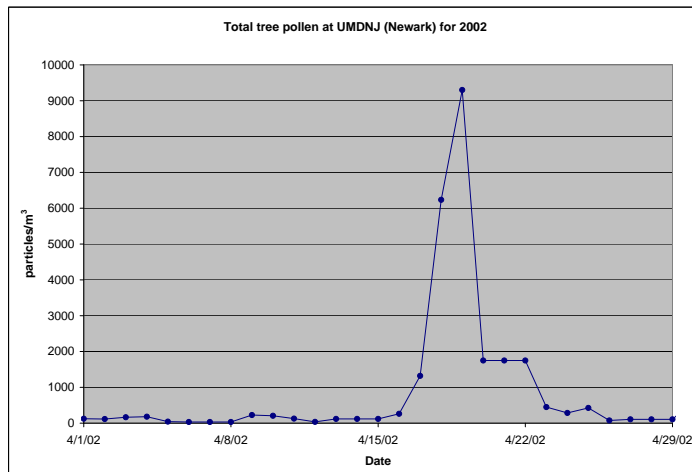
Figure 5.15: Tree pollen counts for the month of April 2002. Data for UMDNJ Newark were provided by Dr. Bielory.
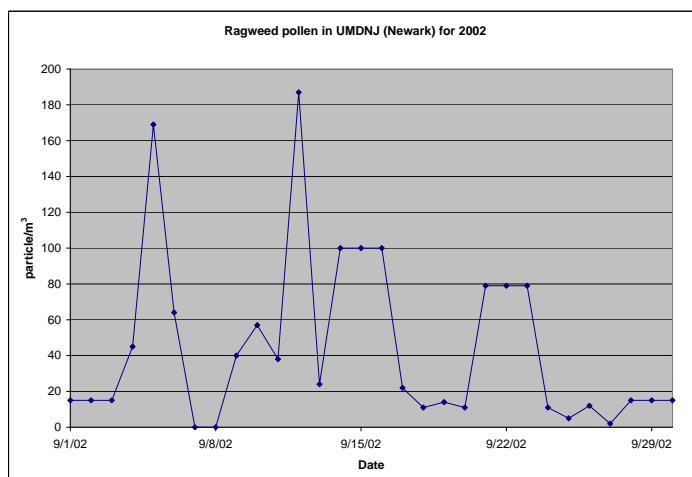
Figure 5.16: Ragweed pollen counts for the month of August 2002. Data for UMDNJ Newark were provided by Dr. Bielory.
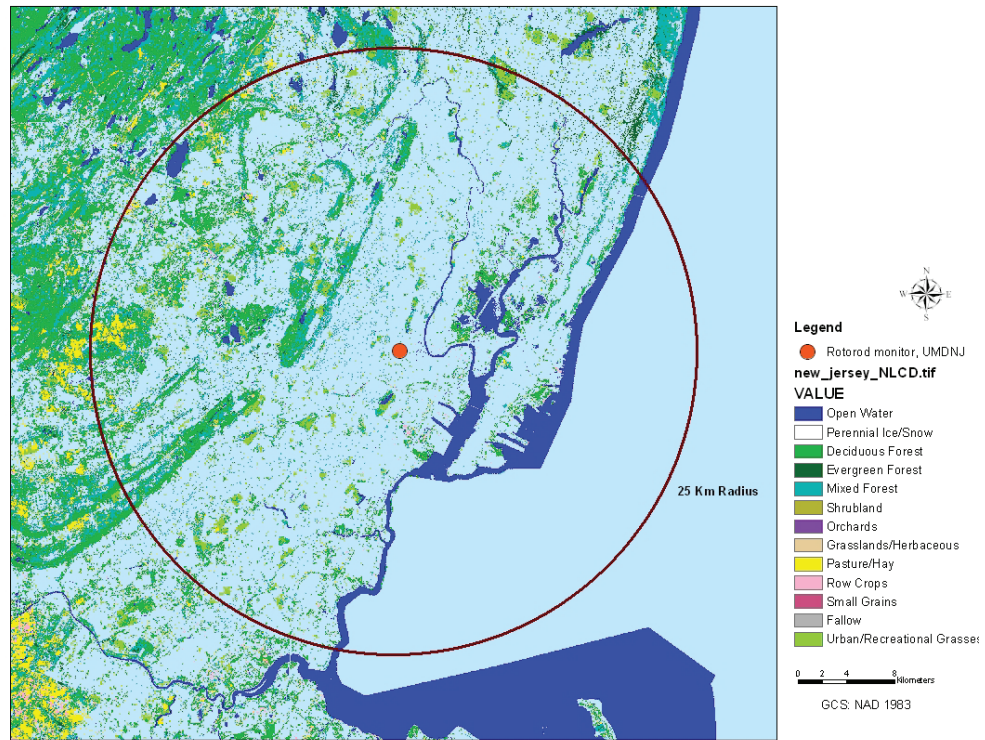
(a)
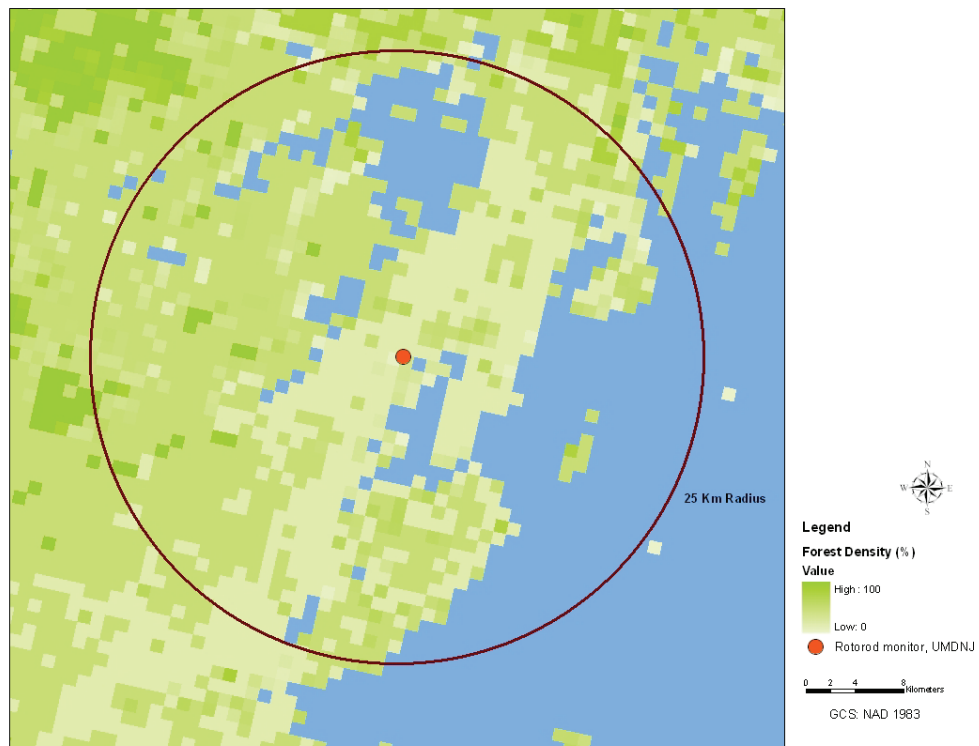
(b)

Figure 5.17: The National Land Cover Database (a) and USGS forest density (b) maps for the area of Newark, NJ
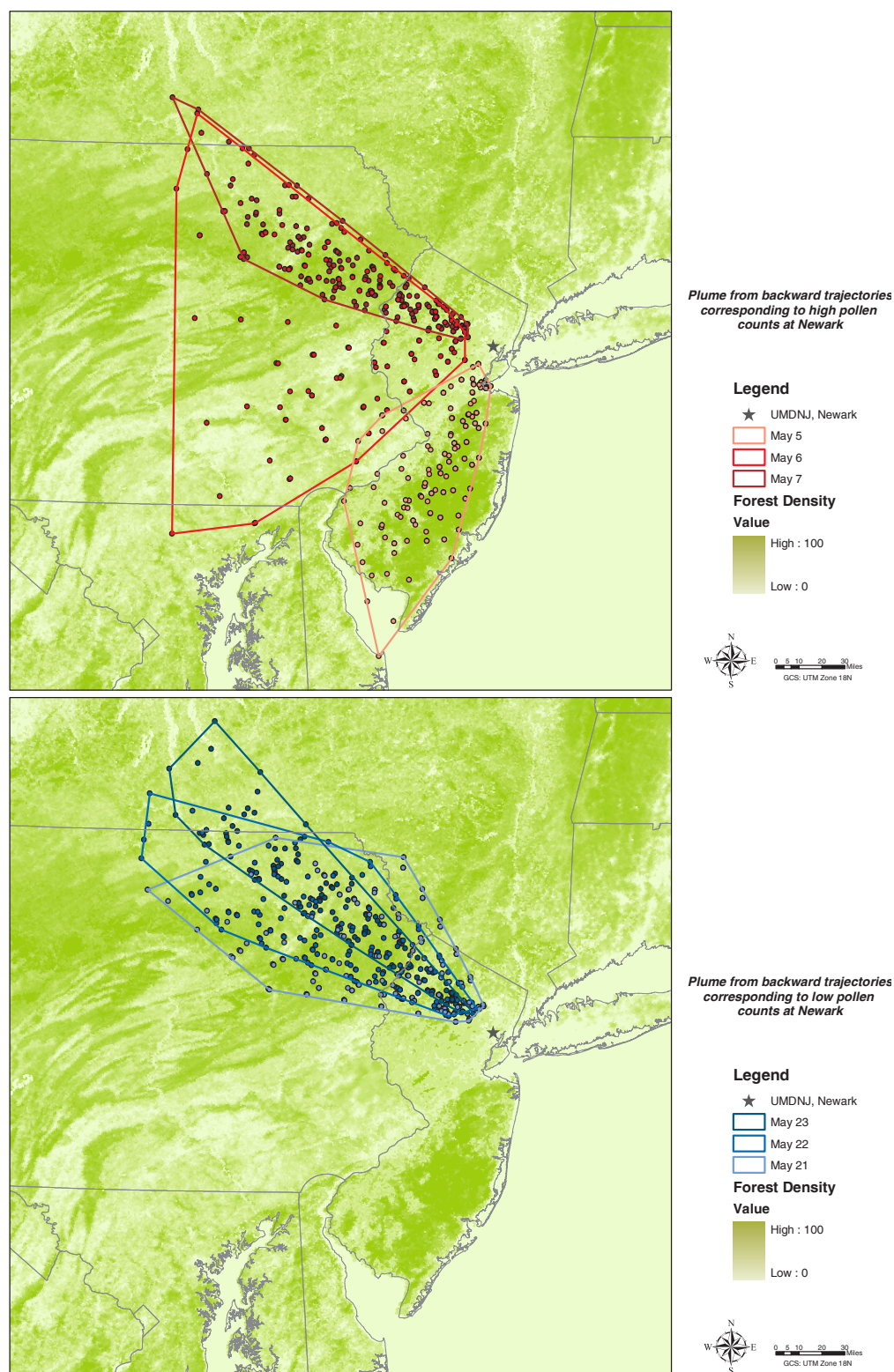
Figure 5.18: Plumes from backward trajectories corresponding to low pollen counts (Top figure: May 5-7) and high pollen counts (Bottom figure: May 21-23) reaching the Newark monitoring location.
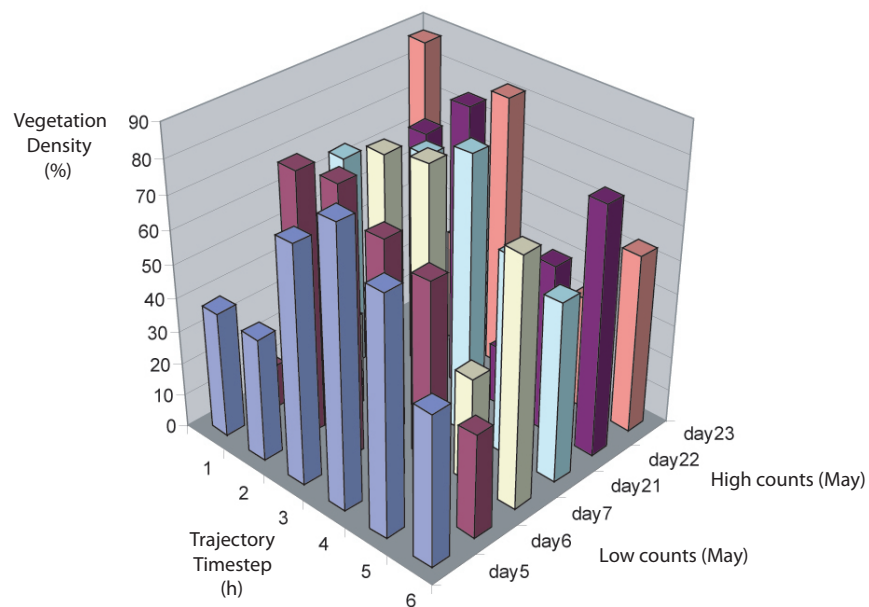
(a) Raw tree density
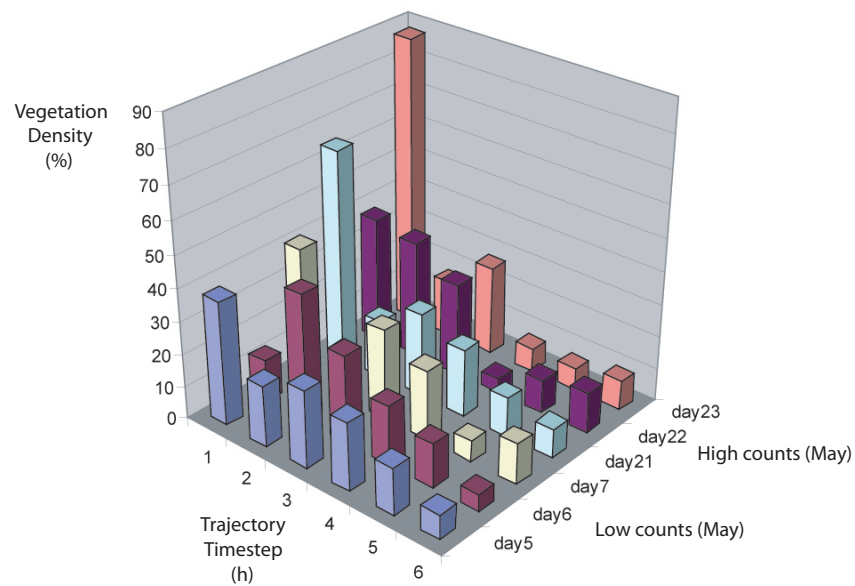
(b) Distance-weighted tree density

Figure 5.19: (a) Raw, and (b) distance-weighted vegetation density metric based on the BELD3 database and the overlapping backward trajectories for low and high pollen counts.
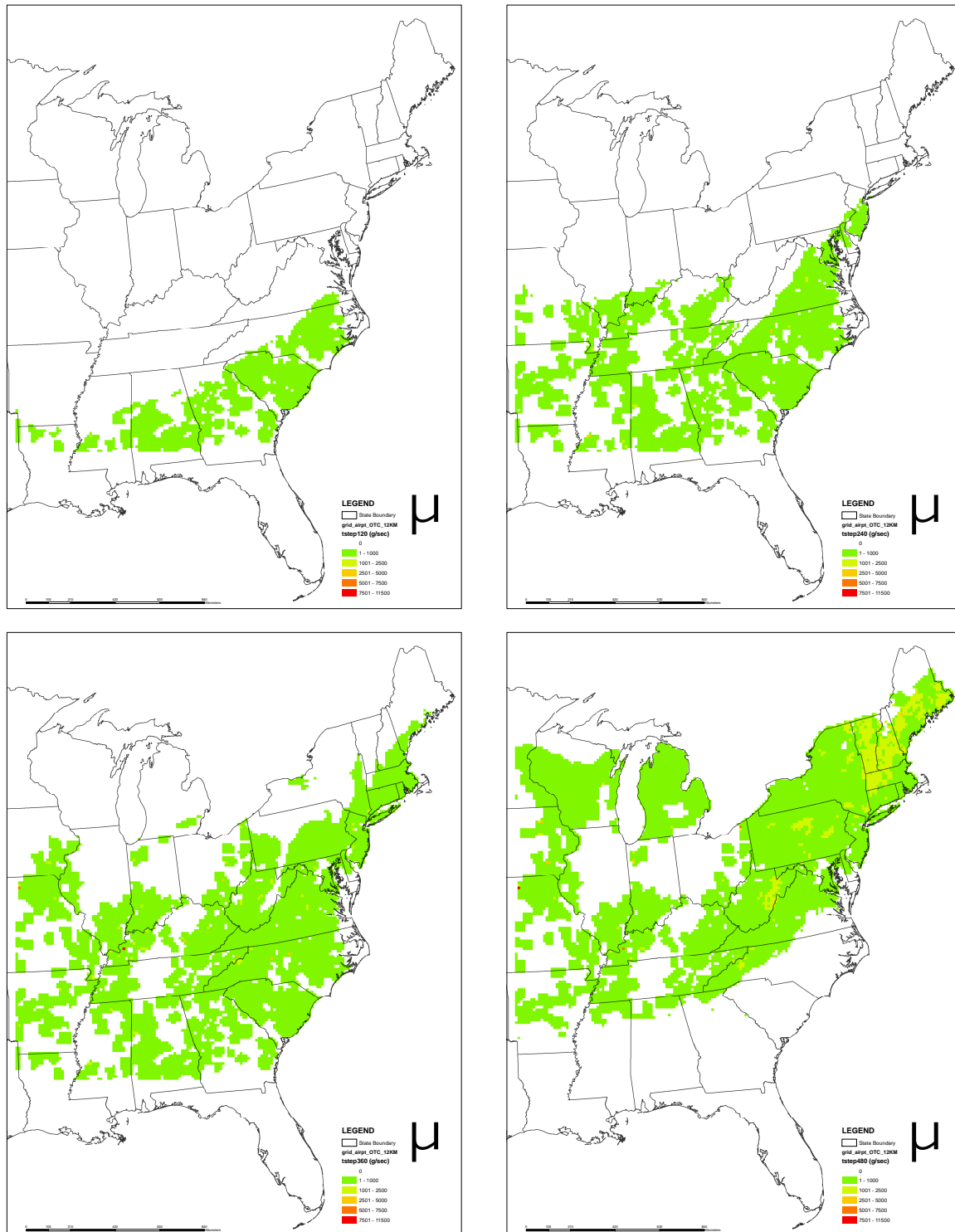
Figure 5.20: Hourly Birch pollen emissions for the 5th, 10th, 15th, 20th, 25th, and 30th day of April (GCS: NAD83).
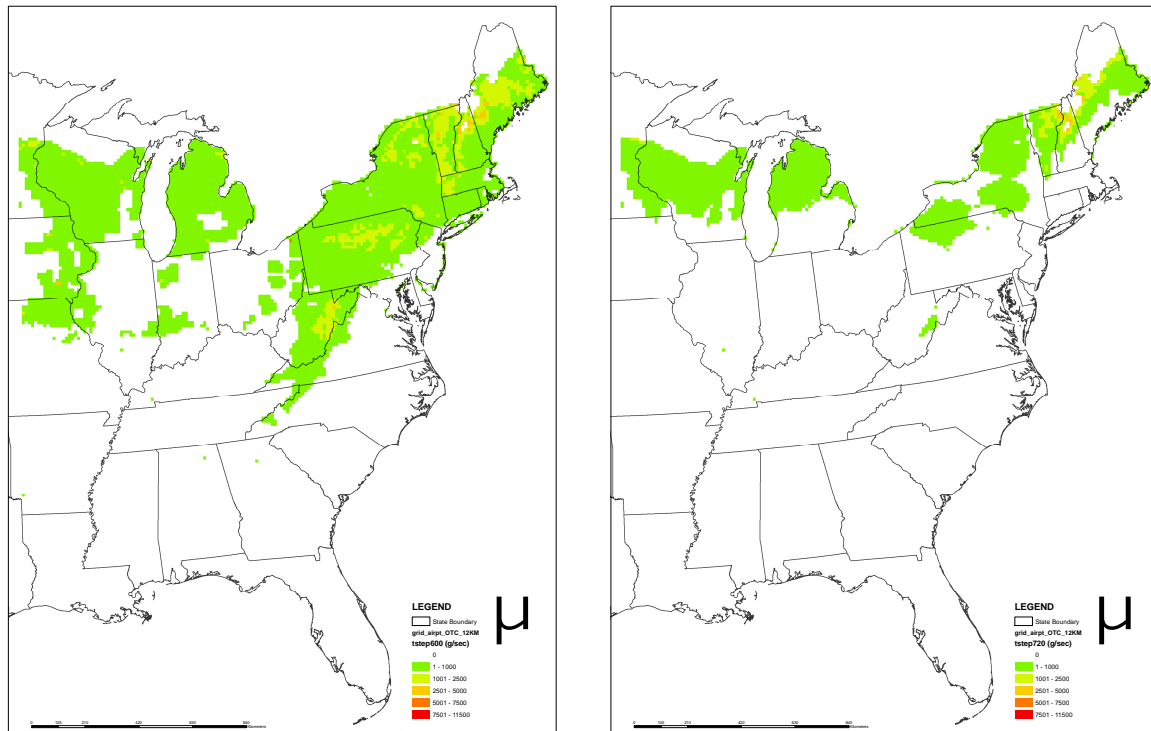
(Continued...) Hourly Birch pollen emissions for the 5th, 10th, 15th, 20th, 25th, and 30th day of April (GCS: NAD83).
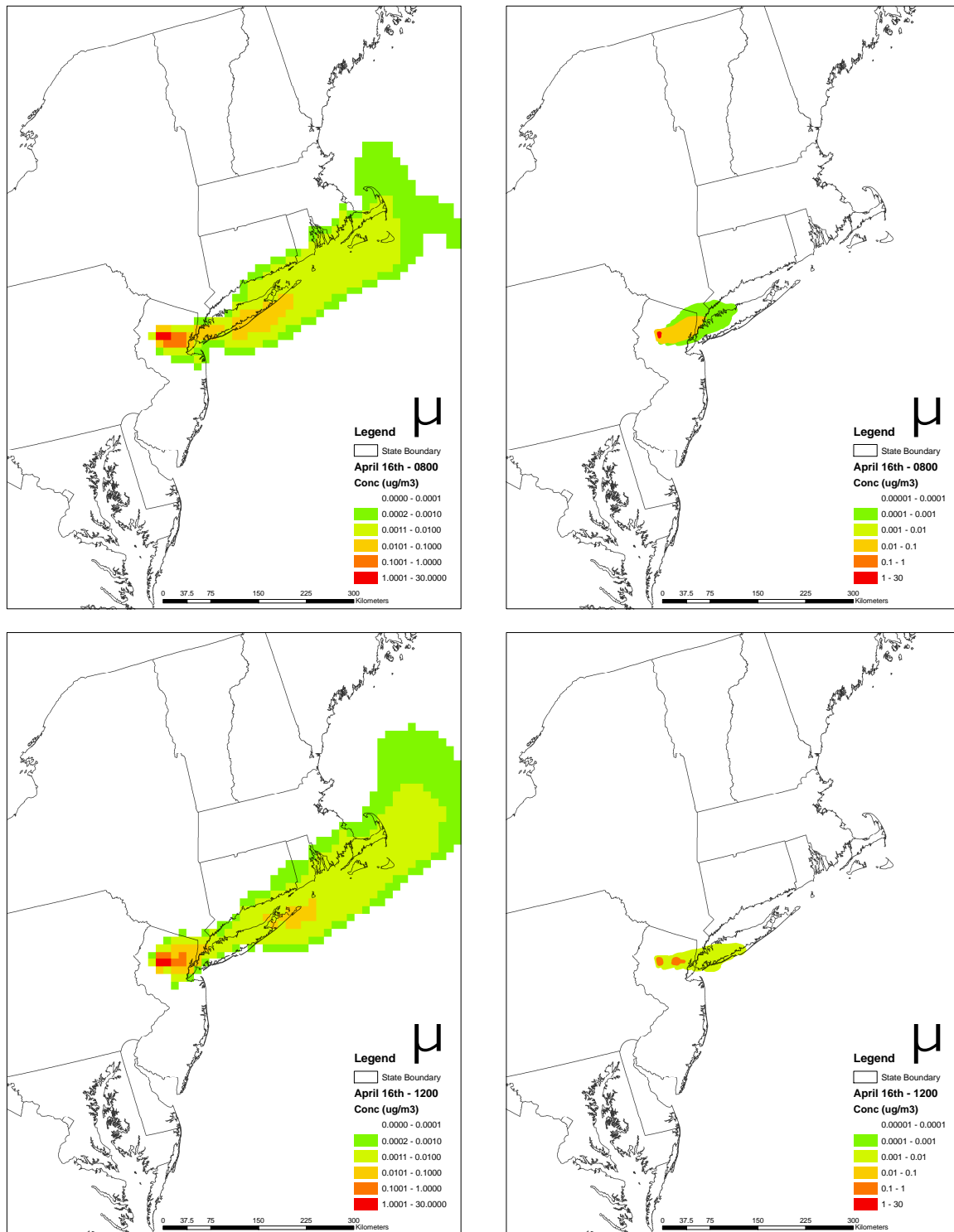
Figure 5.21: Plume comparison plots utilizing CMAQ (left) and HYSPLIT (right) models for a single cell Birch emission during 07:00 - 08:00 and 11:00 -12:00 on April 16 of 2002. The two models closely capture the direction and spread of the plume (GCS: NAD83).
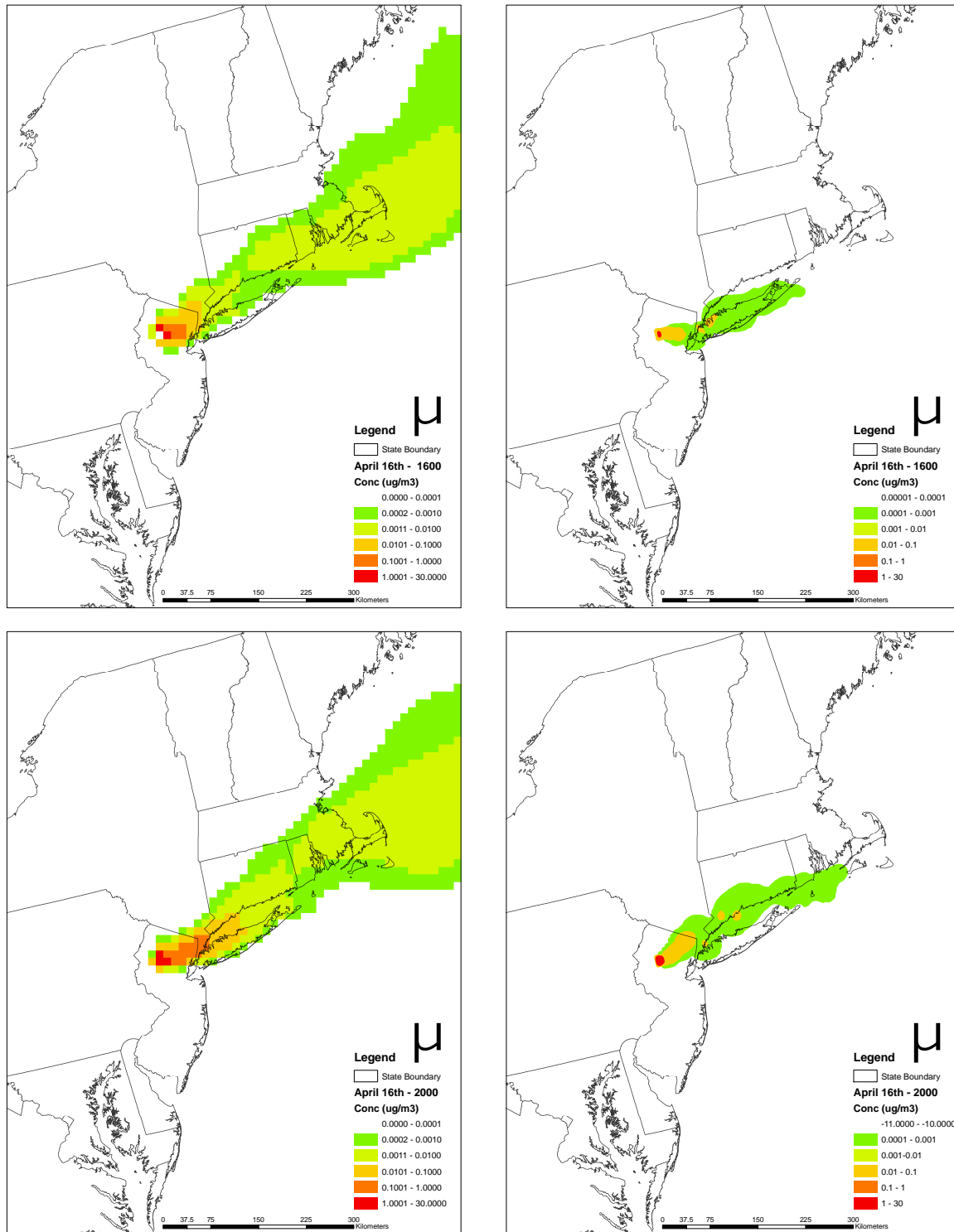
Figure 5.22: Plume comparison plots utilizing CMAQ (left) and HYSPLIT (right) models for a single cell Birch emission during 15:00-16:00 and 19:00-20:00 on April 16th of 2002.
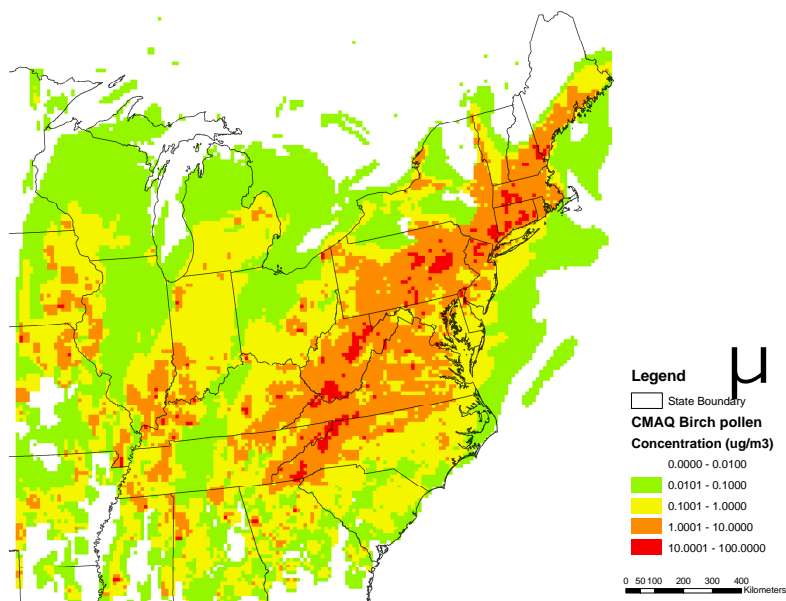
Figure 5.23: Hourly averaged surface pollen concentration calculated with the CMAQ model using Birch emissions for 8am of April 16th 2002 (GCS: NAD83).
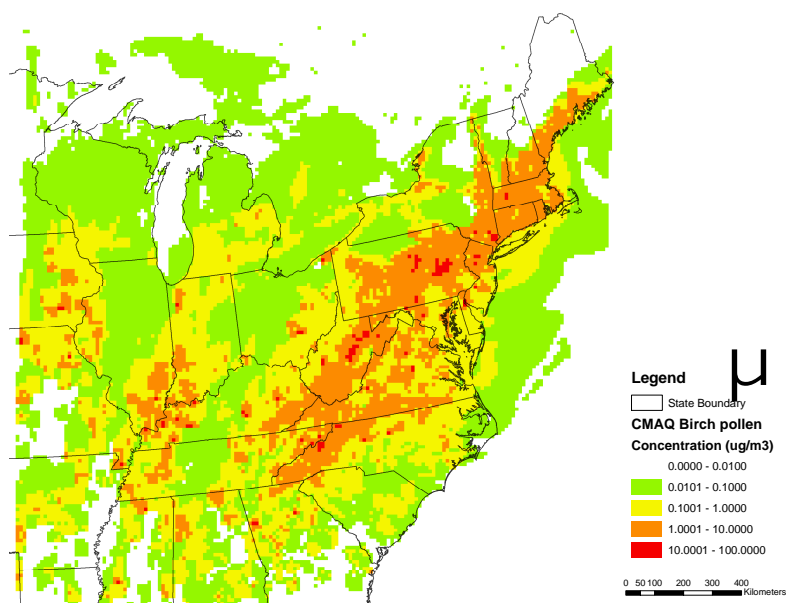
Figure 5.24: Hourly averaged surface pollen concentration calculated with the CMAQ model using Birch emissions for 12pm of April 16th 2002 (GCS: NAD83).
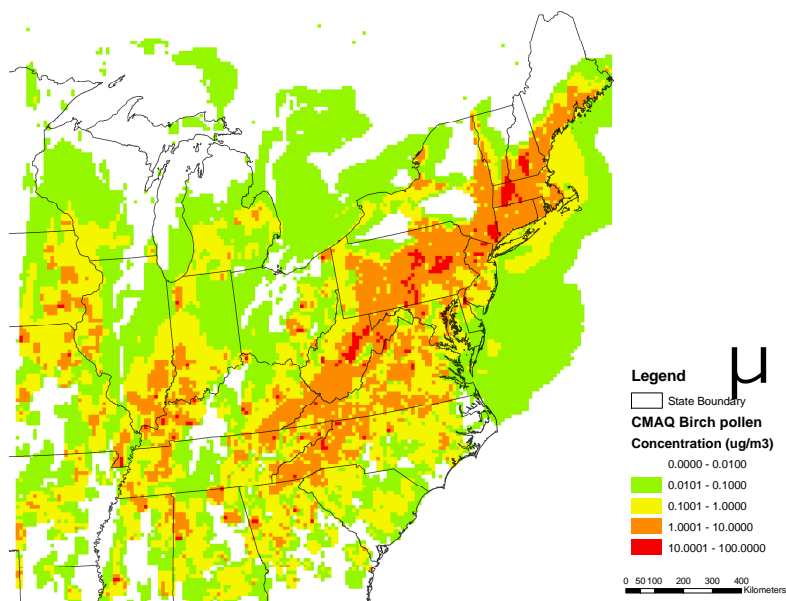
Figure 5.25: Hourly averaged surface pollen concentration calculated with the CMAQ model using Birch emissions for 4pm of April 16th 2002 (GCS: NAD83).
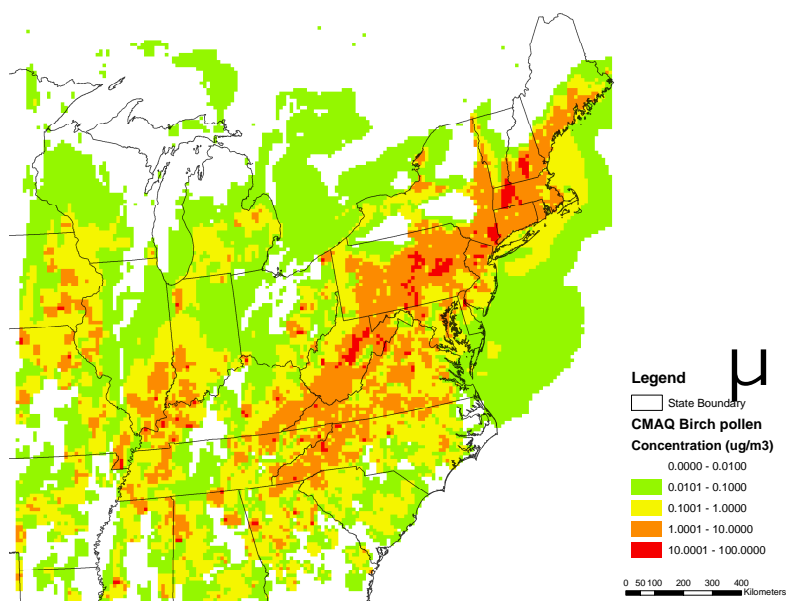
Figure 5.26: Hourly averaged surface pollen concentration calculated with the CMAQ model using Birch emissions for 8 pm of April 16th 2002 (GCS: NAD83).
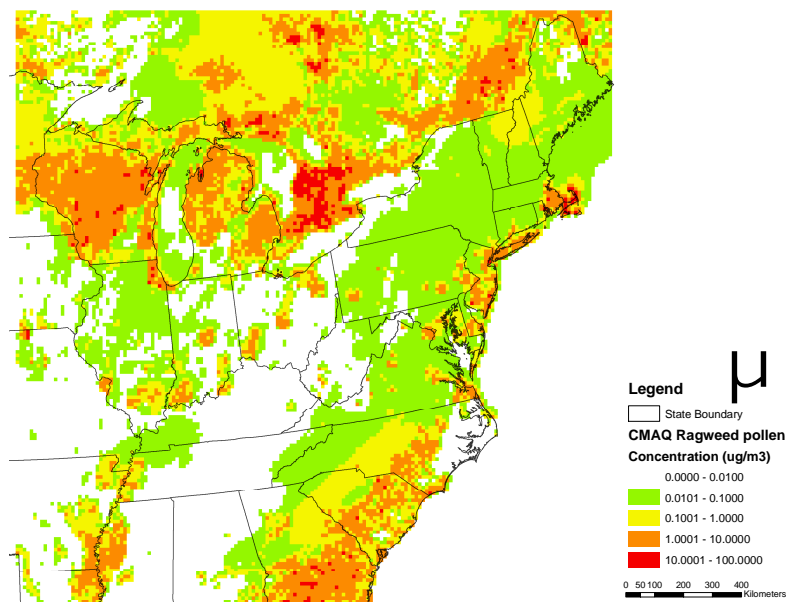
Figure 5.27: Hourly averaged surface pollen concentration calculated with the CMAQ model using Ragweed emissions for 8am of August 15th 2002 (GCS: NAD83).
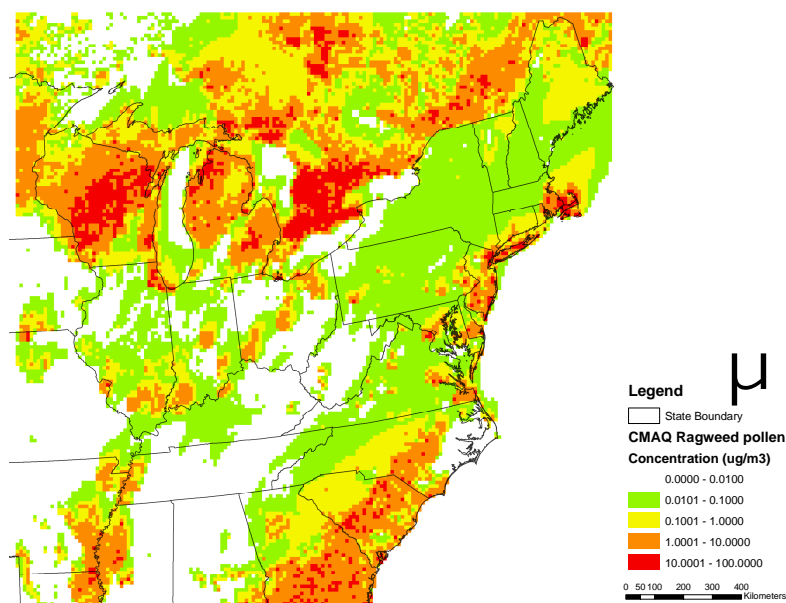
Figure 5.28: Hourly averaged surface pollen concentration calculated with the CMAQ model using Ragweed emissions for 12pm of August 15th 2002 (GCS: NAD83).
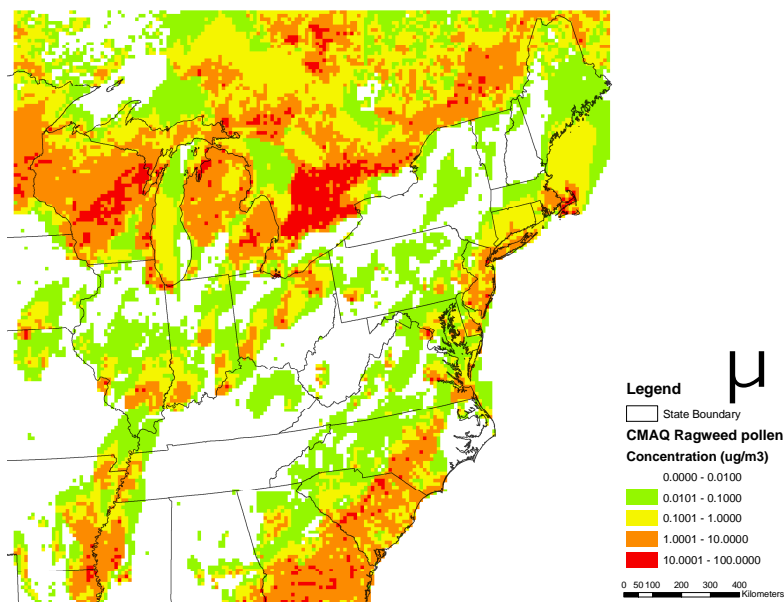
Figure 5.29: Hourly averaged surface pollen concentration calculated with the CMAQ model using Ragweed emissions for 4pm of August 15th 2002 (GCS: NAD83).
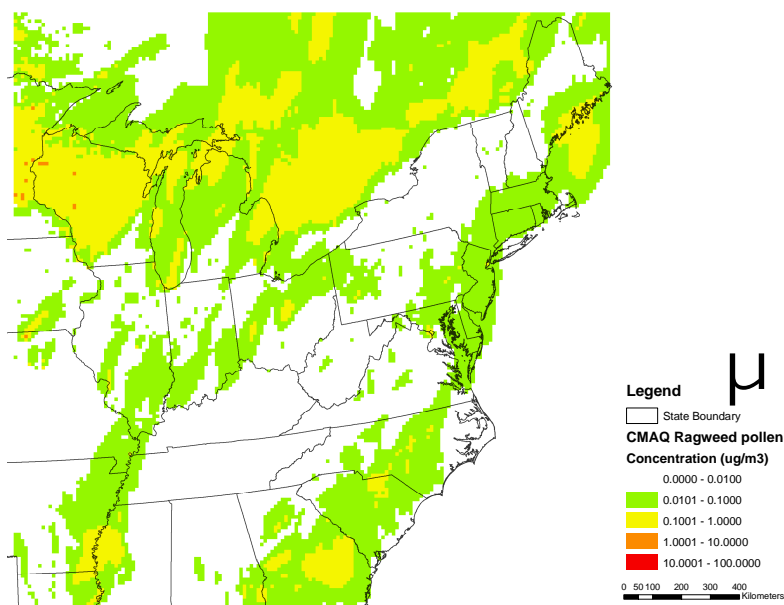
Figure 5.30: Hourly averaged surface pollen concentration calculated with the CMAQ model using Ragweed emissions for 8 pm of April 16th 2002 (GCS: NAD83).
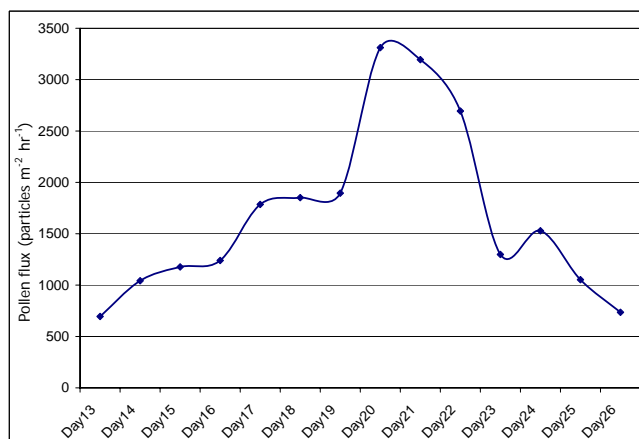
Figure 5.31: Daily averaged surface pollen concentration calculated with the CMAQ model using Birch emissions for the modeled month of April 2002 (GCS: NAD83).
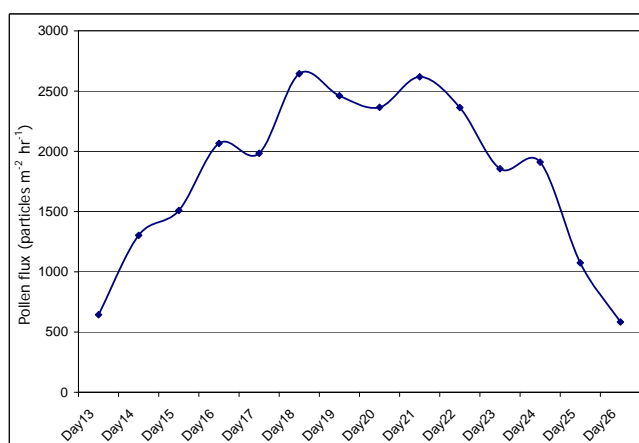
Figure 5.32: Daily averaged surface pollen concentration calculated with the CMAQ model using Ragweed emissions for the modeled month of August 2002 (GCS: NAD83).

Tables

Table 5.1: Predominant pollen shedding species of allergenic potential in the OTC domain (Source: BELD3 database).

	FAMILY	MAJOR SPECIES	Dp (µm)	POLLEN PERIOD	ALLERGEN	OTC BELD3 density (%)
	Quercus	Oaks	19-39	March - June	t7	32.35
	Pinaceae	Pines	53-73	May - June	t16, t73	9.44
	Cupressaceae	Cypress, Juniper, Cedar	20-36	April - May	t6, t17, t23	3.64
	Moraceae	Mulberries	11-25	March - June	t70	< 1
	Betulaceae	Alder, Birch, Hazel	19-32	April - May	t2, t3, t4, t210	3.42
	Oleaceae	Ashes	26-33	March -May	t9,t15	3.15
	Fagaceae	Beech	40-44	May-June	t5	4.80
	Aceraceae	Maples	23-38	April - May	t1	13.90
	Carya	Hickory, Pecan	35-55	May - June	t22	3.64

Table 5.2: Species-specific input parameters for the pollen emission module.

Property	Birch	Ragweed
q_p in pollen grains/m^2	$1 \cdot 10^9$	$2.1 \cdot 10^9$
S in days	15	15
LAI	5	3
h_c in m	20	2
Emission height in m	2	20
Particle size (diameter in μm)	20	20
Particle density (kg/m^3)	1080	800

Table 5.3: Estimated settling velocity for typical pollen grains (cm/s). Adapted from Knox and Inst [1979]

Species	Bodmer (1927)	Knoll (1932)	Dyakowska (1937)	Eisenhut (1961)
Abies alba			38.7	12.0
Larix decidua	12.5 - 22	9.9	12.3	12.6
Picea abies		8.7	6.8	5.6
Pinus silvestris	2.9 - 4.4	2.5	3.7	3.7
Taxus baccata	1.1 - 1.3		2.3	1.6
Abies incana	1.7 - 2.2			2.1
Betula verrucosa	1.3 - 1.7	2.4	2.9	2.6
Carpinus betulus		4.5	6.8	4.2
Quercus robur		2.9	4.0	3.5

Chapter 6

Conclusions and discussion

Biogenic emissions make a significant contribution to the levels of aeroallergens and secondary air pollutants such as ozone, and understanding the major factors contributing to allergic airway diseases requires accurate characterization of emissions and transport/transformation of biogenic emissions. However, biogenic emission estimates are laden with large uncertainties. Furthermore, the current biogenic emission estimation models use low-resolution data for estimating land use, vegetation biomass and VOC emissions. Furthermore, there are currently no established methods for estimating bioaerosol emissions over continental or regional scale. Therefore, there is a need for improvements in the methods for estimating the emissions and transport/transformation of biogenic VOCs and bioaerosols.

6.1   Refinements and Application of the BVOC modules

In the first part of the thesis, an detailed review of different approaches and available databases for estimating biogenic emissions was conducted, and multiple geodatabases and satellite imagery were used in a consistent manner to improve the estimates of biogenic emissions over the continental United States. These emissions represent more realistic, higher resolution estimates of biogenic emissions (including those of highly reactive species such as isoprene). The impact of these emissions on tropospheric ozone levels was studied at a regional scale through the application of the USEPA's Community Multiscale Air Quality (CMAQ) model. Minor, but significant differences in the levels of ambient ozone were observed,

6.2   Development and Application of the pollen modules

In the second part of the thesis, an algorithm for estimating emissions of pollen particles from major allergenic tree and plant families in the United States was developed, extending the

approach for modeling biogenic gas emissions in the Biogenic Emission Inventory System (BEIS). A spatio-temporal vegetation map was constructed from different remote sensing sources and local surveys, and was coupled with a meteorological model to develop pollen emissions rates. This model overcomes limitations posed by the lack of temporally resolved dynamic vegetation mapping in traditional pollen emission estimation methods. The pollen emissions model was applied to study the pollen emissions for North East US at 12 km resolution for comparison with ground level tree pollen data. A pollen transport model that simulates complex dispersion and deposition was developed through modifications to the USEPA's Community Multiscale Air Quality (CMAQ) model. The peak pollen emission predictions were within a day of peak pollen counts measured, thus corroborating independent model verification. Furthermore, the peak predicted pollen concentration estimates were within two days of the peak measured pollen counts, thus providing independent corroboration. The models for emissions and dispersion allow data-independent estimation of pollen levels, and provide an important component in assessing exposures of populations to pollen, especially under different climate change scenarios.

6.3 Discussion: Direct health effects of biogenic emissions

6.3.1 Health effects related to BVOC emissions

Several studies on the inhalation pharmacokinetics of the isoprenoid group have been conducted for a number of species including rats, mice, and monkeys [Dahl et al., 1990; Melnick et al., 1996; Peter et al., 1990]. The major representative, isoprene, is showing no significant relationship to carcinogenesis [Cox et al., 1996]. Toxicological studies on human lung cells suggest that once isoprene is released in the atmosphere, it reacts to form products that induce potentially greater adverse health effects than isoprene itself [Doyle et al., 2004]. Since the ambient levels of isoprene are very low, occupational exposure studies targeted wood-processing environments where the compound can be abundant [Martin et al., 1991]. Other authors emphasized on the formation of strong airway irritants in isoprene mixtures with O_3 and NO_2 [Wilkins et al., 2001]. Nevertheless, biogenic VOCs are important ozone precursors and therefore are of great significance when trying to derive air pollution-related health indicators.

6.3.2   Health effects related to aeroallergens

Allergic diseases represent a major health problem of most modern societies [Ring, 1997]. Pollen allergens are integral pollen constituents. They have to be released during a process of activation in order to become bioavailable [Behrendt and Becker, 2001]. The main pathway of exposure to allergenic pollen grains is through inhalation, while ingestion and dermal exposure are of lessen importance. The two main symptoms of exposure are seasonal allergic rhinitis (hay fever) and asthma. They often coexist and share a genetic background [Braunstahl et al., 2000]. Epidemiologic, pathophysiologic and clinical studies strongly suggest a link between rhinitis and asthma. The reason why pollen causes asthma in some persons and allergic rhinitis in others are obscure. Allergic rhinitis is induced by pollen grains when they make contact with the upper respiratory tract (nostrils, oral cavity, and eyes). A patient may suffer irritation when grains are impacted on the eye at relatively low speeds [Knox and Inst, 1979]. Asthma is an inflammatory disease of the airways, mainly associated with high levels of air pollution [Hiltermann et al., 1997]. If inhaled, pollen may be deposited in the uppermost ciliated portion of the respiratory tract. During an asthmatic reaction, symptoms develop in the deeper, non-ciliated parts of the lung which show accumulation of fluid and secretions in the terminal bronchioles. Symptoms may appear immediately following pollen exposure or be delayed for some hours. The entry of pollen to the lungs depends on the size of pollen and the diameter of the airways. Inhaled particles with a diameter greater than $30\,\mu$m which includes pollens and most fungal spores, are deposited in the trachea and upper bronchi (See Figure 6.1). Any particles deposited in the lungs are removed by alveolar fluid and by macrophages. Experimental inhalation of pollen grains labeled with radioactive technetium (^{99m}Tc), showed that most of the pollen was deposited in the oropharynx and did not reach trachea [Knox and Inst, 1979]. A portion was swallowed and through the process of persorption, passed directly from the stomach to the bloodstream within 45 minutes. The significance of persorption in the initiation of allergic reactions remains to be assessed.

Exposure requires the occurrence of the presence of a potential environmental agent at a particular point in space and time, and the presence of a person or persons at the same location and time. A significant population fraction, with estimates that vary from 2 to 25% [Cookson and Hopkin, 1988; Marsh et al., 1981; Raeburn and Webber, 1994], consists of susceptible individuals,

who, after exposed to a similar mix of environmental stimuli as all others become sensitized and on subsequent contact, develop allergic symptoms. This, is in fact implied in the term allergy meaning "expression of a different response". An interesting observation, confirmed by medical history records, is that even in the susceptible group there is a wide patient-to-patient and family-to-family variability with respect to the spectrum of sensitizing agents (single allergen or effect of a series of unrelated substances) and the clinical presentation (rhinitis, asthma, eczema, alone or associated with each other). Individual liability might depend on both genetic and non-genetic causes. In the presence of a similar reactive background, susceptibility of different target organs may vary under the effect of sex, age, actual environmental exposure, life style, and other associated diseases [Falagiani, 1990].

The term allergen does not refer to pollen itself, but factors that are located on or within it that may induce allergic disease. Allergens are proteins or glycoproteins that are capable of eliciting the formation of specific skin-sensitizing or reaginic antibodies through the body's immune system. The nature of allergic response was first defined as "the acquired, specific, altered capacity to react" [Knox and Inst, 1979]. *Acquired* means that there must have been previous exposure to the allergen to stimulate the immune system and develop hypersensitivity. It also means that once identified, steps can be taken to avoid unnecessary exposure to allergen. *Specific*, refers to the precise molecular relationship that exists between the allergen and the corresponding antibodies produced in response. Related allergens may carry common determinants, allowing in this way for a degree of cross-reaction between them. *Altered capacity to react* describes the different response induced by the same allergen after antibodies have been produced against it. The allergic response may be increased as hypersensitivity, or it may be decreased as a result of increased immunity. Two types of allergic response have been identified: immediate or delayed hypersensitivity (taking place several hours after contact with the allergen).

An allergen is an antigen capable of binding human IgE antibodies. The IgE antibody was first isolated and characterized by [Ishizaka et al., 1970] and shares the particular property of binding to basophils and mast cells. The interaction of allergen and cell-bound IgE induces degranulation of the cells, and at the same time several mediators like histamine are released. Figure 6.2 presents the sequence of events in the production of allergic response. Only a few

molecules of allergen and IgE are required to cause an allergic reaction since the amplification obtained by the release of several molecules of histamine is quite high [Falagiani, 1990]. Recently, an involvement of IgE during the mammalian embryo implantation in the maternal uterus has been described [Cocchiara et al., 1992, 1996].

6.3.3 Populations and microenvironments of concern - synergistic effects of pollen and gaseous air pollutants

Millions of people worldwide are periodically exposed to air pollution levels that exceed health-based air quality guidelines. Epidemiologic studies have demonstrated consistent associations between exacerbations of respiratory disease and air pollution [Bascom et al., 1996]. These associations are most often noted with particulate matter smaller than $10\,\mu m$ (PM_{10}) or with ozone. Harmful effects of air pollution may predominate in the most sensitive subjects of the population, such as asthmatics or patients with chronic obstructive pulmonary disease. A recent study indicates that there is no consistent evidence that children with wheeze, positive histamine challenge, and doctor diagnosis of asthma reacted differently to air pollution from children with wheeze and doctor diagnosis of asthma and children with wheeze only [Jalaludin et al., 2004]. Recent studies also indicate that it is not certain whether factors encountered in a farm environment may protect against the development of allergy or not. A study, conducted in several countries of the E.U. found that living on a farm in childhood was associated with a reduced risk of atopic sensitization in adulthood [Leynaert et al., 2001]. Compared with other adults, those who had lived on a farm as a child were less frequently sensitized to cat and to Timothy grass, and were at lower risk of having nasal symptoms in the presence of pollen. There are two more subpopulations of concern, florists and pregnant women. An epidemiological study among 111,702 children born in Stockholm [Forsberg et al., 1998] between 1988 and 1995 suggests that there is a strong connection between maternal pollen exposure and asthmatic children. The last 12 weeks of pregnancy and the corresponding pollen were pointed as the most significant parameters.

There is also a strong suggestion that certain pollutants that can be found in the urban air can influence the bioavailability of pollen allergen [Behrendt and Becker, 2001]. By the use of fluidized bed reactors, the influence of both gaseous and particulate upon allergen release from

pollen can be studied in a dose-, time-, and humidity- dependent fashion [Behrendt et al., 1997; Risse et al., 2000]. The scanning electron micrographs (SEM) seen in Figure 6.3, show that birch pollen found in urban microenvironment interacts with airborne matter that sticks to the grain coating in a greater degree compared to rural sites [Behrendt et al., 1997]. Exposure of *P.Pratense* pollen to high concentrations of SO_2 induces a significant reduction of liberation of a major allergen. This leads to the assumption that the bioavailability of major grass pollen allergens might be grossly reduced in regions polluted with SO_2 as compared with non-polluted areas. This observation is associated with the well-known paradoxic finding of low asthma and hay fever rates in 5-6 year old children from areas with heavy SO_2 pollution in the former East Germany compared with children living in the West part [Ring et al., 2001; von Mutius et al., 1992]. For the case of NO_2, no change in bioavailability was observed under identical conditions. Binding of Lol p 1, a major grass pollen allergen, to diesel-exhaust particles under experimental conditions has been observed by Knox [Knox and Inst, 1979]. Furthermore, airborne particles agglomerate onto pollen surfaces in heavy-traffic areas, but not in park regions that are devoid of high concentrations of air pollution [Behrendt et al., 1997].

A very interesting part, in terms of modeling the pollen levels and the potential exposure, is the indoor environment. In the indoor environment there are pollutants like NO_2, that can be found in concentrations that approach outdoor levels (due to emission from pilot lights and gas stoves [Gauderman et al., 2000]. In order to investigate the factors affecting indoor and outdoor microenvironmental concentrations of aeroallergens, and the relationships between them, Stock [Stock et al., 1985] took 12-hour samples of airborne pollens and spores from two fixed ambient air monitoring stations and inside and directly outside of 12 houses during the period June to October in Houston. Outdoor concentrations of pollen were spatially less heterogeneous than those of spores, and showed greater seasonal and diurnal variation. Indoor levels of both pollen and spores were uniformly lower than outdoor levels for all 12 air-conditioned homes, with indoor pollen counts on average 30% of outdoor values, and indoor spore counts on average 20% of outdoor values. Indoor levels of both aeroallergens in most homes were not significantly correlated with simultaneous outdoor levels. Variation in exposure to aeroallergens indoors appears largely determined by variations in both infiltration of outdoor air and activities of the household. A study, using dust wipes in order to estimate the level of pollen in residences,

concluded that higher concentrations can be encountered close to the entrance and windows [Forsberg et al., 1998]. The level of humidity is one of the indoor parameters that can also affect the bioavailability of pollen.

6.4 Future work: Biogenic emissions and climatic change

Climate change may increase the frequency and intensity of ozone episodes in future summers in the United States. A warming climate is believed to result in increased morbidity and mortality related to ozone, an impact that is often overshadowed by concerns about the direct effects of increased heat stress. Peak ambient O_3 concentrations are typically observed in summer months, when higher temperatures and increased sunlight enhance O_3 formation and also lead to increased emission of biogenic and fugitive anthropogenic hydrocarbons, important precursors of O_3 formation. Numerous epidemiology studies have reported associations between O_3 and hospital admissions or emergency visits for respiratory conditions, diminished lung function, and a variety of other health outcomes. A relatively recent but growing body of literature has also documented acute effects on mortality in large cities, in many cases while controlling for particulate matter and other pollutants.

Figures

Respiratory System (Anterior view)

Pulmonary vein
Nerve
Pulmonary artery
Mucosal lining
Cartilage
Bronchus
Mucous gland
Bronchiole (cartilage stops)
Smooth muscles
Terminal bronchiole
Elastic fibers
Respiratory bronchiole
Alveolar sacs
Alveolar duct
Atrium
Alveolar sac
Interalveolar septa
Lung tissue
Visceral pleura
Pleural cavity
Parietal pleura

Frontal sinus
Sphenoid sinus
Superior nasal concha
Middle nasal concha
Inferior nasal concha
Pharyngeal orifice of auditory tube
Nasal cavity
Pharynx: nasopharynx oropharynx laryngopharynx
Vestibule of nose
Hard palate
Oral cavity
Epiglottis
Soft palate
Vocal fold
Hyoid bone
Thyroid cartilage
Trachea
Cricoid cartilage
Carina of trachea
Apex of lung
Right and left main bronchii
Superior lobe
Superior lobe
Lobar bronchus: Right superior (red) Right middle (yellow) Right inferior (blue)
Lobar bronchus: Left superior (red) Left inferior (blue)
Horizontal fissure
Lingular division bronchus
Middle lobe
Oblique fissure of left lung
Inferior lobe
Inferior lobe
Intermediate bronchus
Oblique fissure
Cardiac notch
Lingula of lung

Figure 6.1: Anterior view of the human respiratory system (Source: Stedman's Medical Dictionary).
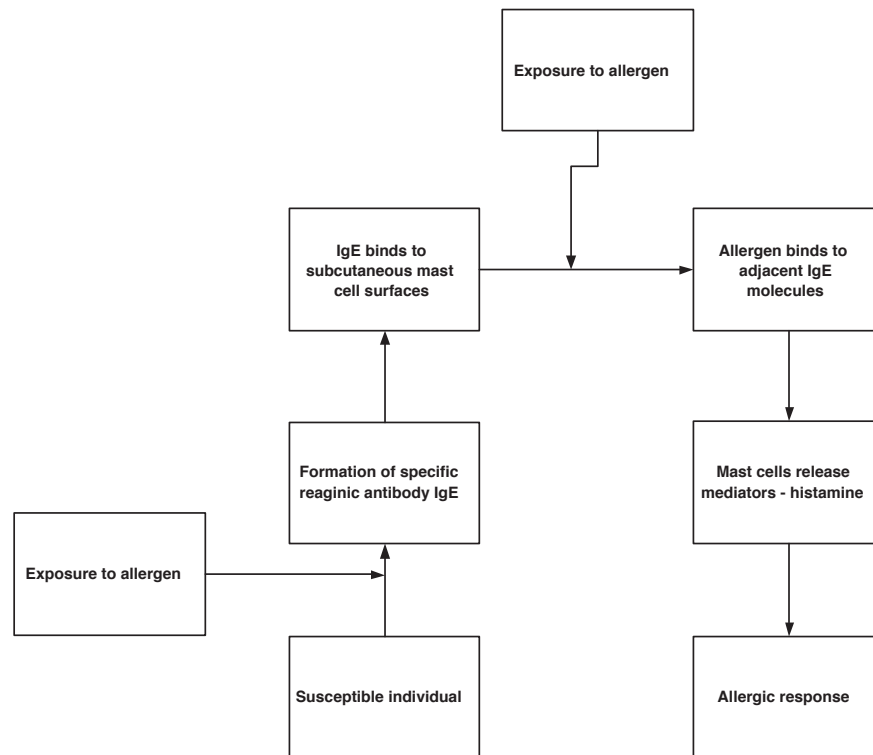
Figure 6.2: Sequence of events in the production of allergic response.
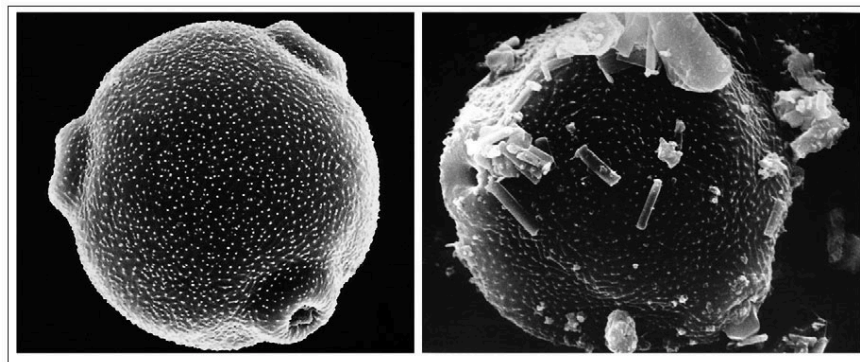
Figure 6.3: Scanning Electron Microscopy image of a ragweed pollen in a polluted and clean atmosphere [Adapted with permission from Behrendt et al., 1997].
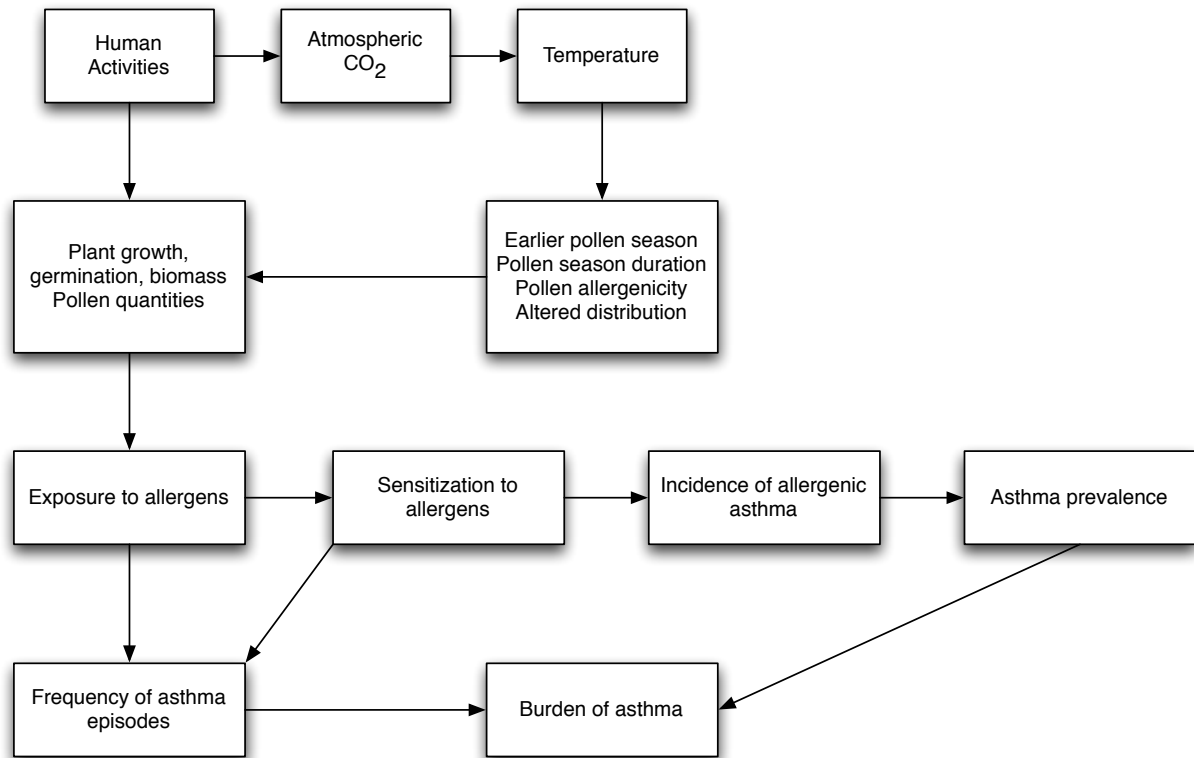
Figure 6.4: Climate change, allergens, and prevalence of asthma - a schematic of the processes involved under a changing climate.

Appendix A

Equations for the estimation of biogenic emissions

A.1 Isoprene Emissions

Isoprene is emitted only during daylight hours from specific deciduous species, such as oak, willow, aspen, and poplar, and only from spruce for the group of coniferous species. In BEIS3, Pierce [2001] uses a slightly modified form of the Guenther et al. [1993] formulation. The emission flux can be defined as:

$$E = \xi \cdot E_s \cdot C_L^A \cdot C_T \cdot A \tag{A-1}$$

where,

$$
\begin{array}{rcl}
E & \to & \text{total emission rate of isoprene } (\mu g\,ha^{-1}\,h^{-1}) \\
\xi & \to & \text{seasonal adjustment coefficient (dimensionless)} \\
E_s & \to & \text{species-specific emission rate of isoprene at } 30\,^{\circ}\mathrm{C} \text{ and } 1000\,\mu mol\,m^{-2}\,s^{-1} \\
C_L^A & \to & \text{ratio of the canopy-adjusted PAR to the PAR above the canopy (dimensionless)} \\
C_T & \to & \text{temperature correction factor (dimensionless)} \\
A & \to & \text{areal extend of the species in the modeled location (ha)}
\end{array}
$$

However, Guenther et al. [1995, 1999b, 2000] have refined their model to estimate isoprene emission according to the following formula:

$$E = \epsilon \cdot D_p \cdot D_f \cdot \gamma_P \cdot \gamma_T \cdot \gamma_A \cdot \rho \cdot A \tag{A-2}$$

where,

$$\epsilon \quad \rightarrow \quad \text{landscape average emission capacity } (\mu g\, g^{-1}\, h^{-1})$$

$$D_p \quad \rightarrow \quad \text{annual peak foliar density } (g\, ha^{-1}g \cdot ha^{-1})$$

$$D_f \quad \rightarrow \quad \text{fraction of foliage present at a particular time of year}$$

$$\gamma_P, \gamma_T, \gamma_A \quad \rightarrow \quad \text{emission activity factors for PPFD, temperature, and leaf age (dimensionless)}$$

$$\rho \quad \rightarrow \quad \text{canopy escape efficiency (dimensionless)}$$

$$A \quad \rightarrow \quad \text{areal extend of the species in the modeled location (ha)}$$

In the revised Guenther formulation [Guenther et al., 2000], $\epsilon \cdot D_p$ is equivalent to E_s in BEIS3, γ_T is equivalent to C_T, and γ_P is equivalent to C_L^A. However, though the parameters are equivalent, the formulation of the parameters may be slightly different. This leaves the Guenther et al. [2000] terms D_f, γ_A, and ρ unaccounted for in the Pierce [2001] BEIS3 formulation.

The canopy adjusted PAR, C_L^A, is computed via a simple canopy model that accounts for the effects of variations of PAR with height in the leaf canopy. C_L^A approaches the value of 1.0 for the case of thin canopies. The canopy model in BEIS3 is based on a leaf energy balance and knowledge of the Leaf Area Index (LAI). C_L^A, or the ratio of the canopy-adjusted PAR to the PAR above the canopy, is calculated for the sunlit and shaded leaves using an empirical expression derived by Campbell and Norman [1998]:

$$C_L^A = L_S^f \cdot C_L(PAR_S) + L_D^f \cdot C_L(PAR_D) \tag{A-3}$$

where,

$$E \quad \rightarrow \quad \text{total emission rate of isoprene } (\mu g\, h^{-1})$$

$$L_S^f \quad \rightarrow \quad \text{fraction of sunlit leaves (dimensionless)}$$

$$L_D^f \quad \rightarrow \quad \text{fraction of shaded leaves (dimensionless)}$$

$$C_L \quad \rightarrow \quad \text{light correction factor (dimensionless)}$$

$$PAR_D \quad \rightarrow \quad \text{the amount of PAR on shaded leaves } (\mu mol\, m^{-2}\, s^{-1})$$

$$PAR_S \quad \rightarrow \quad \text{the amount of PAR on sunlit leaves } (\mu mol\, m^{-2}\, s^{-1})$$

The fractions of sunlit and shaded leaves, L_S^f and L_D^f are estimated as:

$$L_S^f = \frac{1 - \exp\left(-K \cdot LAI\right)}{K \cdot LAI} \tag{A-4}$$

$$L_D^f = 1 - C_S^f \tag{A-5}$$

where K (dimensionless) is the direct beam solar radiation extinction coefficient:

$$K = \frac{\sqrt{1 + [tan(\vartheta)]^2}}{2} \tag{A-6}$$

where ϑ is the solar zenith angle, calculated according to the equation developed by **?**]:

$$\vartheta = \alpha \cos\left[\delta_s \cdot \sin\left(\frac{\pi\varphi}{180}\right) + \sqrt{1.0 - \delta_s^2} \cdot \cos\left(\frac{\pi\varphi}{180}\right) \cdot \cos\left(\frac{15\pi}{180} \cdot t_\vartheta\right)\right] \tag{A-7}$$

$$t_\vartheta = t + \frac{\lambda}{15} - 0.123470\sin\left(t_r\right) + 0.004289\cos\left(t_r\right) - 0.153809\sin\left(t_r + t_r\right) - 0.060783\sin\left(t_r + t_r\right) - 12 \tag{A-8}$$

where φ is the latitude (°C), λ is the longitude (in degrees), t is local time converted to Greenwich Mean Time (hours), t_r is the terrestrial rotation angle (rad) defined by equation A-9, and δ_s is a parameter of the earth's declination to the solar plane defined by equation A-10.

$$t_r = \frac{\pi\Omega t}{180} \tag{A-9}$$

$$\delta_s = \sin\left(\frac{\pi\delta}{180}\right) \cdot \sin\left(t_r + \frac{\pi}{180} \cdot t_\rho\right) \tag{A-10}$$

$$t_\rho = 279.9348 + 1.914827\sin\left(t_r\right) - 0.079525\cos\left(t_r\right) + 0.019938\sin\left(t_r + t_r\right) - 0.00162\cos\left(t_r + t_r\right) \tag{A-11}$$

where Ω is the fraction of complete rotation per day (360/365.242); and δ is the earth's declination to the solar plane (23.443 833 °C). Note that though the formulation of A-10 takes

into account the time of the day, it does not take into account the day of the year. To account for the day of the year, the first term of the equation A-10 should read:

$$\sin\left(\frac{\pi\delta}{180}\sin\left[\frac{\pi}{180}\left(360\cdot\frac{284+n}{365}\right)\right]\right) \tag{A-12}$$

where n is the Julian day of the year (*i.e.* 1 to 365). The PAR for shaded and sunlit leaves is computed via the following two equations:

$$PAR_D = \frac{PAR_d\left[1-\exp\left(-0.61\cdot LAI\right)\right]}{0.61\cdot LAI} + \frac{PAR_b\left[\exp\left(-0.894\cdot LAI\right)-\exp\left(-K\cdot LAI\right)\right]}{2}$$
$$\tag{A-13}$$

$$PAR_S = K\cdot(PAR_b + PAR_d)\cdot PAR_D \tag{A-14}$$

where PAR_d is the amount of PAR from diffuse visible solar radiation defined by equation A-15, and PAR_b is the amount of PAR from direct beam, visible radiation defined by equation A-16:

$$PAR_d = I_r\cdot I_c^v\cdot I_d^v\cdot f \tag{A-15}$$

$$PAR_b = I_r\cdot I_c^v\cdot I_b^v\cdot f \tag{A-16}$$

where I_r is the ratio of the observed, or modeled, solar radiation to the clear sky total solar radiation defined by equation A-23; I_b^v is the fraction of visible solar radiation that is from direct beam solar radiation defined by equation A-17; I_d^v is the fraction of visible solar radiation that is from diffuse beam solar radiation defined in equation A-18; I_c^v is the clear sky total visible solar radiation defined by equation A-19; and f=4.6 is an empirical factor that converts solar radiation in terms of energy to solar radiation in terms of photon flux.

$$\mathrm{I}_b^v = \begin{cases} 0.009550 \cdot \dfrac{I_{cb}^v}{I_c^v} & , \text{ for } I_r \leq 0.21 \\[3ex] \left[1.0 - \left(\dfrac{0.9 - I_r}{0.7}\right)^{2/3}\right] \cdot \dfrac{I_{cb}^v}{I_c^v} & , \text{ for } 0.21 < I_r < 0.89 \\[3ex] 0.941124 \cdot \dfrac{I_{cb}^v}{I_c^v} & , \text{ for } I_r \geq 0.89 \end{cases} \tag{A-17}$$

$$I_d^v = 1 - I_b^v \tag{A-18}$$

$$I_c^v = I_{cb}^v + I_{cd}^v \tag{A-19}$$

where I_{cb}^v is the clear sky, direct beam visible solar radiation defined by equation A-20; and I_{cd}^v is the clear sky, diffuse visible solar radiation defined by equation ??.

$$I_{cb}^v = 600 \cdot \exp\left(-0.185m\right) \cdot \cos\vartheta \tag{A-20}$$

$$I_{cd}^v = 0.42 \cdot \left(600 - I_{cb}^v\right) \cdot \cos\vartheta \tag{A-21}$$

where m is the atmospheric optical thickness defined by the following equation:

$$m = \frac{P}{P_0 \cdot \cos\vartheta} \tag{A-22}$$

where P is the observed pressure (mbar); and P_0 is the standard pressure (1013.25 mbar).

$$I_r = \frac{I}{I_c} \tag{A-23}$$

where I is the observed, or modeled incoming solar radiation; and I_c is the clear sky total solar radiation defined in the following manner:

$$I_c = I_{cb}^i + I_{cd}^i + I_{cb}^v + I_{cd}^v \tag{A-24}$$

where I_{cb}^i is the clear sky, direct beam near infrared solar radiation defined by equation A-25; and I_{cd}^i is the clear sky, diffuse near-infrared solar radiation defined by equation A-26.

$$I_{cb}^i = (720 \cdot \exp(-0.06m) - \omega) \cdot \cos\vartheta \tag{A-25}$$

$$I_{cd}^i = 0.65 \cdot \left(720 - \omega - I_{cb}^i\right) \cdot \cos\vartheta \tag{A-26}$$

where ω is absorption by water of solar radiation in the near-infrared spectrum defined by the following relationship:

$$\omega = 101.64 \cdot (2m)^{0.3} \tag{A-27}$$

Note that in some references, PAR is expressed in $\mu\mathrm{mol\,m^{-2}\,s^{-1}}$, while in others PAR is expressed in units of $\mathrm{W\,m^{-2}}$. Rather than convert the units in equation A-1, and related isoprene equations, the units in the original references are retained. The approximate conversion factor between PAR ($\mu\mathrm{mol\,m^{-2}\,s^{-1}}$)and total solar radiation I (RGRND from MM5 model output is defined in $\mathrm{W\,m^{-2}}$ is:

$$\mathrm{PAR} = 0.5 \cdot 4.6 \cdot \mathrm{I} \tag{A-28}$$

where, 0.5 is an empirical coefficient that indicates approximately 50% of the total incoming solar radiation is PAR, and 4.6 is an empirical conversion factor from $\mathrm{W\,m^{-2}}$ to $\mu\mathrm{mol\,m^{-2}\,s^{-1}}$. The light correction factor, C_L in equation A-3 is calculated as:

$$C_L = \frac{\alpha \cdot c_{L1} \cdot \mathrm{PAR}}{\sqrt{1 + \alpha^2 \cdot \mathrm{PAR}^2}} \tag{A-29}$$

where,

$$\alpha \quad \rightarrow \quad 0.0027 \ (1000\,\mu\mathrm{mol\,m^{-2}\,s^{-1}})$$
$$c_{L1} \quad \rightarrow \quad 1.06 \ (\text{dimensionless})$$
$$\mathrm{PAR} \quad \rightarrow \quad \text{photosynthetically active radiation} \ (\mu\mathrm{mol\,m^{-2}\,s^{-1}})$$

BEIS3.12 uses constant values for the above coefficients as in Guenther et al. [1993]. More

recent work by ?] describes an approach with updated coefficients α and c_{L1} varying with canopy height. Values for α and c_{L1} are calculated as follows:

$$\alpha = 0.001 + 0.0085 \cdot LAI \tag{A-30}$$

$$c_{L1} = 1.42 \exp{-0.3 \cdot LAI} \tag{A-31}$$

where LAI is the cumulative leaf area index above the leaf. The PAR adjustment factor is calculated at each level in the canopy, using the photosynthetic photon flux density at that level, and then integrated to get a whole canopy value. BEIS3 uses the methodology described by Guenther et al. [1993] to estimate the dimensionless temperature correction factor, C_T, appearing in equation $A - 1$:

$$C_T = \frac{\exp\left(\dfrac{c_{T1} \cdot (T - T_S)}{R \cdot T_S \cdot T}\right)}{1 + \exp\left(\dfrac{c_{T1} \cdot (T - T_M)}{R \cdot T_S \cdot T}\right)} \tag{A-32}$$

where,

$$
\begin{aligned}
c_{T1} &\rightarrow 95\,000 \,\mathrm{J\,mol^{-1}} \\
c_{T2} &\rightarrow 230\,000 \,\mathrm{J\,mol^{-1}} \\
T_M &\rightarrow 314 \,\mathrm{K} \\
T_S &\rightarrow \text{normalizing ambient temperature } (303 \,\mathrm{K}) \\
R &\rightarrow \text{Ideal gas constant } (8.314 \,\mathrm{J\,K^{-1}\,mol^{-1}})
\end{aligned}
$$

A.2 Monoterpene Emissions

The sum of monoterpene emissions can estimated following the approach suggested by Guenther et al. [1993]:

$$E = \xi \cdot E_s \cdot C_T \cdot A \tag{A-33}$$

where,

$$E \quad \rightarrow \quad \text{total emission rate of monoterpenes } (\mu\text{g ha}^{-1}\,\text{h}^{-1})$$

$$\xi \quad \rightarrow \quad \text{seasonal adjustment coefficient (dimensionless)}$$

$$E_s \quad \rightarrow \quad \text{species-specific emission rate of total monoterpenes at } 30\,^\circ\text{C and } 1000\,\mu\text{mol m}^{-2}\,\text{s}^{-1}$$

$$C_T \quad \rightarrow \quad \text{temperature correction factor (dimensionless)}$$

$$A \quad \rightarrow \quad \text{areal extend of the species in the modeled location (ha)}$$

The temperature correction factor, C_T, for monoterpenes is dimensionless and is estimated based on leaf temperature, which is assumed to equal ambient temperature, T:

$$C_T = \exp\left(\beta[T - T_s]\right) \tag{A-34}$$

where $\beta = 0.09\ K^{-1}$ is an empirical coefficient that can also be thought as an inverse temperature scale. The monoterpene emissions temperature factor monotonically increases with increasing temperature. This same C_T formula is used by BEIS3 as the OVOC temperature correction factor. The exponential form of equation A-34 is based purely on a statistical fit of measured emission rates [Guenther et al., 1993].

A.3   Biogenic Nitric Oxide Emissions

Biogenic nitric oxide (BNO) is emitted as a result of microbial nitrification-denitrification activities in soil and is enhanced through nitrogen-based fertilizer application [Williams et al., 1992]. BEIS3 uses the empirical model developed by Williams et al. [1992] to estimate BNO emissions E, from soils:

$$E = E_s \cdot C_T \cdot A \tag{A-35}$$

where,

$$E \quad \rightarrow \quad \text{total emission rate of BNO emissions } (\mu\text{g ha}^{-1}\,\text{h}^{-1})$$

$$E_s \quad \rightarrow \quad \text{species-specific emission rate of BNO at } 30\,^\circ\text{C and } 1000\,\mu\text{mol m}^{-2}\,\text{s}^{-1}$$

$$C_T \quad \rightarrow \quad \text{temperature correction factor (dimensionless)}$$

$$A \quad \rightarrow \quad \text{areal extend of the species in the modeled location (ha)}$$

C_T is the dimensionless temperature conversion factor, which is estimated based on soil temperature, T_{soil}

$$C_T = \exp\left(T_3 \cdot [T - T_s]\right) \tag{A-36}$$

where $T_3 = 0.071 \ C^{-1}$ is an empirical scaling parameter that describes the rate of increase of BNO emissions with soil temperature; $30\,°C$ is a constant identical o the temperature scale T_S (expressed as $303\,K$ in equations A-32 and A-34); T_{soil} is the soil temperature, parameterized based on ambient air temperature with the following equation [Williams et al., 1992]:

$$T_{soil} = T_1(T - 273.15K) + T_2 \tag{A-37}$$

where $T_1 = 0.72$ and $T_2 = 5.8\,°C$ are empirical model parameters that relate soil temperature to ambient temperature; $T(C)$ is the leaf temperature which is assumed to be equal to the ambient temperature.

Appendix B

Definitions for statistical measures of model performance

B.1 Unpaired accuracy

This statistical measure compares the accuracy of the maximum measured and predicted ozone concentrations unpaired in time or in space. It should be noted that this statistical measure may not be very meaningful given the large areal extend of the modeling domain. However, it was included in the study since it is one of the recommended metrics in the regulatory analysis [E.P.A., 1991].

$$\text{Unpaired accuracy} = \frac{\text{P}_{max} \text{ - } \text{O}_{max}}{\text{O}_{max}} \cdot \ 100\% \tag{B-1}$$

where, P_{max} and O_{max} are the maximum predicted and observed values, respectively, of all the stations.

B.2 Normalized bias

This statistical measure provides for an estimate of bias in the models. The E.P.A. [1991] recommends a range of $\pm 5\% \ - \ 15\%$ for this statistic as an acceptable level of model performance. The statistic is defined as:

$$\text{Normalized Bias} = \frac{1}{N} \sum \frac{P_i - O_i}{(O_i)} \tag{B-2}$$

where, P_i and O_i are the predicted and observed values, respectively, at station i, and N is the total number of stations.

B.3 Normalized Average Absolute Gross Error

This metric reflects an overall bias between predicted and measured ozone concentrations in contrast to the normalized bias in which the over- or under-predictions could cancel each other out. The E.P.A. [1991] suggested a range of 30% - 35% as an acceptable level of model performance for this metric.

$$\text{Normalized Average Absolute Gross Error} = \frac{1}{N} \sum \frac{\mid P_i - O_i \mid}{(O_i)} \tag{B-3}$$

where, P_i and O_i are the predicted and observed values, respectively, at station i, and N is the total number of stations.

Appendix C

Parameterization of the deposition velocity for typical pollen particles

The air viscosity can be calculated by the following equation which is derived from the Sutherland's equation (valid between $0 < T < 555K$):

$$\eta = \eta_0 \frac{T_0 + C}{T + C} \left(\frac{T}{T_0} \right)^{\frac{3}{2}}$$

(C-1)

where,

$$C \quad \rightarrow \quad \text{Sutherland's constant } [120\,\text{K}]$$
$$T_0 \quad \rightarrow \quad \text{Reference temperature } [291.15\,\text{K}]$$
$$\eta_0 \quad \rightarrow \quad \text{viscosity } [18.27 \times 10^{-6}\,\text{Pa}]$$

With particle diameter assumed to be $20\,\mu$m and the density estimated at $800\,Kg/m^3$, for a range of temperature values between 0 and $20\,°C, it appears that the value of pollen settling velocity is about 1\,\text{cm}\,\text{s}^{-1}. Typic

$$u_s^2 = \frac{2\rho_P V_P g}{\rho_a c_d(u_s) A_P}$$

(C-2)

where, ρ_a and ρ_p are the density are the density of air and of the pollen grain, respectively, V_P and A_P are the volume and cross-sectional area of the pollen grain, c_d is a drag coefficient, and g is gravitational acceleration.

For a spherical particle with diameter D_P, equation $C-2$ becomes:

$$u_s^2 = \frac{4\rho_P D_P g}{3\rho_a c_d(u_s)}$$

(C-3)

which reduces to a well known result for a spherical particle small enough to obey Stokes law.

Over a wide range of Reynolds numbers (including the Re $\sim$ 0.5-2.5 of interest here), the drag coefficient can be represented well by the formulation of Fuchs [1964] and Friedlander [1977]:

$$c_d = \frac{24}{Re_p}(1 + 0.158Re_p^{2/3}) \tag{C-4}$$

where Re_p is the particle Reynolds number based on the characteristic diameter of the pollen grain. For the spheroidal corn pollen grains, D_P in Eq.$C-3$ was replaced by a volume-equivalent diameter, D_e, given by:

$$D_e = \sqrt[3]{L_1 L_2^2} \tag{C-5}$$

applied to a prolate grain with the major and minor principal radius L_1 and L_2. The ratio L_1/L_2 for the corn pollen has been found to be around 1.1 for freshly collected pollen, but in most cases investigators assume it is reasonable to take the dynamical shape factor equal to 1.0 [Aylor, 2002; Fuchs, 1964].

A complicated factor is the increase in density of pollen grains that occurs during drying (since water has a smaller density than the solid material). In changing from a fresh, fully hydrated state to a dehydrated state, the density ρP of corn pollen increases from about 1.25 to $1.45\,\mathrm{g\,cm^{-3}}$, so that the density must be expressed as a function of D_e, and equation $C-3$ becomes:

$$u_s^2 = \frac{4\rho_P(D_e)gD_e}{3\rho_a c_d(u_s)} \tag{C-6}$$

where,

$$\rho_p(D_e) = \rho_{H_2O}\left(1 - \left(\frac{D_d}{D_e}\right)^3\right) + \rho_{solid}\left(\frac{D_d}{D_e}\right)^3 \tag{C-7}$$

where D_d is the diameter of a pollen grain in the dried state. Over the range of diameters encountered here, Eq. $C-7$ can be replaced by a linear function with a maximum error of $\leq 2\%$. The application of the deposition velocity formula as described above (excluding the effects of water content on the particle size) is presented in Figure 5.5.

Bibliography

N. Aberg. Asthma and allergic rhinitis in swedish conscripts. *Clinical and Experimental Allergy*, 19(1):59–63, 1989.

B. Adams-Groom, J. Emberlin, J. Corden, W. Millington, and J. Mullins. Predicting the start of the birch pollen season at london, derby and cardiff, united kingdom, using a multiple regression model, based on data from 1987 to 1997. *Aerobiologia*, 18(2):117–123, 2002.

D. E. Ahl, S. T. Gower, S. N. Burrows, N. V. Shabanov, R. B. Myneni, and Y. Knyazikhin. Monitoring spring canopy phenology of a deciduous broadleaf forest using modis. *Remote Sensing of Environment*, 104(1):88–95, 2006.

P. K. Ajikumar, K. Tyo, S. Carlsen, O. Mucha, T. H. Phon, and G. Stephanopoulos. Terpenoids: Opportunities for biosynthesis of natural product drugs using engineered microorganisms. *Molecular Pharmaceutics*, 5(2):167–190, 2008.

A.L.A. Asthma and children fact sheet. Technical report, American Lung Association, 2007.

A. P. Altshuller. Review: Natural volatile organic substances and their effect on air quality in the united states. *Atmospheric Environment (1967)*, 17(11):2131–2165, 1983.

M. Andersen. Mechanistic models for the seed shadows of wind-dispersed plants. *American Naturalist*, 137(4):476, 1991.

R. A. Anthes and T. T. Warner. Development of hydrodynamic models suitable for air pollution and other mesometerological studies. *Monthly Weather Review*, 106(8):1045–1078, 1978.

J. Arey, S. B. Corchnoy, and R. Atkinson. Emission of linalool from valencia orange blossoms and its observation in ambient air. *Atmospheric Environment. Part A. General Topics*, 25(7): 1377–1381, 1991a.

J. Arey, A. M. Winer, R. Atkinson, S. M. Aschmann, W. D. Long, and C. Lynn Morrison. The emission of (z)-3-hexen-1-ol, (z)-3-hexenylacetate and other oxygenated hydrocarbons from agricultural plant species. *Atmospheric Environment. Part A. General Topics*, 25(5-6): 1063–1075, 1991b.

J. Arey, D. E. Crowley, M. Crowley, M. Resketo, and J. Lester. Hydrocarbon emissions from natural vegetation in california south-coast-air-basin. *Atmospheric Environment*, 29(21):2977– 2988, 1995.

Robert R. Arnts and Sarah A. Meeks. Biogenic hydrocarbon contribution to the ambient air of selected areas. *Atmospheric Environment (1967)*, 15(9):1643–1651, 1981.

S. M. Aschmann, J. Arey, R. Atkinson, and S. L. Simonich. Atmospheric lifetimes and fates of selected fragrance materials and volatile model compounds. *Environmental Science and Technology*, 35(18):3595–3600, 2001.

M. I. Asher, U. Keil, H. R. Anderson, R. Beasley, J. Crane, F. Martinez, E. A. Mitchell, N. Pearce, B. Sibbald, and A. W. Stewart. International study of asthma and allergies in childhood (isaac): rationale and methods. *European Respiratory Journal*, 8(3):483–491, 1995.

R. Atkinson. A structure-activity relationship for the estimation of rate constants for the gas-phase reactions of oh-radicals with organic compounds. *International Journal of Chemical Kinetics*, (19):799–819, 1987.

R. Atkinson. Gas-phase troposhperic chemistry of organic compounds: A review. *Atmospheric Environment*, A(24):1–41, 1990.

R. Atkinson. Gas-phase tropospheric chemistry of volatile organic compounds: 1. alkanes and alkenes. *J. Phys. Chem. Ref. Data*, (26):215–290, 1997.

R. Atkinson. Atmospheric chemistry of vocs and nox. *Atmospheric Environment*, 34(12-14): 2063–2101, 2000.

R. Atkinson and J. Arey. Atmospheric chemistry of biogenic organic compounds. *Accounts of Chemical Research*, 31(9):574–583, 1998.

R. Atkinson and J. Arey. Gas-phase tropospheric chemistry of biogenic volatile organic compounds: a review. *Atmospheric Environment*, 37:S197–S219, 2003a.

R. Atkinson and J. Arey. Atmospheric degradation of volatile organic compounds. *Chemical Reviews*, 103:4605–4638, 2003b.

R. Atkinson and W.P.L. Carter. Kinetics and mechanisms of the gas-phase reactions of ozone with organic compounds under atmospheric conditions. *Chemical Reviews*, (84):437–470, 1984.

R. Atkinson, J. Arey, S.M. Aschmann, S.B. Corchnoy, and Y.H. Shu. Rate constants for the gas-phase reactions of cis-3-hexen-1-ol, cis-3-hexenylacetate, trans-2-hexebal, and linalool with oh and no3 radicals and o3 at 296+/-2 k, and oh radical formation yields from the o3 reactions. *International Journal of Chemical Kinetics*, 27(10):941–955, 1995.

D. E. Aylor. Biophysical scaling and the passive dispersal of fungus spores: relationship to integrated pest management strategies. *Agricultural and Forest Meteorology*, 97(4):275–292, 1999.

D. E. Aylor. Settling speed of corn (zea mays) pollen. *Journal of Aerosol Science*, 33(11): 1601–1607, 2002.

D. E. Aylor. Rate of dehydration of corn (zea mays l.) pollen in the air. *Journal of Experimental Botany*, 54(391):2307–2312, 2003.

D. E. Aylor. Survival of maize (zea mays) pollen exposed in the atmosphere. *Agricultural and Forest Meteorology*, 123(3-4):125–133, 2004.

D. E. Aylor and T. K. Flesch. Estimating spore release rates using a lagrangian stochastic simulation model. *Journal of Applied Meteorology*, 40(7):1196–1208, 2001.

D. E. Aylor and M. E. Irwin. Aerial dispersal of pests and pathogens: implications for integrated pest management - preface. *Agricultural and Forest Meteorology*, 97(4):233–234, 1999.

D. E. Aylor, N. P. Schultes, and E. J. Shields. An aerobiological framework for assessing cross-pollination in maize. *Agricultural and Forest Meteorology*, 119(3-4):111–129, 2003.

B. Baker, A. Guenther, J. Greenberg, and R. Fall. Canopy level fluxes of 2-methyl-3-buten-2-ol, acetone, and methanol by a portable relaxed eddy accumulation system. *Environmental Science and Technology*, 35(9):1701–1708, 2001.

R. Bascom, P. A. Bromberg, D. A. Costa, R. Devlin, D. W. Dockery, M. W. Frampton, W. Lambert, J. M. Samet, F. E. Speizer, and M. Utell. Health effects of outdoor air pollution. *American journal of respiratory and critical care medicine*, 153(1):3–50, 1996.

H. Behrendt and W. M. Becker. Localization, release and bioavailability of pollen allergens: the influence of environmental factors. *Current Opinion in Immunology*, 13(6):709–715, 2001.

H. Behrendt, K. Friedrichs, E. Kainka-Staenicke, U. Darsow, W. M. Becker, and R. Tomingas. Allergens and pollutants in the air–a complex interaction. *New Trends in Allergy III. Berlin, Springer*, pages 467–478, 1991.

H. Behrendt, W. M. Becker, C. Fritzsche, W. Sliwa-Tomczok, J. Tomczok, K. H. Friedrichs, and J. Ring. Air pollution and allergy: Experimental studies on modulation of allergen release from pollen by air pollutants. *International archives of allergy and immunology*, 113(1-3): 69–74, 1997.

M. T. Benjamin and A. M. Winer. Estimating the ozone-forming potential of urban trees and shrubs. *Atmospheric Environment*, 32(1):53–68, 1998.

J.A. Bernstein, N. Alexis, C. Barnes, I.L. Bernstein, A. Nel, D. Peden, D. Diaz-Sanchez, S.M. Tarlo, and P.B. Williams. Health effects of air pollution. *Journal of Allergy and Clinical Immunology*, 114:1116–23, 2004.

N. Bertin, M. Staudt, U. Hansen, G. Seufert, P. Ciccioli, P. Foster, J. L. Fugit, and L. Torres. Diurnal and seasonal course of monoterpene emissions from quercus ilex (l.) under natural conditions application of light and temperature algorithms. *Atmospheric Environment*, 31 (Supplement 1):135–144, 1997.

A. Bist, T. Pandit, A. K. Bhatnagar, and A. B. Singh. Variability in protein content of pollen of castor bean (ricinus communis) before and after exposure to the air pollutants so2 and no2. *Grana*, 43(2):94–100, 2004.

M. T. Boehm and D. E. Aylor. Lagrangian stochastic modeling of heavy particle transport in the convective boundary layer. *Atmospheric Environment*, 39(27):4841–4850, 2005.

G. B. Bonan. Land-atmosphere interactions for climate system models: Coupling biophysical, biogeochemical, and ecosystem dynamical processes. *Remote Sensing of Environment*, 51(1): 57–73, 1995.

Gert-Jan Braunstahl, Alex Kleinjan, Shelley E. Overbeek, Jan-Bas Prins, Henk C. Hoogsteden, and Wytske J. Fokkens. Segmental bronchial provocation induces nasal inflammation in allergic rhinitis patients. *Am. J. Respir. Crit. Care Med.*, 161(6):2051–2057, 2000.

J. M. Bullock and R. T. Clarke. Long distance seed dispersal by wind: measuring and modelling the tail of the curve. *Oecologia*, 124(4):506–521, 2000.

D. Byun and K. L. Schere. Review of the governing equations, computational algorithms, and other components of the models-3 community multiscale air quality (cmaq) modeling system. *Applied Mechanics Reviews*, 59(1-6):51–77, 2006.

D. W. Byun and J. K. S. Ching. Science algorithms of the epa models-3 community multiscale air quality (cmaq) modeling system. Technical report, US Environmental Protection Agency, Office of Research and Development, 1999.

C. Calfapietra, G. S. Mugnozza, D. F. Karnosky, F. Loreto, and T. D. Sharkey. Isoprene emission rates under elevated co2 and o-3 in two field-grown aspen clones differing in their sensitivity to o-3. *New Phytologist*, 179(1):55–61, 2008.

A. Calogirou, D. Kotzias, and A. Kettrup. Atmospheric oxidation of linalool. *Naturwissenschaften*, 82(6):288–289, 1995.

G. S. Campbell and J. M. Norman. *An Introduction to Environmental Biophysics*. Springer, 1998.

W.P.L. Carter. Development of ozone reactivity scales for volatile organic compounds. *Journal of the Air and Waste Management Association*, 44(7):881–899, 1994.

W.P.L. Carter, J.A. Pierce, D.M. Luo, and I.L. Malikna. Environmental chamber study of maximum incremental reactivities of volatile organic compounds. *Atmospheric Environment*, 29(18):2499–2511, 1995.

W. L. Chameides, R. W. Lindsay, J. Richardson, and C. S. Kiang. The role of biogenic hydrocarbons in urban photochemical smog: Atlanta as a case study. *Science*, 241(4872):1473–1475, 1988.

A. Chehregani, A. Majde, M. Moin, M. Gholami, M.A. Shariatzadeh, and H. Nassiri. Increasing potency of zinnia pollen grains in polluted areas. *Ecotoxicology and Environmental Safety*, 58 (2):267–272, 2004.

P. Ciccioli, A. Cecinato, R. Cabella, E. Brancaleoni, and P. Buttini. The contribution of gas-phase reactions to the nitroarene fraction of molecular weight 247 present in carbon particles sampled in an urban area of northern italy. *Atmospheric Environment. Part A. General Topics*, 27(8):1261–1270, 1993.

A. J. Cimorelli, S. G. Perry, A. Venkatram, J. C. Weil, R. J. Paine, R. B. Wilson, R. F. Lee, W. D. Peters, and R. W. Brode. Aermod: A dispersion model for industrial source applications. part i: General model formulation and boundary layer characterization. *Journal of Applied Meteorology*, 44(5):682–693, 2005.

M. Claeys, B. Graham, G. Vas, W. Wang, R. Vermeylen, V. Pashynska, J. Cafmeyer, P. Guyon, M. O. Andreae, P. Artaxo, and W. Maenhaut. Formation of secondary organic aerosols through photooxidation of isoprene. *Science*, 303(5661):1173–1176, 2004a.

M. Claeys, W. Wang, A. C. Ion, I. Kourtchev, A. Gelencser, and W. Maenhaut. Formation of secondary organic aerosols from isoprene and its gas-phase oxidation products through reaction with hydrogen peroxide. *Atmospheric Environment*, 38(25):4093–4098, 2004b.

B. Clot. Airborne birch pollen in neuchatel (switzerland): onset, peak and daily patterns. *Aerobiologia*, 17(1):25–29, 2001.

R. Cocchiara, G. Albeggiani, G. D. Trapani, A. Azzolina, N. Lampiasi, F. Rizzo, L. Diotallevi,

L. Gianaroli, and D. Geraci. Oestradiol enhances in vitro the histamine release induced by embryonic histamine-releasing factor (ehrf) from uterine mast cells, 1992.

R. Cocchiara, N. Lampiasi, G. Albeggiani, A. Azzolina, A. Bongiovanni, L. Gianaroli, F. D. Blasi, and D. Geraci. A factor secreted by human embryo stimulates cytokine release by uterine mast cell. *Molecular Human Reproduction*, 2(10):781–791, 1996.

W. D. Collins, Rasch P. J., Eaton B. E., Fillmore D. W., Kiehl J. T., Beck C. T., and Zender C. S. Simulation of aerosol distributions and radiative forcing for indoex: Regional climate impacts. *Journal of Geophysical Research*, 107(D19), 2002.

W. Cookson and J. M. Hopkin. Dominant inheritance of atopic immunoglobulin-e responsiveness. *Lancet*, 1(8577):86–88, 1988.

S.B. Corchnoy and R. Atkinson. Kinetics of the gas-phase reactions of oh and no3 radicals with 2-carene, 1,8-cineolde, p-cymene, and terpinolene. *Environmental Science and Technology*, (24):1497–1502, 1990.

M. L. Cover and L. C. Change. Modis land cover product algorithm theoretical basis document (atbd) version 5.0. Technical report, 1999.

Jr. Cox, L. A., M. G. Bird, and L. Griffis. Isoprene cancer risk and the time pattern of dose administration. *Toxicology*, 113(1-3):263–72, 1996.

D. Dabdub and R. Manohar. Performance and portability of tan air quality model. *Parallel computing*, (23):2187–2200, 1997.

A. R. Dahl, W. E. Bechtold, J. A. Bond, R. F. Henderson, J. L. Mauderly, B. A. Muggenburg, J. D. Sun, and L. S. Birnbaum. Species differences in the metabolism and disposition of inhaled 1,3-butadiene and isoprene. *Environ Health Perspect*, 86:65–9, 1990.

G. D'Amato and L. Cecchi. Effects of climate change on environmental factors in respiratory allergic diseases. *Clinical and Experimental Allergy*, 38(8):1264–1274, 2008.

F. De Leeuw, N. Moussiopoulos, P. Sahm, and A. Bartonova. Urban air quality in larger conurbations in the european union. *Environmental Modeling and Software*, (16):399–414, 2001.

R. L. Dennis, D. W. Byun, J. H. Novak, K. J. Galluppi, C. J. Coats, and M. A. Vouk. The next generation of integrated air quality modeling: Epa's models-3. *Atmospheric Environment*, 30 (12):1925–1938, 1996.

F. Di-Giovanni and P. M. Beckett. On the mathematical modeling of pollen dispersal and deposition. *Journal of Applied Meteorology*, 29(12):1352–1357, 1990.

F. Di-Giovanni, P. M. Beckett, and J. R. Flenley. Modeling of dispersion and deposition of tree pollen within a forest canopy. *Grana*, 28(2):129–139, 1989.

D. W. Dockery. Epidemiologic evidence of cardiovascular effects of particulate air pollution. *Environmental Health Perspectives*, 109 Suppl 4:483–6, 2001.

D. W. Dockery and 3rd Pope, C. A. Acute respiratory effects of particulate air pollution. *Annu. Rev. Public. Health.*, 15:107–32, 1994.

V. Dose and A. Menzel. Bayesian analysis of climate change impacts in phenology. *Global Change Biology*, 10(2):259–272, 2004.

M. Doyle, K. G. Sexton, H. Jeffries, K. Bridge, and I. Jaspers. Effects of 1,3-butadiene, isoprene, and their photochemical degradation products on human lung cells. *Environ Health Perspect*, 112(15):1488–95, 2004.

R. R. Draxler and G. D. Hess. An overview of the hysplit4 modelling system for trajectories, dispersion, and deposition. *Australian Meteorological Magazine*, 47(4):295–308, 1998.

R. R. Draxler, R. Dietz, R. J. Lagomarsino, and G. Start. Across north-america tracer experiment (anatex) - sampling and analysis. *Atmospheric Environment Part a-General Topics*, 25 (12):2815–2836, 1991.

J. Dudhia. Numerical study of convection observed during the winter monsoon experiment using a mesoscale two-dimensional model. *Journal of the Atmospheric Sciences*, 46(20):3077–3107, 1989.

J. Dudhia and J. F. Bresch. A global version of the psu–ncar mesoscale model. *Monthly Weather Review*, 130(12):2989–3007, 2002.

J. A. Duffie and W. A. Beckman. *Solar Engineering of Thermal Processes.* John Wiley and Sons, 1980.

S. Dupont, Y. Brunet, and N. Jarosz. Eulerian modelling of pollen dispersal over heterogeneous vegetation canopies. *Agricultural and Forest Meteorology*, 141(2-4):82–104, 2006.

John Dwyer. Remotely sensed data available from the us geological survey eros data center. In *Earth Science Satellite Remote Sensing*, pages 18–51. 2006.

K. Eastham and J. Sweet. Genetically modified organisms (gmos): The significance of gene flow through pollen transfer. Technical report, European Environmental Agency, 2002.

E. O. Edney, T. E. Kleindienst, M. Jaoui, M. Lewandowski, J. H. Offenberg, W. Wang, and M. Claeys. Formation of 2-methyl tetrols and 2-methylglyceric acid in secondary organic aerosol from laboratory irradiated isoprene/nox/so2/air mixtures and their detection in ambient pm2.5 samples collected in the eastern united states. *Atmospheric Environment*, 39(29): 5281–5289, 2005.

J. Emberlin. Plant allergens on pauci-micronic airborne particles. *Clinical and Experimental Allergy*, 25(3):202–205, 1995.

J. Emberlin, M. Detandt, R. Gehrig, S. Jaeger, N. Nolard, and A. Rantio-Lehtimäki. Responses in the start of betula (birch) pollen seasons to recent changes in spring temperatures across europe. *International Journal of Biometeorology*, 46(4):159–170, 2002.

E.P.A. Guidelines for regulatory application of the urban airshed model. Technical report, Research Triangle Park, 1991.

N. Estrella, A. Menzel, U. Krämer, and H. Behrendt. Integration of flowering dates in phenology and pollen counts in aerobiology: analysis of their spatial and temporal coherence in germany (1992–1999). *International Journal of Biometeorology*, 51(1):49–59, 2006.

R. C. Evans, D. T. Tingey, M. L. Gumpertz, and W. F. Burns. Estimates of isoprene and monoterpene emission rates in plants. *Botanical Gazette*, 143(3), 1982.

Knut Faegri, Peter Emil Kaland, and Knut Krzywinski. *Textbook of pollen analysis.* Wiley, Chichester [England] ; New York, 4th edition, 1989.

Paolo Falagiani. *Pollinosis.* CRC Press, Boca Raton, Fla., 1990.

F. Fehsenfeld, J. Calvert, R. Fall, P. Goldan, A. Guenther, and C. N. Hewitt. Emission of volatile organic compunds from vegetation and the implications for atmospheric chemistry. *Global Biochemical Cycles*, (6):389–430, 1992.

B. Felzer, D. Kicklighter, J. Melillo, C. Wang, Q. Zhuang, and R. Prinn. Effects of ozone on net primary production and carbon sequestration in the conterminous united states using a biogeochemistry model. *Tellus Series B-Chemical and Physical Meteorology*, 56(3):230–248, 2004.

B. J. Finlayson-Pitts and J. N. Pitts. *Chemistry of the upper and lower atmosphere. Theory, experiments, and applications.* Academic Press, UK, 2000.

A. M. Fiore, D. J. Jacob, I. Bey, R. M. Yantosca, B. D. Field, A. C. Fusco, and J. G. Wilkinson. Background ozone over the united states in summer: Origin, trend, and contribution to pollution episodes. *Journal of Geophysical Research-Atmospheres*, 107(D15):–, 2002.

B. Forsberg, N. Stjernberg, R. Linne, B. Segerstedt, and S. Wall. Daily air pollution levels and acute asthma in southern sweden. *European Respiratory Journal*, 12(4):900, 1998.

T. Franze, M. G. Weller, R. Niessner, and U. Poschl. Protein nitration by polluted air. *Environmental Science and Technology*, 39(6):1673–1678, 2005.

T. Frei and E. Gassner. Climate change and its impact on birch pollen quantities and the start of the pollen season an example from switzerland for the period 1969–2006. *International Journal of Biometeorology*, 52(7):667–674, 2008.

D. A. Frenz. Comparing pollen and spore counts collected with the rotorod sampler and burkard spore trap. *Annals of Allergy, Asthma and Immunology*, 83(5):341–349, 1999.

D. A. Frenz, S. E. Melcher, L. W. Murray, and R. E. Sand. A comparison of total pollen counts obtained 5.6 km apart. *Aerobiologia*, 13(3):205–208, 1997.

M. A. Friedl, D. K. McIver, J. C. F. Hodges, X. Y. Zhang, D. Muchoney, A. H. Strahler, C. E. Woodcock, S. Gopal, A. Schneider, and A. Cooper. Global land cover mapping from modis: algorithms and early results. *Remote Sensing of Environment*, 83(1-2):287–302, 2002.

S. K. Friedlander. *Smoke, dust and haze: Fundamentals of aerosol behavior.* Wiley-Interscience, New York, 1977.

N. A. Fuchs. The mechanics of aerosol. *Pergamon, New York*, 9303:20, 1964.

J. D. Fuentes and D. Wang. On the seasonality of isoprene emissions from a mixed temperate forest. *Ecological Applications*, 9(4):1118–1131, 1999.

J. D. Fuentes, M. Lerdau, R. Atkinson, D. Baldocchi, J. W. Bottenheim, P. Ciccioli, B. Lamb, C. Geron, L. Gu, A. Guenther, T. D. Sharkey, and W. Stockwell. Biogenic hydrocarbons in the atmospheric boundary layer: A review. *Bulletin of the American Meteorological Society*, 81(7):1537–1575, 2000.

J. Fuhrer and F. Booker. Ecological issues related to ozone: agricultural issues. *Environment International*, 29(2-3):141–154, 2003.

J. Gaffney and N. Marley. Tropospheric chemistry of natural hydrocarbons and energy-related pollutants: biosphere/climate feedbacks? In C. Sloane, T. Tesche, and M.I. Chelsea, editors, *Atmospheric Chemistry: Models and predictions for climate and air quality.* Lewis Publishers, Inc., 1991.

S. H. Gage, S. A. Isard, and M. Colunga. Ecological scaling of aerobiological dispersal processes. *Agricultural and Forest Meteorology*, 97(4):249–261, 1999.

J. W. Gauderman, R. O. B. M c Connell, F. Gilliland, S. London, D. Thomas, E. Avol, H. Vora, K. Berhane, E. B. Rappaport, and F. Lurmann. Association between air pollution and lung function growth in southern california children. *American journal of respiratory and critical care medicine*, 162(4):1383–1390, 2000.

P. G. Georgopoulos. A multiscale approach for assessing the interactions of environmental and biological systems in a holistic health risk assessment framework. *Water, Air, and Soil Pollution: Focus*, 8(1):3–21, 2008.

C. Geron, A. Guenther, T. Sharkey, and R. R. Arnts. Temporal variability in basal isoprene emission factor. *Tree Physiology*, 20(12):799–805, 2000a.

C. Geron, R. Rasmussen, R. R. Arnts, and A. Guenther. A review and synthesis of monoterpene speciation from forests in the united states. *Atmospheric Environment*, 34(11):1761–1781, 2000b.

M. W. Gery, G. Z. Whitten, J. P. Killus, and M. C. Dodge. A photochemical kinetics mechanism for urban and regional scale computering modeling. *Journal of Geophysical Research*, 94(D10), 1989.

Z. González Parrado, R. M. Valencia Barrera, C. R. Fuertes Rodríguez, A. M. Vega Maray, R. Pérez Romero, R. Fraile, and D. Fernández González. Alternative statistical methods for interpreting airborne alder (alnus glutimosa (l.) gaertner) pollen concentrations. *International Journal of Biometeorology*, 53(1):1–9, 2009.

J. Goudriaan and H. H. van Laar. *Modelling Potential Crop Growth Processes: Textbook with Exercises*. Kluwer Academic Pub, 1994.

D. F. Greene and E. A. Johnson. A model of wind dispersal of winged or plumed seeds. *Ecology*, 70(2):339–347, 1989.

D. F. Greene and E. A. Johnson. Long-distance wind dispersal of tree seeds. *Canadian Journal of Botany/Revue Canadienne de Botanique*, 73(7):1036–1045, 1995.

Philip Herries Gregory. *The microbiology of the atmosphere*. Wiley, New York,, 2d edition, 1973.

G. A. Grell, J. Dudhia, and D. R. Stauffer. A description of the fifth-generation penn state/ncar mesoscale model (mm5). ncar technical note. Technical report, National Center for Atmospheric Research, Boulder, CO, 1994.

R. J. Griffin, D. Dabdub, and J. H. Seinfeld. Secondary organic aerosol 1. atmospheric chemical mechanism for production of molecular constituents. *J. Geophys. Res*, 107:4332, 2002.

A. Guenther, C. N. Hewitt, D. Erickson, R. Fall, C. Geron, T. Graedel, P. Harley, L. Klinger, M. Lerdau, W. A. Mckay, T. Pierce, B. Scholes, R. Steinbrecher, R. Tallamraju, J. Taylor, and P. Zimmerman. A global-model of natural volatile organic-compound emissions. *Journal of Geophysical Research-Atmospheres*, 100(D5):8873–8892, 1995.

A. Guenther, P. Zimmerman, L. Klinger, J. Greenberg, C. Ennis, K. Davis, W. Pollock, H. West-berg, G. Allwine, and C. Geron. Estimates of regional natural volatile organic compound fluxes from enclosure and ambient measurements. *Journal of Geophysical Research-Atmospheres*, 101 (D1):1345–1359, 1996.

A. Guenther, S. Archer, J. Greenberg, P. Harley, D. Helmig, L. Klinger, L. Vierling, M. Wilder-muth, P. Zimmerman, and S. Zitzer. Biogenic hydrocarbon emissions and landcover/climate change in a subtropical savanna. *Physics and Chemistry of the Earth Part B-Hydrology Oceans and Atmosphere*, 24(6):659–667, 1999a.

A. Guenther, B. Baugh, G. Brasseur, J. Greenberg, P. Harley, L. Klinger, D. Serca, and L. Vier-ling. Isoprene emission estimates and uncertainties for the central african expresso study domain. *Journal of Geophysical Research-Atmospheres*, 104(D23):30625–30639, 1999b.

A. Guenther, C. Geron, T. Pierce, B. Lamb, P. Harley, and R. Fall. Natural emissions of non-methane volatile organic compounds; carbon monoxide, and oxides of nitrogen from north america. *Atmospheric Environment*, 34(12-14):2205–2230, 2000.

A. B. Guenther, P. R. Zimmerman, P. C. Harley, R. K. Monson, and Fall R. Isoprene and monoterpene emission rate variability: Model evaluations andsensitivity analyses. *Journal of Geophysical Research*, (98):12609–12617, 1993.

H. Hakola, T. Laurila, J. Rinne, and K. Puhto. The ambient concentrations of biogenic hydro-carbons at a northern european, boreal site. *Atmospheric Environment*, 34(29-30):4971–4982, 2000.

H. Hakola, V. Tarvainen, T. Laurila, V. Hiltunen, H. Hellen, and P. Keronen. Seasonal variation of voc concentrations above a boreal coniferous forest. *Atmospheric Environment*, 37(12): 1623–1634, 2003.

P. Harley, A. Guenther, and P. Zimmerman. Effects of light, temperature and canopy position on net photosynthesis and isoprene emission from sweetgum (liquidambar styraciflua) leaves. *Tree Physiology*, 16(1-2):25–32, 1996.

P. Harley, A. Guenther, and P. Zimmerman. Environmental controls over isoprene emission in deciduous oak canopies. *Tree Physiology*, 17(11):705–714, 1997.

N Helbig, B Vogel, H Vogel, and F Fiedler. Numerical modelling of pollen dispersion on the regional scale. *Aerobiologia*, 20(1):3–19, 2004.

C. N. Hewitt. *Reactive hydrocarbons in the atmosphere.* Academic Press, San Diego, 1999.

S. I. Higgins, R. Nathan, and M. L. Cain. Are long-distance dispersal events in plants usually caused by nonstandard means of dispersal? *Ecology*, 84(8):1945–1956, 2003.

Hilaire. *Modelling of Birch pollen concentrations using an atmospheric transport model.* PhD thesis, De Bilt, 2007.

T. J N Hiltermann, C. R deBruijne, J. Stolk, A. H Zwinderman, F. Th M Spieksma, W. Roemer, P. A Steerenberg, P. H Fischer, L. vanBree, and P. S Hiemstra. Effects of photochemical air pollution and allergen exposure on upper respiratory tract inflammation in asthmatics. *Am. J. Respir. Crit. Care Med.*, 156(6):1765–1772, 1997.

J. Hodges. Modis mod12 land cover and land cover dynamics products user guide. *Available online at: geography. bu. edu/landcover/userguidelc/intro. html (accessed 13 September 2005)*, 2001.

S. Y. Hong and H. L. Pan. Nonlocal boundary layer vertical diffusion in a medium-range forecast model. *Monthly Weather Review*, 124(10):2322–2339, 1996.

L. W. Horowitz, J. Y. Liang, G. M. Gardner, and D. J. Jacob. Export of reactive nitrogen from north america during summertime: Sensitivity to hydrocarbon chemistry. *Journal of Geophysical Research-Atmospheres*, 103(D11):13451–13476, 1998.

M. Huynen, B. Menne, H. Behrendt, R. Bertollini, S. Bonini, R. Brandao, C. Brown-Fährlander, B. Clot, P. D'Ambrosio De Nuntiis, and K. L. Ebi. Phenology and human health: Allergic disorders. pages 16–17, 2003.

V. Illarionova, J. Kaiser, E. Ostrozhenkova, A. Bacher, M. Fischer, W. Eisenreich, and F. Rohdich. Nonmevalonate terpene biosynthesis enzymes as antiinfective drug targets: Substrate

synthesis and high-throughput screening methods. *Journal of Organic Chemistry*, 71(23): 8824–8834, 2006.

J. G. Isebrands, A. B. Guenther, P. Harley, D. Helmig, L. Klinger, L. Vierling, P. Zimmerman, and C. Geron. Volatile organic compound emission rates from mixed deciduous and coniferous forests in northern wisconsin, usa. *Atmospheric Environment*, 33(16):2527–2536, 1999.

K. Ishizaka, H. Tomioka, and T. Ishizaka. Mechanisms of passive sensitization: I. presence of ige and igg molecules on human leukocytes. *The Journal of Immunology*, 105(6):1459, 1970.

T. Ishizaki, K. Koizumi, R. Ikemori, Y. Ishiyama, and E. Kushibiki. Studies of prevalence of japanese cedar pollinosis among the residents in a densely cultivated area. *Ann Allergy*, 58 (4):265–70, 1987.

V. A. Isidorov, I. G. Zenkevich, and B. V. Ioffe. Volatile organic compounds in the atmosphere of forests. *Atmospheric Environment*, 19(1):1–8, 1985.

D. J. Jacob. Heterogeneous chemistry and tropospheric ozone. *Atmospheric Environment*, 34 (12-14):2131–2159, 2000.

M. Z. Jacobson. *Fundamentals of atmospheric modeling*. Cambridge University Press, Cambridge, UK., 1999.

B. B. Jalaludin, B. I. O'Toole, and S. R. Leeder. Acute effects of urban ambient air pollution on respiratory symptoms, asthma medication use, and doctor visits for asthma in a cohort of australian children. *Environmental Research*, 95(1):32–42, 2004.

N. Jarosz, B. Loubet, B. Durand, A. McCartney, X. Foueillassar, and L. Huber. Field measurements of airborne concentration and deposition rate of maize pollen. *Agricultural and Forest Meteorology*, 119(1-2):37–51, 2003.

N. Jarosz, B. Loubet, and L. Huber. Modelling airborne concentration and deposition rate of maize pollen. *Atmospheric Environment*, 38(33):5555–5566, 2004.

A. M. Jones and R. M. Harrison. The effects of meteorological factors on atmospheric bioaerosol concentrations - a review. *Science of the Total Environment*, 326(1-3):151–180, 2004.

S. K. Kaharabata, P. H. Schuepp, and J. D. Fuentes. Source footprint considerations in the determination of volatile organic compound fluxes from forest canopies. *Journal of Applied Meteorology*, 38(7):878–884, 1999.

J. S. Kain. The kain–fritsch convective parameterization: An update. *Journal of Applied Meteorology*, 43(1):170–181, 2004.

M. Kanakidou, J. H. Seinfeld, S. N. Pandis, I. Barnes, F. J. Dentener, M. C. Facchini, R. Van Dingenen, B. Ervens, A. Nenes, C. J. Nielsen, E. Swietlicki, J. P. Putaud, Y. Balkanski, S. Fuzzi, J. Horth, G. K. Moortgat, R. Winterhalter, C. E. L. Myhre, K. Tsigaridis, E. Vignati, E. G. Stephanou, and J. Wilson. Organic aerosol and global climate modelling: a review. *Atmospheric Chemistry and Physics*, 5:1053–1123, 2005.

D. W. Kang, V. P. Aneja, R. Mathur, and J. D. Ray. Nonmethane hydrocarbons and ozone in three rural southeast united states national parks: A model sensitivity analysis and comparison to measurements. *Journal of Geophysical Research-Atmospheres*, 108(D19):–, 2003.

J. F. Karlik and A. M. Winer. Measured isoprene emission rates of plants in california landscapes: comparison to estimates from taxonomic relationships. *Atmospheric Environment*, 35(6):1123–1131, 2001.

J. F. Karlik, A. H. McKay, J. M. Welch, and A. M. Winer. A survey of california plant species with a portable voc analyzer for biogenic emission inventory development. *Atmospheric Environment*, 36(33):5221–5233, 2002.

S. Kawashima and Y. Takahashi. Modelling and simulation of mesoscale dispersion processes for airborne cedar pollen. *Grana*, 34:142–142, 1995.

S. Kawashima and Y. Takahashi. An improved simulation of mesoscale dispersion of airborne cedar pollen using a flowering-time map. *Grana*, 38(5):316–324, 1999.

C. J. Keijzer. The processes of anther dehiscence and pollen dispersal. i. the opening mechanism of longitudinally dehiscing anthers. *New Phytologist*, 105(3):487–498, 1987a.

C. J. Keijzer. The processes of anther dehiscence and pollen dispersal. ii. the formation and the

transfer mechanism of pollenkitt, cell-wall development of the loculus tissues and a function of orbicules in pollen dispersal. *New Phytologist*, 105(3):499–507, 1987b.

C. J. Keijzer, I. H. S. Hoek, and M. T. M. Willemse. The processes of anther dehiscence and pollen dispersal. iii. the dehydration of the filament tip and the anther in three monocotyledonous species. *New Phytologist*, 106(2):281–287, 1987.

J. Kesselmeier and M. Staudt. Biogenic volatile organic compounds (voc): An overview on emission, physiology and ecology. *Journal of Atmospheric Chemistry*, 33(1):23–88, 1999.

J. Kesselmeier, U. Kuhn, A. Wolf, M. O. Andreae, P. Ciccioli, E. Brancaleoni, M. Frattoni, A. Guenther, J. Greenberg, P. D. Vasconcellos, T. de Oliva, T. Tavares, and P. Artaxo. Atmospheric volatile organic compounds (voc) at a remote tropical forest site in central amazonia. *Atmospheric Environment*, 34(24):4063–4072, 2000.

E. Kinnee, C. Geron, and T. Pierce. United states land use inventory for estimating biogenic ozone precursor emissions. *Ecological Applications*, 7(1):46–58, 1997.

K. Knowlton, M. Rotkin-ellman, and G. Solomon. How global warming could increase ragweed allergies, air pollution and asthma. Technical report, National Resources Defence Council, Oct. 2007 2007.

R. B. Knox and Biology Inst. *Pollen and Allergy*. Edward Arnold, 1979.

S. Koch, R. Winterhalter, E. Uherek, A. Kolloff, P. Neeb, and G. K. Moortgat. Formation of new particles in the gas-phase ozonolysis of monoterpenes. *Atmospheric Environment*, 34(23): 4031–4042, 2000.

M. Kogevinas, J. M. Anto, J. Sunyer, A. Tobias, H. Kromhout, and P. Burney. Occupational asthma in europe and other industrialised areas: a population-based study. european community respiratory health survey study group. *Lancet*, 353(9166):1750–4, 1999.

G. Konig, M. Brunda, H. Puxbaum, C. N. Hewitt, S. C. Duckham, and J. Rudolph. Relative contribution of oxygenated hydrocarbons to the total biogenic voc emissions of selected mid-european agricultural and natural plant-species. *Atmospheric Environment*, 29(8):861–874, 1995.

J. H. Kroll, N. L. Ng, S. M. Murphy, R. C. Flagan, and J. H. Seinfeld. Secondary organic aerosol formation from isoprene photooxidation under high-nox conditions. *Geophysical Research Letters*, 32(18):–, 2005.

J. H. Kroll, N. L. Ng, S. M. Murphy, R. C. Flagan, and J. H. Seinfeld. Secondary organic aerosol formation from isoprene photooxidation. *Environmental Science and Technology*, 40 (6):1869–1877, 2006.

M. Kuhn, P. J. H. Builtjes, D. Poppe, D. Simpson, W. R. Stockwell, Y. Andersson-Skold, A. Baart, M. Das, F. Fiedler, O. Hov, F. Kirchner, P. A. Makar, J. B. Milford, M. G. M. Roemer, R. Ruhnke, A. Strand, B. Vogel, and H. Vogel. Intercomparison of the gas-phase chemistry in several chemistry and transport models. *Atmospheric Environment*, 32(4):693–709, 1998.

A. Kuparinen. Mechanistic models for wind dispersal. *Trends in Plant Science*, 11(6):296–301, 2006.

B. Lamb and Council Coordinating Research. *Review of the Emissions, Atmospheric Chemistry, and Gas/particle Partition of Biogenic Volatile Organic Compounds and Reaction Products*. Atmospheric and Environmental Research, 1999.

B. Lamb, A. Guenther, D. Gay, and H. Westberg. A national inventory of biogenic hydrocarbon emissions. *Atmospheric Environment*, 21(8):1695–1705, 1987.

B. Lamb, D. Gay, H. Westberg, and T. Pierce. A biogenic hydrocarbon emission inventory for the u.s.a. using a simple forest canopy model. *Atmospheric Environment*, (27):1673–1690, 1993.

B. Lamb, T. Pierce, D. Baldocchi, E. Allwine, S. Dilts, H. Westberg, C. Geron, A. Guenther, L. Klinger, P. Harley, and P. Zimmerman. Evaluation of forest canopy models for estimating isoprene emissions. *Journal of Geophysical Research-Atmospheres*, 101(D17):22787–22797, 1996.

A. Lehning, W. Zimmer, I. Zimmer, and J. P. Schnitzler. Modeling of annual variations of oak

(quercus robur l.) isoprene synthase activity to predict isoprene emission rates. *Journal of Geophysical Research-Atmospheres*, 106(D3):3157–3166, 2001.

Walter Hepworth Lewis, Prathibha Vinay, and Vincent E. Zenger. *Airborne and allergenic pollen of North America*. Johns Hopkins University Press, Baltimore, 1983.

B. Leynaert, C. Neukirch, D. Jarvis, S. Chinn, P. Burney, and F. Neukirch. Does living on a farm during childhood protect against asthma, allergic rhinitis, and atopy in adulthood? *American journal of respiratory and critical care medicine*, 164(10):1829–1834, 2001.

DW Li and B Kendrick. Functional relationships between airborne fungal spores and environmental factors in kitchener-waterloo, ontario. *Grana*, 33(3):166–176, 1994.

J. Y. Liang, L. W. Horowitz, D. J. Jacob, Y. H. Wang, A. M. Fiore, J. A. Logan, G. M. Gardner, and J. W. Munger. Seasonal budgets of reactive nitrogen species and ozone over the united states, and export fluxes to the global atmosphere. *Journal of Geophysical Research-Atmospheres*, 103(D11):13435–13450, 1998.

H. K. Lichtenthaler, J. Schwender, A. Disch, and M. Rohmer. Biosynthesis of isoprenoids in higher plant chloroplasts proceeds via a mevalonate-independent pathway. *Febs Letters*, 400 (3):271–274, 1997.

B. Lighthart and B. T. Shaffer. Increased airborne bacterial survival as a function of particle content and size. *Aerosol Science and Technology*, 27(3):439–446, 1997.

H. J. Lim, A. G. Carlton, and B. J. Turpin. Isoprene forms secondary organic aerosol through cloud processing: Model simulations. *Environmental Science and Technology*, 39(12):4441–4446, 2005.

J. A. Logan. Tropospheric ozone: Seasonal behavior, trends and anthropogenic influence. *Journal of Geophysical Research-Atmospheres*, (90):10463–10482, 1985.

C. Loos, R. Seppelt, S. Meier-Bethke, J. Schiemann, and O. Richter. Spatially explicit modelling of transgenic maize pollen dispersal and cross-pollination. *Journal of theoretical biology*, 225 (2):241–255, 2003.

A. A. Lopes, D. C. Baldoqui, S. N. Lopez, M. J. Kato, V. D. Bolzani, and M. Furlan. Biosynthetic origins of the isoprene units of gaudichaudianic acid in piper gaudichaudianum (piperaceae). *Phytochemistry*, 68(15):2053–2058, 2007.

F. Loreto and T. Sharkey. A gas-exchange study of photosynthesis and isoprene emission in quercus rubra l. *Planta*, 182(4):523–531, 1990.

F. Loreto, P. Ciccioli, E. Brancaleoni, A. Cecinato, M. Frattoni, and T. D. Sharkey. Different sources of reduced carbon contribute to form three classes of terpenoid emitted by quercus ilex leaves. *Proceedings of the National Academy of Sciences*, 93(18):9966–9969, 1996.

F. W. Lurmann, W. P. L. Carter, and R. A. Coyner. A surrogate species chemical reaction mechanism for urban-scale air quality simulation models. volume i-adaptation of the mechanism. *EPA, Research Triangle Park, NC, USA*, 1987.

R. C. MacDonald and R. Fall. Detection of substantial emissions of methanol from plants to the atmosphere. *Atmospheric Environment. Part A. General Topics*, 27(11):1709–1713, 1993.

J. Macher and J. M. Macher. Bioaerosols: Assessment and control, 1999.

A. Makela. Implications of the pipe model theory on dry matter partitioning and height growth in trees. *Journal of theoretical biology*, 123:103–120, 1986.

D. G. Marsh, D. A. Meyers, and W. B. Bias. The epidemiology and genetics of atopic allergy. *N Engl J Med*, 305(26):1551–9, 1981.

R. S. Martin, H. Westberg, E. J. Allwine, L. Ashman, J. C. Farmer, and B. Lamb. Measurement of isoprene and its atmospheric oxidation products in a central pennsylvania deciduous forest. *Journal of Atmospheric Chemistry*, 13(1):1–32, 1991.

K. Masaka and S. Maguchi. Modelling the masting behaviour of betula platyphylla var. japonica using the resource budget model. *Annals of Botany*, 88(6):1049, 2001.

S. N. Matsunaga, C. Wiedinmyer, A. B. Guenther, J. J. Orlando, T. Karl, D. W. Toohey, J. P. Greenberg, and Y. Kajii. Isoprene oxidation products are a significant atmospheric aerosol component. *Atmos. Chem. Phys. Discuss.*, 5(6):11143–11156, 2005.

S. Matthias-Maser, V. Obolkin, T. Khodzer, and R. Jaenicke. Seasonal variation of primary biological aerosol particles in the remote continental region of lake baikal/siberia. *Atmospheric Environment*, 34(22):3805–3811, 2000.

H. A. McCartney and M. E. Lacey. Wind dispersal of pollen from crops of oilseed rape(brassica napus l.). *Journal of Aerosol Science*, 22(4):467–477, 1991.

D. J. McGarvey and R. Croteau. Terpenoid metabolism. *Plant Cell*, 7(7):1015–1026, 1995.

R. L. Melnick, R. C. Sills, J. H. Roycroft, B. J. Chou, H. A. Ragan, and R. A. Miller. Inhalation toxicity and carcinogenicity of isoprene in rats and mice: comparisons with 1,3-butadiene. *Toxicology*, 113(1-3):247–52, 1996.

E. J. Mlawer, S. J. Taubman, P. D. Brown, M. J. Iacono, and S. A. Clough. Radiative transfer for inhomogeneous atmospheres: Rrtm, a validated correlated-k model for the longwave. *Journal of Geophysical Research*, 102(16):663–16, 1997.

RT Molina, AM Rodriguez, IS Palacios, and FG Lopez. Pollen production in anemophilous trees. *Grana*, 35(1):38–46, 1996.

R. K. Monson and R. Fall. Isoprene emission from aspen leaves : Influence of environment and relation to photosynthesis and photorespiration. *Plant Physiology*, 90(1):267–274, 1989.

R. K. Monson, P. C. Harley, M. E. Litvak, M. Wildermuth, A. B. Guenther, P. R. Zimmerman, and R. Fall. Environmental and developmental controls over the seasonal pattern of isoprene emission from aspen leaves. *Oecologia*, 99(3-4):260–270, 1994.

J. L. Monteith and M. H. Unsworth. *Principles of Environmental Physics*. Butterworth-Heinemann, 1990.

J. Mullins and J. Emberlin. Sampling pollens. *Journal of Aerosol Science*, 28(3):365–370, 1997.

R. B. Myneni, C. D. Keeling, C. J. Tucker, G. Asrar, and R. R. Nemani. Increased plant growth in the northern high latitudes from 1981 to 1991. *Nature*, 386(6626):698–702, 1997.

R. B. Myneni, S. Hoffman, Y. Knyazikhin, J. L. Privette, J. Glassy, Y. Tian, Y. Wang, X. Song, Y. Zhang, and G. R. Smith. Global products of vegetation leaf area and fraction absorbed par from year one of modis data. *Remote Sensing of Environment*, 83(1):214–231, 2002.

R. Nathan and G. G. Katul. Foliage shedding in deciduous forests lifts up long-distance seed dispersal by wind. *Proceedings of the National Academy of Sciences of the United States of America*, 102(23):8251–8256, 2005.

R. Nathan, U. N. Safriel, and I. Noy-Meir. Field validation and sensitivity analysis of a mechanistic model for tree seed dispersal by wind. *Ecology*, 82(2):374–388, 2001.

R. Nathan, G. G. Katul, H. S. Horn, S. M. Thomas, R. Oren, R. Avissar, S. W. Pacala, and S. A. Levin. Mechanisms of long-distance dispersal of seeds by wind. *Nature*, 418(6896):409–413, 2002.

U.S. National Research Council. Rethinking the ozone problem in urban and regional air pollution. Technical report, National Academy Press, 1991.

K. W. Nicholson. A review of particle resuspension. *Atmospheric Environment (1967)*, 22(12): 2639–2651, 1988a.

K. W. Nicholson. The dry deposition of small particles: A review of experimental measurements. *Atmospheric Environment (1967)*, 22(12):2653–2666, 1988b.

Eugene Cecil Ogden, New York State Museum, Science Service., and U.S. Atomic Energy Commission. *Manual for sampling airborne pollen*. Hafner Press, New York,, 1974.

A. Okubo and S. A. Levin. A theoretical framework for data analysis of wind dispersal of seeds and pollen. *Ecology*, 70(2):329–338, 1989.

T. L. Otte. Whats new in mcip2 (meteorology-chemistry interface processor). In *3rd Annual CMAS Models-3 users conference*, Chapel Hill, NC, 2004.

Spyros N. Pandis, Suzanne E. Paulson, John H. Seinfeld, and Richard C. Flagan. Aerosol formation in the photooxidation of isoprene and [beta]-pinene. *Atmospheric Environment. Part A. General Topics*, 25(5-6):997–1008, 1991.

R. Pasken and J. A. Pietrowicz. Using dispersion and mesoscale meteorological models to forecast pollen concentrations. *Atmospheric Environment*, 39(40):7689–7701, 2005.

E. Pattey, R. L. Desjardins, H. Westberg, B. Lamb, and T. Zhu. Measurement of isoprene emissions over a black spruce stand using a tower-based relaxed eddy-accumulation system*. *Journal of Applied Meteorology*, 38(7):870–877, 1999.

F. Paulot, J. D. Crounse, H. G. Kjaergaard, J. H. Kroll, J. H. Seinfeld, and P. O. Wennberg. Isoprene photooxidation mechanism: resonance channels and implications for the production of nitrates and acids. *Atmos. Chem. Phys. Discuss*, 8:14643–14716, 2008.

S. G. Perry, A. J. Cimorelli, R. J. Paine, R. W. Brode, J. C. Weil, A. Venkatram, R. B. Wilson, R. F. Lee, and W. D. Peters. Aermod: A dispersion model for industrial source applications. part ii: Model performance against 17 field study databases. *Journal of Applied Meteorology*, 44(5):694–708, 2005.

H. Peter, H. J. Wiegand, J. G. Filser, H. M. Bolt, and R. J. Laib. Inhalation pharmacokinetics of isoprene in rats and mice. *Environmental Health Perspectives*, 86:89–92, 1990.

B. Peterson and A. Saxon. Global increases in allergic respiratory disease: the possible role of diesel exhaust particles. *Ann Allergy Asthma Immunol*, 77(4):263–8; quiz 269–70, 1996.

G. Petron, P. Harley, J. Greenberg, and A. Guenther. Seasonal temperature variations influence isoprene emission. *Geophysical Research Letters*, 28(9):1707–1710, 2001.

R.A. Pielke. *Mesoscale Meteorological Modeling.* Academic Press, Orlando, 1984.

P. A. Pier and C. McDuffie. Seasonal isoprene emission rates and model comparisons using whole-tree emissions from white oak. *Journal of Geophysical Research-Atmospheres*, 102(D20): 23963–23971, 1997.

T. Pierce, C. Geron, L. Bender, R. Dennis, G. Tonnesen, and A. Guenther. Influence of increased isoprene emissions on regional ozone modeling. *Journal of Geophysical Research-Atmospheres*, 103(D19):25611–25629, 1998.

T. Pierce, J. E. Pleim, E. J. Kinnee, and L. R. Joyce. Intercomparison of alternative vegetation databases for regional air quality modeling, 2002.

T. E. Pierce and P. S. Waldruff. Pc-beis - a personal-computer version of the biogenic emissions inventory system. *Journal of the Air and Waste Management Association*, 41(7):937–941, 1991.

T.E. Pierce. Beis 3 version 0.9, 2001.

T.E. Pierce, B.K. Lamb, and A.R. Van Meter. Development of a biogenic emissions inventory system from regional scale air pollution models. In *83rd Annual Meeting of the Air and Waste Management Association*, Pittsburgh, PA, 1990.

E. T. Prater and C. Midgley. This year's model: A new air dispersion modeling software is helping create more accurate industrial source models. *ENVIRONMENTAL PROTECTION-WACO-*, 17(3):24, 2006.

S. Pressley, B. Lamb, H. Westberg, A. Guenther, J. Chen, and E. Allwine. Monoterpene emissions from a pacific northwest old-growth forest and impact on regional biogenic voc emission estimates. *Atmospheric Environment*, 38(19):3089–3098, 2004.

K. E. Puls. Der einfluss von witterung und wetter auf blutenanlage, pollenfreisetzung und pollenflug. In Stiftung Deutscher Polleninformationsdienst, editor, *Europaisches Pollenflug-Symposium*, volume 20=21, pages 27–47, 1987.

D. Raeburn and S. E. Webber. Proinflammatory potential of the airway epithelium in bronchial asthma. *European Respiratory Journal*, 7(12):2226–2233, 1994.

H. Ranta, A. Oksanen, T. Hokkanen, K. Bondestam, and S. Heino. Masting by betula-species; applying the resource budget model to north european data sets. *International Journal of Biometeorology*, 49(3):146–151, 2005.

R.A. Rasmussen. Isoprene: identified as a forest-type emission to the atmosphere. *Environmental Science and Technology*, 4:667–671, 1970.

R.A. Rasmussen and F.W. Went. Volatile organic material of plant origin in the atmosphere. *Proceedings of the National Academy of Sciences of the United States of America*, 53:215–220, 1965.

N. S. Reddi. Pollen production in some anemophilous angiosperms. *Grana*, (25):55–61, 1986.

W. H. Reeser, G. M. Lee, A. Taylor, L. Wang, S. F. Arnold, J. S. Ultman, and A. Ben-Jebria. Uptake of ozone in human lungs and its relationship to local physiological response. *Inhalation Toxicology*, 17(13):699–707, 2005.

H. Rempe. Untersuchunged uber die verbreitung des blutenstaubes durch die luftstromungen. *Planta*, (27):93–147, 1938.

T Reponen, SA Grinshpun, KL Conwell, J Wiest, and WJ Anderson. Aerodynamic versus physical size of spores: Measurement and implication for respiratory deposition. *GRANA*, 40 (3):119–125, 2001.

A. M. Reynolds. Prediction of particle deposition on to rough surfaces. *Agricultural and Forest Meteorology*, 104(2):107–118, 2000.

J. Ring. Allergy and modern society: does' western life style'promote the development of allergies? *Int Arch Allergy Immunol*, 113(1-3):7–10, 1997.

J. Ring, B. Eberlein-Koenig, and H. Behrendt. Environmental pollution and allergy. *Annals of Allergy, Asthma and Immunology*, 87(1):2–6, 2001.

U. Risse, J. Tomczok, J. Huss-Marp, U. Darsow, and H. Behrendt. Health-relevant interaction between airborne particulate matter and aeroallergens (pollen). *Journal of Aerosol Science*, 31:27–28, 2000.

F. Rohdich, S. Hecht, K. Gartner, P. Adam, C. Krieger, S. Amslinger, D. Arigoni, A. Bacher, and W. Eisenreich. Studies on the nonmevalonate terpene biosynthetic pathway: Metabolic role of isph (lytb) protein. *Proceedings of the National Academy of Sciences of the United States of America*, 99(3):1158–1163, 2002.

S. J. Roselle. Effects of biogenic emission uncertainties on regional photochemical modeling of control strategies. *Atmospheric Environment*, 28(10):1757–1772, 1994.

S.J. Roselle, K.L. Schere, J.E. Pleim, and A.F. Hanna. Photolysis rates for cmaq. In S.W. Byun and J.K.S. Ching, editors, *Science algorithms of the EPA Models-3 Community Multiscale Air*

Quality (CMAQ) Modeling System. Office of Research and Development, U.S. Environmental Protection Agency, Washingtong, DC., 1999.

M. Rousi and J. Heinonen. Temperature sum accumulation effects on within-population variation and long-term trends in date of bud burst of european white birch (betula pendula). *Tree Physiology*, 27(7):1019, 2007.

A. G. Russell, J. G. Wilkinson, S. Hanna, and J. Vukovich. Review of beis3 formulation and consequences relative to air quality standards. Technical report, EPRI, 17 September 2001 2001.

G. A. Sanadze and G.M. Dolidze. Absorption of molecular hydrogen by illuminated leaves. *Soobshch. Akal. Nauk Gruz. SSR*, 27, 1961.

J. Schaber and F. W. Badeck. Physiology-based phenology models for forest tree species in germany. *International Journal of Biometeorology*, 47(4):193–201, 2003.

C. Schleip, A. Menzel, N. Estrella, and V. Dose. The use of bayesian analysis to detect recent changes in phenological events throughout the year. *Agricultural and Forest Meteorology*, 141 (2-4):179–191, 2006.

C. S. Schopmeyer. *Seeds of woody plants in the United States. For. Serv.* US Dept,. Agric., Agric. Handbk. 1974.

S. Schueler and K. H. Schlünzen. Modeling of oak pollen dispersal on the landscape level with a mesoscale atmospheric model. *Environmental Modeling and Assessment*, 11(3):179–194, 2006.

G. Schuh, A. C. Heiden, Th Hoffmann, J. Kahl, P. Rockel, J. Rudolph, and J. Wildt. Emissions of volatile organic compounds from sunflower and beech: Dependence on temperature and light intensity. *Journal of Atmospheric Chemistry*, 27(3):291–318, 1997.

W. Schurmann, H. Ziegler, D. Kotzias, R. Schonwitz, and R. Steinbrecher. Emission of biosynthesized monoterpenes from needles of norway spruce. *Naturwissenschaften*, 80(6):276–278, 1993.

D. Schwede, G. Pouliot, and T. Pierce. Changes to the biogenic emissions inventory system version 3 (beis3), 26–28 September 2005 2005.

K. I. Scott and M. T. Benjamin. Development of a biogenic volatile organic compounds emission inventory for the scos97-narsto domain. *Atmospheric Environment*, 37:S39–S49, 2003.

N.L. Seaman. Meteorological modeling for air quality assessment. *Atmospheric Environment*, (34):2231–2259, 2000.

J. H. Seinfeld. Ozone air quality models: a critical review. *JAPCA*, 5(38):616–645, 1988.

John H. Seinfeld and Spyros N. Pandis. *Atmospheric chemistry and physics : from air pollution to climate change.* J. Wiley, Hoboken, N.J., 2nd edition, 2006.

P. J. Sellers, Y. Mintz, Y. C. Sud, and A. Dalcher. A simple biosphere model (sib) for use within general circulation models. *Journal of the Atmospheric Sciences*, 43(6):505–531, 1986.

P. J. Sellers, D. A. Randall, G. J. Collatz, J. A. Berry, C. B. Field, D. A. Dazlich, C. Zhang, G. D. Collelo, and L. Bounoua. A revised land surface parameterization (sib2) for atmospheric gcms. part i: Model formulation. *Journal of Climate*, 9(4):676–705, 1996.

D. E. Shallcross and P. S. Monks. New directions: A role for isoprene in biosphere-climate-chemistry feedbacks. *Atmospheric Environment*, 34(10):1659–1660, 2000.

T. D. Sharkey and F. Loreto. Water stress, temperature, and light effects on the capacity for isoprene emission and photosynthesis of kudzu leaves. *Oecologia*, 95(3):328–333, 1993.

T. D. Sharkey and S. S. Yeh. Isoprene emission from plants. *Annual Review of Plant Physiology and Plant Molecular Biology*, 52:407–436, 2001.

T. D. Sharkey, S. Yeh, A. E. Wiberley, T. G. Falbel, D. M. Gong, and D. E. Fernandez. Evolution of the isoprene biosynthetic pathway in kudzu. *Plant Physiology*, 137(2):700–712, 2005.

T. D. Sharkey, A. E. Wiberley, and A. R. Donohue. Isoprene emission from plants: Why and how. *Annals of Botany*, 101(1):5–18, 2008.

P. Siljamo, M. Sofiev, and H. Ranta. An approach to simulation of long-range atmospheric transport of natural allergens: An example of birch pollen. pages 395–402. Springer, 2004.

S. Sillman, M. A. Carroll, T. Thornberry, B. K. Lamb, H. Westberg, W. H. Brune, I. Faloona, D. Tan, P. B. Shepson, A. L. Sumner, D. R. Hastie, C. M. Mihele, E. C. Apel, D. D. Riemer,

and R. G. Zika. Loss of isoprene and sources of nighttime oh radicals at a rural site in the united states: Results from photochemical models. *Journal of Geophysical Research-Atmospheres*, 107(D5-6):–, 2002.

E. L. Singsaas. Terpenes and the thermotolerance of photosynthesis. *New Phytologist*, 146(1): 1–2, 2000.

E. L. Singsaas and T. D. Sharkey. The regulation of isoprene emission responses to rapid leaf temperature fluctuations. *Plant, Cell and Environment*, 21(11):1181–1188, 1998.

E. L. Singsaas and T. D. Sharkey. The effects of high temperature on isoprene synthesis in oak leaves. *Plant, Cell and Environment*, 23(7):751–757, 2000.

G. Sistla, W. Hao, J. Y. Ku, G. Kallos, K. Zhang, H. Mao, and S. T. Rao. An operational evaluation of two regional–scale ozone air quality modeling systems over the eastern united states. *Bulletin of the American Meteorological Society*, 82(5):945–964, 2001.

O. Skarpaas, O. E. Stabbetorp, I. Rønning, and T. O. Svennungsen. How far can a hawk's beard fly. *Measuring and modeling the dispersal of Crepis praemorsa. I: Skarpaas, O. Plant population dynamics in fragmented landscapes, Dr. scient. avhandling, Universitetet i Oslo, Paper IV*, 2003.

M. Sofiev, P. Siljamo, H. Ranta, and A. Rantio-Lehtimäki. Towards numerical forecasting of long-range air transport of birch pollen: theoretical considerations and a feasibility study. *International Journal of Biometeorology*, 50(6):392–402, 2006a.

M. Sofiev, P. Siljamo, H. Ranta, A. Rantio-Lehtimaki, and T. Linkosalo. Evaluation and forecasting of atmospheric concentrations of allergenic pollen in europe. pages 22–24, 2006b.

H. Soons, G.W. Heil, R. Nathan, and G. G. Katul. Determinants of long-distance seed dispersal by wind in grasslands. *Ecology*, 85:3056–3068, 2004.

K. Soudani, G. le Maire, E. Dufrêne, C. François, N. Delpierre, E. Ulrich, and S. Cecchini. Evaluation of the onset of green-up in temperate deciduous broadleaf forests derived from moderate resolution imaging spectroradiometer (modis) data. *Remote Sensing of Environment*, 112(5): 2643–2655, 2008.

F. T. M. Spieksma and A. H. Nikkels. Similarity in seasonal appearance between atmospheric birch-pollen grains and allergen in paucimicronic, size-fractionated ambient aerosol. *Allergy*, 54(3):235–241, 1999.

Robert G. Stanley and H. F. Linskens. *Pollen: biology, biochemistry, management.* Springer-Verlag, Berlin, New York,, 1974.

M. Staudt, N. Bertin, U. Hansen, G. Seufert, P. Cicciolij, P. Foster, B. Frenzel, and J. L. Fugit. Seasonal and diurnal patterns of monoterpene emissions from pinus pinea (l.) under field conditions. *Atmospheric Environment*, 31(Supplement 1):145–156, 1997.

M. Staudt, N. Bertin, B. Frenzel, and G. Seufert. Seasonal variation in amount and composition of monoterpenes emitted by young pinus pinea trees - implications for emission modeling. *Journal of Atmospheric Chemistry*, 35(1):77–99, 2000.

T. H. Stock, D. J. Kotchmar, C. F. Contant, P. A. Buffler, A. H. Holguin, B. M. Gehan, and L. M. Noel. The estimation of personal exposures to air pollutants for a community-based study of health effects in asthmatics-design and results of air monitoring. *Journal of the Air Pollution Control Association*, 35(12):1266–1273, 1985.

W. R. Stockwell, F. Kirchner, M. Kuhn, and S. Seefeld. A new mechanism for regional atmospheric chemistry modeling. *JOURNAL OF GEOPHYSICAL RESEARCH-ALL SERIES-*, 102:25–25, 1997.

R. A. Street, S. C. Duckham, and C. N. Hewitt. Laboratory and field studies of biogenic volatile organic compound emissions from sitka spruce (picea sitchensis bong) in the united kingdom. *Journal of Geophysical Research-Atmospheres*, 101(D17):22799–22806, 1996.

D. Sulla-Menashe and M. A. Friedl. Modis collection 5 land cover type and land cover dynamics: Algorithm refinements and early assessment, 2007.

Earth Resources Observation Systems and USGS. Gtopo30 manual. Technical report, USGS EROS Data Center, 2002.

O. Tackenberg. Modeling long-distance dispersal of plant diaspores by wind. *Ecological monographs*, 73(2):173–189, 2003.

EJ Taylor. *Dorland's illustrated medical dictionary.* W.B. Saunders, Philadelphia, PA, 31st edition, 2007.

T. W. Tesche and D. E. McNally. Superregional ozone modeling and analysis study c final report: Assessment of the reliability of the otag modeling system. *prepared for the Midwest Ozone Group, prepared by Alpine Geophysics, LLC, Ft. Wright, KY*, 1997.

T. W. Tesche, P. Georgopoulos, J. H. Seinfeld, G. Cass, F. W. Lurmann, and P. M. Roth. Improvement of procedures for evaluating photochemical models. *Report to California Air Resources Board for Contract*, 1990.

Gail P. Thelin and Leonard P. Gianessi. Method for estimating pesticide use for county areas of the conterminous united states. Technical Report 00-250, USGS, 2000.

William A. R. Thomson. *Black's medical dictionary.* Barnes and Noble, New York,, 33rd edition, 1981.

G. D. Thurston, K. Ito, P. L. Kinney, and M. Lippmann. A multi-year study of air pollution and respiratory hospital admissions in three new york state metropolitan areas: results for 1988 and 1989 summers. *J Expo Anal Environ Epidemiol*, 2(4):429–50, 1992.

G. D. Thurston, K. Ito, C. G. Hayes, D. V. Bates, and M. Lippmann. Respiratory hospital admissions and summertime haze air pollution in toronto, ontario: consideration of the role of acid aerosols. *Environ Res*, 65(2):271–90, 1994.

D. T. Tingey, M. Manning, L. C. Grothaus, and W. F. Burns. Influence of light and temperature on monoterpene emission rates from slash pine. *Plant Physiol.*, 65(5):797–801, 1980.

D. T. Tingey, R. C. Evans, and M. L. Gumpertz. Effects of environmental conditions on isoprene emission from live oak. *Planta*, 152(6):565–570, 1981.

P. E. Tolbert, M. Klein, K. B. Metzger, J. Peel, W. D. Flanders, K. Todd, J. A. Mulholland, P. B. Ryan, and H. Frumkin. Interim results of the study of particulates and health in atlanta (sophia). *J Expo Anal Environ Epidemiol*, 10(5):446–60, 2000.

P. Turchin. *Quantitative analysis of movement: measuring and modeling population redistribution in animals and plants.* Sinauer Associates, 1998.

U.S.E.P.A. Revised draft user's guide for the aermod meteorological preprocessor (aermet). Technical report, 1998.

U.S.G.S. Usgs land use and land cover (lulc) data. Technical report, US Geological Survey, 1994.

H. T. Valentine. Tree-growth models: derivations employing the pipe-model theory. *Journal of theoretical biology*, 117(4):579–585, 1985.

P. E. Van Laake and G. A. Sanchez-Azofeifa. Mapping par using modis atmosphere products. *Remote Sensing of Environment*, 94(4):554–563, 2005.

W. Vizuete, V. Junquera, and D. T. Allen. Sesquiterpene emissions and secondary organic aerosol formation potentials for southeast texas. *Aerosol Science and Technology*, 38:167–181, 2004.

H. Vogel, A. Pauling, and B. Vogel. Numerical simulation of birch pollen dispersion with an operational weather forecast system. *Int J Biometeorol*, 2008.

J. E. Vogelmann, T. L. Sohl, P. V. Campbell, and D. M. Shaw. Regional land cover characterization using landsat thematic mapper data and ancillary data sources. *Environmental Monitoring and Assessment*, 51(1-2):415–428, 1998.

J. E. Vogelmann, S. M. Howard, L. M. Yang, C. R. Larson, B. K. Wylie, and N. Van Driel. Completion of the 1990s national land cover data set for the conterminous united states from landsat thematic mapper data and ancillary data sources. *Photogrammetric Engineering and Remote Sensing*, 67(6):650–+, 2001.

E. von Mutius, C. Fritzsch, S. K. Weiland, G. Röll, and H. Magnussen. Prevalence of asthma and allergic disorders among children in united germany: a descriptive comparison. *BMJ: British Medical Journal*, 305(6866):1395, 1992.

P. J. Walklate, J. C. R. Hunt, H. L. Higson, and J. B. Sweet. A model of pollen-mediated gene flow for oilseed rape. *Proceedings of the Royal Society B: Biological Sciences*, 271(1538): 441–449, 2004.

K. Y. Wang and D. E. Shallcross. Modelling terrestrial biogenic isoprene fluxes and their potential impact on global chemical species using a coupled lsm-ctm model. *Atmospheric Environment*, 34(18):2909–2925, 2000.

Y. H. Wang, D. J. Jacob, and J. A. Logan. Global simulation of tropospheric o-3-nox-hydrocarbon chemistry 3. origin of tropospheric ozone and effects of nonmethane hydrocarbons. *Journal of Geophysical Research-Atmospheres*, 103(D9):10757–10767, 1998a.

Y. H. Wang, D. J. Jacob, and J. A. Logan. Global simulation of tropospheric o-3-nox-hydrocarbon chemistry 1. model formulation. *Journal of Geophysical Research-Atmospheres*, 103(D9):10713–10725, 1998b.

Y. H. Wang, J. A. Logan, and D. J. Jacob. Global simulation of tropospheric o-3-nox-hydrocarbon chemistry 2. model evaluation and global ozone budget. *Journal of Geophysical Research-Atmospheres*, 103(D9):10727–10755, 1998c.

Y. Q. Wang, X. Y. Zhang, and R. R. Draxler. Trajstat: Gis-based software that uses various trajectory statistical analysis methods to identify potential sources from long-term air pollution measurement data. *Environmental Modelling and Software*, 2009.

B. D. Wardlow and S. L. Egbert. A state-level comparative analysis of the gap and nlcd land-cover data sets. *Photogrammetric Engineering and Remote Sensing*, 69(12):1387–1398, 2003.

P. J. Weathers, S. Elkholy, and K. K. Wobbe. Artemisinin: The biosynthetic pathway and its regulation in artemisia annua, a terpenoid-rich species. *In Vitro Cellular and Developmental Biology-Plant*, 42(4):309–317, 2006.

H. Westberg, B. Lamb, K. Kempf, and G. Allwine. Isoprene emission inventory for the boreas southern study area. *Tree Physiology*, 2000:735–743, 2000.

C. Wiedinmyer, A. Guenther, M. Estes, I. W. Strange, G. Yarwood, and D. T. Allen. A land use database and examples of biogenic isoprene emission estimates for the state of texas, usa. *Atmospheric Environment*, 35(36):6465–6477, 2001.

M. C. Wildermuth and R. Fall. Light-dependent isoprene emission - characterization of a

thylakoid-bound isoprene synthase in salix discolor chloroplasts. *Plant Physiology*, 112(1): 171–182, 1996.

C. K. Wilkins, P. A. Clausen, P. Wolkoff, S. T. Larsen, M. Hammer, K. Larsen, V. Hansen, and G. D. Nielsen. Formation of strong airway irritants in mixtures of isoprene/ozone and isoprene/ozone/nitrogen dioxide. *Environmental Health Perspectives*, 109(9):937–941, 2001.

J. Wilkinson and M. Janssen. Biome3. *Proceedings from the 10th International Emission Inventory Conference, Denver, CO. 0*, 20:40–60, 2001.

E. J. Williams, A. Guenther, and F. C. Fehsenfeld. An inventory of nitric oxide emissions from soils in the united states. *Journal of Geophysical Research*, 97(D7):7511–7519, 1992.

A.M. Winer, D.R. Fitz, and P.R. Miller. Investigation of the role of natural hydrocarbons in photochemical smog formation in california. Technical report, Statewide Air Pollution Research Center, 1983.

A.M. Winer, J. Arey, R. Atkinson, S.M. Aschmann, W.D. Long, Morrison C.L., and Olszyk D.M. Emission rates of organics from vegetation in california's central valley. *Atmospheric Environment*, (26A):2647–2660, 1992.

G. Yarwood, G. Wilson, C. Emery, and A. Guenther. Development of globeis-a state of the science biogenic emissions modeling system. Technical report, 1999.

G. Yarwood, G. Wilson, and S. Shepard. User's guide to the global biosphere emissions and interactions system (globeis) version 3. *ENVIRON International Corporation*, 2002.

Y. Yokouchi and Y. Ambe. Factors affecting the emission of monoterpenes from red pine (pinus densiflora). *Plant Physiol.*, 75(4):1009–1012, 1984.

J. G. Zeidler, H. K. Lichtenthaler, H. U. May, and F. W. Lichtenthaler. Is isoprene emitted by plants synthesized via the novel isopentenyl pyrophosphate pathway? *Zeitschrift Fur Naturforschung C-a Journal of Biosciences*, 52(1-2):15–23, 1997.

X. Zhang, M. A. Friedl, and C. B. Schaaf. Global vegetation phenology from moderate resolution imaging spectroradiometer (modis): Evaluation of global patterns and comparison with in situ measurements. *J. Geophys. Res*, 111, 2006.

P. Zimmerman. Natural source of ozone in houston: Natural organics. In *Proceedings of specialty conference on Ozone/Oxidants - Interactions with the Total Environment*, Pittsburgh, PA, 1979a. Air Pollution Control Association.

P. Zimmerman. Tampa bay area photochemical oxidant study: Determination of emission rates of hydrocarbons fron indigenous species of vegetation in the tampa/st. petersburg, florida area. Technical Report EPA 904/9-77-028, U.S. Environmental Protection Agency, 1979b.

Vita

Christos Efstathiou

1996 Graduated from the Second Lyceum of Voula, Athens, Greece.

2000 Bachelor of Science (B.Sc.) in Environmental Sciences, University of the Aegean, Greece.

2001-09 Research Assistant, Computational Chemodynamics Laboratory, Environmental and Occupational Health Sciences Institute, Piscataway, New Jersey.

2009 Laumbach R. J., Harris G., Kipen H. M., Georgopoulos P., Shade P., Efstathiou C., Isukapalli S., Galea S., Vlahov D., Wartenberg D. Lack of Association Between Estimated WTC Plume Intensity and Respiratory Symptoms among Residents Outside of Lower Manhattan. *American Journal of Epidemiology*, (In Press).

2009 Ph.D. in Environmental Sciences - Exposure Assessment Program, Joint Degree between Rutgers, The State University of New Jersey, and the Graduate School of Biomedical Sciences, University of Medicine and Dentistry of New Jersey.